THE APPLICATION OF CRITICAL STATE SOIL MECHANICS TO PREDICT GROUND DEFORMATIONS BELOW AN EMBANKMENT CONSTRUCTED ON SOFT ALLUVIUM

by

ANDREW ROBERT PICKLES

A Thesis submitted for the degree of

Doctor of Philosophy

CITY UNIVERSITY

Civil Engineering Department

January 1989

CONTENTS

LIST OF TABLES

LIST OF FIGURES

ACKNOWLEDGEMENTS

The London Docklands Development Corporation in conjunction with the London Borough of Newham very kindly allowed City University, with funding from the Science and Engineering Research Council, to assist in monitoring the EGAR embankment during construction and to have access to both soil samples and to the design and construction data. In particular I would like to acknowledge the help of Mr. Mike Lepper, Mr. Ben Kirk and their colleagues for their help in the day to day monitoring of the construction.

My thanks and appreciation are due to Mr. John Evans and Professor John Atkinson for their help and guidance throughout the project. I would also like to thank my colleagues and the students in the Geotechnical Engineering Research Centre and in particular Dr. Matthew Coop, Dr. Neil Taylor and Mr. Rick Woods for the contributions that they have made. In addition, the laboratory testing would not have been possible without Mr. Keith Osborne and his team of technicians.

Finally I would like to thank my wife Lindsay without whose patience and encouragement this work would have taken twice as long to complete.

DECLARATION

I grant powers of discretion to the University Librarian to allow this thesis to be copied in full or in part without further reference to me. This permission covers only single copies made for study purposes, subject to normal conditions of acknowledgement.

ABSTRACT

An embankment has been constructed to a maximum height of approximately twelve metres at Beckton, east London. The embankment is underlain by up to eight metres of alluvium and made ground. The embankment was monitored during construction. Centreline settlements of the order of 0.6m and horizontal movements at the embankment toe of up to 0.15m were measured. The excess pore pressures generated during construction were found to dissipate rapidly.

Soil samples recovered from the site have been tested at City University. The alluvial clay is shown to have extremely variable compression characteristics and it is not possible to determine a single set of critical state soil parameters from the "undisturbed" soil samples. The use in design of parameters derived from reconstituted soil samples is investigated.

Laboratory test results indicate that a small quantity of organic matter in the soil has a large effect on the engineering properties of the alluvial clay. The importance of not drying soils which contain organic matter is highlighted. It is shown that, despite the effects of the organic matter, critical state concepts and in particular the modified Cam clay soil model can be used to predict the behaviour of the alluvial clay in a wide variety of laboratory tests.

Standard methods of determining the yield stress or preconsolidation pressure are shown to be inadequate when used to analyse the results of compression tests performed at a constant rate of loading. An alternative method, the Lambda construction, is proposed and this is shown to be both reliable and objective.

Two distinct testing methods have been used to probe the state boundary surface of the reconstituted alluvial clay samples. The results of these tests appear to indicate the existence of a single state boundary surface for both K_o and isotropically compressed samples. This surface has a shape similar to that predicted by the modified Cam clay soil model. This result conflicts with the findings of many other investigators.

Finite element modelling of the embankment construction has been carried out. A single set of soil parameters derived from tests on the reconstituted clay were used to represent the alluvial stratum. The construction of the embankment was modelled as a drained event. The results are shown to compare favourably with the actual field data.

Glossary of Symbols

E'	Young's modulus in terms of effective stress
G'	elastic shear modulus
G_s	specific gravity of soil grains
H	initial layer thickness
K'	elastic bulk modulus
K_{nc}	value of K_o for one-dimensionally normally compressed soil
K_o	current value of σ'_v/σ'_h for soil constrained to deform one-dimensionally also used to denote one-dimensional compression and swelling
PI	plasticity index
R_o	overconsolidation ratio from σ'_{vc}/σ'_v
R_p	overconsolidation ratio from p'_m/p'
a	(subscript) axial
c'	cohesion
c_h	horizontal coefficient of consolidation
c_u	undrained shear strength
m	(subscript) maximum past value
p'	current value of mean effective stress $(\sigma'_1+\sigma'_2+\sigma'_3)/3$
p'_{cs}	value of p' at critical state
p'_e	equivalent pressure: value of p' at the point on the isotropic normal compression line at the same specific volume
p'_{eo}	value of p' at the point on the K_o normal compression line at the same specific volume
p'_m	maximum past value of p'
p'_p	value of p' at the intersection of the elastic wall and the isotropic normal compression line
q'	current value of deviator stress $(\sigma'_1-\sigma'_3)$
r	(subscript) radial
u	pore pressure
v	specific volume
v_k	specific volume of isotropically compressed soil swelled to p'=1kPa
Γ	specific volume of soil at critical state with p'=1kPa
M	slope of critical state line when it is projected on to a constant volume plane
M_c	value of M for triaxial compression tests
M_e	value of M for triaxial extension tests
N	specific volume of isotropically normally compressed soil at p'=1kPa
N_o	specific volume of K_o normally compressed soil at p'=1kPa
δ	a small increment of ...
ϵ	strain
ϵ_v	volumetric strain $(\epsilon_1+\epsilon_2+\epsilon_3)$
ϵ_s	shear strain for $\epsilon_2=\epsilon_3$, $2(\epsilon_1-\epsilon_3)/3$
κ	slope of swelling line (negative)
λ	slope of normal compression line (negative)
ν'	Poissons' ratio
σ	normal stress
σ'_v	vertical effective stress (axial in triaxial test)
σ'_{vc}	maximum past value of σ'_v
ϕ'	angle of internal friction

ϕ'_c, ϕ'_e angle of internal friction for triaxial compression and extension tests respectively

1 (subscript) major principal
2 (subscript) intermediate principal
3 (subscript) minor principal

CHAPTER 1 INTRODUCTION

1.1 Background to the Research

The Eastern Gateway Access Road (EGAR) has been constructed to link the A13 at Beckton to the new London City airport. The road crosses the Northern Outfall Sewer (NOS) which is an above ground collection of large diameter sewer pipes protected by an earthen embankment approximately four metres high. On either side of the NOS the road is carried on an embankment which forms the abutments to a single span bridge supporting the carriageway. The total length of the embankment is approximately 800 metres and the maximum height of the embankment during construction was approximately twelve metres.

The site is underlain by up to 8m of soft organic alluvial deposits and made ground. A large diameter gas main crosses the site and runs parallel and close to the embankment toe in one area. In order to protect the gas main from potential ground movements, it was necessary to construct a bored pile wall between the embankment toe and the gas main.

The client for the construction of the embankment was the London Docklands Development Corporation (LDDC) who retained the London Borough of Newham (LBN) as the lead consultant for the design of the road and associated structures. Husband and Co. were employed as the specialist geotechnical consultants for the project. The main contractor for the construction of the embankment was J. Laing Construction Ltd.

The LDDC in conjunction with the LBN very kindly allowed City University, with funding from the Science and Engineering Research Council (SERC), to assist in monitoring the embankment during construction. In addition soil samples were recovered during the installation of the

geotechnical instrumentation for testing at City University.

1.2 Rationale and Aims of the Research

A major part of the present investigation is the prediction of ground deformations due to construction of the embankment. The predictions are made using the CRISP finite element package and are compared with the actual field movements. The use of drained finite element analyses to represent embankment construction is investigated.

The choice of a representative soil model for the organic clay stratum is very important. The original Cam clay and modified Cam clay critical state soil models are particularly relevant to normally and lightly overconsolidated clays, Wroth (1977). These models were based on the results of triaxial tests on isotropically compressed samples and their validity, in particular the postulated shape of the state boundary surface, when used to represent one-dimensionally (K_o) compressed soil strata has been questioned, for example Graham et al. (1988), Tavenas and Leroueil (1977).

As part of the present investigation the state boundary surface of both isotropically and K_o compressed reconstituted soil samples is investigated. The determination of a relevant yield stress from compression test data is also examined.

It is generally recommended that engineering parameters for design be derived from the results of both in situ tests and high quality laboratory tests on "undisturbed" soil samples (e.g. Britto and Gunn (1987), Wroth (1984)). The alluvial clay stratum below the embankment is shown to have extremely variable engineering properties. A single set of critical state parameters cannot be derived from

the results of either the in situ testing or laboratory tests on "undisturbed" samples. The use of parameters derived from reconstituted soil samples is investigated.

The effect of drying the alluvial clay, which contains organic peaty material, during sample preparation for the measurement of standard engineering parameters, such as the Atterberg limits, is investigated.

The critical state parameters determined for the reconstituted organic clay are compared to the results of the testing performed during the original site investigation. The results of the original site investigation are also reviewed in the light of critical state theory and the requirements of the finite element analyses.

1.3 Structure of the Dissertation

A number of topics relevant to the construction of the embankment are covered in the dissertation. It has been necessary to include discussion on individual aspects of the investigation at various stages in the body of the report.

A summary of the previous finite element investigations of embankment behaviour is presented in chapter 2. The basic concepts underlying critical state soil mechanics are set out and various modifications to these concepts, proposed by other research workers, are discussed. The effects of organic peat material on the engineering properties of clay soils are also summarised.

A method for determining a yield stress, which is representative of the preconsolidation pressure of a soil sample, from the results of constant rate of loading compression tests in the triaxial apparatus is proposed in chapter 3. A multi-stage stress path test for defining the

shape of the state boundary surface of K_o compressed samples is also discussed.

An extensive site investigation including both pressuremeter and plate dilatometer testing was carried out prior to the construction of the embankment. The results of the investigation are reported in chapter 4. The triaxial test data derived during the original site investigation have been re-plotted in terms of the more usual critical state stress invariants p' and q'. In addition both the pressuremeter and plate dilatometer results have been re-analysed in the light of recent advances in the interpretation of these tests. This work has also been included in chapter 4.

The instrumentation installed below the embankment is described in chapter 5. The data obtained from this instrumentation during construction of the embankment are summarised at the end of this chapter.

Chapters 6, 7 and 8 report the laboratory testing carried out at City University. Chapter 8 includes discussion on the K_o state boundary surface and the stress-strain behaviour of both the reconstituted and the "undisturbed" clay samples. The critical state parameters determined for the reconstituted clay are compared to the original site investigation data, reported in chapter 4.

The finite element modelling procedures and the methods adopted for determining the relevant analysis parameters from both the laboratory and in situ tests are discussed in chapter 9. The results of the finite element analyses are also presented in this chapter and these are compared with the actual field movements.

Chapter 10 comprises a review of the results discussed in the other sections of the dissertation. The various conclusions drawn from the work are summarised in chapter 11.

CHAPTER 2 LITERATURE SURVEY AND BACKGROUND THEORY

2.1 Introduction

A great deal has been written on the subject of the construction of embankments on soft ground. It has also been the subject of a number of prediction symposiums, for example, the Foundation Deformation Prediction symposium held at M.I.T. in 1974 and the Reinforced Earth Embankment symposium held at King's College, London in 1986. As a result much research work has been performed studying various aspects of embankment behaviour.

The majority of this work has been concerned with the assessment of stability during construction. Previous published reports on embankment construction on the soft alluvium of the River Thames (e.g. Marsland and Powell (1978), Marsland and Randolph (1978), Golder and Palmer (1955)) have been primarily concerned with this feature. The most important aspect in these studies has been the determination of reliable estimates of the undrained shear strength of the foundation soils.

The second most common area of research work has been devoted to the prediction of settlements and in particular to the rate of settlement below an embankment. The compressibility and permeability of the foundation material are the most important parameters for the calculation of these values.

Work has also been carried out on the determination of general soil deformations below an embankment, though much of this work has been related to the stability of the embankment. This aspect of embankment construction will become increasingly important as more embankments are constructed close to existing services or structures. In order to calculate these deformations the stress-strain-pore pressure response of the foundation soil has to be predicted for a wide variety of stress changes.

The stress-strain response of an element of soil is both stress path and state dependant and involves both plastic and elastic shearing and volumetric distortions. A number of mathematical soil models have been developed to represent this behaviour, for example the hyperbolic model of Duncan and Chang (1970) and the t_{ij}-clay model of Nakai and Matsuoka (1987). In order to fully exploit these non-linear soil models to predict embankment performance the finite element method is often used.

In the United Kingdom the critical state soil concepts and soil models developed at Cambridge University, Schofield and Wroth (1968), are relatively well known by the geotechnical engineering profession. However the simplicity and versatility of these concepts are not widely appreciated by practicing engineers. The CRISP finite element package is also widely available, although, few examples of the use of this package to model field embankment construction have been published.

This chapter presents a brief summary of the previous research into the prediction of soil deformations below embankments using the finite element method. The basic concepts and parameters used in critical state soil mechanics are defined. Current research into yielding and the shape of the state boundary surface is reported. Finally the determination of relevant soil parameters for the very variable organic peaty clays found at the EGAR site are discussed.

2.2 Soil Deformations below an Embankment

Traditionally engineers have been primarily concerned with the settlement of embankments, for the following main reasons. Firstly, continuing settlements after completion of construction can lead to serviceability problems at the interface between the embankment and other structures, such as bridges, which are generally founded on stiffer

soil strata. Secondly the cost and feasibility of embankment construction can be determined by the settlement magnitude.

Conventional soil mechanics theories, based on the results of oedometer tests, have been relatively successful at predicting the magnitude of these settlements (e.g. Lewis et al. (1975)). The prediction of lateral deformations is more difficult, particularly when the foundation soils experience plastic deformations.

With the advent of more sophisticated non-linear soil models and access to increasingly powerful finite element programs, more complicated elasto-plastic stress-strain analyses incorporating coupled consolidation and creep parameters have been possible. These analyses have been used to predict a number of parameters including the pore pressures developed during construction, rates of settlement and lateral deformations. An extensive body of literature exists on the finite element analysis of embankment behaviour, for example Thoms et al. (1976), Wroth (1977) and Nakai and Matsuoka (1987).

As discussed in section 2.1, a number of mathematical soil models have been developed to represent the stress-strain behaviour of soil. In addition many finite element programs have been developed, for example the FEECON program developed by Simon et al. (1972) and the SSOIL program developed by Thoms et al. (1976). For the purposes of this study the emphasis is placed on finite element analyses using the CRISP finite element program, Britto and Gunn (1987), and incorporating critical state soil models.

A number of investigators have used the CRISP finite element package to analyse centrifuge model tests with critical state soil models, for example Almeida et al. (1986) and Basset et al. (1981). These studies have generally shown relatively good agreement between the

model test results and finite element predictions under controlled laboratory conditions.

Kwok (1987) modified the CRISP package to permit modelling of a reinforcement layer below an embankment. The majority of this research considered parametric studies, performed using finite element analyses, of the many factors involved in reinforced embankment construction. Kwok recommended that an elastic perfectly plastic model with a Mohr-Coulomb yield criterion be used to represent embankment fill in preference to the other soil models available in CRISP.

The majority of field investigations have involved the construction of heavily instrumented test embankments, for example, Almeida and Ramalho-Ortigão (1982) and Wroth (1977). These have generally been constructed rapidly to failure in order to investigate stability criteria. Construction has been modelled as an undrained event. However it has been shown (e.g. Leroueil et al. (1978)) that most real field construction conditions are far from undrained.

The major advantage of Cam clay type soil models over other non-linear elastic models, such as the hyperbolic model of Duncan and Chang (1970), is their ability to calculate pore pressures, Wroth (1977). Coupled consolidation analyses can therefore be performed to estimate longer term deformation trends. The major difficulty in performing these analyses is obtaining appropriate consolidation parameters, Almeida and Ramalho-Ortigão (1982). Almeida and Ramalho-Ortegão modelled embankment construction considering coupled consolidation, undrained and drained analyses with the CRISP program. They found that the drained analysis predicted horizontal displacements of the same magnitude and pattern as the other analyses.

Hird and Kwok (1988) also used the CRISP program to model construction of the Stanstead Abbotts trial embankment. In

common with the other predictors at the Reinforced Earth symposium they found that the consolidation process had not been adequately modelled. Consolidation occurred much faster on site than would have been predicted from the laboratory test results. A drained finite element analysis gave better agreement with the actual inclinometer profiles measured on site than the equivalent coupled consolidation analyses.

With the exception of the analyses reported by Almeida and Ramalho-Ortegão (1982) and Hird and Kwok (1988), no other examples of comparisons between real field construction and analyses using the CRISP finite element package, in which the construction is modelled as a drained event could be found by the author. Shibata et al. (1976) reported good agreement between predicted and observed deformations when analysing embankment construction as a drained event using a soil model developed by Matsuoka (1974).

Burland (1969) performed triaxial tests in which a deviator load was applied under undrained conditions after which the sample was allowed to drain. The results were compared with the equivalent loading applied slowly under drained conditions. He found that at low deviator stresses (up to about 30% of the undrained failure stress) the shear strains for both types of tests were almost identical. At higher stresses the shear strains for the undrained loading case were larger than the equivalent drained test, being about twice as large at 90% of undrained failure. The volumetric strains in both types of tests were almost identical.

These results appear to indicate that, provided only small excess pore pressures are generated, drained finite element analyses are satisfactory for predicting long term deformations. Considering the difficulty associated with determining appropriate consolidation parameters and the fact that most field construction conditions are far from undrained, drained finite element analyses may often be

appropriate. This is particularly the case when vertical drainage elements have been installed as at the EGAR embankment.

2.3 Basic Soil Mechanics

The soil test data reported in this dissertation have been analysed within the framework of critical state soil mechanics, Schofield and Wroth (1968), Atkinson and Bransby (1978). The symbols and definitions of terms used in Atkinson and Bransby (1978) have been adopted throughout the thesis. It is important to note that critical state soil mechanics provides a general framework within which the behaviour of a soil mass can be analysed. There have been many refinements to the original theories which attempt to model observed soil behaviour more closely. Some of these refinements are discussed in sections 2.4 and 2.5.

For a general three-dimensional state of effective stress the stress invariants are

$$p' = (\sigma_1'+\sigma_2'+\sigma_3')/3 \qquad (2.1)$$

$$q' = [(\sigma_1'-\sigma_2')^2+(\sigma_2'-\sigma_3')^2+(\sigma_3'-\sigma_1')^2]^{1/2}/\sqrt{(2)} \qquad (2.2)$$

in the special case of triaxial test data (where $\sigma_2'=\sigma_3'$)

$$p' = (\sigma_a'+2\sigma_r')/3 \qquad (2.3)$$

$$q' = (\sigma_a'-\sigma_r') \qquad (2.4)$$

Similarly the strain invariants in the triaxial test (where $\epsilon_2=\epsilon_3$) are defined as

$$\epsilon_v = (\epsilon_a+2\epsilon_r) \qquad (2.5)$$

$$\epsilon_s = 2(\epsilon_a-\epsilon_r)/3 \qquad (2.6)$$

The strains measured in soil tests are relatively large and as such natural strains are used throughout this thesis. Note that if engineering strains are used in equation 2.5 then, in an undrained triaxial test at large strain, $\epsilon_a > -2\epsilon_r$ and (from eqn. 2.5) $\epsilon_v > 0$. The conversion between natural strains ϵ(nat) and engineering strains ϵ(eng) is as follows

$$\epsilon(\text{nat}) = \ln \frac{1}{\{1-\epsilon(\text{eng})\}} \qquad (2.7)$$

A fundamental concept of critical state soil mechanics is the existence of a state boundary surface in p',q',v space. An example of a constant volume section through the state boundary surface is shown on figure 2.1. The state of a sample cannot lie outside this surface, although the surface can be permanently extended by compressing the sample. For all states on the state boundary surface on the wet side of the critical state line (i.e. $p' > p'_{cs}$) the sample is considered to be normally compressed. It is assumed that the state of samples which have been normally compressed to different stresses, but identical stress ratios, fall on straight lines with a slope of λ in v:ln(p') space, see figure 2.1.

The ultimate state of samples at the end of a shearing test lie on the critical state line which is parallel to the normal compression lines. The critical state stress ratio is plotted as two lines in q':p' space with slopes M_c and M_e for positive and negative values of q', see figure 2.1. The relationship between M_c and M_e depends on the assumed failure criterion. The Mohr-Coulomb failure criterion (ϕ' constant) appears to provide a good fit with experimental data, Bishop (1966). In this case it can be shown, Atkinson and Bransby (1978), that

$$M_c = \frac{6 \sin\phi'}{(3 - \sin\phi')} \qquad (2.8)$$

and

$$M_e = \frac{6 \sin\phi'}{(3 + \sin\phi')} \qquad (2.9)$$

The state of samples inside the state boundary surface must lie on an elastic wall which, in p',q',v space, is perpendicular to the q'=0 plane. The elastic wall projects as a straight line with a slope of κ in v:ln(p') space. The elastic wall intercepts the isotropic compression line on the q'=0 plane at p'_p.

Strains within the state boundary surface are elastic and hence recoverable although not necessarily linear. For states on the state boundary surface plastic and hence irrecoverable strains occur in addition to the elastic strains. The state boundary surface is therefore a yield surface separating purely elastic behaviour from inelastic behaviour. A further extension of critical state soil mechanics is the assumption that the state boundary surface is also a plastic potential (The plastic strain increment vector is orthogonal to a plastic potential). This allows plastic strains to be calculated as the sample state moves across the state boundary surface. The assumed shape of the state boundary surface therefore determines the predicted stress-strain behaviour of a soil element.

2.4 The Shape of the State Boundary Surface

An elastic wall section through the state boundary surface defines the shape of the yield locus. The shape of the original Cam clay yield locus, Schofield and Wroth (1968), was determined from a consideration of the work dissipated during shear and is given by

$$\frac{q'}{M\,p'} + \ln\left\{\frac{p'}{p'_p}\right\} = 0 \qquad (2.10)$$

Other yield loci have been postulated which attempt to give a better fit with experimental data. The most commonly used of these alternative formulations, proposed by Burland (1965) and known as the modified Cam clay yield locus, is defined as follows

$$p'_p = \frac{\{ (q'/p')^2 + M^2 \}}{M^2} p' \qquad (2.11)$$

Both the original Cam clay and the modified Cam clay soil models were developed from the results of triaxial tests performed on isotropically compressed samples. However, the majority of naturally occurring soft clay deposits have been deposited under conditions of zero lateral strain.

Parry and Nadarajah (1973) performed tests on lightly overconsolidated specimens of kaolin consolidated from a slurry under K_o stress conditions. Various drained and undrained tests were performed on these specimens to enable a volumetric yield locus to be defined. The volume change or pore pressure response for each test was plotted against q' or p'(in arithmetic rather than log stress-strain space). The yield point at which a marked change occurred in the behaviour of either the pore pressure response in undrained tests or the volumetric strain in drained tests was determined by the use of simple straight line extrapolations of portions of the curves with different slopes, figure 2.2. A volumetric yield locus was determined and this was compared to the results of an undrained extension test on a K_o compressed sample and an undrained compression test on an isotropically compressed sample. The test results are replotted on figure 2.3.

Many other investigators, for example Clausen et al. (1984), Tavenas and Leroueil (1977), Crooks and Graham (1976), have carried out tests on "undisturbed" and K_o compressed reconstituted clay samples to investigate the shape of the yield envelope. A summary of the results of this testing is given in Graham et al. (1988) and the yield envelopes for a number of different clays are reproduced in figure 2.4. Details of the various tests are reproduced in table 2.1.

It can be seen from figures 2.3 and 2.4 that the yield envelopes for these clays appear to have a very different shape from the yield locus predicted by the modified Cam

clay model (a constant volume section through the modified Cam clay state boundary surface is shown on figure 2.1). It should be noted that all the yield envelopes presented in figure 2.4 have been determined using the bi-linear curve fitting technique adopted by Parry and Nadarajah (1973).

Graham et al. (1988) also present the yield points measured on natural Winnipeg clay normalised by the corresponding value of p'_{eo}, determined from the one-dimensional normal compression line. The results are reproduced on figure 2.5. These results agree more closely with the shape of the modified Cam clay yield locus.

The state of samples that have been isotropically normally compressed will remain on the state boundary surface when tested in either compression or extension. Pender (1978) and Parry and Nadarajah (1973) have compared the yield envelopes for K_o compressed samples with the results of undrained extension tests on K_o normally compressed samples. It is often assumed that the undrained stress path for these tests represents a constant volume section through the state boundary surface. It should be noted however that critical state soil mechanics would predict that the state of a K_o compressed sample when tested in undrained extension will traverse an elastic wall until the state boundary surface is re-engaged at a negative deviator stress, see figure 2.6.

A number of investigators, for example Pender (1978), Atkinson et al. (1987), have proposed alternative mathematical formulations for the K_o yield locus based on the type of test data presented in figures 2.3 and 2.4. The use of these alternative formulations will lead to differing stress-strain predictions between K_o and isotropically compressed samples.

2.5 Measurement of an Appropriate Yield Stress

It was noted in section 2.3 that critical state soil mechanics provides a general framework within which the behaviour of a soil mass can be analysed. An ideal soil behaving exactly as predicted by critical state theory would exhibit a well defined yield point. However when real soils are tested there is always a transitional region between pre-yield and post-yield behaviour. The criteria for identifying a yield point are empirical and require judgement, Graham et al. (1988).

Traditionally the preconsolidation pressure of a soil sample has been measured in an oedometer using the Casagrande (1936) construction, see figure 2.7. The preconsolidation pressure of a soil sample is generally defined as the maximum vertical effective stress (σ'_{vc}) that the sample has experienced at any stage during its' geological history. However, due to effects such as ageing or secondary consolidation, soils often exhibit a higher preconsolidation pressure than would be expected from the loading history of the soil sample. Casagrande recommended that a range of values for σ'_{vc} be used rather than a single value. The preconsolidation pressure is a measure of the vertical yield stress for K_o compression.

The Casagrande (1936) construction was proposed for use with oedometers employing incremental loading steps and considers only the one-dimensional loading case. A test carried out in a triaxial cell can follow a number of different stress paths and this construction may not be appropriate for all these stress paths.

As discussed in section 2.4 the majority of investigators have adopted a bi-linear construction, in arithmetic stress space, when determining a value for the yield stress. However, it is well known that the elastic behaviour of soils below the state boundary surface is non-linear. For example a threshold region of very stiff stress-strain response is exhibited when the direction of

the stress path is reversed, Richardson (1988). In addition, based on the study of a number of laboratory test results, Butterfield (1979) proposed that a better straight line fit to stress-strain data is observed if compression and swelling test data are plotted in ln(v):ln(p') space.

When using the bi-linear construction the fitting of straight lines to a curved set of data points is necessarily subjective, for example see the results presented in figure 2.2. An alternative method of defining the yield point is proposed in section 3.2.

2.6 The Effects of Organic Material on Soil Properties

The alluvial clay at the EGAR site has an extremely variable organic (peat) content. The presence of large amounts of organic matter in soils is usually undesirable from an engineering viewpoint, Mitchell (1976). For example it can lead to high plasticity, high shrinkage, high compressibility and low strength. A comprehensive summary of the morphology and properties of clays with a high organic content is given by Hobbs (1986). Odell et al. (1960) present quantitative analyses of the influences of small quantities (< 10% by weight) of organic matter on the engineering properties of soils from Illinois. However no other data could be found on the properties of clays with a low organic content.

The cation exchange ability of peat is extremely high and this exerts an important influence on the way in which it effects the engineering properties of soils. As discussed above a quantitative indication of the effects of peat on the plasticity characteristics of soil is given by Odell et al (1960). The effects of small changes in the organic content are compared with the influence of changes in the percentage of clay and percentage of montmorillonite in the soil and the results are reproduced in figure 2.8. It

can be seen in this figure that relatively small changes in the organic content of the order of 1% or 2% can lead to large changes in the liquid and plastic limits.

Another important feature is the effect of drying on the properties of peaty soils. At high moisture contents decomposed organic matter may behave as a reversible swelling system, but, at some critical stage during drying this reversibility ceases, Mitchell (1976). This can be observed in a large decrease in the Atterberg limits as a result of drying. For example, Mayne (1987) reported that the liquid limit of air dried samples from a site in Washington D.C. was on average only 63% of the liquid limit of samples tested without drying.

Many engineering properties are derived from the Atterberg limits using both empirical and semi-empirical relationships. For example, the ratio of the undrained shear strength to the vertical effective stress, for a normally consolidated clay, is related to the plasticity index by Skempton (1957) as follows:-

$$Cu/\sigma'_v = 0.11 + 0.0037 * PI \qquad (2.12)$$

and the slope of the critical state line in v:ln(p') space is related to the plasticity index by Schofield and Wroth (1968) as follows:-

$$\lambda = (Gs * PI) / 461 \qquad (2.13)$$

It is important therefore that the correct sample preparation procedure is followed when measuring the Atterberg limits. Many published summaries of laboratory test data from soft clay sites report in situ moisture contents in excess of the measured liquid limit. For example 4 out of the 7 sets of test data summarised on table 2.1 exhibit this feature. It is probable that this is a result of drying during sample preparation for the liquid limit test, although clays with a very high sensitivity (i.e. loss of strength on remoulding) could also exhibit this behaviour.

The standard preparation procedure for the liquid limit test given in BS 1377 (1975) is to dry the sample prior to

testing. However it also recommends that "organic soils should be tested at their natural moisture content", i.e. inferring that the soil should not be dried. No guidance is given on the organic content at which this alteration to sample preparation procedure is important.

When determining the moisture content of organic clay samples many investigators have adopted drying temperatures between 60°C and 90°C to avoid oxidation of the peat, Skempton and Petley (1970). However Skempton and Petley found that drying temperatures had little effect on the measured moisture content of organic samples.

2.7 Summary

The research described in this dissertation endeavours to extend knowledge in the area of the engineering prediction of the deformation of soft soil below an embankment. As discussed in section 2.2, drained finite element analyses to predict deformations may be appropriate to many real embankments. However there are few published examples of comparisons between real field construction and finite element analyses using critical state soil models in which the construction has been modelled as a drained event.

The modified Cam clay soil model, incorporated in the CRISP finite element package, is used in the present investigation to represent the soft alluvial clay stratum below the embankment. As discussed in section 2.4 the shape of the state boundary surface predicted by this soil model, when used to represent K_o compressed soil, has been questioned by a number of investigators.

The difficulties associated with the measurement of a relevant yield stress to determine the preconsolidation pressure was discussed in section 2.5. The effects of small quantities of organic matter on the engineering properties of clay soils were highlighted in section 2.6.

CHAPTER 3 - DEVELOPMENTS AND APPLICATIONS OF THEORY

3.1 Introduction

As discussed in section 2.3 the state boundary surface is a surface in p':q':v space that separates elastic stress-strain response from elasto-plastic behaviour. If the state boundary surface is also assumed to be a plastic potential surface and a yield surface then its shape will determine the predicted stress-strain response of a soil element to any applied loading path. The shape of the state boundary surface has been examined by previous researchers using either the results of undrained tests on normally compressed samples or the results of drained stress path probes.

The difficulty of determining the shape of the state boundary surface from undrained tests on K_o compressed samples when tested in extension was highlighted in section 2.4 and on figure 2.6. The problems associated with defining a yield point from the results of drained stress path probes was discussed in section 2.5.

A method of defining the yield point from the results of constant rate of loading drained probing tests is proposed in this chapter. In addition an alternative method of establishing the shape of the state boundary surface from the results of drained loading tests which traverse the surface is discussed. The procedures adopted for determining the value of ν' from the results of a K_o swelling test and for normalising stress-strain data are also presented.

3.2 Determination of the SBS Yield Point

In critical state theory a lightly overconsolidated soil sample compressed along a drained stress path similar to that shown on figure 3.1a will yield when the stress path

intersects the yield locus (an elastic wall section through the state boundary surface). The size of the yield locus is a function of the past maximum compression stresses. The magnitude of the stresses at which a soil sample yields is dependant on the direction of the stress path probe and the past maximum compression stresses.

When the state boundary surface is being probed the aim is to identify the point at which the state boundary surface is engaged (or the yield locus is intersected). For the purposes of this dissertation the combination of stresses at which the state boundary surface is engaged for a particular stress path has been named the SBS yield point (rather than the more commonly used terminology of the preconsolidation pressure or the yield stress).

Real soils start to yield before the state boundary surface is engaged. Even in carefully controlled laboratory tests it is difficult to determine a clearly defined yield stress, for example, see the results of tests on reconstituted kaolin performed by Parry and Nadarajah (1973) reproduced in figure 2.2. For a stress path probe performed at a constant stress ratio the ideal and real soil behaviour in v:ln(p') space is shown on figure 3.1b. It can be seen on this figure that the SBS yield point is not clearly defined on the v:ln(p') curve for the real soil. A method of determining the SBS yield point from stress path test results is therefore required.

The triaxial stress path cells used at City University perform tests controlled at either a constant rate of loading or a constant rate of straining, see section 6.4. The Casagrande (1936) construction was developed for use with the results of oedometer tests performed using incremental loading steps. The Casagrande (1936) construction is therefore not suitable for use with the type of test procedure employed at City University.

A number of investigators (e.g. Bell (1977) and Graham et al. (1983)) have used a bi-linear approach for determining

a yield stress from the stress-strain response of a drained stress path probe on a soil sample. However the majority of these investigators have used incremental loading techniques. As discussed in section 2.5, the bi-linear construction can be subjective and the results may not be representative of the SBS yield point.

Leroueil (1986) has performed a large number of tests on Champlain sea clays using both constant rate of straining and constant rate of loading test methods. He considered the strain rate to be a rheological parameter and that the measured preconsolidation pressure is therefore a function of the strain rate. No details are given of the method adopted to determine the preconsolidation pressure from the stress-strain curves.

During the present investigation a number of experiments were carried out on both "undisturbed" and reconstituted samples to find a reliable method of determining the SBS yield point from triaxial tests performed at a constant rate of loading. In these tests the samples were compressed to a known stress state, swelled back inside the state boundary surface and then re-compressed to a much higher effective stress. The compression and swelling stages for each soil sample followed either K_o or isotropic stress paths. In this way samples were created with known SBS yield points, or known points at which the state boundary surface would be engaged.

Various combinations of stress and strain parameters and geometric constructions were used to locate the known SBS yield point. The aim was to find a method that accurately measures the known SBS yield point, and its' application is both simple and objective. The procedure finally adopted to determine the SBS yield point from constant rate of loading tests is described below and is referred to throughout this dissertation as the Lambda construction.

At the end of a constant rate of loading test the stresses are held constant until the volumetric strain rate falls below 0.005% per hour. This rate is considered to be sufficiently slow that the assumption that the consolidation is complete can be made. A small tail is produced on the v:ln(p)' plot, see figure 3.2, representing the dissipation of excess pore pressures from the sample. A line is drawn from the base of this tail parallel to the final portion of the v:ln(p') plot. The point at which this line re-crosses the v:ln(p') plot is taken to be the SBS yield point, see figure 3.3. The justification for the use of this construction is considered below.

The magnitude of the excess pore pressure generated during constant rate of loading tests is discussed in Atkinson (1984a). The average excess pore pressure generated during a constant rate of loading test is inversely proportional to the coefficient of consolidation of the sample. For stress states inside the state boundary surface the stress-strain response is relatively stiff and the coefficient of consolidation of the soil is therefore higher than for the same soil in a normally compressed state. The average excess pore pressure generated when consolidating a sample whose state lies inside the state boundary surface is therefore relatively small and the v:ln(p') plot requires no correction for this stage of the test.

When the soil is in a normally compressed state the average excess pore pressure generated is relatively large. The position of the normal compression line can only be determined by stopping the loading stage and holding the stresses constant, until the excess pore pressure has dissipated. In order accurately to locate the normal compression line the test should be stopped in this way a number of times. However it can be shown experimentally that the volume change resulting from the dissipation of the excess pore pressure is approximately constant for a given soil, when tested at a constant rate

of loading. A line drawn through the end point parallel to the uncorrected v:ln(p') plot is therefore a good approximation to the actual normal compression line for the soil. The point of intersection with the initial portion of the v:ln(p') plot then defines the SBS yield point with reasonable accuracy.

The test results obtained using the Lambda construction are discussed in section 8.4.

3.3 Probing the State Boundary Surface

As discussed in section 2.4 the method adopted by the majority of investigators to determine the shape of the state boundary surface has been to use drained stress path probes directed onto the state boundary surface. For each individual probe a new sample must be used. In order to define the shape of the yield locus either all the samples must have identical preconsolidation pressures or the results must be normalised with respect to the known preconsolidation pressure of each sample.

If the critical state parameters of the soil are known and it is assumed that the shape of the state boundary surface is regular, then an alternative method of probing the surface is possible. The results of a drained stress path test directed across the state boundary surface can be normalised to give a section through the state boundary surface. It is current practice to normalise test data with respect to the equivalent pressure p'_e, Graham et al. (1988), Atkinson (1984b). This will reveal a constant volume section through the state boundary surface. In order to define a yield locus or elastic wall section through the surface the results should be normalised against p'_p. From the geometry of figure 3.4

$$v = N - \lambda \ln(p'_p) + \kappa \{\ln(p'_p) - \ln(p')\} \qquad (3.1)$$

then $$(\lambda - \kappa)\ln(p'_p) = N - v - \kappa\ln(p') \qquad (3.2)$$

$$p'_p = \exp \frac{\{N - v - \kappa\ln(p')\}}{(\lambda - \kappa)} \qquad (3.3)$$

For states below the state boundary surface the normalised test data for a drained probe will fall onto a line parallel to the actual test data in q':p' space (p'_p is constant). When the state boundary surface is engaged the normalised stress state will trace out a yield locus on the state boundary surface.

In order to investigate the shape of the state boundary surface for K_o compressed samples tested in extension the following test procedure was used. A sample was initially K_o normally compressed to a point on the state boundary surface. A multi-stage drained extension test was then performed on the sample. The direction of the effective stress paths for the test stages are shown on figure 3.5. The test stages are directed outside the current yield locus but are designed to extend the yield locus by only a small amount. In this way the sample experiences only relatively small plastic strains thereby keeping disturbance of the soil structure to a minimum and only relatively small excess pore pressures are generated while testing. This method of testing is referred to as a Type 1 probing test throughout the dissertation.

The standard method adopted by other investigators of using drained stress path probes directed onto the state boundary surface from an initially overconsolidated sample state is referred to as a Type 2 probing test.

The results of both Type 1 and Type 2 probing tests are discussed in more detail in chapter 8.

3.4 Determination of ν' from K_o Swelling Tests

For a triaxial sample in a K_o normally compressed state the ratio of radial to axial effective stresses is given by

$$K_{nc} = \sigma'_{rm}/\sigma'_{am} \qquad (3.4)$$

If the axial effective stress is decreased to σ'_a and the sample is allowed to K_o swell such that $\delta\epsilon_r=0$ the radial effective stress σ'_r is given by

$$K_o = \sigma'_r/\sigma'_a \qquad (3.5)$$

and for an elastic material

$$\delta\epsilon_r = 0 = [(\sigma'_{rm}-\sigma'_r)(1-\nu')-\nu'(\sigma'_{am}-\sigma'_a)]/E' \qquad (3.6)$$

rearranging (3.6) gives

$$\nu' = \frac{(\sigma'_{rm}-\sigma'_r)}{(\sigma'_{am}-\sigma'_a) + (\sigma'_{rm}-\sigma'_r)} \qquad (3.7)$$

and substituting for σ'_{am}, σ'_a, σ'_{rm} and σ'_r from (3.4) and (3.5) into (3.7) and making use of

$$R_o = \sigma'_{am}/\sigma'_a \qquad (3.8)$$

gives

$$\nu' = \frac{(K_{nc}R_o - K_o)}{(R_o - 1 + K_{nc}R_o - K_o)} \qquad (3.9)$$

Either (3.7) or (3.9) can be used to determine a value for ν' from the results of a K_o swelling stage performed on a K_o normally compressed sample, see section 8.6.3.

Rearranging (3.9) gives

$$K_o = K_{nc}R_o - \frac{\nu'(R_o-1)}{(1-\nu')} \qquad (3.10)$$

Equation (3.10) was proposed by Wroth (1975) to determine the in situ horizontal stresses acting on a lightly overconsolidated soil stratum, see section 9.2.3.

3.5 Normalising Stress-Strain Data

Soil behaviour depends on many factors but principally on the magnitudes of the effective stresses and the specific volume. In order to compare soil test data on a common basis the data should be normalised to common effective stresses and specific volumes. Details of appropriate normalising procedures are given in Atkinson (1984b) and only a brief outline of the procedures relating to stress-strain behaviour are included in this section.

It is shown in Atkinson (1984b) that the incremental stress-strain relationships for the original Cam clay soil model, modified to include elastic shear strains, can be formulated as

$$\delta\epsilon_s = \frac{1}{vp'}\left[\frac{(\lambda-\kappa)}{(M-\eta')M} + \mu'\kappa\right]\delta q' + \frac{(\lambda-\kappa)}{vp'M}\delta p' \qquad (3.11)$$

$$\delta\epsilon_v = \frac{(\lambda-\kappa)}{vp'M}\delta q' + \frac{1}{vp'}\left[\frac{(M-\eta')(\lambda-\kappa)}{M} + \kappa\right]\delta p' \qquad (3.12)$$

where $\mu' = \frac{2(1+\nu')}{9(1+2\nu')}$ and $\eta' = \frac{q'}{p'}$

equations 3.11 and 3.12 can be written as

$$v\delta\epsilon_s = A\frac{\delta q'}{p'} + B\frac{\delta p'}{p'} \qquad (3.13)$$

$$v\delta\epsilon_v = C\frac{\delta q'}{p'} + D\frac{\delta p'}{p'} \qquad (3.14)$$

where the moduli A,B,C and D depend on the (constant) soil parameters λ,κ,M and μ' and on the current stress ratio η'. Therefore the stress-strain behaviour of soil can be normalised by plotting stresses divided by p' and strains multiplied by v. Normalised stress-strain plots are used in section 8.8 to compare the behaviour of the soft alluvial clay stratum at the site with the Cam clay and modified Cam clay soil models.

CHAPTER 4 - SITE INVESTIGATION, DESIGN AND CONSTRUCTION OF THE E.G.A.R. EMBANKMENT

4.1 Introduction

This chapter presents details of the design and construction of the EGAR embankment and summarises the extensive site investigation and laboratory testing programme performed prior to construction. Although the test data presented in this chapter is based on information outlined in various site investigation reports, some further analysis of the pressuremeter, plate dilatometer and triaxial test data has been included. This re-analysis has been carried out in the light of recent improvements in the interpretation of the in situ test data and for comparison of the triaxial test results with the testing carried out during the present research.

The initial site investigation carried out for the LBN by Groundworks Ltd. (1984) revealed that the area is underlain by up to eight metres of made ground and soft alluvium. The dual problems of both stability during construction and long term settlements were envisaged at the design stage. In addition to these potential problems, the proposed route of the approach road to the East London River Crossing (ELRIC) touches on the eastern edge of the EGAR embankment and provision for this had to be considered in the design of the embankment. In order to monitor the performance of the embankment during construction approximately £50,000 worth of geotechnical instruments were installed.

4.2 Site Location and Geology

4.2.1 Site location

The site is situated on the alluvial floodplain on the north bank of the River Thames at Beckton, London E15. The

location of the site is shown on figure 4.1 and a more detailed site layout is shown on figure 4.2. The centre of the site is at approximately National Grid Reference TQ 4385 8265

4.2.2 Site History

This area of London is referred to in verse by Alfred Stokes who in the 1850's describes the area as dead flats, full of water rats, onions, greens, black ditches and foul drains, Soils Engineering Ltd. (1987). In 1868 the Gas, Coke and Light Company purchased the land, which was then known as the East Ham Marshes, to form the site of the Beckton Gas Works.

Over the years of the development of the Gas Works complex, ancillary works were constructed to produce chemicals from the by-products of gas production. The largest of these, the Tar and Ammonia Products Works was erected at the Southern end of the EGAR site, to the south of the NOS. This plant produced tar for road construction, sulphate of ammonia for fertilizers, printing ink, dyes and chemicals for the manufacture of explosives. The Tar and Ammonia Works had been demolished prior to the construction of the EGAR embankment. The site is now covered by between 2 and 4 metres of made ground comprising demolition rubble and fill material which had been placed to form a suitable surface upon which development of the gasworks could take place. This area of the site is generally flat at a height of approximately 3.5 metre above Ordnance Datum.

The area to the north of the NOS remains largely undeveloped and the land is used predominantly for grazing and allotment gardens. Immediately adjacent to the NOS the Thames Water Authority has constructed a sludge lagoon, bounded by an embankment of natural materials from within the site. This facility is intended to impound untreated sewage should the pumps at the local sewage works

breakdown. The area is generally flat at a level of approximately 1.5 metre above Ordnance Datum and parts of the site are inundated by water at times of high rainfall.

4.2.3 Site Geology

A comprehensive site investigation was performed prior to the construction of the embankment. A total of 13 boreholes were drilled to a maximum depth of 20 metres to determine the site geology and to recover soil samples for laboratory testing. In addition to the exploration boreholes a large number of in situ tests were carried out at the site. The positions of the relevant boreholes and in situ tests are shown on figure 4.2. In addition to the site investigation borehole logs, the drillers' logs from the installation of the geotechnical instrumentation have been used to determine appropriate soil sections. Full details of the site investigation are given in Groundworks (1984).

Published geological records of the area indicate that the site is underlain by deposits of Alluvium and Flood Plain Gravels associated with the River Thames, which is approximately one mile to the south of the site. These superficial deposits are underlain by stiff to very stiff fissured London Clay, which was shown in the site investigation to attain a maximum thickness of 7.5 metres. The London Clay is underlain by the Woolwich and Reading Beds. For the purposes of the present investigation, only the superficial surface deposits are considered. The London Clay and lower horizons have little effect on both the ground movements below the embankment and stability considerations during construction. Full details of these lower horizons are given in Husband and Co. (1985).

As discussed in section 4.2.2 the site to the south of the NOS is covered by between 2 and 4 metres of made ground. The made ground is underlain by a variable thickness of soft alluvial organic silty clay with bands of clayey

peat. This stratum typically extends to a total depth of between 7 and 8 metres and is underlain by medium dense to dense sandy gravel.

To the north of the NOS there is no evidence of any previous development and the site is underlain by the alluvial organic silty clay stratum to a depth of between 4 and 5 metres. This is in turn underlain by medium dense to dense sandy gravel.

The ground water table was recorded with piezometers at various locations across the site prior to construction. To the north of the NOS the water table is at a depth of approximately 1.5 metres below ground level. To the south of the NOS the ground water table appears to coincide with the base of the made ground. It is likely that this represents a perched water table, although this was difficult to establish accurately from the available data. The water table did not appear to be affected by tidal fluctuations in the nearby River Thames.

Soil profiles below the embankment, based on an interpretation of the site investigation and extrapolation/interpolation between boreholes, at instrument sections EE and DD (see figure 4.2) are shown on figure 4.3. The various soil horizons are discussed in more detail in the following paragraphs.

Made Ground

The made ground comprises a mix of a wide variety of materials which near ground level include ash, gravel and general demolition rubble. The lower horizons of this made ground are described as containing soft silty clay and it is considered that this material is the result of contamination by the naturally occurring alluvial deposits, Husband and Co. (1985). Most of the made ground is granular and it is assumed that this stratum will behave as a free draining material. The made ground is contaminated by a variety of substances resulting from the

Tar and Ammonia Works. SPT tests performed in this stratum gave values between 2 and 70 and this indicates a very variable state of compaction.

Organic Silty Clay

The organic silty clay stratum was encountered over the whole site, the thickness varying between approximately 4 and 6 metres. The composition is extremely variable, ranging from a firm desiccated silty clay to a soft clayey peat. Very occasional gravel fragments and thin bands of sand were also encountered. The major influence on the engineering behaviour of this stratum is the organic content, which varies between approximately 2 and 40 percent. The more peaty material was recorded in bands up to two metres thick. However the thickness and extent, both vertically and laterally, of these bands is extremely variable and it is impossible accurately to predict reliable soil profiles based on the exploration boreholes. The drillers logs for the installation of geotechnical instrumentation were not recorded in sufficient detail to be of much assistance in this regard.

North of the NOS the organic silty clay horizon occurs at ground level where desiccation has resulted in varying degrees of overconsolidation. The overconsolidated crust extends in places to a depth of up to two metres, below which the clay tends towards a more normally consolidated condition.

To the south of the NOS this overconsolidated crust appears to have reached a fully softened state, probably as a result of a perched water table at the base of the made ground. The clay in this area also appeared to be contaminated by waste products from the Tar and Ammonia Works.

The following description of the organic clay stratum is based on the site investigation borehole logs and a visual inspection of the soil samples recovered for testing at

City University. Where the stratum is encountered at a low organic content it is a brown mottled grey, soft to firm, intact silty CLAY with occasional organic plant remains and very occasional thin bands of sand. Samples with a high organic content are described using the method proposed by Hobbs (1986) as dark brown, slight to moderately decomposed, wet clayey fine to coarse fibrous PEAT with occasional woody fragments, odourless, plastic limit test possible.

The results of both in situ and laboratory tests carried out on samples recovered from this stratum are described in more detail in the sections 4.3 and 4.4.

4.3 In Situ Testing

4.3.1 Pressuremeter Tests

A total of nine self-boring pressuremeter tests at three boreholes were performed at the site by PM Insitu Techniques during July 1984. The position of the various tests are shown on figure 4.2 and full details of the testing can be found in PM Insitu Techniques (1984).

The test results for all 9 tests are summarised on table 4.1. Plots of cavity pressure-cavity strain for the 3 tests at borehole SBP5 and SBP7 are presented on figures 4.4 and 4.5. It should be noted that these stress-strain plots have been generated by the author from a best fit curve constructed through the data points presented in the PM Insitu report. The results presented in the PM Insitu report represent the average values for the three strain arms of the pressuremeter. The stress-strain curves on figures 4.4 and 4.5 were used by the author to derive the in situ shear stress-shear strain curves presented on figures 4.6 and 4.7 for tests performed at borehole 5 and 7 respectively, using the method proposed by Palmer (1972). The stress-strain curves are considered in more

detail in section 9.2.3. The undrained shear strengths measured from these plots are summarised on table 4.1. It should be noted that all the other data in table 4.1 was derived from the original plots of cavity pressure-cavity strain presented in the PM Insitu report.

The undrained shear strength can also be calculated assuming that the soil behaves as an elastic perfectly plastic material using the method proposed by Gibson and Anderson (1961). The undrained shear strength calculated using this approach is also included in table 4.1 and can be seen to agree fairly well with the strength calculated using Palmers' method.

The in situ total lateral stress can be assessed directly from the field stress-strain curves by identifying the pressure at which the membrane first starts to expand, making allowance for a membrane correction. In order to estimate the effective lateral stress the in situ porewater pressure must be measured. There is no record of porewater pressure measurements included in the field data and the in situ pressure has been estimated from piezometer readings recorded at the time of the investigation. However, this estimated value of the porewater pressure could be in error by as much as $\pm$ 10kPa. It is also extremely difficult to estimate the lift off pressure, from the stress-strain curves, to an accuracy better than approximately 10kPa. In soft clay strata at relatively shallow depths the in situ lateral effective stress is likely to be in the range 10kPa to 50kPa and the error of the pressuremeter derived value could thus be large.

4.3.2 Plate Dilatometer Tests

Plate dilatometer testing was also performed at the site by PM Insitu Techniques. The test positions are shown on figure 4.2 and full details of the testing are given in PM Insitu (1984). The dilatometer used and method of

operation was similar to that described by Marchetti (1980). The dilatometer results were used to determine profiles of the in situ stresses for the finite element analyses (see section 9.2.3).

Three parameters, the material index (Id), the horizontal stress index (Kd), and the dilatometer modulus (Ed), can be derived from the results. These parameters are related by empirical correlations to the overconsolidation ratio, coefficient of earth pressure at rest (Ko), undrained shear strength, stiffness, density and soil type.

The correlations given in Marchetti (1980) were used to analyse the data in the PM Insitu report. It should be noted that these correlations are based predominantly on a study of natural Italian clays. Recent work by the Building Research Establishment into the use of the dilatometer at British soft clay sites, Powell and Uglow (1988), has shown that some of the original Marchetti correlations may not be appropriate for U.K. soils. Improved correlations with the overconsolidation ratio and the coefficient of earth pressure at rest for use with the plate dilatometer have been suggested. However, the Marchetti correlation with undrained shear strength was found to be reasonable for young clays, less than 70,000 years old.

The results presented in the PM Insitu report have been re-analysed using the correlations suggested by Powell and Uglow. Figures 4.8, 4.9 and 4.10 show respectively derived values for the undrained shear strength, in situ K_o and the overconsolidation ratio. On each figure two sets of data are presented. The results of 8 tests performed to the south of the NOS and 6 tests performed to the north of the NOS are summarised showing both the average value and the spread of the results with depth. Also included on figures 4.9 and 4.10, for comparison purposes, are the average values for the in situ K_o and overconsolidation ratio calculated using the original Marchetti (1980) correlations.

It can be seen from figure 4.8 that the overconsolidated crust extends to a depth of between 1m and 1.5m below ground level to the north of the NOS, tests DMT6A to E and DMT7A. Figure 4.8 also shows that the undrained shear strength of the alluvial clay horizon to the south of the NOS is approximately 30% greater than the equivalent horizon to the north of the NOS.

The Powell and Uglow (1988) correlation predicts values for the overconsolidation ratio of less than unity, figure 4.10, which is clearly impossible. A site specific correction is therfore used in section 9.2.3 to determine the in situ preconsolidation profile. The in situ K_o value generally lies between 0.6 and 0.8 in the alluvial clay horizon, figure 4.9. Both these sets of results indicate the normally or very lightly overconsolidated condition of the alluvial clay stratum, particularly to the south of the NOS.

4.3.3 In situ Permeability Tests

The results of in situ permeability tests carried out in the organic clay stratum are summarised on table 4.2.

4.3.4 In situ Vane Tests

In situ shear vane testing of the alluvial deposits was performed at the site by Soils Engineering Limited. The results are summarised in figure 4.11. Full details of the in situ vane tests are given in Soils Engineering (1985).

The results show the organic silty clay to have a vane sensitivity, the ratio of the peak to the residual shear strength, in the range 1.5 to 4.6 with an average value of 2.9. The measured shear strength shows no discernable trend with depth. The average peak strength for tests performed to the south of the NOS is 71 kN/m2 and the residual value is 31 kN/m2. The equivalent values for

tests to the north of the NOS are 44 and 16 respectively. These values are significantly higher than those measured in either the triaxial tests or by the pressuremeter and plate dilatometer. The vane test results are probably affected by a combination of the rate of testing, consolidation and the presence of fibrous organic matter. Marsland and Powell (1978) reported that, even after applying the correction factors suggested by Bjerrum (1972), the vane shear test seriously over-estimated the undrained shear strength of the soft Thameside alluvium at Littlewood power station, about 10 miles east of the site.

4.3.5 Standard Penetration Tests

Standard Penetration tests (SPT) were performed in the made ground horizon to the south of the NOS. The results are shown on figure 4.12. The SPT N-values indicate that the made ground has a state of compaction varying from loose to dense. However the results will be affected by the very variable nature of the mixture of materials encountered in this deposit.

4.4 Laboratory Testing at Site investigation Stage

4.4.1 Introduction

Most of the laboratory testing relevant to the soft alluvial strata was performed by Foundation Engineering Limited during the period of September 1984 to January 1985. The test results are given in Foundation Engineering (1985). Further index and consolidation test results are given in Groundworks Ltd. (1984). All soil tests were carried out in accordance with BS1377 (1975). This section summarises the results of the laboratory testing.

4.4.2 Index Test Results

A summary of the index test results determined during the site investigation is given on table 4.3. It can be seen from this table that the Atterberg limits of the organic clay stratum are extremely variable. In addition, the natural water content is reported in a number of cases to be in excess of the liquid limit of the relevant sample.

4.4.3 Oedometer and Rowe Cell Test Results

Seven oedometer consolidation tests were carried out on samples of the peat and organic silty clay. The results are summarised on figure 4.13 in v:ln(p') space. The derived values for the coefficients of compressibility and consolidation are given on table 4.4.

Six 250mm diameter Rowe cell consolidation tests drained radially outwards under plane strain conditions were carried out, using the methods set out by Rowe and Barden (1966). The results are summarised on figure 4.13 in v:ln(p') space. The derived values for the coefficients of compressibility and consolidation are given in table 4.5.

It can be seen from figure 4.13 that the compressibility of undisturbed samples of the organic clay stratum is extremely variable. It is also not possible to discern any trend with either depth or position across the site.

The coefficient of consolidation of the organic clay stratum is also extremely variable. As may be expected the samples show a large decrease in permeability with increasing confining pressure. It would however be difficult to determine a reliable value for the permeability of the soil based on this test data. It has often been observed, for example Smith and Hobbs (1976), Lewis et al. (1975), that laboratory measured values of permeability can badly underestimate the actual field values.

The preconsolidation pressure for the various soil samples has been determined by the author using the Casagrande (1936) construction and the results are summarised on table 4.6. The determination of appropriate preconsolidation pressures is discussed in more detail in section 3.2.

4.4.4 Undrained Unconsolidated Triaxial Compression Tests

Twelve sets of unconsolidated undrained triaxial compression tests were carried out on samples of the organic clay and peat trimmed from U100 tubes. Each set comprised three tests at cell pressures of between 35 and 475 kPa on specimens 76mm long and 38mm diameter. The test results are summarised on figure 4.14.

Although no stress-strain curves were presented in the report, the type of failure for all the tests was described as plastic. The failure strains were in the range four to twenty percent.

4.4.5 Consolidated Undrained Triaxial Tests

Thirteen sets of consolidated undrained triaxial compression tests with pore pressure measurements were performed on undisturbed samples of the organic silty clay and peat. Each set comprised three tests at different effective cell pressures on specimens 76mm long and 38mm in diameter. The tests were strain controlled at a strain rate of approximately 1% per hour. One test in each set was performed after consolidation to the approximate in situ stress state. The stress state at the end of each test, at an axial strain of between 10% and 20%, is summarised on figure 4.15.

Plots of deviator stress versus axial strain were presented in the site investigation report and these show that the samples, including those recompressed to the in

situ stress state, do not exhibit peak deviator strengths at low strains. The average ratio of mean effective stress at the end of consolidation stage to the mean effective stress at critical state was 1.94. The average ratio of the undrained shear strength to the consolidation stress was 0.30. Ultimate effective stress strength parameters of $c'=0$ and $\phi'=29°$ have been determined by the author from these results. The results are considered in more detail in section 8.8.4.

4.4.6 Consolidated Drained Triaxial Tests

Six sets of consolidated drained triaxial compression tests were performed on samples of the organic clay and peat. Each set comprised three tests at different cell pressures on samples 76mm long and 38mm in diameter. The tests were strain controlled at a strain rate of approximately 0.2% per hour. The test results are summarised on figure 4.16. Ultimate effective stress strength parameters of $c'=0$ and $\phi=25°$ have been determined by the author from these results. The results are considered in more detail in section 8.8.4.

4.5 Design and Construction of the EGAR Embankment

The design criteria for the embankment are discussed in detail in Husband and Co. (1985). Stability analyses, based on the results of the undrained triaxial tests, indicated that it would not be possible to build the embankment rapidly to the full height in one lift. It was therefore proposed to construct the embankment in three stages, allowing time between each stage for the foundation materials to consolidate. Monitoring of the development and dissipation of excess pore pressures was proposed to control construction rates. Concern about potentially large secondary consolidation settlements, particularly at the bridge abutments, meant that

surcharging of the embankment would also be desirable if time was available.

Based on estimates of the coefficient of consolidation measured in the various in situ and laboratory tests it was considered necessary to include vertical drainage elements in order to accelerate consolidation times. It was therefore decided to install wick drains below the embankment, extending into the gravel horizon at the base of the soft organic clay.

The value of the horizontal coefficient of consolidation c_h of the organic clay stratum was assumed at the design stage to lie in the range $2m^2$/year to $8m^2$/year. The time t to achieve a degree of consolidation U was calculated from the relationship given by Hansbo et al. (1981)

$$t = \frac{D^2}{8c_h} * \left[\ln \frac{D}{d} - 0.75 \right] * \ln \left[\frac{1}{1-U} \right] \quad (4.1)$$

where D = Diameter of the zone of influence of the drain

d = Equivalent diameter of the vertical drain

The wick drain spacing adopted in the final design is 1.0m in the area of sections AA and BB and 0.5m in the area of sections CC to FF (figure 4.2). Using these spacings 90% consolidation would be expected within one month of construction of Stages 1 and 2 and within two months of the construction of Stage 3 at sections CC to FF. As these times are approximately equivalent to the planned construction periods for the embankment stages, the construction of the embankment was considered to be essentially a drained loading case at the design stage.

The embankment was constructed during the period of October 1986 to June 1987. To the south of the NOS construction proceeded in the three stages as originally planned. However, based on the results of monitoring of the instrument sections to the north of the NOS, the embankment in this area was constructed in a continuous

operation. Details of the geotechnical monitoring and embankment construction rates are given in chapter 5.

The embankment fill material was a sea dredged, fine to medium sand with numerous shell fragments. The engineering properties of this material, measured at City University, are discussed in section 8.9. The average bulk unit weight of the compacted sand, based on a number of in situ measurements, is 17kN/m3.

The embankment sand is underlain by a drainage blanket comprising a free draining, sea dredged, sand and gravel. The drainage blanket varies in thickness from approximately 0.5 to 0.8 metres. The engineering properties of the blanket and fill materials are similar.

4.6 Summary

A road embankment rising to a maximum height of nine metres has been constructed at Beckton in the East end of London. The site investigation revealed that the embankment is underlain by up to eight metres of made ground and soft organic silty clay.

A comprehensive series of both laboratory and in situ tests have shown that the compressibility of the soft organic clay is extremely variable. The organic content and Atterberg limits of clay samples were also extremely variable. The natural water content of some samples are reported to be in excess of their measured liquid limit.

The measured preconsolidation pressures suggest that the organic clay stratum is generally lightly overconsolidated with the overconsolidation ratio in the range one to two. A desiccated crust, up to approximately 1.5m thick, was revealed by the plate dilatometer profiles to the north of the NOS.

The results of the various in situ tests indicate that the organic clay stratum to the south of the NOS has a higher undrained shear strength profile than the equivalent stratum to the north of the NOS. It appears likely therefore that the placement of approximately 3m of made ground to the south of the NOS, many years prior to the construction of the embankment, has brought the organic clay stratum to an almost normally compressed state in this area.

The ultimate or end of test effective strength parameters of the organic clay were measured by both consolidated drained and undrained triaxial compression tests. The effective strength parameters used in the design of the embankment were c'= 10kPa and ϕ'=23. Further analysis by the author of the triaxial test results has determined that the effective strength parameters are c'=0 and ϕ' varying between 25° and 29° for drained and undrained tests respectively. The reasons for this discrepancy between the drained and undrained friction angles is discussed in section 8.8.4.

In order to accelerate consolidation during construction vertical wick drains were installed through the soft alluvial surface deposits. Based on laboratory and in situ measured values of the coefficient of consolidation, approximately 90 percent consolidation of the organic clay stratum was expected during the construction of the embankment. In order to ensure complete primary consolidation and to limit potential secondary consolidation settlements after completion of construction the embankment was surcharged.

CHAPTER 5 INSTRUMENTATION AND MONITORING OF THE EMBANKMENT

5.1 Introduction

Geotechnical instrumentation was installed at six cross sections of the EGAR embankment in order to control the construction of the embankment. The positions of the instrumented cross sections are shown in figure 4.2. The instrumentation included hydraulic piezometers, magnet extensometers and inclinometers. The instrumentation installed at each cross section are shown on figures 5.1 to 5.3.

The instrumentation was installed by Geotechnical Instrumentation Ltd. during the period July to September 1986. Details of the piezometers, extensometers and inclinometers are given in sections 5.2.1 to 5.2.3.

Monitoring of the embankment during construction was performed jointly by the London Borough of Newham and City University. After completion of construction the monitoring was continued by City University in order to establish longer term trends.

The results have been stored and analysed at City University on an IBM PC compatible microcomputer using the VP Planner spreadsheeting software. VP Planner is a joint spreadsheet and database package which has allowed rapid manipulation of data and continuous updating of information. This has enabled movement and pore pressure trends to be readily plotted, aiding planning the monitoring programme. Based on the results of the present investigation this type of software package was highly successful and its use would be advantageous in other similar monitoring projects.

Phase 2 of the EGAR contract, comprising road and bridge works, was awarded to Percy Bilton Construction Ltd. in September 1987. At this time the majority of the extensometers were removed in order to facilitate

construction. Major earthworks, including the construction of haul roads, landscaping and stockpiling of materials in the areas of the instrumentation, rendered some of the later readings of the piezometers and inclinometers unreliable.

5.2 Instrumentation Installation and Monitoring Details

5.2.1 Piezometers

A total of thirty twin tube hydraulic piezometers were installed at the six cross-sections. The piezometers at sections EE and FF were driven approximately 0.3m below the base of individual boreholes and a 0.5m thick bentonite plug placed at the bottom of the borehole. The borehole was then backfilled with a weak cement/bentonite grout to ground level. The piezometers at all the other cross-sections were installed in the middle of a 0.6m long sand pocket, overlain by 0.5m of bentonite pellets and then grouted to ground level. The leads from all ten piezometers at each pair of cross-sections (AA/BB, CC/DD and EE/FF) were connected to a single pressure transducer in a small instrument cabinet positioned close to the relevant instrument lines. The readings were measured with an accuracy of approximately ±2kPa.

During the early stages of the monitoring the piezometers required de-airing almost every other day. This problem was initially thought to be due to methane produced in the organic clay. However pressure testing of the valve boards revealed a number of faulty connections and valves. After these had been replaced de-airing was only required every one or two months.

During the winter months the piezometer cabinets were heated by greenhouse paraffin heaters. On two occasions the heaters failed during particularly cold spells leading to freezing of the water in the piezometer lines. The

pressure transducer was damaged on both occasions and some piezometric data was subsequently lost.

The wick drain pattern was amended in order to avoid damage to the piezometers during the installation of the vertical wick drains. No wick drains were installed within approximately 2 metres of a piezometer (i.e. an effective drain spacing of 4 metres). The drain spacing under the rest of the embankment was between 0.5m and 1.0m. The change of spacing has a large effect on the pore pressure response during consolidation. A first order approximation, based on the method outlined in section 4.5, indicates consolidation rates approximately 20 times slower in the area around a piezometer when compared with the rest of the embankment. Due to a combination of both stress redistribution and vertical drainage this is likely to be an overestimate of the effect. It is however assumed that the measured porewater pressure response represents an upper-bound on the actual average value below the embankment. The measured values represent a conservative estimate for stability calculation purposes but could not be considered as high quality research data.

5.2.2 Inclinometers

A total of thirteen inclinometers were located outside the embankment toe. The inclinometer tubing comprised 53mm internal diameter aluminium tubing with a wall thickness of 2.3mm. The inclinometer tubes were installed in boreholes extending at least four metres into the dense sand and gravel horizon below the soft alluvium. Three of the inclinometers were equipped with spider magnets to act as extensometers. The inclinometer tubes were cut off just above ground level and were fitted with lockable topcaps.

Measurement of the horizontal deflection was made in the usual way by lowering an inclinometer probe to the base of each tube and taking readings at half metre intervals as the probe was pulled towards the top. The probe was then

rotated through 180 degrees and the process repeated to allow for any zero offset effects. The accuracy of this type of measurement is approximately 0.5mm/m length of tube. However the results on site appeared to be repeatable to within ±2mm over the full depth range, between subsequent sets of readings.

Inclinometer 13 on Section EE appeared to have been slightly damaged by construction traffic towards the end of the monitoring period and the readings after July 1987 are not reliable. A number of inclinometer tubes were lost after the phase 2 contract was started due to various construction activities on the site, but only small movements were occurring at this time. No other problems were experienced with the inclinometers.

5.2.3 Extensometers

Nine magnet extensometers were installed at the site. The three extensometers located at the toe of the embankment were constructed around the inclinometer tubing. The six other extensometers, extending through the embankment fill material, were constructed using 20mm internal diameter plastic tubing located in boreholes and extending at least four metres into the dense sand and gravel horizon below the soft alluvium. Spider magnets were located at various levels within the soft alluvium and a number of plate magnets were placed in the fill during construction.

Measurement of the position of the magnets was made in the usual way by lowering a reed switch connected to a tape measure down the tube.

The combined inclinometer/extensometers at the embankment toe gave no problems during the project. The two extensometers at section AA and the extensometer at the centreline of section DD were irreparably damaged during construction of the embankment. The two centreline extensometers were replaced after a short delay and some

settlement data was inevitably lost. On a number of other occasions the extensometers were slightly damaged by construction plant, leading to embankment sand blocking the tubes. The lower 4 magnets of extensometer 29 on Section DD were rendered permanently inaccessible in this way.

All the extensometers within the embankment fill were removed shortly after the start of the phase 2 contract because of construction activities. Only small secondary consolidation settlements were being measured at this point in the project.

5.3 Results of the Monitoring

5.3.1 Introduction

Complete results of the monitoring programme are given in Pickles (1988c). Typical results for the various types of instrumentation are discussed in sections 5.3.2 to 5.3.4. The settlement at the embankment centreline, maximum horizontal movement at the embankment toe and the excess pore pressures recorded at the centrelines of sections AA, DD and EE are summarised on figures 5.4 to 5.6 respectively. In addition, some further settlement and horizontal deformation profiles at the instrumented cross sections are given in chapter 9 where the results are compared with finite element predictions.

5.3.2 Piezometers

In general the piezometers recorded the development of only small excess pore pressures, of the order of 20kPa, during construction of the embankment, see figures 5.4 and 5.5. The only exception to this trend were piezometers 2 and 3 located below the centreline of section EE, figure 5.6. A maximum excess pore pressure of 80kPa was

developed at piezometer 2. As discussed in section 5.2.1 the excess pore pressures recorded at these piezometers are likely to represent an overestimate of the actual average value below the embankment.

5.3.3 Inclinometers

The inclinometer profiles at the end of construction are given in chapter 9. The maximum movements at the embankment toe during construction are shown on figures 5.4 to 5.6 for section AA, DD and EE respectively. These figures reveal that the horizontal movements immediately after construction of the embankment are typically between 40% and 80% of the long term values. The horizontal movements appear to lag behind the vertical movements, see section 5.3.4.

5.3.4 Extensometers

The settlement profiles at the end of construction are given in chapter 9. The settlement at the embankment centreline is shown on figures 5.4 to 5.6 for sections AA, DD and EE respectively. It can be seen on these figures that the centreline settlements immediately after construction of the embankment are typically between 60% and 80% of the long term values.

The strains between the various extensometer magnets for the centreline extensometer at section EE are shown on figure 5.7. It can be seen on this figure that the strains between the magnets located within the organic clay layer are comparable to each other, despite the large range in the compressibilities measured during the initial site investigation. This finding is discussed in more detail in section 8.5.2.

CHAPTER 6 LABORATORY TESTING APPARATUS AND PROCEDURES

6.1 Introduction

This chapter presents details of the laboratory testing apparatus, sample preparation techniques and test procedures. The testing program and test results are given in chapter 7. An analysis of the test data and a discussion of the results are presented in chapter 8.

6.2 Classification Testing

6.2.1 Atterberg Limits

As discussed in section 2.6, the standard method of sample preparation given in BS 1377 is to dry the soil prior to testing. However it is also recommended that "organic soils should be tested at their natural moisture content", i.e. inferring that the soil should not be dried. No guidance is given on the organic content at which this alteration to the sample preparation procedure is important. A number of samples were therefore tested using both sample preparation techniques. In tests where the sample was not dried care was taken to attempt to remove soil particles greater than 0.425mm during mixing in order to obtain consistent results.

Comparison of the effects of using site water rather than distilled water during the mixing operation were made on samples prepared using both of the methods discussed above.

The British Standard recommends that certain soils ,for example soils containing halloysite or gypsum, be dried at not more than 80°C and certain investigators have adopted drying temperatures between 60°C and 80°C to avoid oxidation of peat samples, Skempton and Petley (1970). In order to confirm that the drying temperature has no effect

on the measured Atterberg limits of the clay stratum at the EGAR site a number of tests were performed on samples prepared at their natural moisture content and then dried at oven temperatures of either 70°C or 105°C.

6.2.2 Organic Content

The organic contents of a number of the samples were measured using the dichromate method, Test 8 of BS 1377 (1975). As part of this test the volume of ferrous sulphate required to change the colour of a solution, containing the oxidised organic material, from blue to green is measured. The results of the test are valid if this volume falls within the range 5 to 8 ml. The volume required depends on the organic content of the soil and the mass of soil used in the test. It was found to be very difficult to judge the mass of soil required to obtain a successful test result without prior knowledge of the organic content, Pickles and Horrocks (1988). The accuracy of the test appeared questionable when checked by testing soils with known organic contents.

In addition to the above, the colour change noted in BS 1377 for the sodium diphenylaminesulphonate indicator is incorrect. BDH Limited (1988), the manufacturers of the chemicals used in the City University tests, say that the correct colour change should be specified as red/violet to green for this indicator.

Where the organic content of a sample was greater than approximately 20 percent the loss on ignition method presented by Skempton and Petley (1970) was used. After drying at 105°C, the sample was placed in a furnace set at 550°C and left for 3 hours. No problems were encountered using this method.

6.2.3 Grading and Specific Gravity

The grading of the organic clay samples was determined using Test 7(A) and 7(C) of BS 1377 (1975). The grading of the embankment sand was determined using Test 7(B) of BS 1377 (1975). The specific gravity of all samples was determined using Test 6 of BS 1377 (1975).

6.3 Variation of Organic Content Tests

6.3.1 Introduction

A series of tests on samples reconstituted at known organic contents were performed. The Atterberg limits, specific gravity and compression characteristics of samples with organic contents in the range 2 to 10 percent were tested. The testing is described in detail in Pickles and Horrocks (1988). The test procedures are summarised in the following sections.

6.3.2 Sample Preparation

The samples were prepared by mixing known quantities of material from two batches of the organic clay. The first batch comprised a mix of clay samples with a low organic content, typically less than 3%, taken from various parts of the site. The second batch comprised a mix of peaty clay samples with organic contents greater than approximately 30%.

After thorough mixing, the moisture content and organic content of each batch was determined using the methods set out in section 6.2.2. The determinations were carried out a number of times in order to check the repeatability of the results. Mixes of known quantities of each batch were then used to create samples with known organic contents and these mixed samples were used for all subsequent

testing. Care was taken at all times to prevent the samples drying out. However, a quantity of the samples created with 2% and 10% organic content were taken and dried in an oven set at 105°C and these samples were used to examine the effect of drying on the Atterberg limits and on the isotropic compression characteristics of the clay.

6.3.3 Index Tests

The Atterberg limits and specific gravities of the samples were determined using the methods set out in section 6.2.1. The Atterberg limits were determined without drying except for the two samples detailed above. Site ground water was used in the determination of the liquid limit. The organic content of each sample was determined using the methods set out in section 6.2.2, but it is thought that the organic contents calculated from the mix proportions are more representative of the actual values.

6.3.4 Isotropic Compression Testing

Samples for compression testing were prepared in 38mm diameter floating ring oedometers using the method set out in section 6.5.3. The final sample length was typically between 76mm and 80mm. The samples were extruded directly onto the base platen of a standard triaxial cell and set up with filter side drains, top platen and a single membrane. Drainage was only possible through a porous stone at the base of the sample. The volume change was measured using an Imperial College type volume gauge of 50ml capacity. The cell and porewater pressures were monitored using Druck type PDCR 10-15 bar pressure transducers. Full details of the volume gauge and pressure transducers are given by Clinton (1987).

The samples were initially compressed isotropically to an effective stress of 100kPa using a back pressure of 100kPa

and this stress was maintained for 24 hours. After this time the volumetric strain rate was less than 0.01% per hour which was considered to be sufficiently slow to allow the assumption of 100% consolidation to be made. The effective stress was then increased in single step isotropic stress increments of 100kPa to a maximum effective stress of between 400kPa and 500kPa. Each stress increment was maintained for 24 hours. The volume change after 24 hours was noted. At the end of a test the drainage valve was closed and after reducing the cell pressure, the sample was quickly removed from the cell and weighed. The moisture content of the whole sample was determined.

6.4 Stress Path Testing System

6.4.1 Introduction

Stress path tests were performed on 38mm diameter specimens cut from 100mm diameter piston samples and on 38mm diameter reconstituted samples and 100mm diameter piston samples. The 38mm testing was performed in hydraulic triaxial cells, similar to those described by Bishop and Wesley (1975). The stresses and/or strains imposed on the sample were controlled by microcomputer systems which also logged the test data. Two distinct control systems were used. The first, known as the SPECTRA system, is described in detail by Atkinson et al. (1985). This system is capable of controlling up to six triaxial cells at one time. The second, known as the BBC system, is described in detail by Clinton (1987) and has one BBC microcomputer dedicated to each triaxial cell.

The 100mm diameter sample testing was performed in large triaxial cells described by Clinton (1987). The principle of the cell operation is based on the hydraulic loading principle, Atkinson (1973), and is similar to that of the Bishop and Wesley (1975) cell, but is capable of testing

samples up to 100mm in diameter. The system is controlled by a BBC microcomputer in exactly the same manner as the single cells for testing 38mm diameter samples.

The control and logging program used on the SPECTRA system is described in detail by Richardson (1988). The control and logging program, TRILOG3, used on the BBC cells was developed during the present research and full details are given in Pickles (1988b). Section 6.4.2 briefly describes the stress path cells and section 6.4.3 the TRILOG3 computer program used on the BBC cells. The major differences between the BBC system and the SPECTRA system are described.

6.4.2 The Triaxial Cell

The triaxial cell with the recording and control system in use on the BBC cells is illustrated in figure 6.1. Full details of the operation and specifications for the various stress and strain transducers, including typical calibration curves are given in Clinton (1987).

The overall accuracy obtained for the pressure transducers, load cells, axial strain and volumetric strain gauges are summarised on tables 6.1 and 6.2, for the 38mm and the 100mm stress path cells respectively. The various sources of inaccuracy include hysteresis, drift and noise. Where applicable hysteresis in the volume gauge was avoided by manually changing the direction of travel of the piston in the volume gauge between test stages. This was achieved by either pumping in or bleeding out a small quantity of water from the gauge and rezeroing the strains.

The axial load is applied hydraulically through the axial ram. This arrangement allows stress controlled axial loading tests to be performed. However by turning valve A shown on figure 6.1 the axial ram pressure chamber is connected to a Bishop ram. The Bishop ram is turned by a

stepper motor operating through a gearbox. Turning the Bishop ram at a constant speed allows strain controlled axial loading to be performed.

The radial strain is controlled indirectly by varying the cell pressure. The radial strain is calculated from a combination of both the axial and volumetric strains. Radial strain belts have been used at City University, although Loxham (1988) has shown that they do not significantly influence the results obtained from the testing. Radial strain belts were not used during the present investigation.

The only major difference between the BBC and the SPECTRA triaxial cells is in the operation of the pressure manostats and the Bishop ram. In the BBC system the manostats and Bishop ram are operated through incremental stepper motors whereas in the SPECTRA system they are operated by conventional electric motors which are either switched on or off in the appropriate direction.

6.4.3 The Control and Logging Program

The stresses and strains in each of the individually operated triaxial cell are controlled by a BBC microcomputer using the TRILOG3 logging and control program. The microcomputer operates the stepper motors through an interface unit and relay box. Full details of this system are given by Clinton (1987). Full details of the TRILOG3 program are given in Pickles (1988b) and only a brief summary is presented in this section.

The main control loop for the TRILOG3 program is presented in figure 6.2. The computer continually passes through this control loop scanning the output from the five stress and strain transducers and calculating the current values of the stresses and strains. The appropriate stress or strain path to be followed by the sample can be input at the computer terminal. At preset intervals the computer

controls this stress or strain path by operating the appropriate stepper motors. At predetermined intervals a record of the current stresses and strains is taken. At any stage in a test the stress path direction can be altered or the test changed between stress and strain control.

The minimum stress control increment for the cell and pore pressures is 0.4kPa and for the axial stress is approximately 1kPa. The accuracy of the strain control is limited by the resolution of the strain measurements made by the interface unit. Typically the strains can be controlled to the nearest 0.02%.

The program makes an area correction for changes in axial and volumetric strain when calculating the axial stress. No correction is included in the program for either load cell or volume gauge compliance. These corrections are discussed in section 7.4.2.

The major differences between the BBC and the SPECTRA system are listed below:-

- The resolution of the SPECTRA interface is approximately ten times greater than the Spectra Micro-ms used in the BBC system.

- The SPECTRA system cannot follow predetermined stress paths when under strain control, except for conventional drained axial compression or extension tests.

All the triaxial stress path cells used during the investigation were calibrated regularly. Full details of the calibration procedures are given in Lau (1988).

6.5 Sample Preparation, Preliminary and Final Test Procedures

6.5.1 100mm Diameter Piston Samples

All 100mm samples were prepared from 100mm diameter piston samples taken during the installation of geotechnical instrumentation. Samples for testing in the 100mm diameter triaxial cells were extruded directly from the piston tube and trimmed to a length of approximately 200mm on a sample cradle using a thin wire saw and a rigid metal straight edge. Particular attention was paid to ensuring that the top and bottom faces of the sample were perpendicular to the axis of the sample. As discussed in chapter 3, many of the samples had a significant organic content. While trimming the ends of these samples small fragments of the peaty organic material could easily be torn out of the soil matrix. Any small holes remaining in the sample were filled with remoulded clay material taken from the sample trimmings. An initial estimate of the soil moisture content was also made using the soil trimmings.

After weighing, a sample, with pre-soaked filter paper discs at either end, was set up on the base pedestal of the triaxial cell. Filter side drains (Wykeham Farrance type WF11045) were wrapped around the sample ensuring a good connection with the porous stone at the base of the sample. A single 0.32mm thick rubber membrane, which had been pre-soaked in ground water, was placed over the sample. The membrane was clamped to the base pedestal and top cap, which had previously both been lightly coated with silicon vacuum grease, with 2 O-rings at either end.

The 100mm diameter triaxial cells require the top cap to be rigidly connected to the load cell prior to fixing the cell body. The cell and axial pressure were then raised at the same rate until the measured pore pressure was approximately 100kPa. The drainage leads and porous stone were then flushed with de-aired water and the sample was left for 24 hours with the drainage tap closed.

To ensure that the sample was saturated before testing Skempton's pore pressure parameter "B" was measured, Skempton (1957). The all round stress on the sample was raised by 50kPa and the pore pressure response measured. Provided the "B" value was greater than 0.97 the saturation was considered acceptable and the triaxial testing commenced. In a few cases it was necessary to raise the pore pressure to 200kPa and to leave the sample for a further 24 hours in order to achieve the required pore pressure response.

At the end of a test the sample was removed from the cell and its dimensions and weight measured. The sample was then cut horizontally into three approximately equal parts and the moisture content of the top, middle and bottom sections determined. The zero readings of the axial stress, cell pressure and pore pressure transducers were then checked.

6.5.2 38mm Diameter Undisturbed Samples

The standard method adopted for preparing 38mm diameter undisturbed samples was to extrude a 100mm diameter piston sample directly into a 38mm internal diameter thin walled brass tube (0.8mm wall thickness). The brass tube was clamped rigidly above the piston sample, coaxial with its' centreline. The front edge of the tube was pushed approximately 10mm into the piston tube and then the soil was extruded from the piston tube into the brass tube. Care was taken to remove excess soil from around the outside of the brass tube in order to minimise drag on the sample. The soil sample was then immediately extruded from the brass tube and trimmed to a length of 76mm on a sample cradle.

The area ratio of the brass tube is 8% which is approximately equivalent to a standard 100mm piston sample with a wall thickness of 2mm. The brass tubes were lightly

coated with a silicone oil prior to use and the condition and sharpness of the leading edge checked.

After weighing and measuring, the sample, with pre-soaked filter paper discs on the top and bottom, was set up on a porous stone on the base pedestal of a triaxial cell. A filter side drain (Wykeham Farrance type WF10670) was wrapped around the sample ensuring a good connection with the porous stone. If an extension test was to be performed on the sample the side drain was prepared by making a number of cuts in each column of the drain, approximately two thirds of the way across the column, figure 6.3. The cuts were made at a spacing of approximately 3mm, staggered on either side of the column such that alternate cuts overlap each other. In this way the filter is easily extended while maintaining hydraulic conductivity. This type of drain was both quick and easy to prepare and no problems were encountered placing the drains on the sample.

A 0.28mm thick rubber membrane which had been pre-soaked in site ground water was placed over the sample. The membrane was fixed to the top and bottom platens, which had been lightly greased, with two O-rings at either end.

The connection between the top cap and the load cell can be made at any time after the cell body has been positioned. In general the saturation procedures detailed in section 6.5.1 were completed before connection of the top cap. The top cap has a conical rubber seal which is designed to mate with a short truncated cone fixed to the load cell, figure 6.4. Details of the procedure followed to connect the top cap are given in Lau (1988).

After a test had been completed the sample was removed from the cell and its' dimensions and weight measured. The complete sample was then placed in an oven to determine its' moisture content. Finally readings of the axial stress, pore pressure and cell pressure transducers were

checked to ensure that there had been no drift on the transducers during the test.

6.5.3 38mm Diameter Reconstituted Organic Clay Samples

A single large batch of the organic clay was prepared for making mixed samples. The batch was mixed from a number of samples from both the U100 and piston tubes taken at various locations over the site. The soil was mixed by hand and any large organic peat fragments or gravel sized soil particles discovered were removed. A small quantity of site ground water was added to the batch to ensure that the soil did not dry out during the mixing process. The main batch was split into two halves for ease of storage.

The various samples used are listed in table 6.3 and the index properties of the batch are presented on table 6.4. The remixed samples made from the two halves are designated either MIXn or BOXn, where n is the sample number. The MIX samples were used in the earlier tests but it should be noted that there is no intrinsic difference between the two sets of samples.

The initial Atterberg limit and compression tests on samples with different organic contents had demonstrated the significant effect that drying has on the engineering properties of the organic clay. Care was therefore taken to avoid allowing the mixed sample to lose moisture.

Triaxial test specimens of the mixed sample were prepared in a perspex 38mm floating oedometer tube. This comprises a 38mm internal diameter, thick walled, perspex tube equipped with two close fitting hollow pistons with porous stones on their internal faces. A small quantity of the bulk mixed sample was thoroughly mixed with site water to its' liquid limit moisture content. The consistency of the sample was checked using the standard drop cone liquid limit apparatus. Starting with one piston close to the top of a tube the mix was slowly "squeezed" into the tube

using sweeping strokes of a palette knife across the top of the tube. A light finger pressure was placed on the base of the piston to slow the progress of the soil being squeezed into the tube. In this way it was possible to create a reconstituted soil sample with few or no air bubbles trapped inside.

After insertion of the top piston the samples were consolidated by applying weights to a hanger arrangement suspended from the top cap seated on the sample. Drainage from the sample can only take place axially, ensuring that the sample consolidates uniformly across any radial section. The final weight on the hangers varied between 4kg and 8kg depending on the test to be performed on the sample. The final weight was left on the sample for at least four days prior to testing, to ensure complete dissipation of excess pore pressures. A height of approximately 95mm of the soil at its' liquid limit was required to create a sample with a final length of 76mm.

The samples were extruded directly onto the base pedestal of the triaxial cell after having been measured and weighed. The setting up procedure then followed exactly the same routine as for 38mm diameter specimens trimmed from the piston samples. As confirmation of the success of this method of preparation it should be noted that it was possible to attain a "B" value of at least 0.97 for all samples, immediately after setting up in the triaxial cell.

At the end of a test the moisture content of the whole sample was determined using the procedure set out in section 6.5.2.

6.5.4 Kaolin Samples

A limited number of tests on 38mm diameter kaolin samples were performed to study the shape of the state boundary surface for K_o compressed samples and to assess the effect

of the strength of the filter paper side drains. The samples were prepared in a floating oedometer from a slurry mixed at a water content of approximately 1.5 times the liquid limit of kaolin. Full details of the sample preparation technique are given in Ho (1988). The sample was set up in the triaxial cell in the manner detailed in section 6.5.3.

6.5.5 Embankment Sand Samples

Two triaxial tests were performed on the embankment sand fill. Although the grading of the sand indicates that particles up to a maximum size of 20mm are present within this material, 85% of the matrix of the embankment fill has a particle size smaller than 2mm (see figure 7.1 for a grading curve). The triaxial tests were performed on 38mm diameter samples of material passing the 2mm sieve.

A vacuum sample former was set up on the base pedestal of the triaxial cell with a 0.28mm thick rubber membrane almost full of de-aired water. A known mass of the dry sand was covered with water and de-aired. The saturated sand was then carefully spooned into the sample former. Loose samples were formed by pluviating the sand through the water whilst attempting not to disturb the sample former. Dense samples were formed by tamping the sand with a short metal rod, in layers not exceeding 5mm. After placing the top cap the sample dimensions were measured whilst maintaining a small suction on the porewater. The cell body was then positioned and the cell pressure raised until a pore pressure of 100kPa was indicated. The saturation of the sample was checked using the method described in section 6.5.1. A "B" value of greater than 0.97 was always obtained using this method.

At the end of a test the moisture content of the bulk of the sand sample was determined. Any sand remaining on the membrane, top cap and filter stone was carefully washed

into a weighing tin in order to check on the mass of the sand sample.

6.6 Test Procedures

6.6.1 Compression and Swelling Stages

All compression stages were performed using a constant rate of loading rather than incremental step loading. In determining the rate of loading the methods proposed by Atkinson (1984a) were used as a guideline. Using this approach a loading rate is calculated to keep the average undissipated excess pore water pressure less than a predetermined value.

In the 38mm diameter cells a loading rate of 3kPa per hour was used for isotropic compression and swelling. For the 100mm samples the equivalent rate was 1kPa per hour. In one-dimensional compression tests the axial stress was increased at 3kPa per hour for 38mm diameter samples and 1kPa per hour for 100mm diameter samples. The average undissipated excess pore water pressure was calculated to be less than 10kPa during compression stages using these rates. The methods described in section 3.2 are used to plot the actual compression and swelling lines.

An estimate of the excess pore pressure generated during loading can be checked by stopping a test part way through, closing the drainage valve and observing the pore pressure response of the sample. For the 38mm samples an excess pore pressure of between 4kPa and 8kPa was noted and for the 100mm samples the equivalent pressure was between 10kPa and 15kPa. These values agreed reasonably well with the values predicted from measurements of the coefficient of consolidation. The measured excess pore pressure using this method is likely to be an overestimate of the actual value as a result of secondary consolidation effects. If a small amount of secondary consolidation

occurs the sample will want to compress, but with the drainage tap closed the volume cannot change and the effective stress must decrease to compensate for this effect.

At the end of a compression or swelling stage, in order to ensure that the excess pore pressures had dissipated, the final stresses were held on the sample until the rate of volume change was less than 0.005% per hour. This rate was generally achieved after one or two days. However for the more organic samples the effects of secondary consolidation are significant and much longer time periods are required before the rate of volume change has dropped to 0.005% per hour. The volume change at constant stress forms the basis of the Lambda construction to determine the SBS yield stress, described in section 3.2.

One-dimensional compression was performed by controlling the radial stress to maintain zero radial strain. The radial strain was calculated from the measured axial and volumetric strains, assuming that the sample deforms as a right cylinder. Only small variations in the radial stress were required in order to control the radial strain to within 0.02%. One-dimensional swelling was performed in a similar manner.

Compression and swelling of the kaolin samples was carried out at a rate of 10kPa per hour. Compression and swelling of the embankment sand samples was carried out at a rate of 25kPa per hour although much faster rates could have been used.

6.6.2 Shearing Stages

The majority of the shearing tests were performed in at least two stages. During the initial part of a test (at low stress ratios) the stress-strain response of the soil was relatively stiff and a stress controlled stage was used to control the rate of loading. On the approach to

failure the test was strain controlled in order to maintain control of the sample deformations. The loading rates were determined as reported above (6.6.1) and depended on whether the test was drained or undrained and if drained, on the stress path direction.

For drained tests directed onto the state boundary surface, the rate of volumetric strain is a function of the rate at which the yield locus is being extended. This in turn is proportional to the magnitude of the undissipated pore pressure and as such has a significant effect on the choice of loading rate. The testing rate adopted for a particular test was determined by the requirement that the excess pore pressure should not exceed 5kPa.

For standard drained compression or extension tests the axial stress was changed at a rate of 3kPa per hour. The test was switched to strain control when the strain rate approached 0.2% per hour. The test was then continued at this rate to the limit of the axial ram travel, which was generally approximately 20% axial strain.

For constant p' stress paths the deviator stress was increased at a rate of 4kPa per hour. The test was changed to strain control as detailed above.

For tests performed at a constant deviator stress the loading rate was maintained at 3kPa per hour.

The loading rate for undrained tests can be considerably faster than for drained tests. As a result of the constraining effects of the platens on the sample, the pore pressure regime throughout the sample is not uniform. The loading rate adopted should make allowance for equalisation of this pore pressure. A maximum loading rate of 15kPa per hour was used for undrained tests. The tests were changed to stress control as the strain rate approached 0.2% per hour. The strain rate was then held constant at this value until the limit of the travel of

the axial ram was reached at approximately 20% axial strain.

The strain rates discussed above were also used for the tests on kaolin. It should be noted however that because of the higher permeability of kaolin, faster testing rates could have been adopted.

As discussed above the strain controlled shearing stages were continued to an axial strain in excess of 20%. This is particularly important when performing drained compression tests and is discussed in more detail in section 8.8.4. However in extension tests necking of the sample was observed at strains of the order of 10 to 15%.

CHAPTER 7 LABORATORY TESTING PROGRAM AND RESULTS

7.1 Introduction

This chapter presents the results of the laboratory testing performed at City University. Details of the testing program and the procedures adopted to correct the raw triaxial test data are also described. Analysis of the test data and discussion of the results are given in chapter 8. All the soil samples tested at City University were recovered from the instrumentation boreholes.

7.2 Classification Tests

7.2.1 Atterberg Limit - Variation with Test Procedure

The results of a pilot series of plastic limit tests, test 3 of BS 1377 (1975), and liquid limit drop cone tests, test 2(A) of BS 1377 (1975) confirmed the apparently unpredictable variability reported in the original site investigation reports. A program of further tests was designed to assess the following factors

- sample preparation procedure for the liquid limit test, i.e. dried or at natural moisture content

- the use of distilled water rather than the in situ soil water during sample preparation for the liquid limit test

- Oven drying temperature for moisture content determination

Details of the test procedures are given in section 6.2.1. The results of this series of tests are summarised on tables 7.1 to 7.3.

7.2.2 Atterberg Limit - Variation with Organic Content

It can be seen on table 7.1 that the Atterberg limits are extremely variable and the values appear to be a function of the organic content. A second series of tests was performed to look at the effect of different organic contents on the measured Atterberg limits. The sample preparation and testing procedures are detailed in section 6.3. All the samples except two were reconstituted without drying. The results of this series of tests are given in table 7.4.

As discussed in section 6.2.2 the organic contents presented in table 7.4 have been determined from the mix proportions. It is thought that these are more representative than the values determined by Test 8 of BS1377 (1975).

7.2.3 Grading Analyses

The results of grading analyses performed on samples of the organic clay and on a sample of the embankment fill are presented on figure 7.1.

7.2.4 Specific Gravity Determinations

The results of specific gravity determinations on samples of the organic clay are presented on table 7.5. Also included on this table are the results of tests performed on the samples with known organic contents and on a sample of the embankment fill. These values are required when calculating specific volumes.

7.3 Isotropic Compression Tests at Varying Organic Contents

The organic content of the alluvial clay is extremely variable. In order to study the effect of this variation on the compression characteristics of this material a series of tests was performed on samples of the alluvial clay, reconstituted at different known organic contents. The samples were prepared and tested using the methods set out in section 6.3. In general the samples were reconstituted without drying, although two of the samples, one at 2% and one at 10% organic content, were dried prior to testing. The positions of the isotropic normal compression lines in v:ln p' space are plotted in figure 7.2 and the critical state parameters derived from the results are summarised in table 7.6.

7.4 Analysis of Triaxial Stress Path Tests

7.4.1 Correction of Raw Test Data Prior to Analysis

The specific volume of the sample at the end of a test was calculated from the final moisture content of the whole sample.

The raw test data comprises records of the axial stress, radial stress and pore pressure, the axial and volumetric strain and the time at which each record was taken. The data is stored on a floppy disc at the end of each test stage. As discussed in section 6.4 two separate computer systems were used to record the data. Procedures were developed during this research to transfer data from both the BBC and Epson microcomputers onto an IBM compatible PC. Full details of these procedures are given in Pickles (1988a). Once the data had been transferred to the IBM compatible PC it was analysed using the VP Planner spreadsheeting software.

Prior to performing any analyses on the test data, corrections must be made to allow for the effects of both load cell and volume gauge compliance and for the stiffness of the membrane and filter paper side drain. Details of the various corrections are given in sections 7.4.2 and 7.4.3. All versions of the triaxial logging programs used during the present investigation make an area correction, based on the axial and volumetric strains, when calculating the axial stress. No further area correction is therefore required.

The corrected results, referred to as the basic test data, are used for all subsequent analyses. All strains presented in the thesis are natural strains.

7.4.2 Load Cell and Volume Gauge Compliance

The SPECTRA control program incorporates a linear correction factor for load cell compliance. However at small deviator stresses the load cell compliance is non-linear and, when using an Imperial College type load cell, there is a step change of approximately 0.2mm as the deviator stress changes from compression to extension. The Surrey University load cells, although stiffer, also exhibit a non-linear response at small deviator stresses. No allowance is made in the BBC control program for load cell compliance. In addition to the load cell deflection the triaxial apparatus itself is not completely rigid and allowance must be made for both load cell and apparatus compliance when calculating the axial strain.

A number of tests were therefore performed, using dummy steel samples, to measure the system compliance of each set of triaxial apparatus to axial loading. The axial strain measured in the triaxial tests on soil samples were then corrected using the results of the tests with dummy samples for the appropriate triaxial cell and stress path.

No allowance is made for volume gauge compliance in the BBC control program. However all the tests were performed maintaining a constant back pressure in the volume gauge and as such no correction is required.

7.4.3 Membrane and Filter Paper Side Drain Stiffness

Filter paper side drains were used in the triaxial tests both to minimise the excess pore pressures generated during drained compression and shearing stages and to aid the equalisation of pore pressures throughout a sample during undrained shearing tests. When testing soft soils the strength of the filter paper side drain can have a significant effect on the measured deviator stress.

A number of investigators have studied the effects of membrane and side drain stiffness on the results of triaxial tests and a summary of this work can be found in Richardson (1986). The corrections most often applied are those given by Bishop and Henkel (1962). They recommend that a reduction of 14kPa should be applied to the deviator stress at peak strength for a sample tested with both a membrane and a side filter drain. The equivalent correction for a membrane alone is approximately 3kPa. These results are appropriate for 38mm diameter samples.

It should be noted however that the correction is both stress path and strain dependant. The maximum correction for the filter paper stiffness was found by Duncan and Seed (1967) to be reached at approximately 3% accumulated axial strain. The equivalent strain for the membrane is approximately 15%, Richardson (1986).

The corrections required for the membrane stiffness arise from both the axial and hoop strains which occur in the membrane. Richardson (1986) has shown that the correction to both radial and axial stresses is typically less than 3kPa. The corrections are also dependent on the

accumulated strains in the membrane and on the setting up procedure.

In order to determine appropriate corrections for use in the present investigation, 4 tests were performed using 38mm diameter reconstituted kaolin samples. Two of the tests were equipped with side drains and two without side drains. All four samples were tested in undrained compression at an axial strain rate of 0.5% per hour. Plots of deviator stress v natural shear strain for the four tests are given on figure 7.3. All the samples had experienced at least 6% axial strain during the consolidation stage, prior to testing in undrained compression. Kaolin samples were used for this series of tests because the relatively high permeability of this material would ensure good equalisation of pore pressures during the undrained shearing stages.

At axial strains greater than approximately 3% the difference between the results of tests with and without side drains is fairly constant and lies in the range 9kPa to 12kPa. At strains of less than approximately 3% the two tests with side drains exhibited peak strengths up to 16kPa greater than the tests without side drains. As noted above the samples had experienced at least 6% axial strain prior to testing. This effect is possibly due to non-equalisation of pore pressures in the samples without side drains, during the early stages of the strain controlled testing.

Based on these test results and the work of Richardson (1986), Bishop and Henkel (1962) and Duncan and Seed (1967), the following procedures were adopted for correction of the triaxial test data.

. For accumulated compressive axial strains of up to 3% a reduction of 4kPa/% axial strain for 38mm diameter samples and 1.3kPa/% axial strain for 100mm diameter was applied to the axial stress.

- For accumulated compressive axial strains of greater than 3% a reduction of 12kPa and 4kPa was applied to the axial stress calculated for 38mm and 100mm diameter samples respectively.
- No correction was applied to allow for membrane stiffness.
- No correction was applied to the axial stress for samples tested in extension. For all samples which were tested in extension the accumulated axial strain during the compression stage prior to shearing was greater than the axial strain during the extension shearing stage. It should also be noted that, as discussed in section 6.5, a modified side drain was used for all extension tests.

7.5 Stress Path Tests on Piston Samples

7.5.1 Introduction

Triaxial stress path tests on piston samples of the organic clay stratum were performed to confirm the results of the original site investigation and for comparison with the tests on reconstituted samples of the organic clay. The test results are presented in sections 7.5.2 and 7.5.3. The results of the compression and swelling stages and the shearing stages are discussed in section 8.5.2. and 8.5.3 respectively.

7.5.2 Compression and Swelling Stages

A number of tests were performed on piston samples of the organic clay stratum to measure the compression and swelling characteristics of this material. In situ permeability tests and Rowe cell tests, Rowe (1966), on 200mm diameter piston samples, had been performed as part of the initial site investigation. No further attempt was made to determine the permeability characteristics of the

soil. The testing program was designed to confirm the variability of the stiffness of this material and to derive further data on the preconsolidation pressure of this stratum. Both 100mm and 38mm diameter samples were tested. Sample preparation and testing procedures are outlined in sections 6.5 and 6.6.

The test details are summarised on table 7.7 and the test results are summarised on table 7.8. Plots of v:ln(p') for the various tests are presented in figure 7.4. The preconsolidation pressure for each sample, determined using the Lambda construction, proposed in section 3.2, is given in table 7.8.

Three samples (U063, U161 and U171) were compressed to a normally consolidated state, swollen back to an OCR of approximately 3 and then recompressed beyond the previous preconsolidation stresses. These tests were used to confirm the applicability of the Lambda construction, discussed in section 3.2.

7.5.3 Shearing Stages

A limited number of tests were carried out to study the behaviour of the piston samples when sheared. The shearing stages performed on these samples are summarised on table 7.9 and the test results are summarised on table 7.10. The basic test data for each of the tests are presented on figure 7.5.

7.6 Stress Path Tests on Reconstituted Samples

7.6.1 Introduction

Triaxial stress path testing was performed on reconstituted samples of the organic clay to determine a unified set of critical state parameters for use in the

finite element analyses. In addition the test results were required to investigate the applicability of critical state concepts for this material and to study the stress-strain behaviour of K_o compressed samples.

7.6.2 Compression and Swelling Stages

The sample states at the end of the compression and swelling stages are summarised on table 7.11. The compression test data for the isotropically compressed samples are plotted in v:ln(p') space on figure 7.6 and for the K_o compressed samples on figure 7.7.

Tests MIX1 and MIX13 were compressed, allowed to swell and then recompressed along the same stress path. Test MIX1 followed K_o stress paths and test MIX13 followed isotropic stress paths. These tests were performed to calibrate the Lambda construction, proposed in section 3.2, for use with the reconstituted organic clay samples. The test results are presented in v:ln(p') space in figure 7.8. The state of the samples at the end of each compression and swelling stage are summarised in table 7.11.

7.6.3 Shearing Stages

Details of the various shearing stages carried out on the samples are summarised on table 7.12. The sample state at the end of each shearing stage is also presented on this table. The basic test data for the shearing stages are presented on figure 7.9. The ultimate state of the samples at the end of the shearing stages are plotted in v:ln(p') space on figure 7.10. Only those shearing stages where the ultimate shear strain is greater 10% are included on this diagram.

7.6.4 Stages Probing the State Boundary Surface

A number of tests were performed to determine the shape of the state boundary surface for K_o compressed samples. As discussed in section 3.3 there are two methods available for probing the state boundary surface. In the first method the sample is K_o normally compressed and then a series of stress path test stages, similar to the stress path shown on figure 3.4, are carried out from this state, which traverse the state boundary surface. The test results are then normalised to give an elastic wall section through the state boundary surface. Tests BOX5 and BOX6, reconstituted organic clay samples, and test KKE1, a reconstituted kaolin sample, followed this type of test procedure referred to as a type 1 probing test. The basic test data for these tests are presented on figure 7.11. The state of the samples at the end of each test stage are summarised in table 7.12.

In the second method the sample is K_o normally compressed and then allowed to swell back to an overconsolidated state within the state boundary surface. The sample is then compressed along a second stress path which is directed onto the state boundary surface. The point at which the state boundary surface is engaged is then determined from the test results. Tests BOX4, BOX8 and BOX9 followed this type of test procedure referred to as a type 2 probing test. The test results for the second compression stage of each test are presented in figure 7.12. The state of the samples at the end of each test stage are summarised on table 7.11.

7.6 Stress Path Tests on the Embankment Fill Material

Preliminary finite element analyses of the embankment construction (see section 9.2.2) had shown the predicted ground deformations to be relatively insensitive to the

stiffness and strength parameters chosen for the embankment fill. However, in order to determine representative parameters for use in the finite element analyses two triaxial tests were performed on samples of the embankment fill material.

Sample EMB1 was created at a loose state of compaction and sample EMB2 was created at a dense state of compaction. The sample preparation procedures are presented in section 6.5.5. Both samples were isotropically compressed to an effective stress of 500kPa and then allowed to swell back to an effective stress of 150kPa. Sample EMB1 was then sheared in undrained triaxial compression and sample EMB2 was sheared in drained triaxial compression. The sample testing procedures are given in section 6.6.

The compression and swelling test results for the 2 tests are presented in v:ln(p') space in figure 7.13. The basic test data for the two shearing stages are summarised on figure 7.14.

CHAPTER 8 ANALYSIS AND DISCUSSION OF TEST RESULTS

8.1 Introduction

This chapter presents an analysis of the results of the laboratory testing carried out at City University. The procedures adopted to analyse the test data are given and the results of each series of tests discussed. Critical state parameters for the organic clay stratum are derived. These parameters are used in chapter 9 for predictions of the ground deformations during embankment construction using finite element analyses. The strength and stress-strain data measured in triaxial tests on reconstituted samples of the organic clay are shown to be adequately represented by the modified Cam clay soil model. The results of probing tests indicate the existence of only one state boundary surface for both K_o and isotropically compressed samples. The shape of this state boundary surface is also shown to be well represented by the modified Cam clay soil model. The results of the laboratory testing on both the piston and reconstituted samples of the organic clay are compared with the results presented in the original site investigation.

8.2 Classification Test Results

8.2.1 Effects of Test Procedure on the Atterberg Limits

It can be seen from the results given in table 7.1 that drying the soil during sample preparation has a large effect on the measured Atterberg limits. Drying the soil prior to testing dropped the average plasticity index of all the samples tested from 61 to 35. This compares well with the results reported by Mayne (1987), summarised in section 2.6.

The results presented in table 7.2 confirm that the addition of distilled water, instead of site ground water,

during preparation of the sample for the liquid limit test has little effect on the measured limits. Similarly the results summarised in table 7.3 indicate that using an oven temperature of 70°C rather than 105°C for drying moisture content samples has a negligible effect on the measured limits.

It was noted in section 4.4.2 that, in the original site investigation report, the natural water content of a number of samples were reported to be in excess of their measured liquid limits. This observation is in common with the results of tests on a number of soft alluvial soils reported in the literature, see section 2.6. Based on the results of the testing performed at City University it appears that drying the soil during sample preparation may be a likely cause of this effect.

As discussed in section 2.6 the Atterberg limits of a sample are often used with semi-empirical relationships to determine other engineering properties for the soil. It is probable that a sample preparation procedure which affects the measured Atterberg limits will also exhibit a strong influence on other engineering properties of the soil. Based on the results of these tests the soil was not dried during the preparation of reconstituted samples.

8.2.2 Effects of Organic Content on the Atterberg Limits

It can be seen from the test results given in table 7.4 that there is a general increase in both the plastic and liquid limit with increasing organic content. The plasticity index shows a similar increase, although the variation is not as marked. The data highlights the general trends but there are insufficient measurements to establish a quantitative relationship. However the results agree with the findings of Odell et al. (1960).

The results of the two tests on samples with 2% and 10% organic contents which had been dried prior to testing are

given in table 7.1. As discussed in the previous section one effect of drying the soil during sample preparation is to lower the measured Atterberg limits. It can also be seen that the two sets of results for the dried samples exhibit only a relatively small variation in the measured limits despite the relatively large change in the organic content. For example the difference between the liquid limit for the 2% and 10% organic content samples which had been dried during sample preparation is only 5%. The equivalent difference between the 2% and 10% samples which had been tested without drying is 26%.

The average plasticity index of all the samples that were dried during sample preparation is 35%. The plasticity index of the sample with 2% organic content tested without drying is 57% which represents an increase in the plasticity index by a factor of 1.63 over the plasticity index of the dried samples. The equivalent factor for the sample with 10% organic content tested without drying is 1.91. It can be seen from these results that the presence of small quantities of organic matter has a relatively larger effect on the Atterberg limits than the actual amount of the organic matter.

The effects of organic matter in soils are both chemically and physically complex, Mitchell (1976): organic particles may be adsorbed on mineral surfaces and this adsorption modifies both the properties of the minerals and the organic material itself. At high moisture contents, decomposed organic matter may behave as a reversible swelling system but at some critical stage during drying this reversibility ceases. This factor highlights the importance of careful sample preparation when testing organic soils.

8.2.3 Grading of the Organic Clay

The grading curves for the organic clay samples, shown on figure 7.1, fall in a relatively narrow envelope. The

particle size distribution is well graded between the clay and medium sand fractions. The clay content is approximately 25%.

8.3 Isotropic Compression of Clay at Different Organic Contents

The results of isotropic compression tests on triaxial samples reconstituted at different known organic contents are presented in figure 7.2 and summarised in table 7.4. It can be seen on this figure that samples with a high organic content are slightly more compressible and also exhibit higher specific volumes at any given effective stress. Also shown on figure 7.2 are the results of two tests, one at 2% and one at 10% organic content, in which the samples were dried and reconstituted before testing. The isotropic normal compression lines of these two samples fall close to each other but lie below the other test results, once again highlighting the effect of drying on the behaviour of the soil.

Although there is a spread in the compression test results it is possible that the variation for undisturbed samples is even greater. The organic material is inevitably highly disturbed during the mixing process and this will tend to drive water from the organic material into the soil matrix. The results of this series of tests can therefore only give an indication of the likely variation to be expected for the undisturbed soil.

8.4 The SBS Yield Point

As discussed in section 3.2 the standard methods for determining the preconsolidation pressure of a soil sample, such as the Casagrande (1936) construction, are not suitable for samples which are compressed using either

constant rate of loading or constant rate of straining techniques. The Lambda construction for determining the SBS yield point was proposed in section 3.2. In order to calibrate this method three tests were performed on piston samples and two on reconstituted samples of the organic clay. In each test the sample was compressed, either isotropically or K_o, to a known stress state on the state boundary surface and then allowed to swell back to an R_o value of approximately three. Each sample was then recompressed along a stress path passing through the known maximum previous stress state.

The complete loading, unloading, reloading cycle for each test is presented in v:ln p' space in figure 7.4 for the piston samples and in figure 7.8 for the reconstituted samples. The SBS yield point was then determined from the results of the recompression stage using the Lambda construction. The results of the tests are summarised in table 8.1. Typical examples of the Lambda construction for two of the tests, one sample K_o compressed and one sample isotropically compressed, are shown on figures 8.1 and 8.2 respectively. The effect of changing the rate of compression can also be seen on figure 8.1. The test results at the two testing rates fall on approximately parallel lines.

The results of two tests performed by other investigators at City University, following the stress cycle discussed above, were analysed using the Lambda construction and the results are also included in table 8.1. The data for the test on a kaolin sample are given in Wheatley (1984) and on a Woolwich and Reading beds clay sample in Loxham (1988). There are no other published data of constant rate of loading compression tests following a similar stress cycle with which the results may be compared.

Based on the results of this limited series of tests it appears that the Lambda construction gives a reasonable estimation of the SBS yield point. On average the method overestimated the known yield stresses by 2% and the

standard deviation of the results was approximately 6% of the known values. The data from two of the tests were also analysed, using the Lambda construction, by ten independent investigators in order to assess the objectivity of the method. The standard deviation of the estimated SBS yield point value was found to be less than 4% of the average value for the ten determinations.

A number of other methods for determining the SBS yield point were also evaluated. These methods included the Casagrande (1936) construction and the bi-linear construction in v:p' space, described in section 2.4, adopted by many other investigators. It was found that none of these methods reliably predicted the known SBS yield point. The Casagrande construction badly overestimated the SBS yield point and the bi-linear approach was found to be extremely subjective. The Lambda construction was therefore adopted for determining the SBS yield point for all constant rate of loading compression tests.

8.5 Triaxial Stress Path Testing of Piston Samples

8.5.1 Introduction

A number of stress path tests were performed on piston samples of the organic clay horizon for the following reasons:-

- to provide test data to confirm the applicability of the Lambda construction, proposed in section 3.2, for determining the SBS yield point from the piston samples.

- to confirm the test results reported in the original site investigation.

- for comparison with the stress path tests carried out on reconstituted samples.

The testing programme and results of tests performed on piston samples of the organic clay are summarised in section 7.5. The results of the tests are discussed in sections 8.5.2 and 8.5.3.

8.5.2 Compression and Swelling of Piston Samples

The results of the compression and swelling stages performed on piston samples of the organic clay are presented in v:ln(p') space in figure 7.4. The critical state parameters derived from the data are summarised in table 7.8.

It can be seen in figure 7.4 that the compression characteristics of the organic clay stratum are extremely variable. The results show a similar spread to that measured during the initial site investigation, see figure 4.13. The spread in the results is a consequence of the variation in the organic content between the samples. However it should be noted that large variations in the organic content are also present within individual samples. For example the moisture content of the top, middle and bottom third of sample F301 varied from 30% through 60% to 120%.

The compression δH of a normally compressed stratum of soil of initial thickness H can be calculated from:-

$$\delta H = H * (\lambda * \ln(p_2'/p_1')) / (N - \lambda * \ln(p_1')) \qquad (8.1)$$

where p_1' = the initial mean effective stress $(1+2*K_o)*\sigma_v'/3$
p_2' = the final mean effective stress

It can be shown that despite a factor of 8.8 in the measured range of λ values presented in table 7.8 the equivalent range for the percentage compression of a

stratum containing the various soils is only a factor of 3.2 for a change in the mean effective stress from 100kPa to 200kPa.

The above relationship tends to limit the extreme variability in settlement predictions that may initially be suggested from the laboratory compression test results. In addition the natural averaging effect of considering the complete organic clay stratum when making settlement predictions allows a single set of compression parameters to be used. It is shown in chapter 9 that the actual settlement measured below the embankment, at the various instrumented sections, was accurately predicted using only a single set of critical state parameters for the organic clay stratum. The compression between adjacent extensometer magnets is also accurately predicted.

8.5.3 Shearing of Piston Samples

The shearing tests carried out on piston samples of the organic clay are summarised in table 7.9 and the results presented in table 7.10 and figure 7.5. The final state of the samples at the end of each test are plotted in v:ln(p') space in figure 8.3. It can be seen on this figure that there is no clearly defined critical state line. This result is consistent with the compression test data.

The ultimate state of the samples tested in triaxial undrained compression are plotted in q':p' space in figure 8.4. A linear regression of the results gives ultimate strength parameters of c'=2kPa and ϕ'_c=29.5°. An average value for M_c of 1.24 has been determined using a linear regression with the best fit line fixed at the origin. This is equivalent to an ultimate angle of friction of 31°. The results are comparable to those measured during the original site investigation for samples tested in undrained compression, figure 4.15.

In order to compare the various stress paths followed in q':p' space it is helpful to normalise the test results. As a consequence of the variability in the compression characteristics of the soil it is impossible to obtain a single set of critical state soil parameters for the undisturbed soil with which to normalise the test data. However for isotropically normally compressed samples, when tested undrained, it is possible to normalise with respect to the equivalent consolidation pressure p'_e. If the assumption is made that the modified Cam clay yield locus is appropriate for this material then the equivalent pressure can also be determined for the K_o compressed samples. For the purposes of this calculation the ratio of κ/λ is also required. Based on the results of the tests performed on reconstituted samples (see sections 8.6.2 and 8.6.3) this ratio was assumed to be 0.2.

The normalised stress paths for 7 of the tests are plotted in figure 8.5. Constant volume sections through the modified Cam clay and the Cam clay state boundary surface are also included. Although the results are not conclusive it appears that the modified Cam clay soil model may be more appropriate for this soil than the original Cam clay soil model. Sample U174 was taken from the desiccated crust of the organic clay stratum. The results appear to indicate that the sample had not been consolidated to a normally compressed state prior to testing.

The two 100mm diameter samples F301 and F031, which had been K_o normally compressed prior to shearing, show significant peak stresses. After the peak stress had been reached the samples continued shearing at approximately constant stress ratio but with decreasing deviator stress. This behaviour has been noted by other investigators when testing K_o compressed samples, for example Ho (1988). However, the two samples had exhibited significant creep movements at the end of the compression stages. The above phenomenon may be a result of secondary compression which could also lead to the observed strain softening behaviour.

8.6 Triaxial Stress Path Tests on Reconstituted Samples

8.6.1 Introduction

The results of tests on piston samples taken from the organic clay stratum have shown this material to be extremely variable. It is not easy to determine a representative set of critical state parameters for the organic clay stratum from these results. It is also difficult to normalise the stress-strain data from these tests to confirm the applicability of critical state soil models for this material. As an alternative strategy a series of tests on reconstituted samples of the organic clay was carried out. The test series was designed to yield the following information:-

- A consistent set of critical state parameters for use in finite element analyses.

- The shape of the state boundary surface for both one-dimensionally and isotropically compressed samples.

- Confirmation of the validity of critical state concepts when applied to the organic clay.

- A set of stress-strain data for comparison with single element soil model predictions. These results are required to establish the most representative soil model for use in the finite element analyses.

The sample preparation and testing techniques are discussed in sections 6.5 and 6.6. The testing programme and the results of the tests on reconstituted organic clay samples are presented in sections 7.6.2 to 7.6.4 and in figure 7.9. The procedures used to derive the critical state parameters for the reconstituted organic clay are presented in sections 8.6.2 to 8.6.4. The shape of the state boundary surface and stress-strain behaviour of the clay is discussed in sections 8.7 and 8.8.

8.6.2 Determination of N, Γ, N_o and λ

The states of the reconstituted samples at the end of the compression stages are summarised on table 7.11. The data are also presented on a v:ln(p') plot in figure 7.6 for the isotropically compressed samples and figure 7.7 for the K_o compressed samples.

It can be seen from figures 7.6 and 7.7 that there is some scatter in the results of the various tests. The sample preparation procedure prevented the soil from being sieved and fine gravel sized particles were removed by hand during the mixing process. An approximate measure of the effect of a coarse fraction in the soil matrix can be determined by assuming the inclusion of a large particle in the soil matrix which constitutes X% by volume of the soil mass. If the soil matrix without the large particle has a voids ratio e then the measured voids ratio of the soil mass e_m which includes the large particle is given by

$$e_m = \frac{(100e - Xe)}{(100 + Xe)} \qquad (8.2)$$

Using equation 8.2 it can be shown that only small quantities of the gravel particles, of the order of only 2% by volume, would be required to account for the scatter in the results presented in figures 7.6 and 7.7.

As discussed in section 6.5.3 the reconstituted samples were prepared from two sub-batches of the mixed bulk sample, referred to as the MIX and BOX batches. Closer inspection of figure 7.6 and 7.7 reveals that the results from each of the two batches fall on two fairly well defined lines with the BOX test results lying slightly below the MIX test results. There are two possible reasons for this discrepancy. Firstly the original bulk sample may not have been sufficiently well mixed prior to splitting into the two sub-batches. Secondly, as discussed in section 6.5.3, the BOX sub-batch was used for the later test series and some drying of the soil may have occurred during storage. The effect of drying on the compression

characteristics of the organic clay has been demonstrated in section 8.2.1 to be consistent with this behaviour.

Isotropic and K_o normal compression lines have been fitted to the data from the MIX series of tests, plotted on figure 8.6. The critical state parameters derived from these results for N, N_o and λ are 3.90, 3.84 and 0.27 respectively. The isotropic normal compression line was fitted to the test data using a linear regression. The data point for test MIX2 was not included in the regression analysis as it is thought that this test result may have been badly affected by gravel in the clay matrix. The K_o normal compression line has been drawn "by eye" through the data parallel to the isotropic normal compression line. A statistical analysis of the data is strongly affected by the position of the two data points at high stress. The line drawn "by eye" is likely to be more representative of the true K_o normal compression line.

The ultimate state of the samples at the end of the shearing stages, calculated from the measured final moisture content, are shown on figure 7.10. There is some scatter in these data points due to the combined effects of natural sample variation and the apparent difference, noted above, between the MIX and BOX samples. In order to determine the position of the critical state line more accurately using all the available data the following procedure was adopted.

The specific volume of each sample at the end of the compression stage prior to shearing was calculated based on the known final stresses and the normal compression lines shown on figure 8.6. For undrained tests this value was then used as the specific volume for the shearing stage. For drained tests the change in specific volume during the shearing stage was measured and the calculated value at the end of the compression stage adjusted accordingly. The corrected critical state points are shown in figure 8.7.

The corrected results show slightly less scatter than the data presented on figure 7.10. Sample MIX13 was tested at an OCR of 10 and a distinct shear plane formed leading to brittle failure before the whole sample had reached a critical state. Samples MIX15, BOX4 and BOX6 were all tested in extension and necking of the sample occurred at relatively low strains. A linear regression of the data, with the exception of the four results noted above, gave the best fit critical state line shown on figure 8.7. The values for the critical state parameters Γ and λ determined for this line are 3.62 and 0.252 respectively.

These results indicate that the critical state line is not parallel to the isotropic normal compression line, which is incompatible with the basic concepts of critical state soil mechanics. However the two lines would cross at a stress of approximately 6000MPa, based on the measured critical state values. This stress is far greater than the typical stress levels encountered in geotechnical engineering. The difference may also be due to experimental errors.

As discussed in chapter 5 the construction of the embankment was essentially a drained event and the majority of the organic clay stratum strains at a low stress ratio; i.e. the state of the soil is closer to the isotropic normal compression line than the critical state line. The critical state parameters input into the CRISP finite element package to characterise the organic clay stratum include Γ and λ. There is no provision for specifying the position of the isotropic normal compression line separately. For the purposes of the finite element analyses the critical state line was assumed to be parallel to the isotropic normal compression line. The values for Γ and λ were taken to be 3.72 and 0.27 respectively. The position of this line is shown on figure 8.7. This modification has only a small effect on the results of the analyses but is thought to be more realistic for this particular application.

8.6.3 Determination of κ and ν'

The elastic parameters κ and ν' are used in the finite element analyses, reported in chapter 9, to determine the elastic volumetric and elastic shear strains below the embankment. The selection of relevant elastic parameters to model embankment construction is discussed in more detail in section 9.2.2.

The value for κ can be determined from the swelling and recompression stages carried out on the reconstituted samples. The elastic swelling line is, in critical state theory, straight in v:ln(p') space. However in practice the line is generally curved as a result of factors such as the threshold effect, Richardson (1988), discussed in section 2.5. A closed loop is usually generated on a v:ln(p') plot when a soil is allowed to swell from a normally compressed state and is then recompressed back to that state. In addition, during constant rate of loading testing small excess pore pressures are generated which tend to increase the magnitude of the loop generated.

Typical swelling and recompression stage results are shown in figure 7.8. The value of κ is a function of both the size of the swelling stage (i.e. the maximum value of R_p where $R_p = p'_m/p'$) and the stress level at which the test was performed.

A summary of the κ values determined from the tests on reconstituted samples of the organic clay is given on table 8.2. The value of κ for each test has been determined by considering the state of the sample at the beginning and end of each swelling and recompression stage and calculating an average value for κ from the results. The average value of κ has been determined from all the test results to be 0.054.

The value of ν' can be determined directly from the results of a drained compression test on an overconsolidated sample where the radial effective stress

remains constant. From the generalised Hooke's law it can be shown that when $\delta\sigma'_r=0$

$$\nu' = -\delta\epsilon_r/\delta\epsilon_a \qquad (8.3)$$

An alternative method of determining ν' is from the K_o unloading path where $\delta\epsilon_r=0$. In this case it was shown in section 3.4 that

$$\nu' = \frac{(K_{nc} * R_o - K_o)}{(R_o - 1 + (K_{nc} * R_o) - K_o)} \qquad (8.4)$$

Three of the swelling stages carried out on reconstituted samples of the organic clay were analysed using the above relationship to determine ν'. The results of the analyses are presented on figure 8.8. It can be seen in this figure that ν' increases slightly as the overconsolidation ratio increases. However for R_o values in the range 1 to 3 a value for ν' of 0.25 appears reasonable.

8.6.4 Determination of M_c and M_e

The ultimate state of the reconstituted organic clay samples at the end of the shearing stages are summarised in table 7.12. The data is replotted in q':p' space in figure 8.9. Values for M_c and M_e of 1.17 and -0.85 have been determined from the results using a linear regression of the data with the best fit line fixed at the origin. The result from test BOX3 was not included in the regression analysis as this one data point would have unduly weighted the result. The equivalent ultimate drained angles of internal friction, ϕ'_c and ϕ'_e, are 29.3° and 29.7° respectively. The results from both drained and undrained tests are included on this figure.

Figure 8.9 can be compared with the results of the tests on both piston samples, figure 8.4, and the tests carried out during the original site investigation, figures 4.15 and 4.16. There is good agreement between the various sets of test results with the exception of the drained triaxial tests carried out during the original site investigation. These tests gave a value for M_c of only 1.0, equivalent to

ϕ'_c=25.4°. The tests were taken to a maximum axial strain of between 10% and 20% and it is possible that the tests were stopped before the sample had reached critical state. This inference will be discussed in more detail in section 8.8.4.

As discussed in section 6.6.2 samples tested in extension tended to neck at strains of between 10% and 15% and there is some scatter in the results. However the value for M_e of -0.85 is consistent with a Mohr Coulomb failure criterion (i.e. ϕ' is constant).

8.7 The State Boundary Surface

8.7.1 Introduction

The shape of the state boundary surface is an important soil property when considering the stress-strain behaviour of a soil. As discussed in section 3.3 there are two methods available for investigating the position of the state boundary surface. If the critical state parameters of the soil are known, it is possible to normalise the results of any test which traverses the state boundary surface to give a section through the surface (Type 1 probing). Alternatively the stresses at which the state boundary surface is engaged can be determined from the results of stress path probes directed onto the surface from within the surface (Type 2 probing).

This section presents the results of tests probing the state boundary surface for both isotropically and K_o compressed samples. Details of the methods used to normalise the results are given in section 3.3. The results are compared with both the Cam clay and modified Cam clay state boundary surfaces.

8.7.2 Isotropically Compressed Samples

The results of the shearing stages carried out on isotropically compressed samples of the organic clay have been used to determine the shape of the state boundary surface for the isotropically compressed soil. The results have been normalised with respect to p'_p, the value of p' at the intersection of the current elastic wall with the isotropic normal compression line. Details of the various test stages are given in table 7.12. The critical state parameters used to normalise the results are given in table 8.3. The specific volume at the beginning of each shearing stage has been calculated using the critical state parameters determined in section 8.6 and the known effective compression stresses and R_p value for the compression and swelling stages prior to the shearing stage.

The normalised stress paths are shown in figure 8.10 together with sections through the Cam clay and modified Cam clay state boundary surfaces. The Cam clay and modified Cam clay yield curves have been constructed assuming M_c and M_e are 1.17 and -0.85 respectively, as determined in section 8.6.4.

It can be seen from figure 8.10 that the normalised stress paths for the isotropically normally compressed samples sheared in compression fall slightly below the modified Cam clay yield curve but are of similar shape. The stress path for the undrained extension test, MIX15, lies outside the modified Cam clay yield curve. The abrupt change in the direction of the normalised stress path for test MIX15 is probably the result of the sample necking prior to reaching a critical state stress ratio (the calculated sample area is incorrect). The value determined for M_e may be too low as a consequence of the necking.

Test BOX2 is a drained compression test with R_p=2. The normalised stress path for this test should, theoretically, be a straight line at a slope of 3:1 until

the state boundary surface is engaged, see section 3.3. Closer inspection of figure 8.10 reveals that the normalised stress path tends to bend back before the state boundary surface is engaged, indicating that the soil is beginning to yield prior to the surface being engaged.

8.7.3 K_o Compressed Samples - Type 1 Probing

The basic test data for the Type 1 probing tests are shown in figure 7.11. The normalised stress paths for tests carried out on K_o compressed samples are shown on figures 8.11 and 8.12. The tests have been normalised with respect to p'_p. The specific volume at the beginning of each shearing stage has been calculated using the critical state parameters listed in table 8.3. and the known compression stresses and R_p values determined from the relevant compression and swelling stages.

Figure 8.11 presents the stress paths for tests on K_o normally compressed samples. Tests MIX4 and MIX5 are undrained compression stages, tests MIX6 and MIX8 are undrained extension stages and tests BOX5 and BOX6 are drained extension stages following a stress path similar to the one shown in figure 3.5. The stress paths for the undrained compression stages and the drained extension tests fall close to and are of a similar shape to the modified Cam clay yield locus. The normalised stress paths for the undrained extension tests have plotted inside this yield locus.

The two drained extension tests, BOX5 and BOX6, had both experienced less than 2% shear and 2% volumetric strain as the sample state changed from the initial K_o compressed to an isotropic stress state (the point at which the axial and radial stresses are equal on figure 7.11). This represents only a small disturbance of the soil structure resulting from the initial K_o compression. Test BOX6 was continued to failure in extension and follows a normalised stress path very similar to that of test MIX15, an

undrained extension test on an isotropically compressed sample, in figure 8.10.

It can be seen on figure 8.11 that the deviator stress in both the undrained compression tests decreases at an almost constant stress ratio towards the end of each test. These continuing deviatoric stress changes may be due partly to errors in the measurement of sample dimensions at large strains, effects of end platen restraint or secondary compression (a test takes approximately five days). This phenomenon can also be observed at the end of the tests on isotropically compressed samples, although the fall in the deviator stress is relatively smaller for these tests.

The stress paths followed by the two undrained extension tests should, theoretically, either move around the state boundary surface or remain on an elastic wall at constant p', until the state boundary surface is re-engaged. It can be observed on figure 8.11 that the value of p' decreases throughout the test. This is consistent with yielding of the soil, which would lead to a decrease in p' in a constant volume test. Intuitively this behaviour may be expected. The soil mass is experiencing a change in the ratio of the principal stresses and individual soil grain contacts are liable to slip as the stress regime alters. This is equivalent to a limited yielding of the soil mass.

Figure 8.12 shows the normalised stress paths for samples that were initially K_o compressed and then a number of different stress paths followed to take each sample to the starting stress state shown on the figure. The various tests are discussed in the following paragraphs.

Sample BOX3 was initially K_o compressed and then K_o swelled to an isotropic stress state. The sample was then isotropically normally compressed to a stress slightly higher than the initial compression stresses. In this way an isotropically normally compressed sample was created with a soil structure similar to a K_o normally compressed

sample. The sample then followed a drained constant p' compression stage to failure. The normalised stress path for this test stage is similar to the normalised stress paths for K_o normally compressed samples presented on figure 8.11.

Sample BOX5 was initially K_o compressed and then a drained extension stage to an isotropically normally compressed stress state was performed. The result of this test stage is presented on figure 8.11. After the drained extension stage was completed the drainage valve was closed and an undrained compression test performed on the sample, starting from the isotropic stress state. The normalised stress path for this stage is presented on figure 8.12. The normalised stress path followed after the peak deviator stress had been reached is once again similar to the normalised stress paths for K_o normally compressed samples presented on figure 8.11. At low stress ratios the normalised stress path is closer to the results of the undrained tests on isotropically compressed samples.

Sample BOX4 was initially K_o compressed and then followed a series of swelling and compression stress paths to take the state of the sample to a point on the state boundary surface at a negative deviator stress. A drained extension test was then carried out on the sample. The normalised stress path can be compared with the results of test MIX15 (undrained extension of an isotropically compressed sample) in figure 8.10 and test BOX6 (drained extension of a K_o compressed sample) in figure 8.11.

Test MIX7 and MIX10 were allowed to swell one-dimensionally to an R_o of 2 and 4 respectively. Test MIX7 then followed a drained constant p' compression stage to failure and test MIX10 an undrained compression stage. The normalised stress paths for these two tests are included on figure 8.12.

8.7.4 K_o Compressed Samples - Type 2 Probing

A total of three Type 2 probing tests were performed on K_o compressed samples. The basic test data for each of the tests is presented in figure 7.12. The test data for tests BOX8 and BOX9 have been replotted in both v:ln(p') in figure 8.13. The SBS yield point for these tests, determined using the Lambda construction, fall close to the modified Cam clay yield locus, shown on figure 8.14. Test BOX4 was stopped too early to allow the Lambda construction to be properly used.

The test data for tests BOX8 and BOX9 are also plotted in v:p' space in figure 8.13. It can be seen on this figure that, as discussed in section 2.5, the yield stress determined using the bi-linear construction is extremely subjective. The yield points determined from the results are shown on figure 8.14. Also shown on this figure is the bi-linear yield point determined from test BOX4. These points fall well inside the yield curve predicted by both the Type 1 probing test results and the modified Cam clay yield locus.

It is not possible to determine accurately the shape of the state boundary surface from the limited number of Type 2 probing tests. However the results appear to agree with the modified Cam clay predictions and the Type 1 probing test results. In addition the final state on the normalised stress paths for tests BOX8 and BOX9, shown on figure 8.14, also fall close to the modified Cam clay yield locus which reinforces this finding.

8.7.5 Summary of probing test results

The results of both the Type 1 and Type 2 probing tests appear to confirm the existence of only one state boundary surface for the soil. This surface has a shape which is similar to the modified Cam clay state boundary surface.

In order to assess whether this finding was applicable to other soils a Type 1 probing test was also carried out on a K_o compressed reconstituted kaolin sample. The stress path followed is similar to the path shown on figure 3.5 and the basic test data are presented in figure 7.11. The critical state parameters for the kaolin, determined by Atkinson et al. (1987), are 3.23, 0.19 and 0.05 for N_o, λ and κ respectively. A normalised stress path for the test, presented on figure 8.15, is of a similar shape to the modified Cam clay yield locus. The shape of the normalised stress path differs markedly from the volumetric yield locus for K_o compressed kaolin presented by Parry and Nadarajah (1973), reproduced on figure 2.3.

This comparison demonstrates the difference between the yield locus determined by a Type 1 probing test and a yield locus determined using the bi-linear construction, adopted by Parry and Nadarajah and many other investigators. In addition, the problems associated with relying on only undrained stress paths to determine the shape of the state boundary surface are also highlighted.

There is no clearly defined yield point on the v:p' plots in figure 8.13. This characteristic possibly results from yielding of a limited number of individual soil grain contacts as the state boundary surface is approached, rather than full plastic yielding associated with traversing the state boundary surface. This "pre-yielding" is likely to be more pronounced for larger changes in the direction of the stress path. These results emphasise the difficulty of determining a single representative yield stress. A yield point may be more pronounced in sensitive undisturbed soils where soil structure plays a more important role.

8.8 Stress-Strain Behaviour of the Reconstituted Clay

8.8.1 Introduction

A set of critical state parameters have been determined for the reconstituted organic clay. The state boundary surface for both isotropically and K_o compressed samples of the clay has been shown to be similar to the modified Cam clay state boundary surface. In order to confirm the applicability of the derived soil parameters and the modified Cam clay soil model for use in finite element analyses the stress-strain data from the triaxial tests are compared with single element model predictions. The stress-strain data are presented in this section.

8.8.2 Single Element Modelling

The computer program WORM3 was used to compare the triaxial stress-strain data with both the Cam clay and modified Cam clay soil model predictions. The computer program is described in Stallebrass (1988) and only a brief description is given in this section.

The computer program considers a single element of soil with the standard triaxial stress system acting on it. Any triaxial stress or strain path can be applied to the element in a number of increments. The maximum increment size is limited to maintain the yield ratio less than 1.05. The yield ratio is defined as the value of p_p' at the end of an increment divided by the value of p_p' at the start of the increment. Both drained or undrained tests can be modelled.

Either the Cam clay or modified Cam clay soil model can be specified. Recoverable elastic shear strains were not included in the original Cam clay or modified Cam clay soil models but are incorporated in the WORM program. The elastic shear strains are calculated using the equation

$$\delta\epsilon_s = \frac{2\kappa(1+\nu')}{9\,v\,p'\,(1-2\nu')} * \delta q'$$

The program outputs the axial and radial stresses, pore pressure and the axial, radial and volumetric strains at the end of each increment. The data were then analysed on the VP Planner spreadsheet in a similar manner to the triaxial stress path test data.

The critical state parameters presented on table 8.3 were used for the single element modelling.

8.8.3 Stress-Strain Results

Normalised stress-strain plots have been used to compare the results of the various tests. As discussed in section 3.5 the deviator stress has been divided by the current value of p' and the shear strain multiplied by the current specific volume. This allows tests performed at different stresses which follow equivalent stress paths to be compared. The results of drained tests are presented on figure 8.16 and undrained tests on figure 8.17.

It can be seen from figure 8.16 that the modified Cam clay soil model shows good agreement with the two constant p' compression tests. The drained compression test BOX2 was also well represented by modified Cam clay. The drained extension test BOX6 followed a three stage loading path similar to the path shown on figure 3.5. Greater shear strains were measured in the early stages of the test than would have been predicted by the modified Cam clay model.

The results of undrained compression and undrained extension tests on both isotropically and K_o compressed samples of the organic clay are compared to the Cam clay and modified Cam clay predictions on figure 8.17. For the K_o compressed samples the Cam clay and modified Cam clay predictions are similar and as such have been shown as one plot. It can be seen from these results that both soil models compare reasonably well with the triaxial test data. At large changes of stress ratio (i.e. approaching failure in extension for the K_o compressed samples and

failure in compression for the isotropically compressed samples) the reconstituted samples tend to yield more than would be predicted by the soil models. It can also be seen on figure 8.17 that the modified Cam clay soil model predicts the stress-strain response of both K_o and isotropically compressed samples with comparable accuracy.

It can be seen from the above that the modified Cam clay soil model provided reasonable predictions of the stress-strain response, measured in the triaxial apparatus, for both K_o and isotropically compressed samples for a wide variety of drained and undrained stress paths. The major difference in behaviour is a tendency for the real soil to yield more than would be predicted as the sample approaches failure.

8.8.4 Drained and Undrained Ultimate Stress Ratio

It was noted in section 4.7 that the ultimate stress ratio measured in the original site investigation varied from 1.0 in drained triaxial compression tests to 1.2 in undrained tests. Using the soil parameters given in table 8.3 the stress-strain response of a sample, isotropically normally compressed to 100kPa, was modelled for both a drained and an undrained compression test, using the modified Cam clay soil model. The results of the analysis are shown on figure 8.18.

It can be seen from figure 8.18 that the stress-strain response for the two tests are very different. In the undrained test the maximum stress ratio is reached at an axial strain of approximately 5%, while in the drained test the stress ratio is still increasing at an axial strain of 30%.

The drained triaxial tests in the original site investigation were generally stopped at an axial strain of between 15% and 20%. It can be seen in figure 8.18 that the modified Cam clay soil model would predict a stress

ratio of approximately 1.0 at this strain level and this compares well with the actual results.

8.9 Embankment Sand Fill Properties

Preliminary finite element analyses indicated that the strength and stress-strain parameters used for the embankment sand fill do not greatly effect the soil deformations below the embankment. Both the Cam clay and modified Cam clay soil models are applicable to normally and lightly overconsolidated soil. For the purposes of the finite element analyses the embankment sand fill is modelled as an elastic perfectly plastic material. Values for the elastic modulus, Poissons' ratio and a representative friction angle are therefore required.

The results of swelling and compression stages on a loose and a compact triaxial sample of the embankment sand are given in figure 7.13. The average value of κ for the two tests is 0.0035.

A value for ν' can be calculated from the results of a drained compression test where $\delta\sigma_r'=0$, then

$$\nu' = -\delta\epsilon_r/\delta\epsilon_a$$

However at the very small strain levels measured at the beginning of a drained test on sand it is difficult to obtain an accurate value for ν'. A value for ν' in the range 0.1 to 0.3 was determined from the results of test EMB2 (see figure 7.14 for the basic test data). A typical value for fine grained sand is 0.25, Bowles (1968), and this value was used for the finite analyses.

The ultimate stress ratio measured in tests EMB1 and EMB2 was 1.53 and 1.5 respectively (see figure 7.14 for the basic test data). An ultimate friction angle of 37° was determined from these results and this value was used in the finite element analyses reported in chapter 9. This represents a conservative estimate of the strength of the fill. However preliminary finite element analyses

indicated that no point in the embankment fill would approach a failure condition.

8.10 Summary of Laboratory Test Results

The laboratory testing carried out at City University has confirmed the results of the original site investigation. The organic clay stratum has been shown to have extremely variable compression characteristics and this has been linked to the variable organic content of the soil. Small quantities of organic peaty material have been shown to have a relatively large effect on the engineering properties of the soft clay stratum. The effect of drying on the engineering properties of the organic clay has also been demonstrated.

Reconstituted samples of the clay were prepared without drying. A set of critical state parameters for the reconstituted organic clay have been derived and these are summarised in table 8.3.

In general the ratios $(\lambda-\kappa)/\lambda$ and p'_p/p'_{cs} have been found to be approximately 0.8 and 2 respectively for inorganic soils, Wroth (1984). The equivalent ratios determined using the parameters measured for the reconstituted organic clay, presented in table 8.3, are 0.8 and 2.26 respectively.

Schofield and Wroth (1968) proposed the concept of the Ω point at which all critical state lines cross in v:ln(p') space. The coordinates of this point are v=1.25, p'=10.3MPa. The specific volume predicted by the parameters measured for the reconstituted organic clay for p'= 10.3MPa is 1.22, which shows good agreement with the data for other soils.

It was shown in sections 8.7 and 8.8 that the modified Cam clay soil model represents the behaviour of both "undisturbed" and the reconstituted organic clay better

than the original Cam clay model. This is also in agreement with data for the majority of normally and lightly overconsolidated clays.

It was noted in section 4.4.5 that the average value of p'_e/p'_{cs} for the consolidated undrained triaxial tests performed on "undisturbed" samples in the original site investigation was 1.94 which agrees reasonably well with the modified Cam clay prediction of 1.74 (based on the reconstituted organic clay parameters presented in table 8.3). The average value of Cu/p'_e for these tests was 0.30 which also compares well with the modified Cam clay prediction of 0.34.

The ultimate stress ratio measured in the various triaxial tests on both piston samples and reconstituted samples is approximately 1.2. The drained triaxial tests in the original site investigation measured an ultimate stress ratio of only 1.0. The modified Cam clay soil model has been used in section 8.8.4 to show that this may be the consequence of ending the test before the critical state had been reached.

The state boundary surface for K_o compressed samples has been probed using two separate methods. Although only a limited number of tests were performed the results appear to indicate the existence of only one state boundary surface for both K_o and isotropically compressed samples. This state boundary surface has a similar shape to the modified Cam clay state boundary surface. Samples experiencing a large change in stress ratio, in both drained and undrained triaxial tests, exhibit a "pre-yielding" behaviour as the state boundary surface is approached. This pre-yielding is thought to be the result of a limited number of grain contacts failing rather than full plastic yielding associated with traversing the state boundary surface.

Single element modelling has shown that the modified Cam clay soil model can adequately predict the stress-strain

response of soil samples tested on a wide variety of both drained and undrained stress paths. The model works equally well for both K_o and isotropically compressed samples.

It can be seen therefore that although the organic material alters the engineering properties of the soft clay stratum, critical state concepts and in particular the modified Cam clay soil model can be used successfully to predict the behaviour of this material in a wide variety of tests.

CHAPTER 9 FINITE ELEMENT ANALYSES

9.1 Introduction

This chapter describes the finite element analyses carried out during the present investigation. The results of the analyses are presented and these are compared with the actual data measured on site during and after construction of the embankment.

The finite element analyses have been kept deliberately uncomplicated. For example only one set of soil parameters were used to represent the organic clay stratum and the construction was assumed to be a drained event.

9.2 The CRISP Program, Modelling Parameters and Procedures

9.2.1 Introduction

The CRISP finite element program was developed by the Cambridge University Soil Mechanics Group. The 1984 version of CRISP is installed on the Gould computer at City University. The CRISP finite element program is fully described in Britto and Gunn (1987). Only those features relevant to the present investigation are discussed in this section. Use was also made of the pre and post processing packages developed at City University for mesh generation and mesh plotting.

The monitoring results obtained from section EE of the EGAR embankment represent the most comprehensive set of records taken during the present investigation. This cross section was therefore used to assess the importance of the various modelling parameters and analysis techniques. The results obtained from the evaluation of this cross section were then applied to the other instrumented cross sections at the EGAR site.

9.2.2 Soil Models

A number of soil models are available in the CRISP finite element package. These include linear elastic, anisotropic elastic, elastic-perfectly plastic and elastoplastic models. The choice of the most representative soil model for each soil stratum is important.

Organic clay stratum

The laboratory test results and single element stress-strain comparisons have indicated that the modified Cam clay soil model is appropriate for the organic clay stratum. Britto and Gunn (1987) recommend that the critical state parameters used in the finite element analyses be derived from the results of both in situ tests and high quality laboratory tests on "undisturbed" samples. However, the results of in situ tests and tests on "undisturbed" samples have shown this material to be extremely variable. It is not possible to determine a single set of representative critical state parameters from these results.

Two alternative methods were considered in order to overcome this problem. Firstly the organic clay stratum could be modelled as a number of different materials based on the results of individual tests on "undisturbed" samples. This method is not appropriate as the material variability cannot be predicted in either the lateral or vertical direction and representative cross sections are therefore impossible to establish.

Alternatively a single set of critical state parameters can be derived from either a statistical analysis of the results of tests on the "undisturbed" samples or from the results of tests on an "average" reconstituted sample, mixed from a batch of various samples from the stratum. This latter course of action was adopted in the present

investigation. The critical state parameters, derived for the reconstituted clay, are presented in Table 8.3.

The soil model is specified by the position of the critical state line in v:ln(p') space and values for λ and κ. In addition, the calculation of elastic shear strains requires a value for elastic shear modulus to be stipulated. CRISP allows the user to specify either a constant value for ν' or G'. Experimental evidence suggests that G' varies approximately with p', Britto and Gunn (1987), although the soil behaviour is then not truly elastic, Zytynski et. al. (1978). Britto and Gunn recommend that a constant value of ν' be specified such that G' varies in the same way as K'. This procedure has been adopted in the present investigation.

Embankment sand fill

Preliminary finite element analyses indicated that the strength and stiffness of the embankment fill has only a small effect on the predicted ground deformations. In addition, no point in the embankment fill material approaches a failure condition. As discussed in section 2.2, Kwok (1987) found that an elastic-perfectly plastic model with a Mohr Coulomb yield criterion was preferable to the other models available in CRISP to represent the embankment fill. This type of soil model was therefore used in the analyses to represent the embankment fill.

The stiffness of the first embankment lift has the biggest influence on the predicted deformations. Values for κ and ν' of 0.0035 and 0.25 were determined for the embankment sand fill (see section 8.9). A value for the elastic modulus E' is give by Atkinson and Bransby (1978) as

$$E' = \frac{3\ v\ p'(1-2\nu')}{\kappa} \qquad (9.1)$$

A first lift of approximately 3.0m was used in the analyses. The approximate value of p' at mid depth of this layer would be 30kPa and the specific volume of the

compacted fill is approximately 1.5. A value for E' of 20MPa is predicted and this value was used in the analyses.

The relative insensitivity of the deformation predictions to the embankment fill stiffness can be seen on figure 9.1. In this figure the elastic modulus of the embankment fill has been varied between 5MPa and 80MPa and embankment construction modelled in three stages (see section 9.2.6). All the other analysis parameters were left unchanged.

An ultimate friction angle of 37° was used for the fill although, as discussed above, this parameter is relatively unimportant as no point in the embankment fill approaches failure.

Made ground

The made ground to the south of the NOS (see figure 4.2) is extremely variable (see section 4.2.3). The only test data available for this stratum is from the SPT testing carried out during the initial site investigation, reported in section 4.3.5 and shown summarised in figure 4.12. Visual inspection of this stratum has shown the material to be generally granular and to have a variable, though generally loose, state of compaction.

In the absence of other information, the data obtained from the extensometers installed at section EE have been used to derive an elastic modulus of 5MPa for this material. An elastic perfectly plastic model was adopted and the values chosen for ν' and ϕ' are 0.25 and 30° respectively. It should be noted that the made ground is only present to the south of the NOS. An appropriate method of obtaining design parameters for this stratum would be to perform in situ plate loading tests.

9.2.3 In Situ Stresses

For finite element analyses involving Cam clay type soil models it is important to establish the in situ stress state as accurately as possible. This is because the displacements predicted by an analysis are sensitive to the relative amounts of elastic and plastic straining that take place. The program requires the initial horizontal and vertical effective stresses to be specified in addition to the pore water pressure and the pre-consolidation profile.

The position of the water table was discussed in section 4.2.3. The vertical effective stress has been calculated assuming that the unit weight of the organic clay material and the made ground are 16kN/m^3 and 15kN/m^3 respectively. The preconsolidation profile and horizontal stress at any depth depends on the geological history of the site.

Estimates of the preconsolidation pressure have been obtained from the results of oedometer and Rowe cell tests carried out during the initial site investigation, the SBS yield point determined in triaxial tests performed during the present investigation and from the plate dilatometer profiles. The results of all these tests are presented on figure 9.2. The preconsolidation pressure is presented on this figure as p'_p. The value of p'_p has been calculated from the test results by assuming that the modified Cam clay yield locus is appropriate for the soil.

The plate dilatometer profiles presented on figure 9.2 have been calculated from the average R_o values, presented on figure 4.10, determined using the Powell and Uglow (1988) correlations (see section 4.3.2). It should be noted that the profiles presented on figure 4.10 are the average of 8 individual tests performed to the south of the NOS and 6 tests performed to the north of the NOS.

It can be seen on figure 9.2 that there is a relatively large spread in the various test results and it is difficult to establish a representative profile from this data. It is considered however that the dilatometer profiles give a reasonable indication of the shape of the preconsolidation profile, though not necessarily the correct magnitude.

As discussed in section 4.7 approximately 3m of made ground was placed to the south of the NOS many years prior to the construction of the embankment. Pressuremeter derived shear stress-shear strain curves are presented in figures 4.6 and 4.7 for tests carried out to the south and north of the NOS respectively. It can be seen from these results that the organic clay stratum to the south of the NOS is approximately 50% stronger than the equivalent stratum to the north of the NOS. It is likely that the clay to the south of the NOS is close to a normally compressed state. Based on this assumption and the profile from the dilatometer tests, the preconsolidation profile shown on figure 9.2 has been used in the finite element analyses for the cross sections to the south of the NOS. A scaling factor of 1.25 has been derived from the dilatometer data to the south of the NOS to convert the plate dilatometer preconsolidation pressure to the actual preconsolidation pressure.

No development of the site has previously taken place to the north of the NOS. The organic clay stratum is present at ground level. Below a desiccated crust the material is lightly over-consolidated. The plate dilatometer test results indicate that the desiccated crust extends to a depth of between 1m and 1.5m. The preconsolidation profile assumed for this area has been constructed based on the plate dilatometer profile and the scaling factor derived from the data to the south of the NOS.

The SBS yield point results agree reasonably well with the assumed preconsolidation profiles. The preconsolidation pressures measured in the oedometer and Rowe cell tests

appear to overestimate the in situ preconsolidation pressure. It should be noted however that only four loading increments were used in these tests (25kPa, 50kPa, 100kPa and 200kPa) and it is difficult to determine an accurate stress-strain curve from only four data points.

The in situ horizontal effective stress can be determined from the pressuremeter test results, but, as discussed in section 4.3.1, the error in the pressuremeter derived values is relatively large. An alternative approach is to calculate the stress from the assumed preconsolidation profiles. A value for K_{nc} of 0.55 has been determined from the triaxial test results. It is shown in section 3.4 that for K_o swelling

$$K_o = R_o * K_{nc} - \frac{\nu'}{(1-\nu')} * (R_o - 1) \qquad (9.2)$$

The horizontal effective stress has been calculated from the preconsolidation profiles shown on figure 9.2 and equation 9.2. This method gives only an approximate estimate of the stress as the measured preconsolidation pressures may result from secondary compression in addition to K_o unloading. The K_o values calculated using equation 9.2 show reasonably good agreement with the average plate dilatometer values, shown in figure 4.9, determined using the Powell and Uglow (1988) correlations.

9.2.4 Drainage Assumptions

Drained, undrained or coupled consolidation analyses can be performed using the CRISP finite element package. As reported in section 4.6, vertical wick drains were installed below the embankment at a spacing varying between 0.5m and 1.0m. Using these spacings 90% consolidation of the organic clay stratum was expected to occur within one month of the construction of an embankment lift (see section 4.6). As this time is approximately equivalent to the planned construction period for each embankment lift, the construction was

considered to be essentially a drained event at the design stage.

The piezometer results presented in figures 5.4 to 5.6 have confirmed this design assumption. As discussed in section 5.2.1, the measured piezometer results are likely to represent an upper bound estimate of the actual excess pore pressures below the embankment.

All the cross sections were analysed assuming full drainage of the organic clay stratum. It should be noted that it would be extremely difficult to model accurately the inclusion of vertical drainage elements at such a close spacing. In addition the measurement of representative soil permeabilities is also extremely difficult, particulary as permeability is also a function of the void ratio. There is no allowance within the CRISP program for varying permeability with stress level.

9.2.5 The Finite Element Mesh

The CRISP finite element package can model 2-D plane strain or axisymmetric and 3-D problems. 2-D plane strain analyses were used in the present study.

A number of element types can be specified in the CRISP finite element package. Britto and Gunn (1987) recommend that linear strain triangles (LST) are used in plane strain analyses and between 50 and 100 LSTs are required to model a typical geotechnical problem. As the name suggests the strains vary linearly across an LST element.

Cubic strain triangles (CUST) have the strains varying as a cubic function across the element. Typically only 20 to 30 CUSTs are required to model a geotechnical problem. Fewer CUST elements are therefore required for the analysis of the embankment construction, making the data preparation quicker though the computer analysis time is much longer with this type of element.

The effect of using different finite element meshes and element types was investigated at cross section EE. The meshes used are shown on figure 9.3. Mesh "ewc1" has exactly the same geometry as mesh "ew11", however the LST elements are replaced by CUST elements. Mesh "ew12" has approximately four times the number of the elements used in mesh "ew11".

The results of analyses, using a common set of soil parameters and embankment construction modelling procedures, show that the various meshes predict similar deformations. The agreement between the meshes is closer than 2% of the predicted deformation at any point within the mesh. The ratio of the computer time taken to run an analysis using meshes "ew11" and "ewc1" was found to be in the ratio of 1:6. The analysis time for mesh "ew12" is approximately the same as for mesh "ewc1".

9.2.6 Modelling Embankment Construction

The modelling of embankment construction is facilitated by the addition of blocks of elements to the finite element mesh. The stiffness of each block of elements is incorporated into the total mesh stiffness as soon as the element block is specified. However the application of the mass of the element block can be spread over a number of analysis increments. In this way embankment construction is modelled in a number of "increment blocks".

For elasto-plastic soil models the size, and therefore number, of loading increments has an influence on the predicted results. Britto and Gunn (1987) recommend that sufficient increments should be used to limit the yield ratio (see section 8.8.2) at any integration point within the mesh to less than 1.02. Typically, in the present investigation, this restriction would require the construction to be modelled with approximately 200 increments.

The effect of varying the number of loading increments on the predicted settlement profile at ground level can be seen in figure 9.4. In this figure the number of loading increments used to model the first stage of embankment construction has been varied between 5 and 50. It can be seen from these results that there is little advantage to be gained from using more than approximately 20 increments. The maximum yield ratio at any point in the analysis using 20 increments is 1.04. The use of only 5 increments would tend to underestimate the centreline settlement by only 9%. Similar results are obtained for the horizontal displacement profile at the toe of the embankment.

Mesh "ewl3", figure 9.3, was prepared to investigate the effect of changing the number increment blocks used to model construction. The mesh differs from "ewl2" only in the number of elements used to model the embankment. Three analyses were performed modelling construction of the embankment at instrument section EE. In each analysis the construction was modelled using a total of 30 increments, while the number of increment blocks was varied from 1 to 6. The settlement profiles at ground level for the analyses are compared on figure 9.5. It can be seen on this figure that using more than 3 increment blocks has only a relatively small effect on the predicted settlement profile.

9.3 Finite Element Modelling Results

9.3.1 Introduction

The finite element meshes used to model the instrumented cross sections are shown on figures 9.6 to 9.10. The soil parameters discussed in section 9.2.2 and summarised in table 9.1 were used in all the analyses. Embankment construction was modelled using each level of elements, shown on figures 9.6 to 9.10, within the embankment fill

as separate increment blocks. Twenty increments were used for the application of each increment block.

The lowest level of embankment elements in sections AA, CC and DD, figures 9.8 to 9.10, represent the drainage blanket at the base of the embankment fill. The initial zero readings for the instrumentation at these 3 cross sections were taken approximately 2 months after this layer had been placed. The ground deformations resulting from the application of this layer have not been included in the results. Ten increments were used to model the addition of this block of elements.

Base fixity was assumed at the interface between the soft organic clay stratum and the dense sand and gravel layer at all the cross sections. The meshes were assumed to have free vertical movement at the embankment centreline and outer boundary but no horizontal movements were allowed at these boundaries. The assumed initial stresses, preconsolidation profile and position of the water table at each cross section are given in figures 9.6 to 9.10.

The results of the analyses at each cross section are summarised in sections 9.3.2 to 9.3.6 and on figures 9.11 to 9.17. The predicted deformations are compared with both the actual movements measured on site immediately after construction of the embankment section and also the "long term" movements. The "long term" movements are the measurements either immediately prior to the construction of the next embankment lift (section EE west) or at the end of the monitoring period.

9.3.2 Section EE West

The finite element mesh used to model the western half of instrument section EE is shown on figure 9.6. The actual construction of the embankment in this area was completed in three separate lifts, as originally planned at the design stage. The three lifts are represented by the three

levels of embankment elements shown on figure 9.6. A surcharge was placed on the embankment and this has been included in the top row of elements.

The predicted settlement profile at ground level and horizontal movement profile at the position of inclinometers I9, I12, I13 and I14 (see figure 5.1) are compared with the actual site movements on figures 9.11 and 9.12 respectively. The side slope of the embankment was landscaped with the addition of the volume of material shown as triangle PFQ on figure 9.6. The landscaping was performed by tipping quantities of fill into piles and dozing these into shape. The ground deformations resulting from the landscaping have been included in stage 3 of the loading.

9.3.3 Section EE East

The finite element mesh used to model the eastern half of instrument section EE is shown on figure 9.7. This half of the embankment was constructed in one lift and the modelling was also performed using only one increment block.

The results of the analysis are shown on figure 9.13 where the predicted horizontal ground deformations are compared with the inclinometer profiles both immediately after construction of the embankment and at the end of the monitoring period.

9.3.4 Section DD

The finite element mesh used to model instrument section DD is shown in figure 9.8. The embankment was constructed in a continuous operation (see figure 5.5). A bored pile wall was constructed close to the toe of the embankment to protect a large diameter gas main which is situated close to the embankment. The position of the wall is shown on

figure 9.8. Free vertical movement but no horizontal movement has been allowed at the wall.

The results of the finite element analysis are shown on figure 9.14 where the predicted ground deformations are compared with the movements measured on site both immediately after completion of construction of the embankment and at the end of the monitoring period. The predicted centreline settlement and horizontal deformation at the toe of the embankment are compared with the actual movements measured on site during construction of the embankment on figure 9.15. The centreline extensometer was damaged and replaced during construction of the embankment. The results shown on figures 9.14 and 9.15 for the centreline settlement have been extrapolated from the data of both extensometers.

9.3.5 Section CC

The finite element mesh used to model instrument section CC is shown on figure 9.9. The embankment was constructed in a continuous operation in this area. The side slope of the embankment was landscaped with the addition of the volume of material shown as triangle OEP on figure 9.9. The landscaping was performed by tipping quantities of fill into piles and dozing these into shape. It is possible that inclinometer I23 (see figure 5.2) was damaged during this procedure.

The horizontal deformations measured outside the toe of the embankment at the end of construction and after the landscaping operation had been completed are shown on figure 9.16. There were no extensometers installed at this cross section.

9.3.6 Section AA

The finite element mesh used to model instrument section AA is shown on figure 9.10. The embankment was constructed in a continuous operation in this area.

The results of the finite element analysis are shown on figure 9.17 where the predicted deformations are compared with the results measured on site both immediately after construction and at the end of the monitoring period.

A haul road was cut into the side slope of the embankment and the inclinometer at the toe of the embankment was destroyed before the end of the monitoring period. In addition the centreline extensometer was damaged and replaced during construction of the embankment. The results shown on figure 9.17 for the centreline settlement have been extrapolated from the data of both extensometers.

9.4 Summary of the Finite Element Analysis Results

As discussed in section 9.1, a single set of critical state parameters has been used to represent the soft organic clay stratum. The critical state parameters were derived from the results of tests on reconstituted samples of the clay. The construction of the embankment was modelled as a drained event.

The results of analyses modelling embankment construction at the five cross sections, which had been instrumented to measure ground movements, generally show very good agreement with the field results. The centreline settlements were predicted to within 10% of the actual long term values. The immediate settlements were typically between 60% and 80% of the long term values.

The maximum horizontal movements close to the toe of the various embankment sections were predicted to within 20% of the actual long term values, with the exception of inclinometer I37 at section AA and I23 at section CC which were both damaged before the end of the monitoring period. The immediate horizontal movements were typically between 40% and 80% of the long term values. The actual horizontal movements appear to lag behind the vertical movements, see figure 9.15.

The finite element predictions for the horizontal movements of the inclinometers positioned more than approximately 10m from the toe of the embankment did not show as good agreement. However it should be noted that only small movements of the order of 4mm were measured at these inclinometers and this is approximately the same order of magnitude as the accuracy of the measurements.

As discussed in section 9.2.2 the elastic-perfectly plastic soil parameters used to model the made ground were derived from the SPT testing and monitoring results. The results of the finite elements analyses at sections EE east and west may have been improved by using a more representative soil model for this stratum. In situ plate loading tests would probably give the most reliable data to determine a more representative soil model for this stratum.

It can be seen from the results that despite the relative simplicity of the finite element analyses (i.e. using only one set of parameters to model the very variable organic clay horizon and performing drained rather than coupled consolidation analyses) good agreement has been obtained with the ground deformations measured on site. The use of soil parameters derived from reconstituted soil samples appears to have been justified. The implications of using soil parameters derived from tests on either "undisturbed" samples or from soil index properties are discussed in section 10.4.1.

CHAPTER 10 DISCUSSION

10.1 Introduction

The original site investigation for and design and construction of the EGAR embankment was assessed in chapter 4. The laboratory testing performed at City University and analysis of the results within a critical state framework was discussed in chapter 8. The prediction of deformations below the embankment by the finite element method, using a critical state soil model to represent the soft foundation stratum, was considered in chapter 9. This chapter brings together the differing aspects of the investigation. The conclusions drawn from the work are summarised in Chapter 11.

10.2 The Application of Critical State Concepts to Embankment Construction

10.2.1 Laboratory Test Results on Reconstituted Samples

Oedometer and triaxial tests on piston samples of the organic clay stratum revealed that the compression characteristics of this material are very variable. This variability was linked in section 8.2 to the organic content of the clay. In order to study the engineering properties of the clay stratum within the framework of critical state soil mechanics it was convenient to create a single batch of the clay with consistent engineering properties. The results from the various tests were then normalised to reveal the basic patterns of behaviour corresponding to the "average" reconstituted sample.

Critical state soil parameters for the reconstituted organic clay were determined in section 8.6 and these are presented in Table 8.3. The ratios determined for $(\lambda-\kappa)/\lambda$ and p'_p/p'_{cs} are 0.8 and 2.26 respectively. These values show good agreement with the ratios found for other

inorganic soils, Wroth (1984). In addition, the critical state line passes very close to the Ω point proposed by Schofield and Wroth (1968). Using the relationship between λ and the plasticity index proposed by Schofield and Wroth (see equation 2.13) an estimate for λ of 0.31 for the reconstituted soil has been obtained and this compares reasonably well with the actual measured value of 0.27.

The results of probing tests on overconsolidated samples following constant stress ratio stress paths directed onto the state boundary surface (Type 2 probing) do not exhibit a well defined yield point. The sample begins to yield before the state boundary surface is engaged. A first yield point is difficult to define as the region of elastic stress-strain behaviour is neither linear in v:p' nor v:ln(p') space. The SBS yield point was proposed in section 3.2 to represent the combination of stresses at which the state boundary surface is engaged for a particular stress path. The Lambda construction to determine the SBS yield point was proposed in section 3.2 and this is considered in section 10.4.2.

The state boundary surface of both K_o and isotropically compressed samples was probed using specimens of the reconstituted organic clay. Two different experimental techniques were used and these are considered in sections 8.7.3 and 8.7.4. Although only a limited number of tests were performed the results indicate the existence of only one state boundary surface for both K_o and isotropically compressed samples. The shape of an elastic wall section through this state boundary surface is similar to the modified Cam clay yield locus.

This result conflicts with the findings of a number of other investigators (for example Parry and Nadarajah (1973), Graham et al. (1988), Atkinson et al. (1987)), reported in section 2.4, who have proposed that the yield locus for a K_o compressed soil sample differs markedly from that of an isotropically compressed sample. These earlier findings were based on the shape of the stress

paths measured in undrained triaxial tests or from the locus of yield points determined from drained triaxial tests using the bi-linear construction. The potential shortcomings in these methods were discussed in chapter 2. Stress-strain data from triaxial tests on samples of the reconstituted organic clay were compared to the predictions made using the Cam clay and modified Cam clay soil models. The results, presented in section 8.8, show that the modified Cam clay soil model provides a reasonable prediction of the stress-strain behaviour for a wide variety of both drained and undrained stress paths for both K_o and isotropically compressed samples. The major difference in the behaviour is a tendency for the real soil to yield more than predicted by modified Cam clay as the sample approaches failure.

10.2.2 Laboratory Test Results on Piston Samples

It was demonstrated in section 8.10 that the undrained strength of the organic clay piston samples compares well with the modified Cam clay prediction, based on the critical state parameters derived for the reconstituted organic clay.

The end of test stress ratio measured in the undrained and drained triaxial tests on the organic clay piston samples in the original site investigation was 1.2 and 1.0 respectively (see Figures 4.15 and 4.16). The modified Cam clay soil model was used in section 8.8.4 to demonstrate that this may be the consequence of ending the drained triaxial tests before the critical state has been reached.

It was difficult to model the stress-strain behaviour of the piston samples because of the extreme variability of the compression characteristics of these samples (see Figures 4.13 and 7.4).

10.3 Review of the Finite Element Analyses

It was demonstrated in Chapter 9 that finite element analyses of embankment construction gave good agreement with the ground deformations measured on site. The maximum vertical and horizontal deformations below the embankment were predicted to within approximately 10% and 20% respectively of the actual measured movements. The shape of the predicted settlement and horizontal deformation profiles showed excellent agreement with the measured profiles.

The most important feature of the finite element work was the relative simplicity of the analyses. A single set of critical state soil parameters was used to represent the very variable organic clay stratum in the analysis of all five instrumented cross sections of the embankment. The critical state parameters were determined from the results of triaxial tests performed on reconstituted soil samples. The soil samples were reconstituted from a single batch, made up from several samples of the organic clay stratum taken from various parts of the site. Alternatively a set of parameters could have been determined from a statistical analysis of tests on "undisturbed" samples. This alternative is considered in section 10.4.1.

The construction was modelled as a drained event. The permeability of a soil stratum is affected by many factors including soil type, stress level, fissuring, and micro/macro structural features. It is one of the most difficult engineering parameters both to measure accurately and to model correctly. However it is often found that field permeabilities are greater than the equivalent permeabilities measured in both in situ and laboratory tests (for example Lewis et al. (1975), Smith and Hobbs (1976)). Drained analyses may therefore be relevant to a significant number of embankments constructed on soft ground, particularly in cases similar to the EGAR embankment where vertical drainage elements are installed.

10.4 A Review of the Original Site Investigation Results and Embankment Design

10.4.1 Deformation Predictions

A comparison of the centreline settlement predicted at the design stage by Husband and Co. (1985) with the finite element predictions and the actual settlement is given in table 10.1. It can be seen in this table that the original settlement calculations, based on the oedometer and Rowe cell test results, overestimated the centreline settlement by an average of 60%. This compares with an average underestimate by the finite element analyses of only 3%, based on soil parameters measured on reconstituted soil samples. The very close agreement achieved by the finite element analyses is perhaps fortuitous, nevertheless the fact that good agreement was obtained at all the cross sections modelled using a single set of critical state parameters justifies the use of reconstituted soil parameters.

It is pertinent to consider whether the finite element analyses could have been performed on the basis of the original site investigation data.

The embankment construction was envisaged as essentially a drained event at the design stage, see section 4.6. The in situ stresses and preconsolidation profile used in the finite element analyses were determined from a combination of the in situ test results and a knowledge of the site history. A set of critical state soil parameters to represent the organic clay stratum could have been derived from a statistical analysis of the oedometer and Rowe cell test data and from the results of the consolidated undrained triaxial compression tests.

Finite element analyses using critical state parameters derived from a statistical analysis of the oedometer and Rowe Cell test results have not been carried out. However, a first order approximation, based on the piston sample

test results shown in Table 7.8 and using equation 8.1, indicates that the movements would be approximately 20% greater than the predictions using the reconstituted clay parameters. It is interesting to note that a similar result would have been achieved had critical state soil parameters based on the index test results for the average reconstituted sample and the relationships discussed in section 10.2.1 been adopted.

10.4.2 Applicability of the Original Site Investigation Data

The data from the plate dilatometer was used in section 9.2.3 to obtain profiles of the preconsolidation pressure and the in situ horizontal stress for the organic clay stratum. The interpretation of dilatometer data proposed by Powell and Uglow (1988) gave a better correlation with the other site investigation test results than the original interpretation proposed by Marchetti (1980). Site specific correlations with other test results were nevertheless required.

The standard method of performing oedometer and Rowe cell tests in which the vertical load is doubled at each loading increment was not suitable for the determination of preconsolidation pressures. Too few data points are produced and the choice of a relevant yield stress is extremely subjective. A greater number of smaller loading increments are required to produce a reliable stress-strain curve. This has the obvious disadvantage of increased testing times.

Constant rate of loading tests may constitute an improved testing technique. This type of test can take less time than the conventional oedometer test and a continuous stress-strain curve is produced. The excess pore pressures generated during the loading must be considered when interpreting the results of the test.

The Lambda construction to locate the SBS yield point from the results of a constant rate of a loading test was proposed in section 3.2. This method was shown in section 8.4 to give reasonable agreement with known yield stresses in a limited number of controlled tests.

The pressuremeter testing provided the only in situ measurement of the total horizontal stress, but there is no record of pore pressure measurements included in the field records. Based on the level of the water table at the time of the investigation the calculated in situ horizontal effective stress was unrealistically low (the in situ stress ratio would be greater than the critical state stress ratio measured in the triaxial tests). As discussed in section 4.3.1 the accuracy of the pressuremeter readings at the very low stress levels encountered in soft clays is relatively poor.

A comparison of the results of the consolidated drained and undrained triaxial tests carried out at the original site investigation were discussed in section 10.2.2. The drained strength parameters for the organic clay stratum used for the embankment design were c'=10kPa and ϕ'=23°. The equivalent critical state strength parameters based on the testing carried out at City University are c'=0 and ϕ'=29.5°. It is thought that the critical state strength parameters are more representative of the true strength of this material.

The organic clay specimens used for the Atterberg limit tests reported in the original site investigation report were dried during sample preparation. Drying the soil during sample preparation for these tests was shown, in section 8.2.1, to decrease substantially the measured values of both the plastic and the liquid limit. As discussed in section 2.6, Atterberg limit test results are often used with semi-empirical relationships to determine other engineering properties for a soil. It is recommended that soil samples which contain even small quantities of organic material be tested without drying.

CHAPTER 11 CONCLUSIONS

11.1 Soil Mechanics and Laboratory Testing

A number of investigators have proposed that the state boundary surface for a K_o compressed soil differs markedly from that of an isotropically compressed soil. As the majority of real soils are deposited under K_o conditions this factor has an important bearing on the validity of critical state soil models derived from the results of tests on isotropically compressed samples when used to model real construction events.

In the present investigation two separate test procedures were adopted to probe the state boundary surface of K_o compressed reconstituted organic clay samples. The results of these tests appear to indicate the existence of only one state boundary surface for both K_o and isotropically compressed samples. This surface has a similar shape to that predicted by the modified Cam clay soil model. A similar result was obtained from a test on a reconstituted kaolin sample.

The probing tests were performed using a constant rate of loading rather than incremental loading. Standard methods for determining the yield stress from the results of these tests, such as the Casagrande (1936) construction, were found to be inaccurate. The Lambda construction, which is appropriate for drained probing tests carried out at a constant rate of loading, has been proposed to locate the SBS yield point (the stress at which the state boundary surface is engaged). A limited number of tests has shown this construction to be both reliable and objective.

It has been demonstrated that the presence of organic matter alters the engineering properties of the soft clay stratum. Soil samples which contain even small quantities of organic material should not be dried when measuring engineering parameters for the material which are relevant for design. Despite the effects of the organic matter,

critical state concepts and in particular the modified Cam clay soil model can be used to predict the behaviour of this material in a wide variety of tests.

11.2 Modelling Embankment Construction

Finite element modelling of the EGAR embankment was carried out and predictions made of the ground deformations at five cross sections below the embankment. The results of the modelling show good agreement with the actual field measurements.

A large number of closely spaced vertical drains were installed below the embankment and only small excess pore pressures were generated during construction. As a result, drained finite element analyses were found to adequately model embankment construction. The rapid dissipation of pore pressures during embankment construction is a relatively common occurrence, particularly in cases where vertical drains have been installed. Drained analyses may therefore be relevant to a significant number of embankments constructed on soft ground.

Laboratory tests on undisturbed samples of the alluvial clay indicate that this stratum has extremely variable compression characteristics. Nevertheless, it was possible to represent this stratum in the finite element analyses using only a single set of critical state soil parameters derived from tests on reconstituted soil samples.

Determination of the preconsolidation pressure from standard oedometer and Rowe cell tests was found to be extremely difficult. Improved testing techniques, for example using a constant rate of loading, are needed to measure this parameter more accurately. The in situ stresses for the finite element analyses were determined from the results of the plate dilatometer tests and from a knowledge of the site history.

11.3 Implications of the Research and Further Work

A consistent set of critical state soil parameters have been derived for the reconstituted organic clay. This set of data can be added to the existing body of knowledge on critical state soil properties. Analysis of the commercial site investigation data within a critical state framework has lead to a better understanding of the various test results and should lead to an improved confidence in the choice of relevant design parameters. For example the difference between the end of test stress ratio measured in drained and undrained triaxial tests in the original site investigation can be explained by the use of critical state theory.

The relative simplicity and success of the finite element modelling has confirmed the potential for this type of analysis in the design process. For example, the magnitude and extent of the ground deformations at the EGAR site could have been predicted, based on a careful assessment of the initial site investigation data, using this analysis method.

The identification of a single state boundary surface for both K_o and isotropically compressed samples should improve the confidence with which critical state soil models are applied to engineering design. Further testing, using the probing and analysis techniques implemented during the present investigation, is required to confirm whether this result is valid for other soils when tested in a similar manner.

The Lambda construction has been proposed to determine a yield point in compression tests carried out at a constant rate of loading. The method was validated using samples of the organic clay which had been consolidated to known stress states. Further tests on other types of soil are required to establish the general applicability of this construction for measuring the preconsolidation pressure or yield stress of overconsolidated soil samples.

REFERENCES

REFERENCES

Almeida M.S.S., Britto A.M. and Parry R.H.G., (1986). "Numerical modelling of a centrifuged embankment on soft clay". Canadian Geot. Jnl., Vol. 23, pp 103-114.

Almeida M.S.S. and Ramalho-Ortegão J.A., (1982). "Performance and finite element analyses of a trial embankment on soft clay". Cambridge University Engineering Department, CUED/D-Soils, TR 121.

Atkinson J.H., (1973). "The deformation of undisturbed London Clay". PhD Thesis, University of London.

Atkinson J.H., (1984a). "Rate of loading in drained and undrained stress path tests". City University research report No. GE/84/1.

Atkinson J.H., (1984b). "Some procedures for normalising soil test results". City University research report No. GE/84/3.

Atkinson J.H. and Bransby P.L., (1978). "The mechanics of soils : An introduction to critical state soil mechanics". McGraw Hill, Maidenhead, England.

Atkinson J.H. and Clinton D.B., (1984). "Stress path tests on 100mm diameter samples". In: Conference on site investigation practice, Guildford. Proceedings. (Geological Society)

Atkinson J.H., Evans J.S. and Scott C.R., (1985). "Developments in microcomputer controlled stress path testing equipment for measurement of soil parameters". Ground Engineering, Vol. 18, No. 1, pp. 15-22.

Atkinson J.H., Richardson D. and Robinson P.J., (1987). "Compression and extension of K_o normally consolidated kaolin clay". ASCE, Jnl. Geot. Engng., Vol. 113, No. 12, pp 1468-1482.

Bassett R.H., Davies M.C.R. Gunn M.J. and Parry R.H.G., (1981). " Centrifugal models to evaluate numerical models". Proc. 10th Int. Conf. SM&FE, Stockholm.

BDH Limited, (1988). Private communication.

Bell A.L., (1977). "A geotechnical investigation of post-glacial estuarine deposits at Kinnegar, Belfast Lough". PhD thesis, Queen's University, Belfast.

Bishop A.W., (1966). "The strength of soils and engineering materials". Geotechnique, Vol. 16, No. 2, pp 89-130.

Bishop A.W and Henkel D.J., (1962). "The measurement of soil properties in the triaxial test". 2nd Edition, Edward Arnold.

Bishop A. W. and Wesley L.D., (1975). "A hydraulic triaxial apparatus for controlled stress path testing". Geotechnique, Vol. 25, No. 4, pp. 657-670.

Bjerrum L., (1972). "Embankments on soft ground". Proceedings, speciality conference on performance of earth and earth supported structures, Purdue University, Vol. 2, pp. 1-54.

Bowles J.E., (1968). "Foundation analysis and design". McGraw-Hill Book Co., London, p 86.

Britto A.M. and Gunn M.J., (1987). "Critical state soil mechanics via finite elements". Ellis Horwood Limited, Chichester, England.

BS 1377, (1975). "Methods of test for soils for engineering purposes". Br. Standards Institution, London.

Burland J.B., (1965). "The yielding and dilation of clay". Geotechnique, Vol. 15, pp 211-214.

Burland J.B., (1969). "Deformation of soft clay beneath loaded areas". Proc. 7th Int. Conf. on SM&FE, Mexico, pp 55-63.

Butterfield R., (1979). "A natural compression law for soils". Geotechnique, Vol. 29, No. 4, pp 469-480.

Casagrande A., (1936). "The determination of pre-consolidation load and its practical significance". Proc. 1st. Int. Conf. SM&FE., Volume 3.

Clausen C.-J.F., Graham J. and Wood D.M., (1984). "Yielding in soft clay at Mastemyr, Norway". Geotechnique, Vol. 34, No. 4, pp 581-600.

Clinton D.B., (1987). "The determination of soil parameters for design from stress path tests". PhD Thesis, City University, London.

Crooks J.H.A. and Graham J., (1976). "Geotechnical properties of the Belfast estuarine deposits". Geotechnique, Vol. 26, No. 2, pp 293-315.

Duncan J.M and Chang C.Y., (1970). "Non linear analysis of stresses and strains in soils". ASCE, Jnl. Soil Mech. Found. Div., Vol. 96, pp 1629-1653.

Duncan J.M. and Seed H.B., (1967). "Corrections for strength test data". Jnl. of soil mechanics and foundations division, ASCE, Vol. 94, SM5, pp 121-137.

Foundation Engineering Limited, (1985). "Eastern Gateway Access Road and London Industrial Park Link Road and Bridge - Report on laboratory testing - Volume 1". Foundation Engineering Limited, Report No. CF.669/2506, May 1985.

Gibson R.E. and Anderson W.F., (1961). "Insitu measurement of soil properties with the pressuremeter". Civ. Eng. Public Wks. Rev., Vol. 56, No. 658, pp. 615-618.

Golder H.Q. and Palmer D.J., (1955). "Investigation of a bank failure at Scrapgate, Isle of Sheppey, Kent". Geotechnique, Vol. 5, pp 55-73.

Graham J., (1974). "Laboratory testing of a sensitive clay from Lyndhurst, Ontario". Royal Military College of Canada, Kingston, Ontario, Civil Engineering research report CE74-2.

Graham J., Crooks J.H.A. and Lau S.L.K., (1988). "Yield envelopes : identification and geometric properties". Geotechnique, Vol. 38, No. 1, pp 125-134.

Graham J., Noonan M.L. and Lew K.V., (1983). "Yield states and stress strain relationships in a natural plastic clay". Can. Geotech. Jnl., Vol. 20, No. 3, pp 502-516.

Groundworks Ltd., (1984). "Site investigation for the Eastern Gateway Access Road and the London Industrial Park Link Road Bridge, Beckton, London". Groundworks Report No. S.200/6, December 1984.

Hansbo S., Jamiolkowski M. and Kok L., (1981). "Consolidation by vertical drains". Geotechnique Vol. 31, No. 1, pp. 45-66.

Hird C.C. and Kwok C.M.R., (1988). "Predictions for the Stanstead Abbotts trial embankment based on the finite element method". submitted for publication in Proc. Reinforced Earth symposium, King's College, London, in preparation.

Ho E.W.L., (1988). "Geotechnical properties of deep ocean sediments: a critical state approach". PhD Thesis, City University, London. (in preparation)

Hobbs N.B., (1986). "Mire morphology and the properties of some British and foreign peats". Qtly. Jnl. Eng. Geol., Vol. 19, pp 7-80

Husband and Co., (1985). "Eastern Gateway Access Road-Site investigation interpretative report". Husband and Co., Report No. L8422, March.

Kwok C.M.R., (1987). "Finite element studies of reinforced embankments on soft ground". PhD thesis, Sheffield University, England.

Lau W.H.W., (1988). "The behaviour of clay in simple shear and triaxial tests". PhD Thesis, City University, London.

Lewis W.A., Murray R.T. and Symons I.F., (1975). "Settlement and stability of embankments constructed on soft alluvial soils". Proc. Instn. Civ. Engrs., Part 2, 59, Dec., pp 571-593.

Leroueil S., (1986). "Recent developments in consolidation of natural clay". Proc. 10th Canadian Geotechnical Colloquium, Laval University, Quebec, Canada.

Leroueil S., Tavenas F., Mieussens C. and Peighaud M., (1978). "Construction pore pressures in clay foundations under embankments, Part II: Generalised behaviour". Can. Geot. Jnl., No. 15, pp 66-82.

Loxham R., (1988). PhD Thesis in preparation, City University.

Nakai T. and Matsuoka H., (1986). "A generalised elastoplastic constitutive model for clay in three-dimensional stresses". Soils and Foundations, Vol. 26, No 3.

Marchetti S., (1980). "Insitu tests by flat dilatometer". ASCE. Geo. Eng. Div., No. GT3, pp. 299-321.

Marsland A. and Powell J.J.M., (1978). "The behaviour of a trial bank constructed to failure on soft alluvium of the River Thames". Building Research Establishment, Report No. CP11/78.

Marsland A. and Randolph M.F., (1978). "A study of the variation and effects of water pressures in the pervious strata underlying Crayford Marshes". Geotechnique, Vol. 28, No. 4, pp 435-464.

Matsuoka H., (1974). "Stress-strain relationships of sands based on the mobilised plane". Soils and Foundations, Vol. 14, No. 2, pp 47-61.

Mayne P.W., (1987). "Determining preconsolidation stress and penetration pore pressures from DMT contact pressures". Geotechnical Testing Jnl., GTJODJ, Vol. 10, No. 3, pp 146-150.

Mitchell K.J., (1976). "Fundamentals of soil behaviour". John Wiley and Sons, New York, pp 175-178.

Nakai T. and Matsuoka H., (1987). "Elastoplastic analyses of embankment foundations". Proc. 8th Asian Reg. Conf on SM&FE, Kyoto, Japan.

Odell R.T., Thornburn T.H. and McKenzie L.J., (1960). "Relationships of Atterberg limits to some other properties of Illinois soils". Proc. of the Soil Science Society of America, Vol. 24, No. 4, pp 297-300.

Palmer A.C., (1972). "Undrained plane strain expansion of a cylindrical cavity in clay : a simple interpretation of the pressuremeter test". Geotechnique, Vol. 22, No. 3, pp 451-457.

Parry R.H.G and Nadarajah V., (1973). "A volumetric yield locus for lightly overconsolidated clay". Geotechnique, Vol. 23, No. 3, pp 450-453.

Pender M.J., (1978). "A model for the behaviour of overconsolidated soil". Geotechnique, Vol. 28, No. 1, pp 1-25.

Pickles A.R., (1988a). "Transfer of triaxial test data from the BBC to the IBM microcomputer". City University research report No. GE/88/7.

Pickles A.R., (1988b). "TRILOG3 Triaxial data logging and control programme". City University research report No. GE/88/12.

Pickles A.R., (1988c). "The EGAR embankment monitoring results". City University research report No. GE/88/24.

Pickles A.R. and Horrocks L., (1988). "An investigation of the properties of soils with low percentage organic matter content". City University research report No. GE/88/25.

PM Insitu Techniques, (1984). "London Docklands - Results of self-boring pressuremeter tests and dilatometer tests". PM Insitu Report No. T78-R1.

Powell J.J.M. and Uglow I.M., (1988). "The interpretation of the Marchetti dilatometer test in UK clays". Building Research Establishment, report in preparation.

Richardson D., (1986). "Effect of membrane and filter stiffness on the stress-strain behaviour of triaxial samples". City University research report No. GE/86/4.

Richardson D., (1988). "Investigations of threshold effect on soil deformations". PhD Thesis, City University, London.

Rowe P.W. and Barden L., (1966). "A new consolidation cell". Geotechnique, Vol. 16, No. 2, pp. 162-170.

Schofield A.N. and Wroth C.P., (1968). "Critical state soil mechanics". McGraw-Hill Book Co., London.

Simon R.M., Ladd C.C. and Christian J.T., (1972). "Finite element programme FEECON for undrained analysis of granular embankments on soft clay foundations". MIT research report No. 72-9.

Shibata T., Tominaga M and Matsuoka H., (1976). "FE analysis of soil movements below a test embankment". 2nd Int. Conf. on Num. Methods in Geomechanics, Virginia, USA.

Skempton A.W., (1957). "Discussion on planning and design of the new Hong Kong airport". Proc. Instn. Civil Engrs., Vol. 7, p 306.

Skempton A.W. and Petley D.J., (1970). "Ignition loss and other properties of peats and clays from Avonmouth, King's Lynn and Cranberry Moss". Geotechnique, Vol. 20, No. 4, pp 343-356.

Smith I.M. and Hobbs R., (1976). "Biot analysis of consolidation beneath embankments". Geotechnique, Vol 26, No. 1, pp 149-171.

Soils Engineering Ltd., (1987). "Report on a site investigation on Gaslands north of Royal Docks Beckton". Soils Engineering Ltd., Report No. C.3702, April.

Soils Engineering Ltd., (1985). "Report on in-situ vane testing for the proposed Eastern Gateway Access Road". Soils Engineering Ltd., Report No. C.3339, May.

Stallebrass S.E., (1988). "Short term memory effects in overconsolidated clays" City University research report No. GE/88/26.

Tavenas F., Des-Rosiers J.P., Leroueil S., La Rochelle P. and Roy M., (1979). "The use of strain energy as a yield and creep criterion for lightly overconsolidated clays". Geotechnique, Vol. 29, No. 3, pp 285-304.

Tavenas F. and Leroueil S., (1977). "The effects of stresses and time on yielding of clays". Proc. 9th Int. Conf. Soil Mech. Fdn. Engng., Tokyo 1, pp 319-326.

Thoms R.L., Pecquet R.A. and Arman A., (1976). "Numerical analyses of embankments over soft soils". Proc. 2nd Int. Conf. on Numerical Methods in Geomech., Virginia, USA.

Wheatley R.J., (1984). "The consolidation properties of reconstituted kaolin clay". City University, Final year undergraduate project report.

Windle D. and Wroth C.P., (1977). "The use of a self-boring pressuremeter to determine the undrained properties of clays". Ground Engineering, Vol. 10, No. 1.6, pp 37-46.

Wroth C.P., (1975). "In-situ measurement of initial stresses and deformation characteristics" Proc. of the Speciality Conf. In-situ Measurement of Soil Properties, ASCE, Rayleigh, North Carolina, pp 181-230

Wroth C.P., (1977). "The predicted performance of soft clay under a trial embankment loading based on the Cam-clay model". In : Finite elements in geomechanics, John Wiley and sons, New York, pp 191-208.

Wroth C.P., (1984). "The interpretation of in situ tests". Geotechnique, Vol. 34, No. 4, pp 449-489.

Zytynski M., Randolph M.F., Nova R. and Wroth C.P., (1978). "Modelling the unloading-reloading behaviour of soils". Short communication, Int. J. Num. Anal. Meth. in Geomech., No. 2, pp 87-94.

TABLES

Site	Water content %	Liquid limit %	PI %	Activity	OCR
1 Rang de Fleuve	80	70	50	-	1.0-1.2
2 Belfast (a)	35-55	40-60	20-40	0.6	1.6-2.0
2 Belfast (b)	60-80	75-110	50-70	1.5	1.2-1.8
3 Winnipeg	54-63	65-85	35-60	0.67	2.4
4 St. Alban	90	50	23	0.38	2.2
5 Lyndhurst	45	36	13-16	0.25	1.5
6 Mastemyr	40	26	5-13	-	1.2

Reference:-

1 Tavenas et al., 1979

2a Bell, 1977

2b Crooks & Graham, 1976

3 Graham et al., 1983

4 Tavenas & Leroueil, 1977

5 Graham, 1974

6 Clausen et al., 1984

Table 2.1 Classification data for clay yield envelopes on Figure 2.4 (after Graham et al., 1988)

Borehole/ Test No.	Depth m	Total Lateral Stress kN/m^2	Shear Modulus MN/M^2	Cv (*1) m^2/Yr	Cu (*2) kN/m^2	Cu (*3) kN/m^2
SBP5/1	4.3	55	2.2		34	35
SBP5/2	5.3	60	1.9	57	37	42
SBP5/3	6.3	60	3.0		31	35
SBP7/1	1.0	35	2.7		15	16
SBP7/2	2.0	20	2.5	31	36	42
SBP7/3	3.1	20	1.0		20	17
SBP10/1	1.0	25	1.8		19	
SBP10/2	2.0	40	.9	50	50	
SBP10/3	3.0	40	.5		8	

Notes

(*1) Coefficient of consolidation from holding test

(*2) Cu using Gibson and Anderson (1961) method

(*3) Cu using Palmer (1972) method

Table 4.1 Summary of pressuremeter test results

Borehole	Depth m	Permeability m/s
5	3.6	1.20E-08
7	2.5	4.90E-10

Table 4.2 Summary of in situ permeability test results

Borehole	Depth m	Moisture Content %	Liquid Limit %	Plastic Limit %	Organic Content %
3	5.1		60	42	
4	4.5	60	71	39	
5	5.7	73	54	37	
6	1.0	58	70	42	3.2
6	2.0				5.4
6	3.7	60	42	18	
7	.1	44	60	41	
7	1.6	38	52	29	
7	3.6	44	36	19	
8	.1	35	66	42	
8	1.6	51	61	31	
9	.1	27	62	42	
9	1.6	38	66	24	
9	2.6	32	25	16	
11	1.0	35	59	42	
11	2.0	156	78	65	

Table 4.3 Summary of index properties, Groundworks (1984)

Borehole	Depth m	Sample Description	Pressure kN/m^2	Mv m^2/MN	Cv m^2/Yr	Permeability m/s
5/1	3.4	Organic Clay	0-25	3.40	1.2	1.29E-09
			25-50	2.20	.4	2.79E-10
			50-100	1.80	.2	1.31E-10
			100-200	1.10	.2	7.32E-11
			200-50	.25	.6	4.44E-11
5/3	4.75	Silty Clay	0-22	1.90	4.4	2.65E-09
			22-54	1.00	4.1	1.30E-09
			54-107	1.00	1.5	4.76E-10
			107-214	.84	1.0	2.66E-10
			214-429	.49	1.0	1.52E-10
6/4	3.5	Organic Clay	0-21	2.90	2.4	2.21E-09
			21-54	2.20	.7	4.53E-10
			54-107	2.00	.3	2.16E-10
			107-215	1.10	.2	5.93E-11
			215-429	.82	.1	3.12E-11
7/1	1.75	Silty Clay	0-27	.80	2.0	5.07E-10
			27-54	.51	2.0	3.23E-10
			54-107	.34	2.5	2.70E-10
			107-214	.21	3.7	2.46E-10
			214-428	.19	1.9	1.14E-10
7/2	2.75	Peat	0-25	2.50	19.0	1.51E-08
			25-50	1.70	10.0	5.39E-09
			50-100	1.90	3.6	2.17E-09
			100-200	1.30	1.3	5.36E-10
			200-400	.85	.6	1.67E-10
7/3	3.50	Peat	0-27	2.00	8.5	5.39E-09
			27-54	1.80	13.0	7.42E-09
			54-107	.98	7.6	2.36E-09
			107-215	1.70	.6	3.34E-10
			215-429	.94	.5	1.37E-10
9/4	2.25	Peat	0-22	.82	20.0	5.20E-09
			22-54	.52	18.0	2.97E-09
			54-107	.42	17.0	2.26E-09
			107-215	.71	12.0	2.70E-09
			215-429	.74	.7	1.57E-10

Table 4.4 Summary of oedometer test results

Borehole	Depth m	Description	Pressure kN/m^2	Mv m^2/MN	Cv m^2/Yr P.W.P	Cv m^2/Yr Vol	Permeability m/s
5/1	3.5	Organic Clay	0-25	1.30	2.9	.9	1.20E-09
			25-50	2.40	.9	.5	7.15E-10
			50-100	1.60	.6	.4	2.79E-10
			100-200	1.10	.4	.3	1.43E-10
			200-50	.15	1.4	1.5	6.66E-11
5/2	4.3	Organic Clay	0-25	.64	177.0	663.0	3.59E-08
			25-50	.53	36.0	41.0	6.05E-09
			50-100	.50	14.0	7.8	2.22E-09
			100-200	1.30	2.6	1.5	1.07E-09
			200-400	.76	1.2	1.1	2.89E-10
5/3	5.3	Organic Clay	0-25	1.40	8.0	17.0	3.55E-09
			25-50	.85	3.5	8.3	9.43E-10
			50-100	.92	3.3	2.0	9.63E-10
			100-200	1.00	1.3	1.2	4.12E-10
			200-50	.12	1.0	3.7	3.81E-11
5/5	6.2	Organic Clay	0-25	.49	500.0	500.0	7.77E-08
			25-50	.64	476.0	85.0	9.66E-08
			50-100	.48	13.0	6.6	1.98E-09
			100-200	1.18	2.4	4.1	8.98E-10
			200-50	.15	30.0	4.6	1.43E-09
7/2	3.0	Peat	0-25	1.49	188.0	95.0	8.88E-08
			25-50	3.02	621.0	169.0	5.95E-07
			50-100	2.63	132.0	108.0	1.10E-07
			100-200	1.97	65.0	37.0	4.06E-08
			200-50	.35	30.0	13.0	3.33E-09
7/3	3.5	Clayey Peat	0-25	2.90	22.0	88.0	2.02E-08
			25-50	2.60	2.7	1.3	2.23E-09
			50-100	1.80	2.6	2.2	1.48E-09
			100-200	1.40	1.3	.9	5.77E-10
			200-50	.21	2.0	1.2	1.33E-10

Table 4.5 Summary of Rowe cell test results

Borehole	Depth m	Test type	Preconsolidation Pressure kPa
	North of the NOS		
7	-3	Rowe	74
7	-3.5	Rowe	81
10	-1.2	Oedometer	100
10	-2.8	Oedometer	49
11	-2.3	Oedometer	55
6	-3.5	Oedometer	80
7	-1.75	Oedometer	200
7	-2.75	Oedometer	80
9	-2.25	Oedometer	140
	South of the NOS		
5	-3.5	Rowe	76
5	-4.3	Rowe	93
5	-5.3	Rowe	81
5	-6.2	Rowe	95
5	-3.4	Oedometer	101
5	-4.7	Oedometer	121
5	-4.2	Oedometer	140

Table 4.6 Preconsolidation pressure from Rowe cell and oedometer

Sources of Inaccuracies	Deviator Stress kPa	Pore/Cell pressure kPa	Axial strain %	Volume strain %
Hysteresis	1.5	0.5	0.01	(Note 1)
Drift	1.0	0.5	0	0.01
Noise	0.5	0.5	0.005	0.005
Overall	3.0	1.5	0.015	0.015
Resolution (Note 2)				
Spectra	0.2	0.2	0.005	0.003
BBC	0.5	0.2	0.02	0.02

Table 6.1 Typical values of inaccuracies and resolutions for measurements with the 38mm stress path cell

Sources of Inaccuracies	Deviator Stress kPa	Pore/Cell pressure kPa	Axial strain %	Volume strain %
Hysteresis	0.5	0.5	0.005	(Note 1)
Drift	0.3	0.5	0	0.005
Noise	0.2	0.5	0.002	0.002
Overall	1.0	1.5	0.007	0.007
Resolution	0.1	0.2	0.01	0.005

Table 6.2 Typical values of inaccuracies and resolutions for measurements with the 100mm stress path cell

Note 1 See section 6.4.2

Note 2 Resolution depends on voltage output
Typical values quoted

Borehole	Depth m	Quantity kg
BM1	4.8	1.5
BM1	5.8	1.5
2A	6.3	1.5
6	6.5	1.0
13	5.0	1.0
18	3.0	1.5
23	3.3	1.0
28	1.4	1.0
30	4.2	1.0
34	4.2	1.0
47	2.2	1.0

Table 6.3 Soil samples used in the reconstituted sample

Liquid Limit	95
Plastic Limit	42
Plasticity Index	53
Organic Content	3.2%
% passing 0.063mm	55%
% passing 0.002mm	25%
Specific Gravity	2.66

Table 6.4 Index properties of the reconstituted sample

Borehole /Sample	Depth m	Organic Content %	Liquid Limit %	Plastic Limit %	P.I.	Sample Preparation
18	5.5	4.1	66	31	35	Dried
18	5.5	4.1	89	39	50	Natural
7	4.0	4.2	78	34	44	Dried
7	4.0	4.2	113	40	73	Natural
6	5.5	1.8	54	27	27	Dried
6	5.5	1.8	86	30	56	Natural
Org2		2.0	59	25	34	Dried
Org2		2.0	88	31	57	Natural
Org10		10.0	64	32	31	Dried
Org10		10.0	114	47	66	Natural
11	4.3	5.7	76	40	36	Dried
11	4.3	5.7	122	44	78	Natural
18	2.5	3.8	59	35	24	Dried
18	2.5	3.8	88	41	47	Natural
Average	All		65	32	35	Dried
Average	All		100	39	61	Natural

Table 7.1 Summary of the effect of drying during sample preparation on the measured Atterberg limits

Borehole /Sample	Depth m	Organic Content %	Liquid Limit %	Plastic Limit %	P.I.	Sample Preparation
6	5.5	1.8	86	30	56	Distilled
6	5.5	1.8	85	31	54	Site water
3	5.0	3.8	99	36	63	Distilled
3	5.0	3.8	99	35	64	Site water
6	7.0	3.6	93	39	54	Distilled
6	7.0	3.6	94	38	56	Site water

Table 7.2 Summary of the effect of using site ground/ distilled water on the measured Atterberg limits

Borehole /Sample	Depth m	Organic Content %	Liquid Limit %	Plastic Limit %	P.I.	Drying Temperature Celcius
16	4.5	5.4	83	32	51	105
16	4.5	5.4	83	32	51	70
6	5.5	1.8	85	31	54	105
6	5.5	1.8	84	31	53	70
7	4.0	4.2	113	40	73	105
7	4.0	4.2	115	41	74	70

Table 7.3 Summary of the effect of drying temperature on the measured Atterberg limits

Sample	Organic Content %	Liquid Limit %	Plastic Limit %	P.I.
Org2	2	88	31	57
Org4	4	91	33	58
Org6	6	96	36	60
Org8	8	110	40	70
Org10	10	114	47	67

Table 7.4 Summary of the effects of different organic contents on the measured Atterberg limits

Borehole /Sample	Depth m	Specific Gravity
3	4.5	2.63
18	3.0	2.63
33A	3.2	2.62
16	4.5	2.65
MIX		2.66
BOX		2.66
Org2		2.72
Org4		2.70
Org6		2.62
Org8		2.56
Org10		2.53
Embankment Fill		2.65

Table 7.5 Summary of Specific Gravity determination tests

Sample	Organic Content	P.I.	N	Lambda
Org2	2	57	4.06	0.31
Org4	4	58	3.89	0.27
Org6	6	60	3.91	0.27
Org8	8	70	4.43	0.33
Org10	10	67	4.52	0.33
Org2*	2	34	3.56	0.25
Org10*	10	31	3.74	0.29

* Sample dried during prepararion

Table 7.6 Summary of consolidation test data for samples with varying organic content

Sample	Borehole	Depth m	Iso/Ko Comp	Rate kPa/Hr	Sig *1 V max kPa	Test Stages	Initial Sp Vol
U061	6	6.5	Iso	3	100	1	2.787
U062	6	6.5	Iso	6	200	1-2	2.876
U063	6	6.5	Iso	10	500	3-6	2.823
U161	16	4.5	Iso	4	300	1-4	3.050
U064	6	4.5	Ko	3	130	1-3	3.290
U121	12	4.2	Ko	3	200	1-2	3.580
U122	12	4.2	Ko	3	150	1	3.670
U171	17	2.8	Ko	3	400	2-6	2.334
U174	17	2.6	Iso	5	200	2	2.068
F031	3	4.5	Ko	1	230	3-5	2.894
U181	18	3.0	Ko	5	400	1	2.095
U182	18	3.0	Iso	5	300	1	2.158
UBM6	BM6	6.5	Iso	2	190	1-2	2.850
F481	48	2.8	Iso	1	200	1-3	6.00
U421	42	2.8	Ko	5	220	1-2	7.46
F301	30	4.4	Ko	1	200	1-2	2.895
U342	34	3.9	Iso	2	100	1	5.62
U341	34	4.3	Ko	5	200	1	3.941

*1 Maximum axial effective stress during consolidation

Table 7.7 Compression test data for organic clay piston samples

Sample	Final Sp Vol	Lambda	Kappa	N or N_o *1	SBS Yield Stress *2 kPa	Ko *3
U061	2.591					
U062	2.420	0.31		4.08	61	
U063	2.283	0.31	0.07	4.07	69	
U161	2.430	0.40	0.06	4.24	52	0.52
U064	2.890	0.42	0.08	4.89	60	0.57
U121	3.168	0.46	0.08	5.21	50	0.46
U122	3.150	0.46		5.16	43	0.47
U171	2.152	0.14	0.02	2.82	120	0.56
U174	1.953					
F031	2.443	0.32		4.06	55	0.52
U181	1.909	0.16		2.78	110	0.63
U182	1.936	0.15		2.79	117	
UBM6	2.715					
F481	4.77	1.00	0.02	10.00	69	
U421	5.43	1.33		11.80	37	0.37
F301	2.457	0.35		4.19	31	0.46
U342	4.62					
U341	3.117	0.57		5.99	39	0.43

*1 N for isotropically compressed samples otherwise N_o

*2 Determined by the Lambda construction (see Section 3.2)

*3 At the end of the compression stage

Table 7.8 Summary of compression test results on organic clay piston samples

Sample	Borehole	Depth m	Diameter mm	*1 Test Type	Specific Volume	*2 Sig V max kPa	Test Stages
FB1	BM1	4.9	100	UUC S	3.111	30	1
U061	6	6.7	38	CUCIS	2.591	100	3,4
U062	6	6.7	38	CUCIS	2.420	200	3,4
U063	6	6.7	38	CUCIS	2.283	500	7-9
U211	11	3.4	38	CUCIS	4.600	65	3,4
U172	17	2.8	38	CUCKS	2.089	50	3,4
U173	17	2.8	38	CUEIS	1.984	50	3-6
U174	17	2.8	38	CUCIS	1.953	200	4-6
F031	3	4.5	100	CUCKS	2.443	230	6,7
U181	18	3.0	38	CUCKS	1.909	400	2
U182	18	3.0	38	CUCIS	1.936	300	2,3
F301	30	4.4	100	CUCKS	2.457	200	3,4

*1 Test type = ABCDE
- A U=Unconsolidated C=Consolidated
- B U=Undrained
- C C=Compression E=Extension
- D I=Isotropically K=Ko compressed sample
- E S=Shearing stage

*2 Maximum axial effective stress during consolidation

Table 7.9 Details of shearing stages on organic clay piston samples

Sample	*1 OCR	q' Peak kPa	Shear Strain Peak %	p' Ult kPa	q' Ult kPa	Shear Strain Ult %	q'/p' Ult
FB1	?	36	3	22	30	20	1.36
U061	1	76		62	75	12	1.21
U062	1	120	12	94	118	15	1.26
U063	10	145	10	110	139	20	1.26
U211	?	50	12	36	50	19	1.39
U172	?	79		53	79	15	1.49
U173	?	-106	-5	82	-71	-13	-0.86
U174	1	186	5	124	180	15	1.45
F031	1	139	4	90	98	19	1.09
U181	1	250	12	202	240	19	1.19
U182	1	233	12	186	226	19	1.22
F301	1	122	1	69	96	20	1.39

*1 Sample assumed to have been compressed to a normally compressed state

Table 7.10 Summary of results of shearing stages on organic clay piston samples

Test	Compression Stage	p'max	q'max	Spec. Volume	Swelling Stage	p'min	q'min	Spec. Volume
MIX1	1	69	28	2.704	2	30	0	2.756
MIX1	3	217	108	2.387	4	27	-11	2.549
MIX2	1	96	-12	2.637				
MIX3	1	105	49	2.593				
MIX4	1-2	203	128	2.383				
MIX5	2-3	311	190	2.260				
MIX6	2-3	311	191	2.276				
MIX7	1	137	77	2.509	2	84	24	2.529
MIX8	1	132	84	2.539				
MIX10	1	205	125	2.420	2	72	5	2.483
MIX11	1	296	-12	2.357				
MIX12	1	77	-10	2.730				
MIX13	1	246	-12	2.416	2	50	0	2.510
MIX13	3-4	496	-12	2.232	5	50	0	2.389
MIX14	1	496	-12	2.223				
MIX15	1	196	-12	2.474				
BOX2	1	196	-12	2.413	2	100	0	2.439
BOX3	1	296	-12	2.315	2	200	0	2.326
BOX3	6	400	0	2.245				
BOX4	1	137	76	2.501	2	96	61	2.522
BOX5	1	140	90	2.431				
BOX6	1	203	128	2.374				
BOX7	1-2	70	45	2.592				
BOX7	3	270	45	2.264				
BOX8	1	143	86	2.455	2-3	84	12	2.477
BOX8	4	300	0	2.306				
BOX9	1	136	78	2.498	2	60	-30	2.555
BOX9		300	150	2.288				
KKE1	1-2	151	73	2.237				

Table 7.11 Summary of compression and swelling test results on reconstituted organic clay samples

Test	Stages	Shearing Stage Description *1		p'ult kPa	q'ult kPa	Shear Strain %	Spec. Volume
MIX3	2-3	Undr. Comp.	(Ko 1)	60	74	16.3	2.593
MIX4	3-4	Undr. Comp.	(Ko 1)	127	160	14.5	2.383
MIX5	4-6	Undr. Comp.	(Ko 1)	206	240	16.3	2.260
MIX6	4-5	Undr. Ext. *1	(Ko 1)	206	-195	-14.0	2.276
MIX7	3-4	Const p' Comp.	(Ko 2)	80	95	17.4	2.518
MIX8	2-3	Undr. Ext. *1	(Ko 1)	83	-82	-14.8	2.539
MIX10	3-4	Undr. Comp.	(Ko 4)	92	127	17.4	2.483
MIX11	2-3	Undr. Comp.	(Iso 1)	153	185	19.6	2.357
MIX12	2-3	Undr. Comp.	(Iso 1)	36	52	22.3	2.722
MIX13	6-8	Undr. Comp.	(Iso10)	106	138	22.3	2.389
MIX14	2-3	Undr. Comp.	(Iso 1)	251	288	22.3	2.223
MIX15	2-3	Undr. Ext. *1	(Iso 1)	142	-112	-18.2	2.474
BOX2	3-6	Dr. Comp.	(Iso 2)	158	173	22.3	2.313
BOX3	3-4	Const p' Comp.	(Iso1½)	195	176	3.3	2.312
BOX3	7-8	Const p' Comp.	(Iso 1)	399	426	22.3	2.111
BOX4	3	Undr. Ext. *1	(Ko 1)	102	-54	-3.84	2.522
BOX4	5	Const q' Comp.	(Ko 1)	173	-54	-.4	2.454
BOX4	6-8	Undr. Ext. *1	(Ko 1)	132	-116	-10.8	2.454
BOX5	2	Dr. Ext. *2	(Ko 1)	210	0	-1.0	2.353
BOX5	4-5	Undr. Comp.	(Iso 1)	130	151	16.6	2.353
BOX6	2	Dr. Ext. *3	(Ko 1)	350	-3	-1.1	2.304
BOX6	3	Const p' Ext.	(Ko 1)	350	-156	-3.8	2.259
BOX6	4	Dr. Ext. *1	(Ko 1)	316	-257	-20.8	2.209
KKE1	3	Dr. Ext. *3	(Ko 1)	241	-17	-.8	2.177
KKE1	4	Const p' Ext.	(Ko 1)	241	-95	-4.0	2.138
KKE1	5	Dr. Ext. *1	(Ko 1)	221	-163	-16.1	2.121

Key:- (Ko 1) = One dimensionally compressed OCR 1
(Iso 2) = Isotropically compressed OCR 2
*1 = Decreasing axial stress
*2 = Increasing radial stress
*3 = Change in q'/Change in p' = -1

Table 7.12 Summary of shearing stages performed on reconstituted organic clay samples

Test	Loading Type	p' Actual kPa	p' Lambda Method kPa	p' Casagrande Method kPa	p' Bi-linear Method kPa
MIX1	Ko	70	73	92	87
MIX13	Isotropic	250	261	272	280
U063	Isotropic	150	150	200	173
U161	Ko	50	53	57	50
U171	Ko	135	148	159	149
K7	Isotropic	255	245	300	235
37	Isotropic	320	290	350	330

Test K7 on recostituted kaolin, Wheatley (1984)

Test 37 on reconstituted Woolwich and Reading clay, Loxham (1988)

Table 8.1 Determination of the SBS yield point Summary of results

Test	p'max	Specific Volume	p'min	Specific Volume	Max R_p	Kappa (Ave)
MIX1	69	2.704	30	2.756	2.3	.062
MIX1	217	2.387	27	2.549	8.0	.078
MIX7	137	2.509	84	2.529	1.6	.041
MIX10	205	2.420	72	2.483	2.8	.060
MIX13	246	2.416	50	2.510	4.9	.059
MIX13	496	2.232	50	2.389	9.9	.068
BOX2	196	2.413	100	2.439	2.0	.039
BOX3	296	2.315	200	2.326	1.5	.028
BOX4	137	2.501	96	2.522	1.4	.059
BOX8	143	2.455	84	2.477	1.7	.041
BOX9	136	2.498	60	2.555	2.3	.070

Table 8.2 Summary of κ values determined for tests on reconstituted organic clay samples

Parameter	Value
λ	.27
κ	.054
N	3.9
N_o	3.84
Γ	3.72
M_c	1.17
M_e	-.85
ν'	.25

Table 8.3 Critical state parameters determined for the reconstituted organic clay

Material		Organic Clay		Embankment Fill	Made Ground
Soil Model		Modified Cam clay		Elastic Plastic	Elastic Plastic
Property *1 P(1)	κ	0.054	E kN/m2	20000	5000
P(2)	λ	0.27	ν'	0.25	0.25
P(3)	$\Gamma-1$	2.72	c' kN/m2	0.0	0.0
P(4)	M	1.17	ϕ Degrees	37.0	30.0
P(5)	ν'	0.25	-	0	0
P(6)	-	0	Yield Criterion	Mohr/ Coulomb	Mohr/ Coulomb
P(7)	Kw kN/m2	100000	Kw kN/m2	100000	100000
P(8)	Density kN/m3	16.0	Density kN/m3	17.0	15.0
P(9)	Kx m/s	0	Kx m/s	0	0
P(10)	Ky m/s	0	Ky m/s	0	0

Kw = Bulk modulus of water

Kx = Permeability in X direction

Ky = Permeability in Y direction

*1 Parameter used in CRISP programme

Table 9.1 Soil Parameters used in the finite element analyses

Instrument Section	Centreline Settlement		
	*1 Predicted at Design Stage m	Finite Element Prediction m	Actual m
EE	0.84	0.59	0.62
DD	1.00	0.57	0.62
AA	0.70	0.38	0.37

*1 Husband and Co. (1985)

Table 10.1 Comparison of predicted and actual centreline settlements

FIGURES

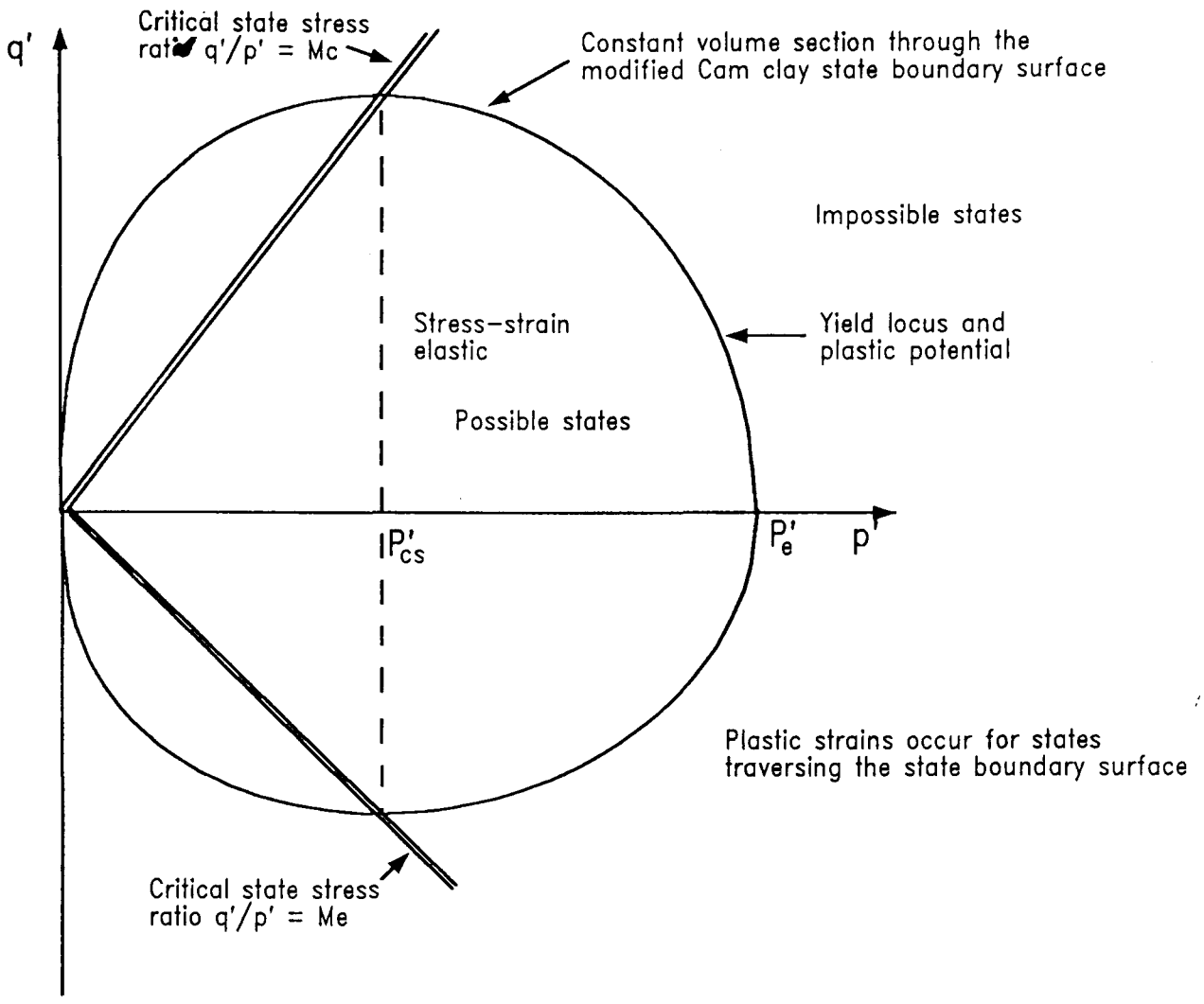

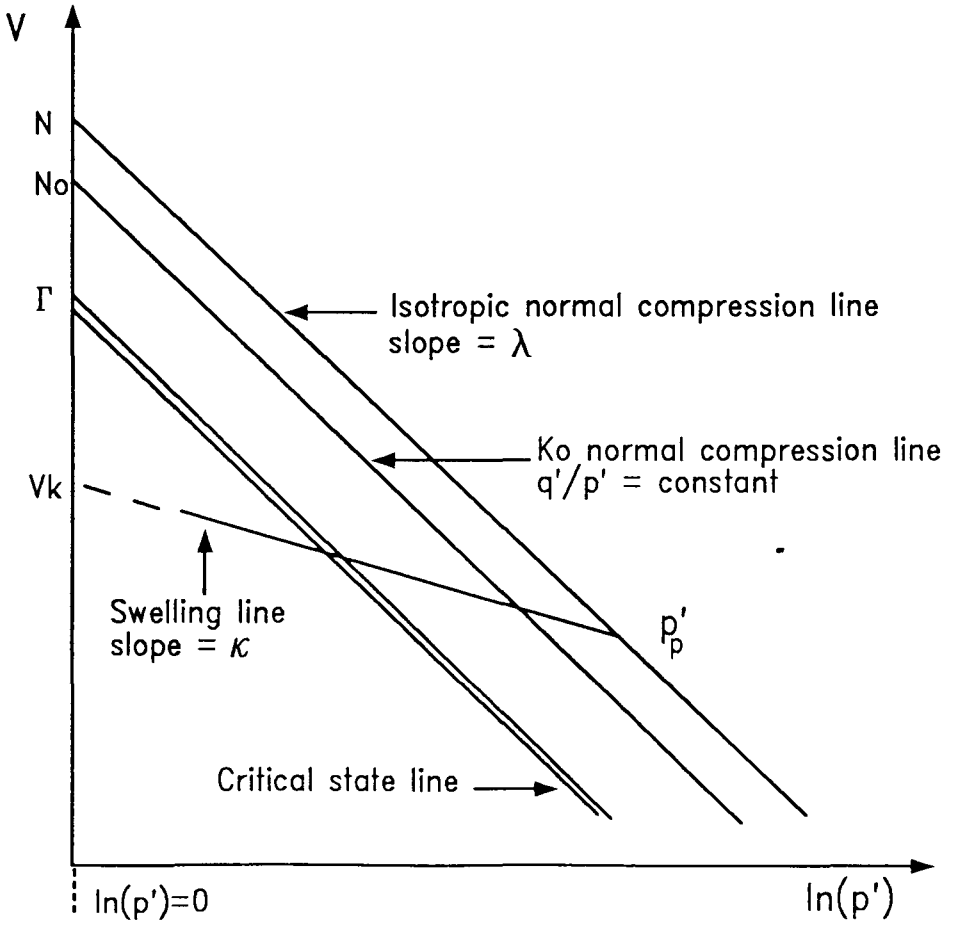

Figure 2.1 Basic critical state parameters and concepts

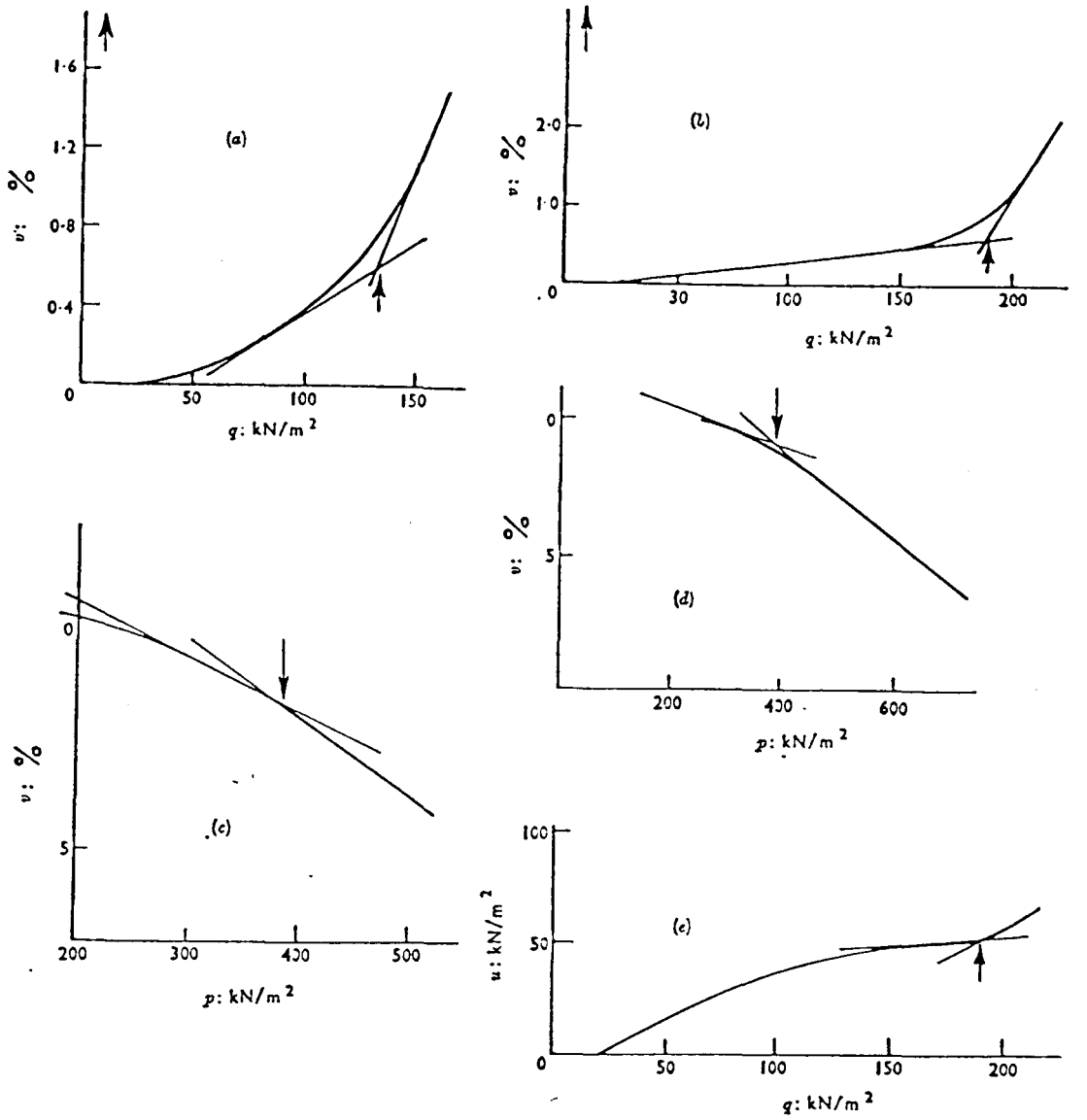

Figure 2.2 Determination of yield points using the Bi-linear method (after Parry and Nadarajah, 1973)

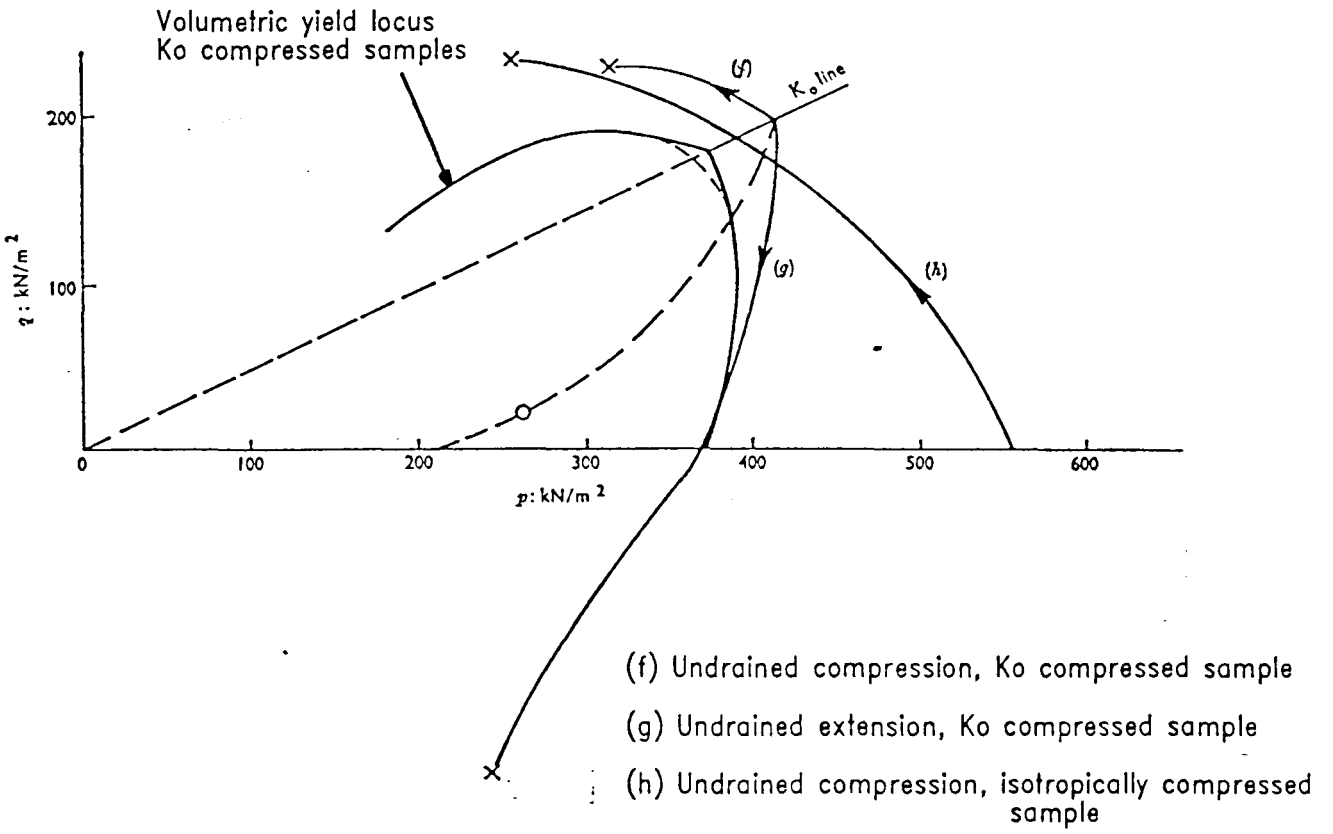

Figure 2.3 Volumetric yield locus and undrained stress paths (after Parry and Nadarajah, 1973)

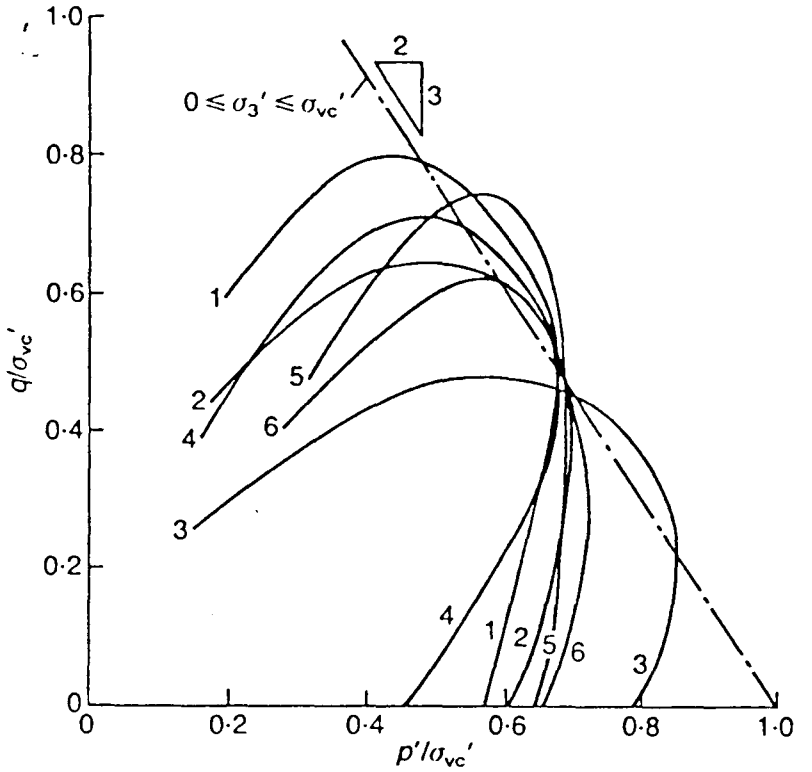

Figure 2.4 Examples of normalised yield envelopes for the various sites listed in Table 2.1 (after Graham et al., 1988)

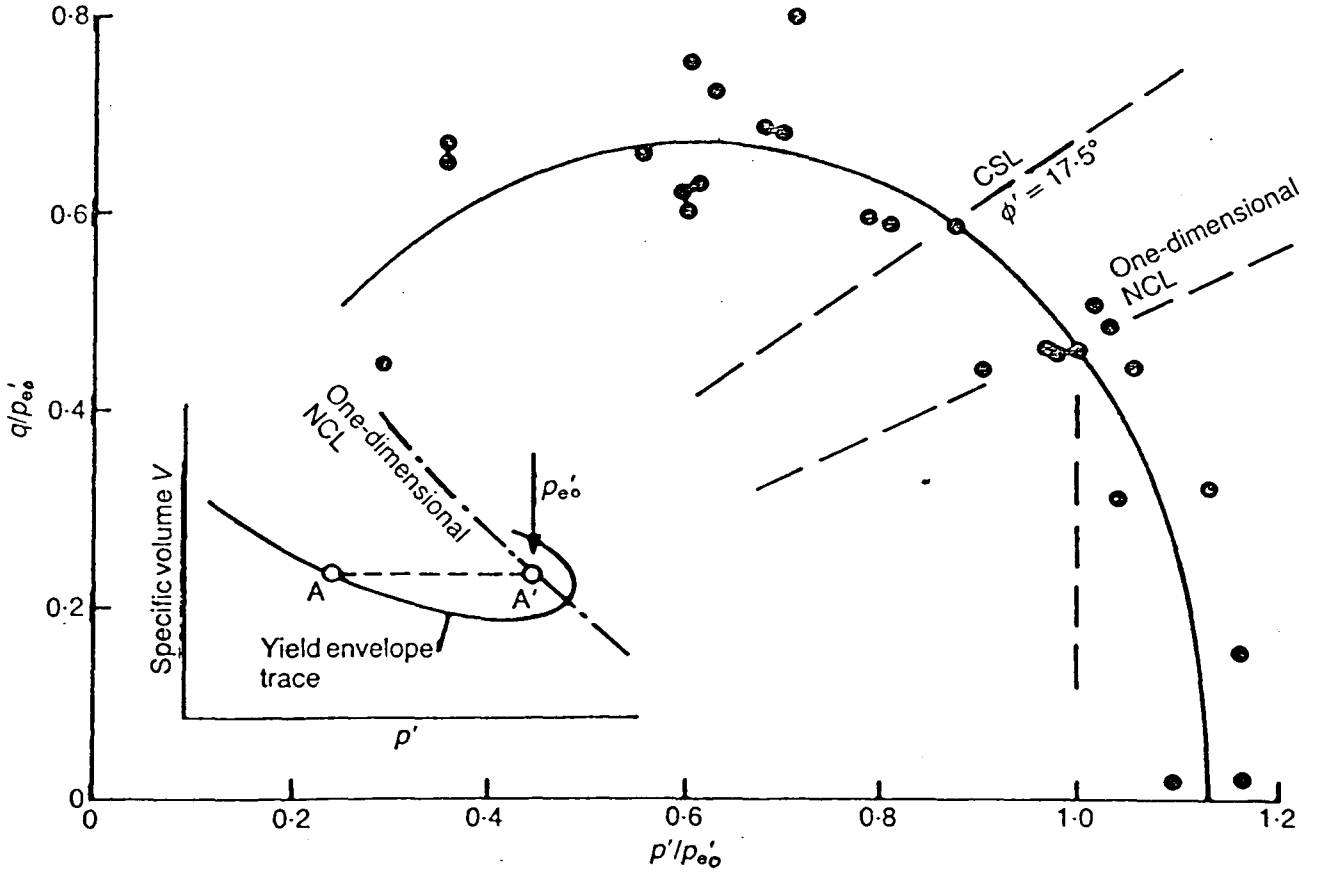

Figure 2.5 Yield envelope for natural Winnipeg clay normalised by the equivalent pressure p_{eo}' on the one-dimensional NCL for the field deposit (after Graham et al., 1988)

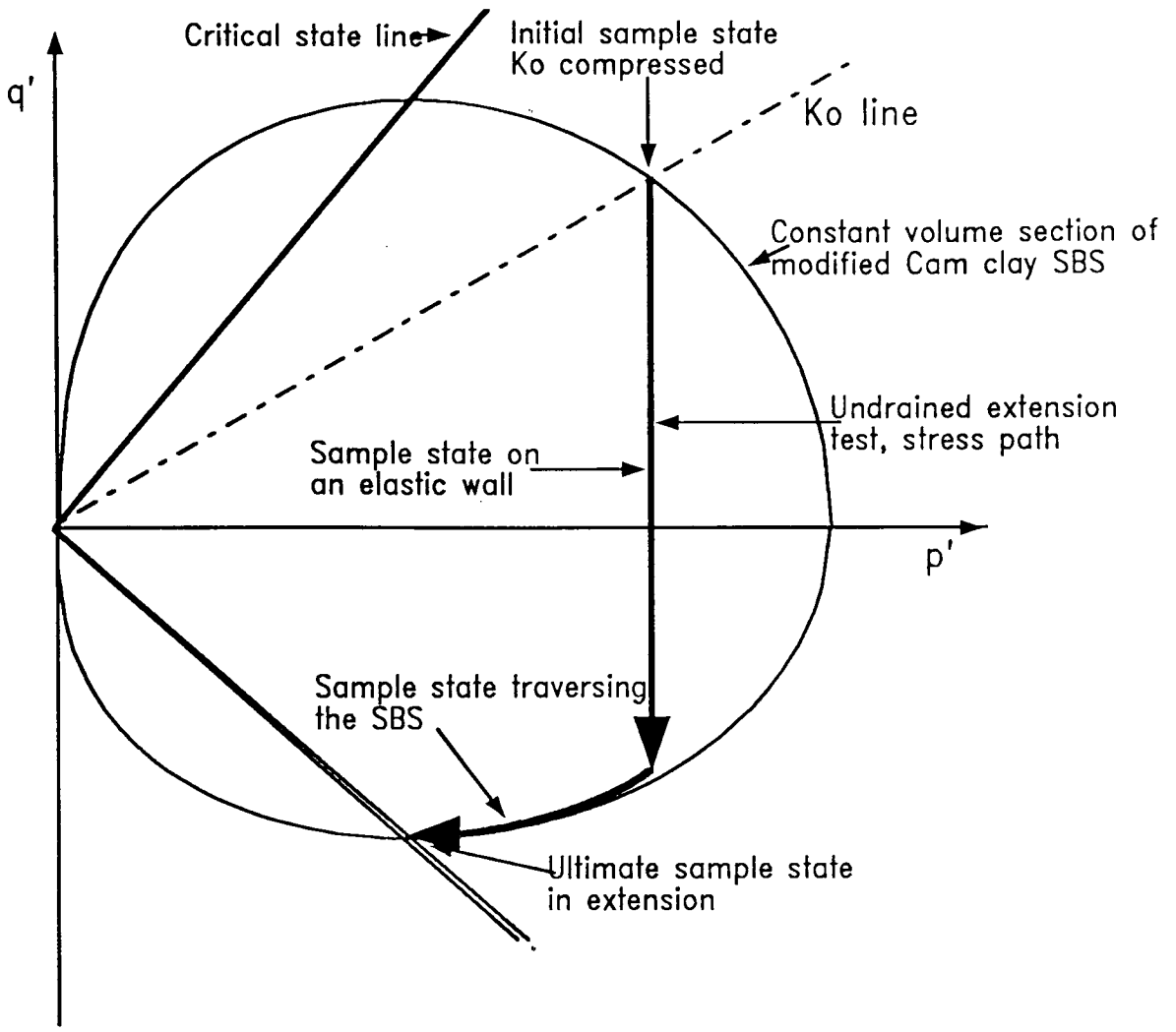

Figure 2.6 Stress path predicted by critical state soil mechanics for an undrained extension test on a Ko compressed sample

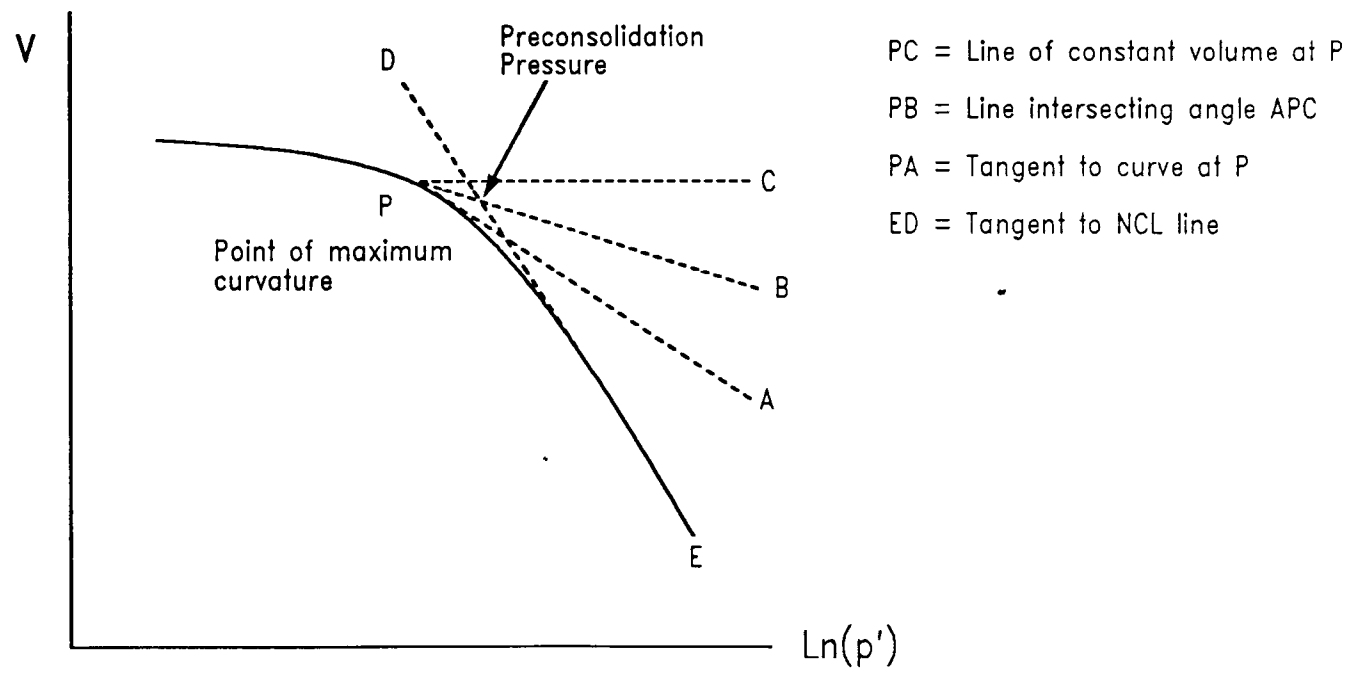

Figure 2.7 The Casagrande (1936) construction

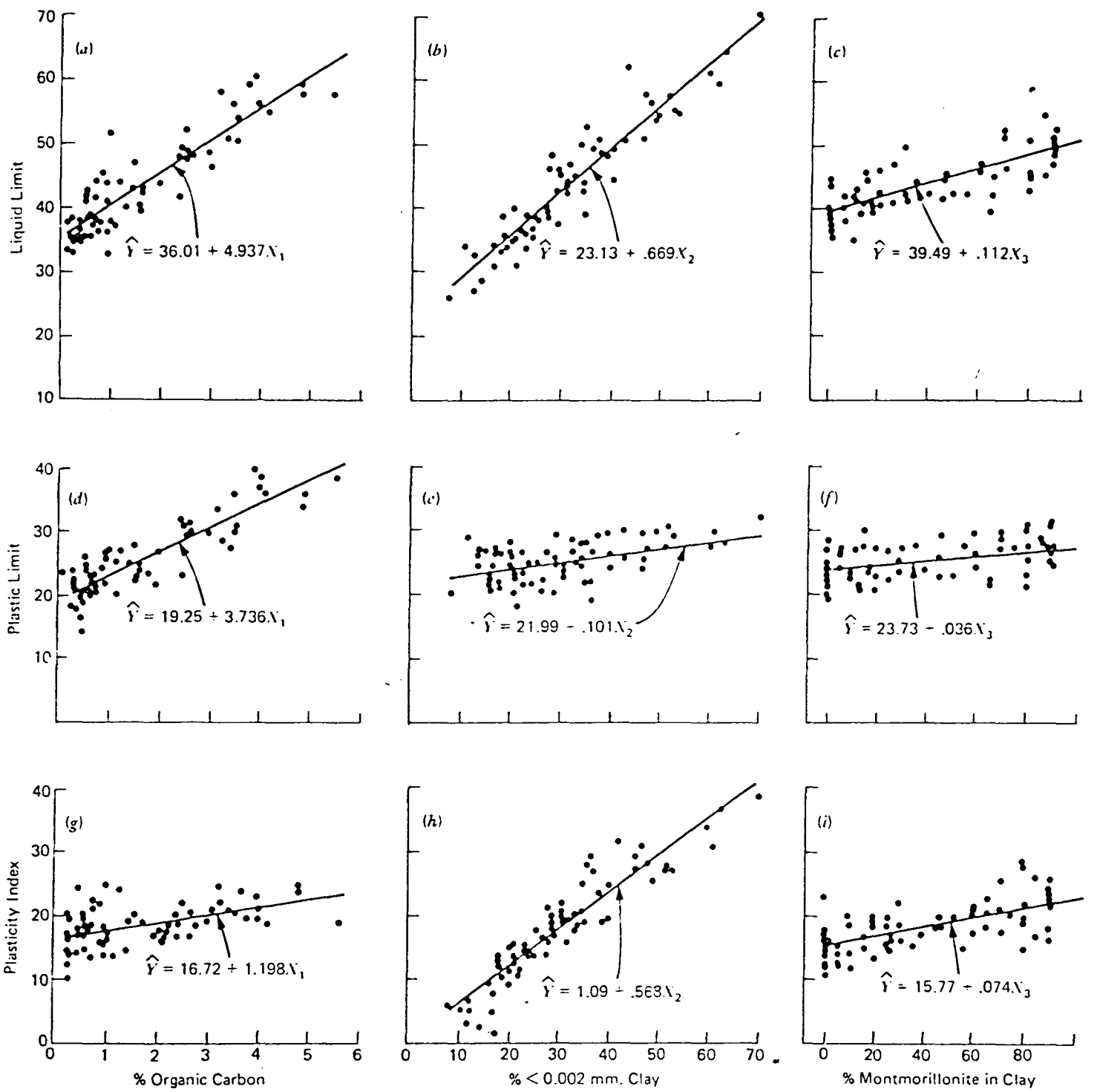

Figure 2-8 Relationships between the Atterberg limits and content of organic carbon, less than 0.002mm clay and montmorillonite in clay (after Odell, Thornburn and McKenzie, 1960)

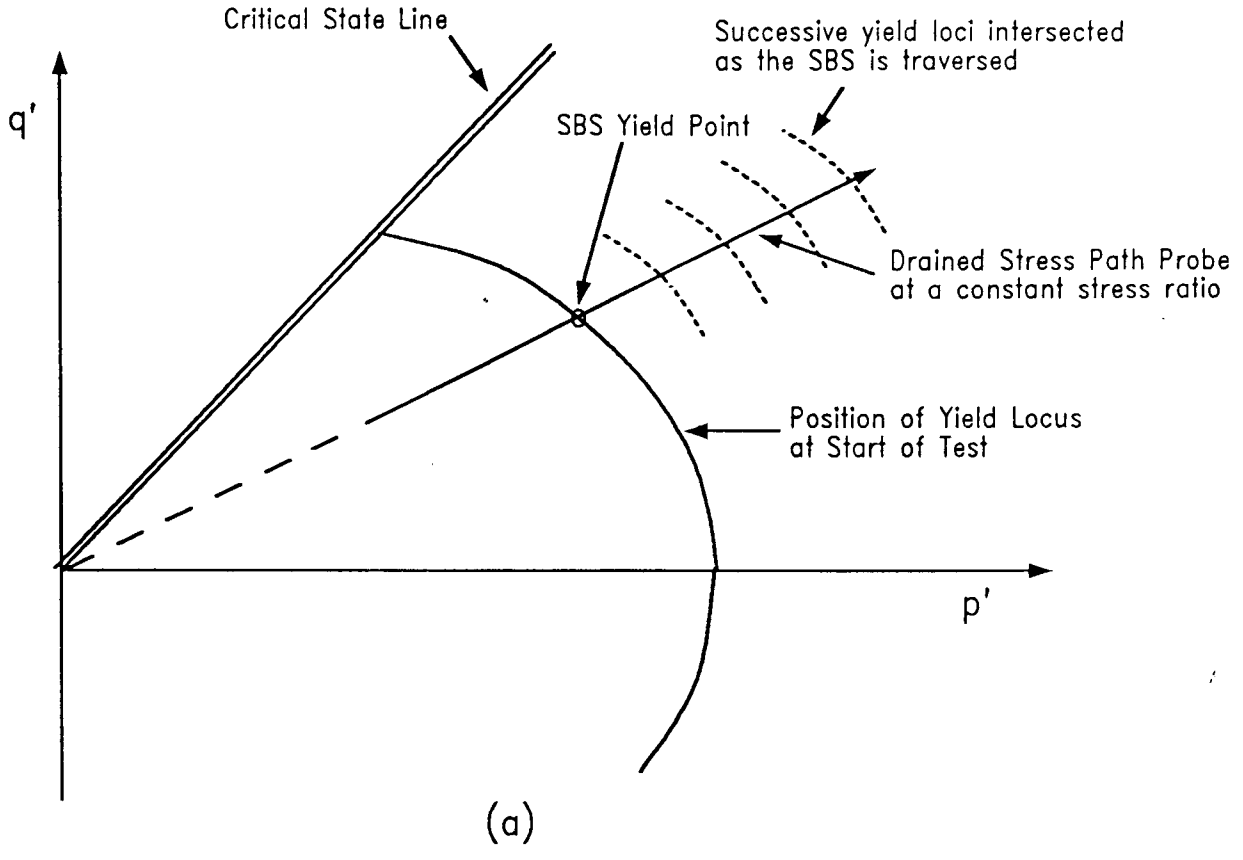

Figure 3.1 Definition of the SBS Yield Point

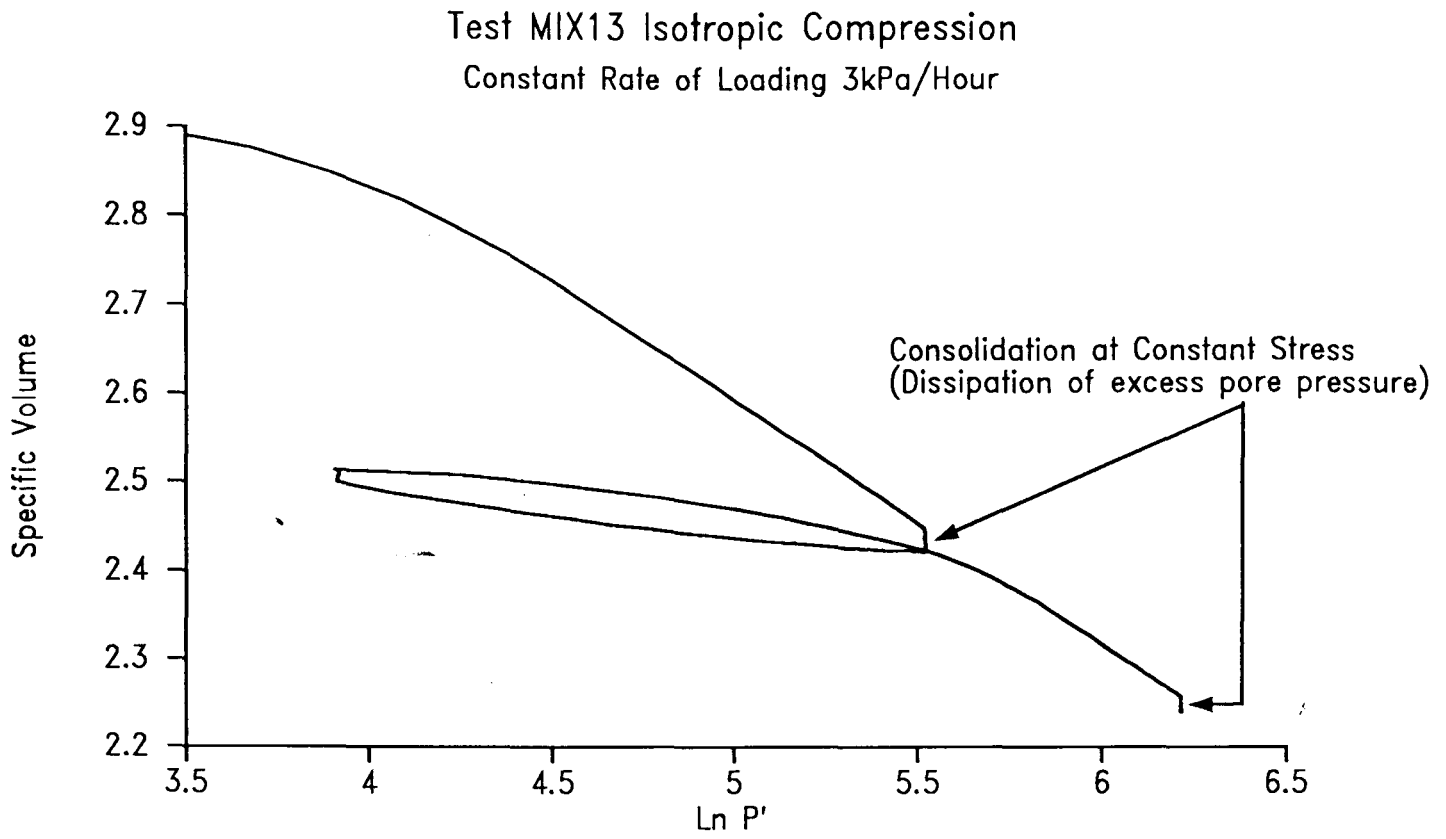

Figure 32 Dissipation of excess pore pressure at end of constant rate of loading triaxial test stage

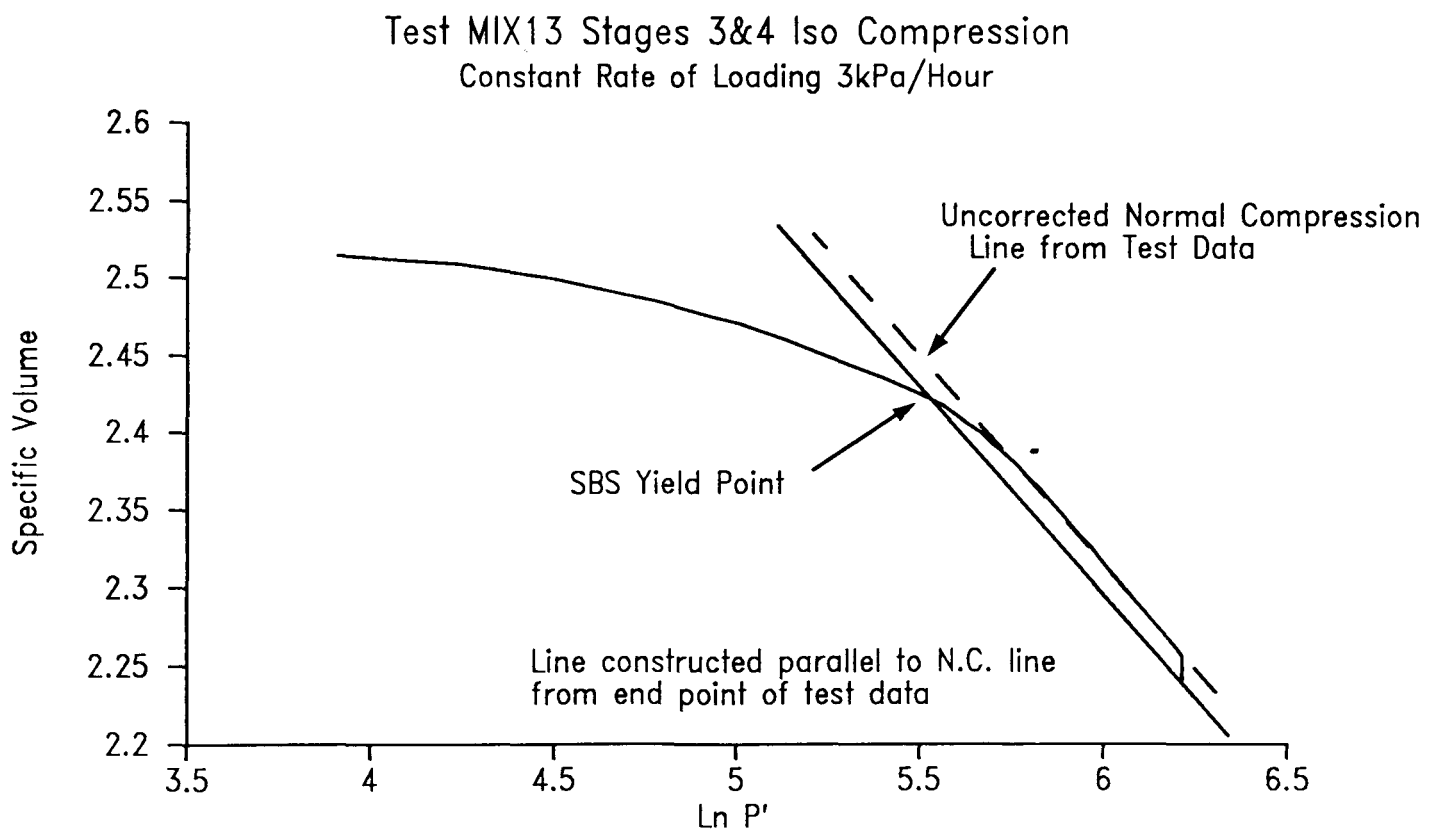

Figure 33 Example of the Lambda construction to determine the SBS yield point

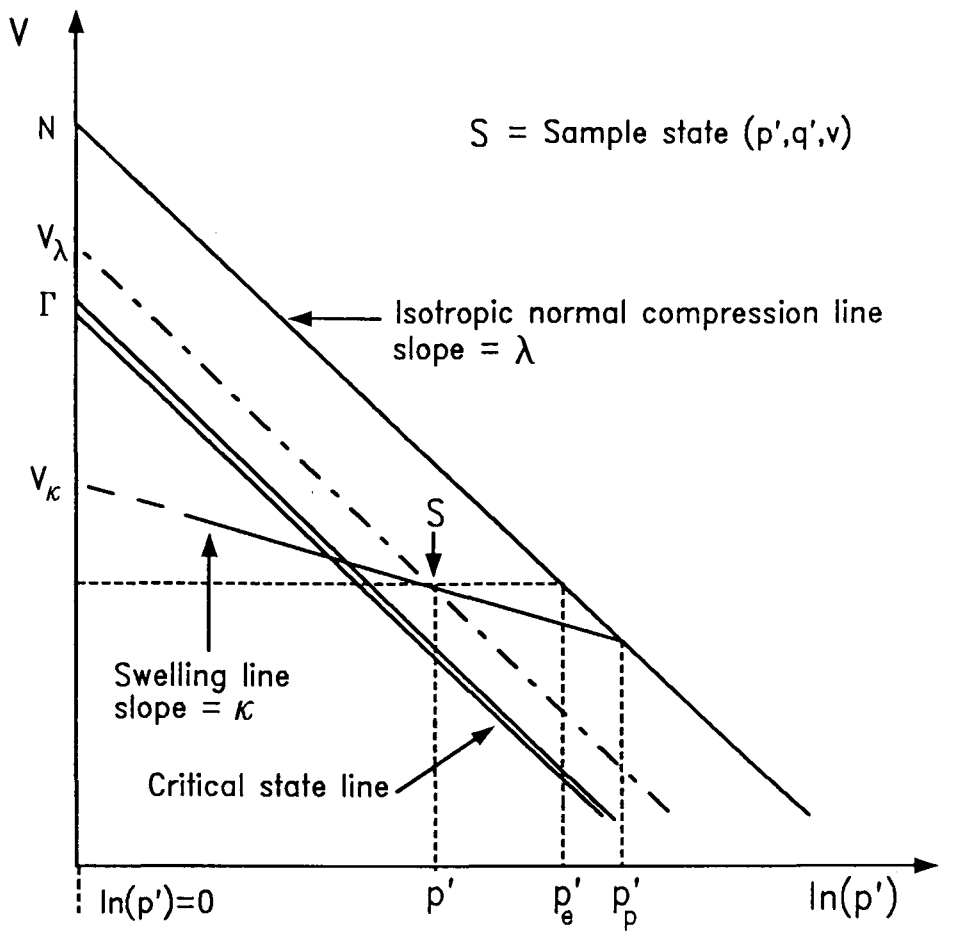

Figure 34 Normalising parameters (after Atkinson, 1984b)

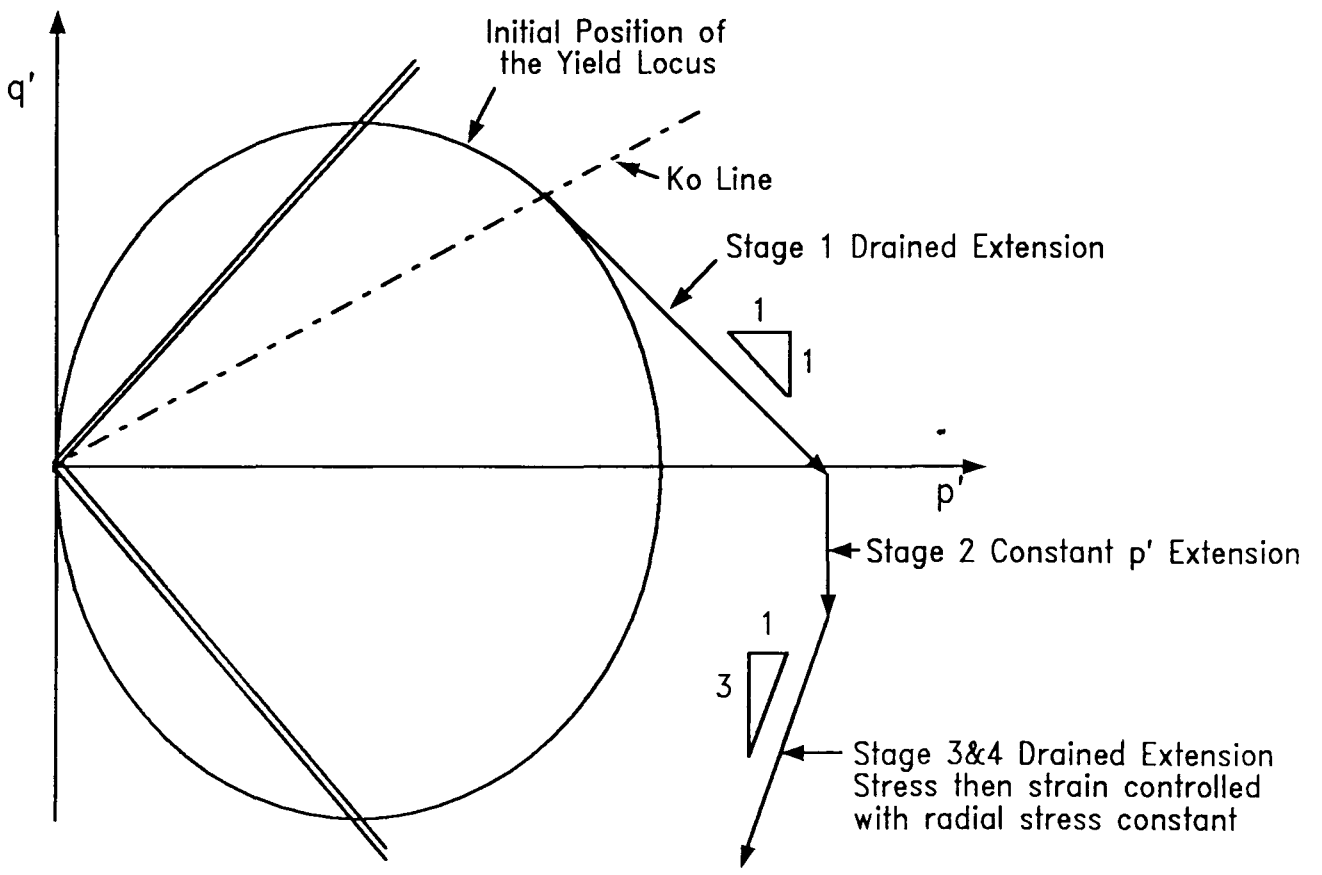

Figure 35 . Effective stress path for Type 1 probing test

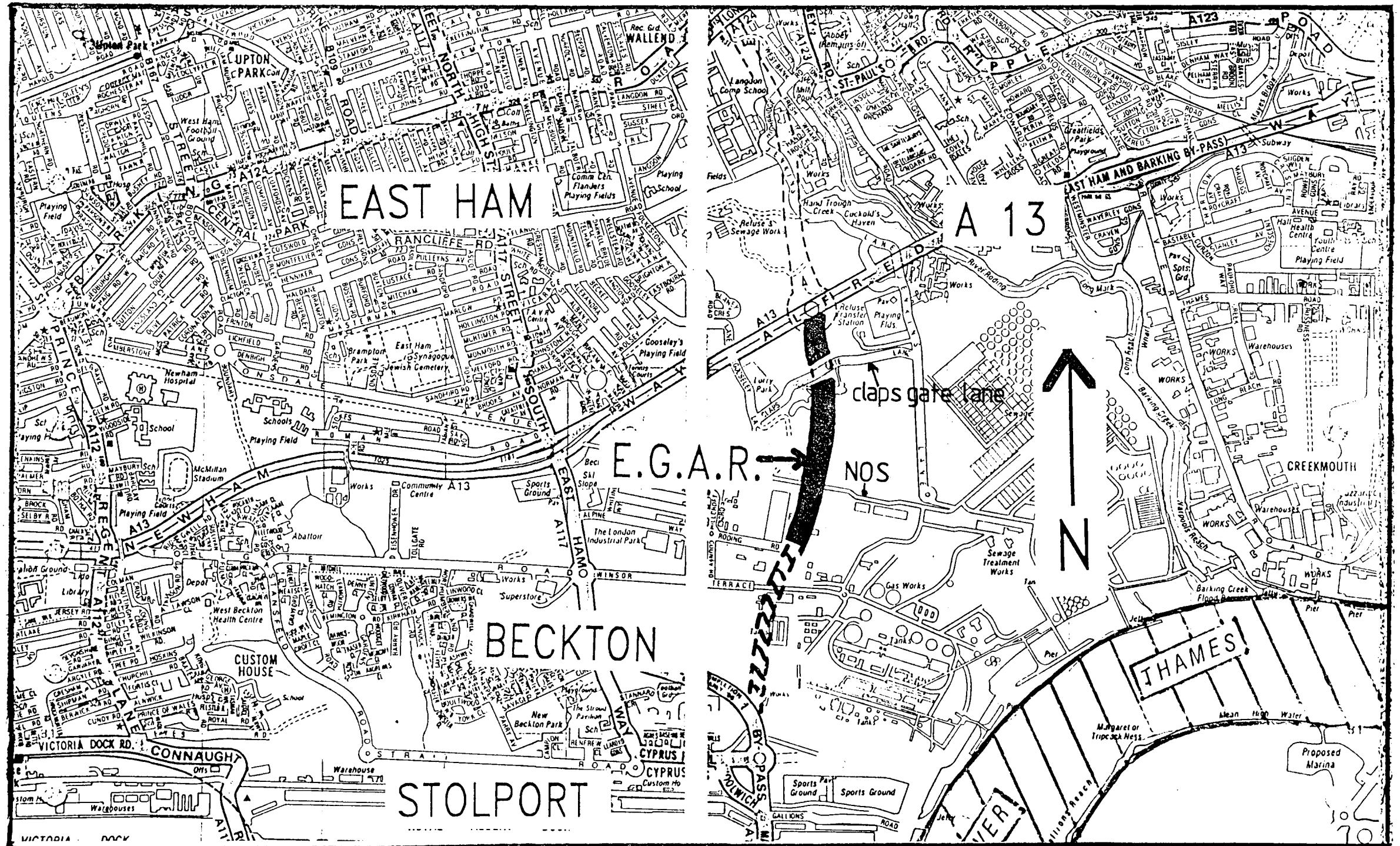

FIGURE 4.1 EASTERN GATEWAY ACCESS ROAD SITE LOCATION

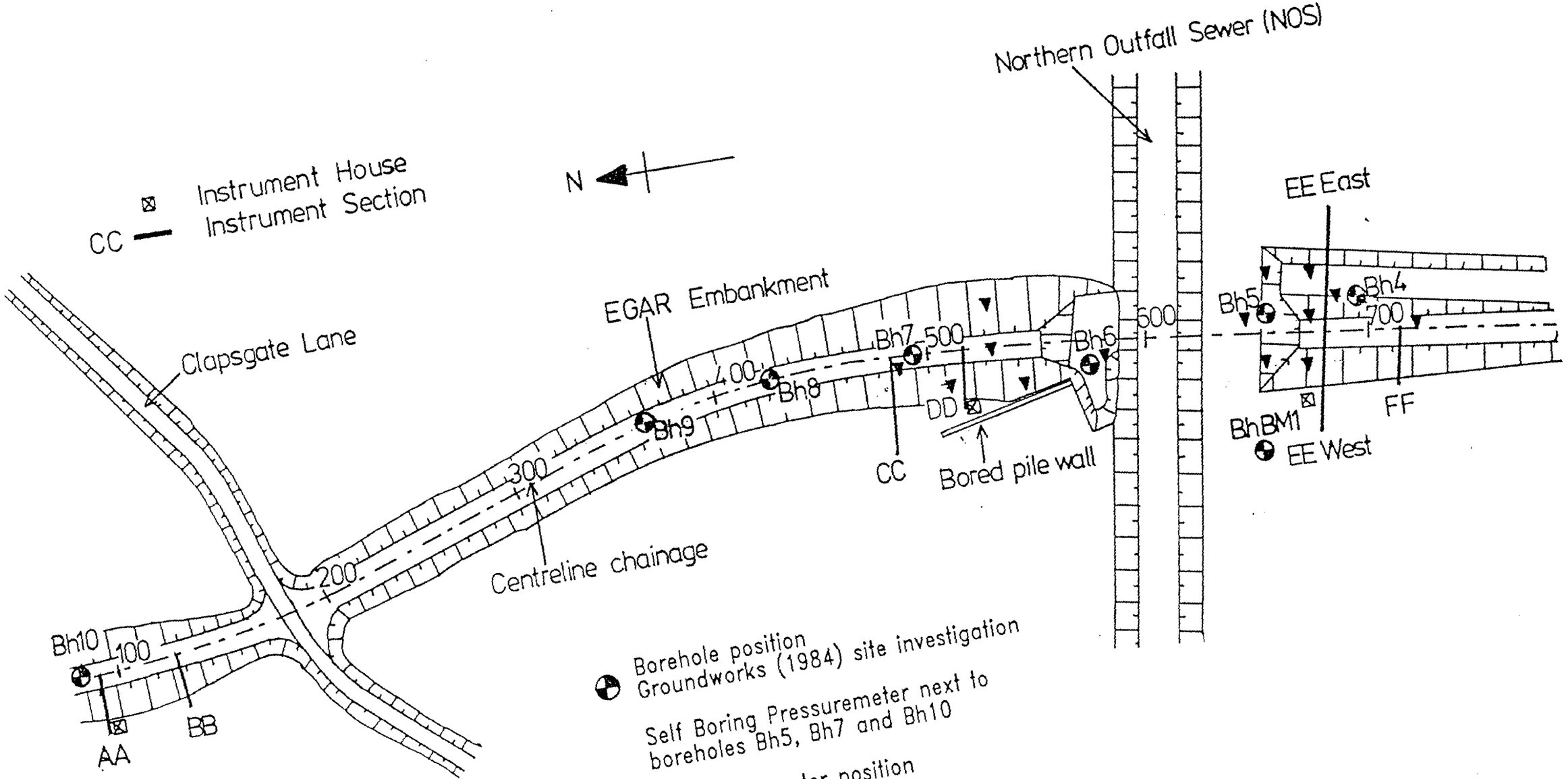

Figure 4.2 Site layout and borehole and in situ test positions

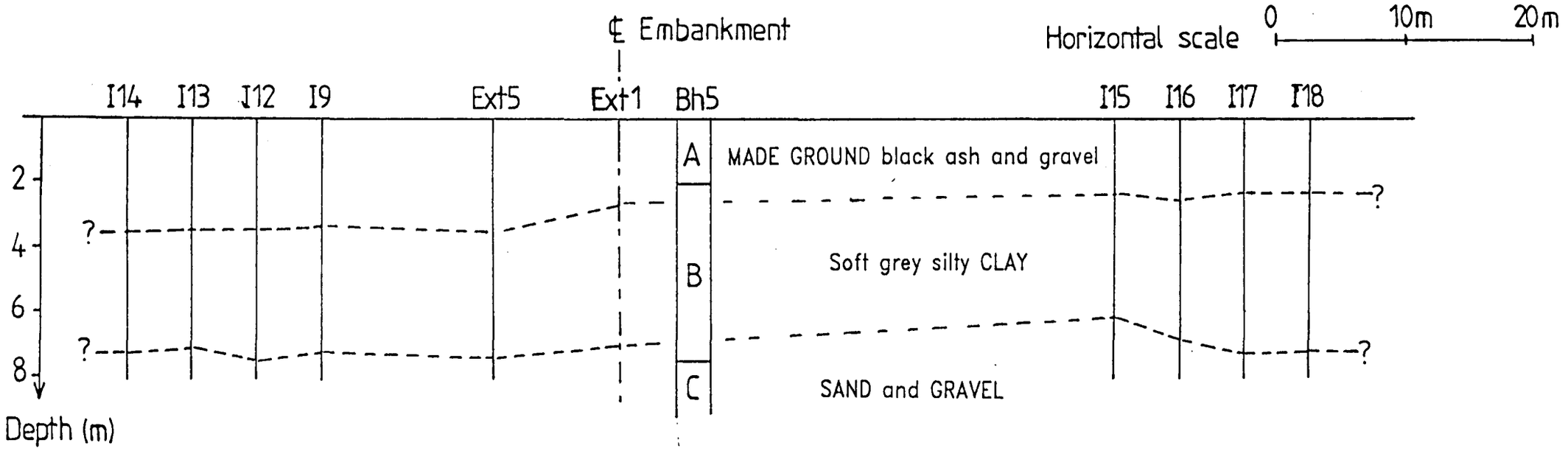

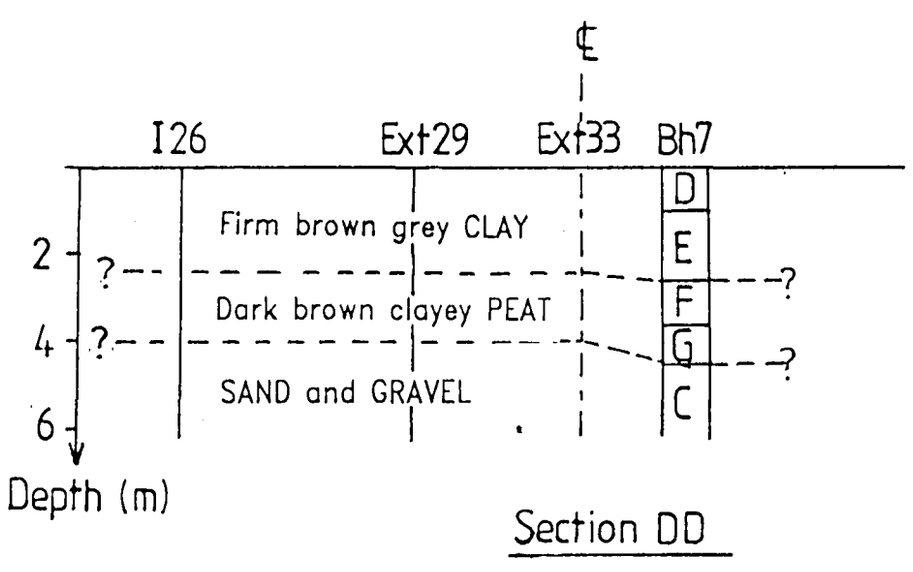

Note:-
for position of instrumentation see
Figure 5.1 (section EE) and Figure 5.2 (section DD)

for position of boreholes see Figure 4.2

Drillers soil description shown on the cross sections

Soil description Groundworks (1984)

A	MADE GROUND Loose, black cinders, ash, sand, some brick and concrete fragments becoming clayey with depth
B	Soft grey silty CLAY with some plant remains, contaminated with oily substance (coal tar)
C	Medium dense brown sandy subangular and rounded GRAVEL
D	Stiff becoming firm with depth brown silty sandy CLAY with some fine gravel and plant remains
E	Firm brown mottled grey silty CLAY
F	Soft dark brown fibrous clayey PEAT
G	Soft light brownish grey silty, sandy, peaty CLAY

Figure 4.3 Soil profiles at sections DD and EE

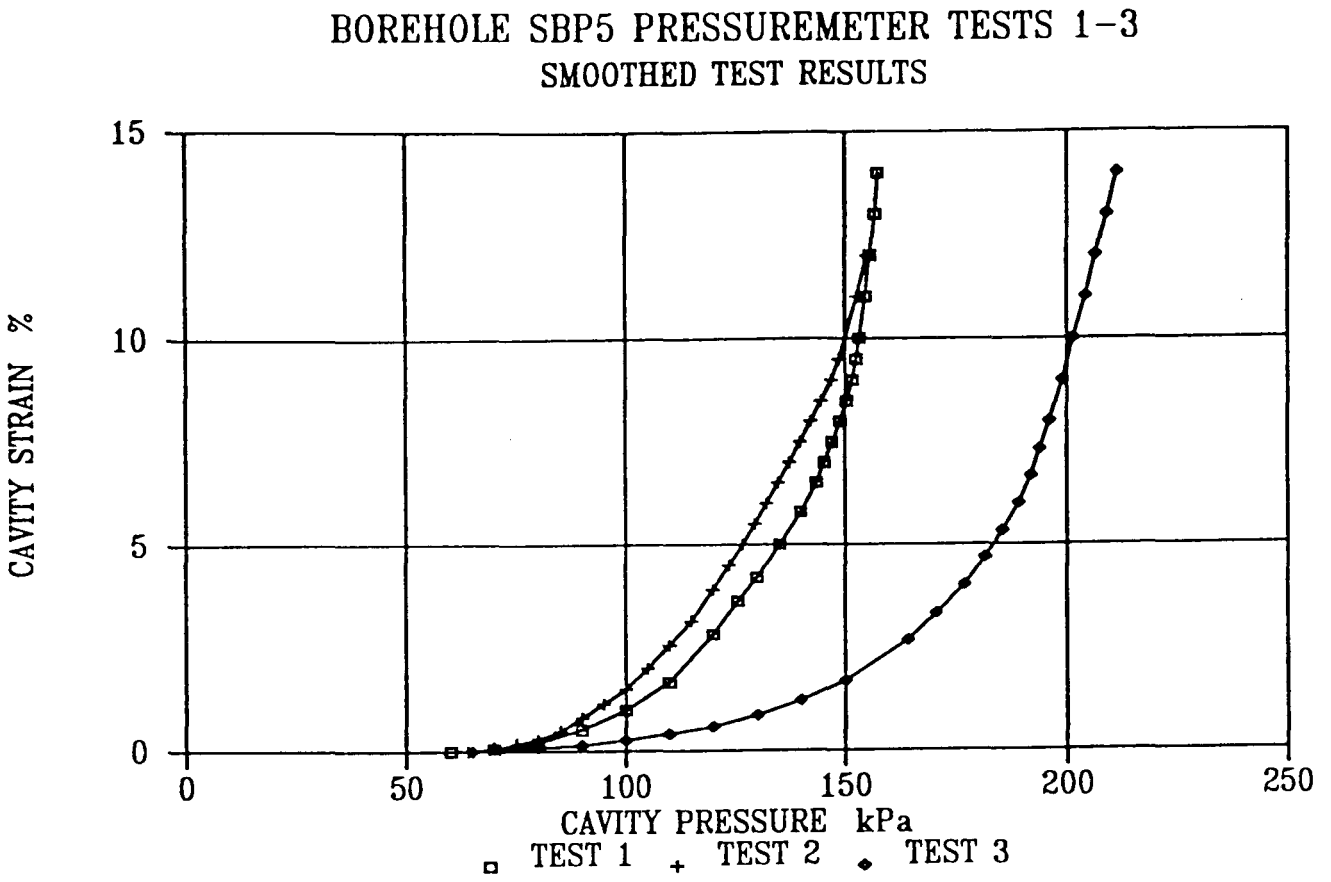

Figure 4.4 Pressuremeter results at borehole SBP5

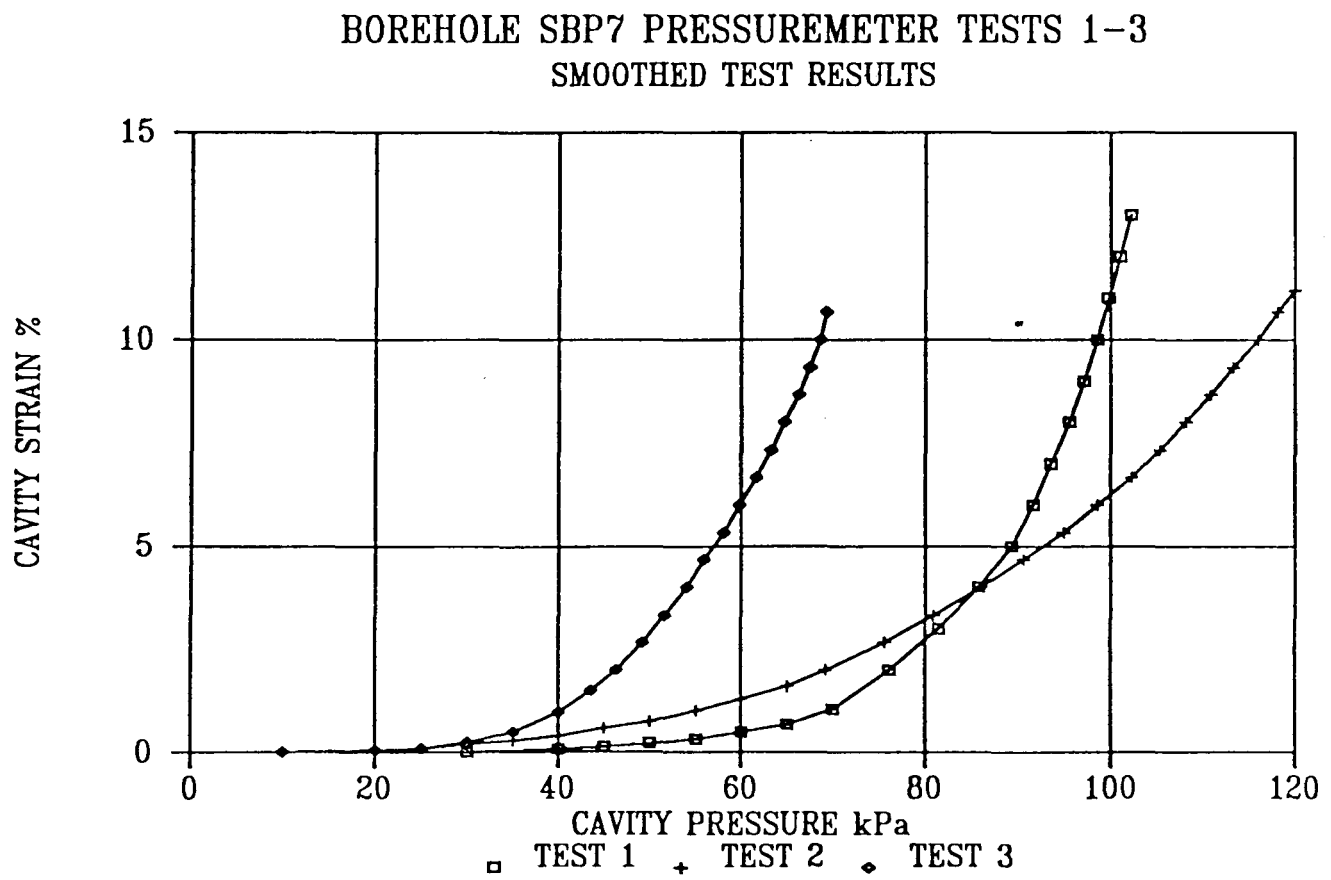

Figure 4.5 Pressuremeter results at borehole SBP7

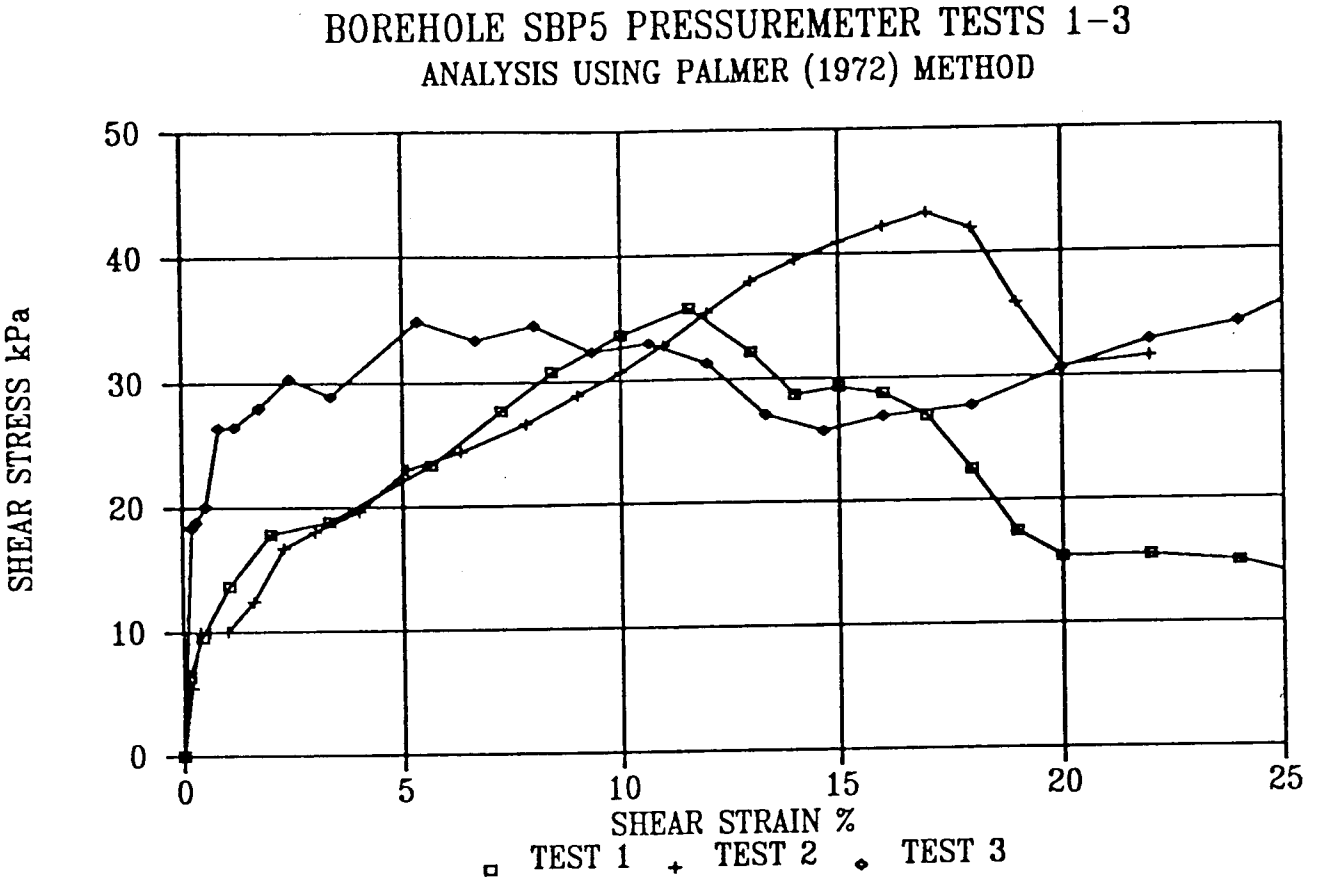

Figure 4.6 Palmer (1972) analysis of pressuremeter tests SBP5/1-3 (South of the NOS)

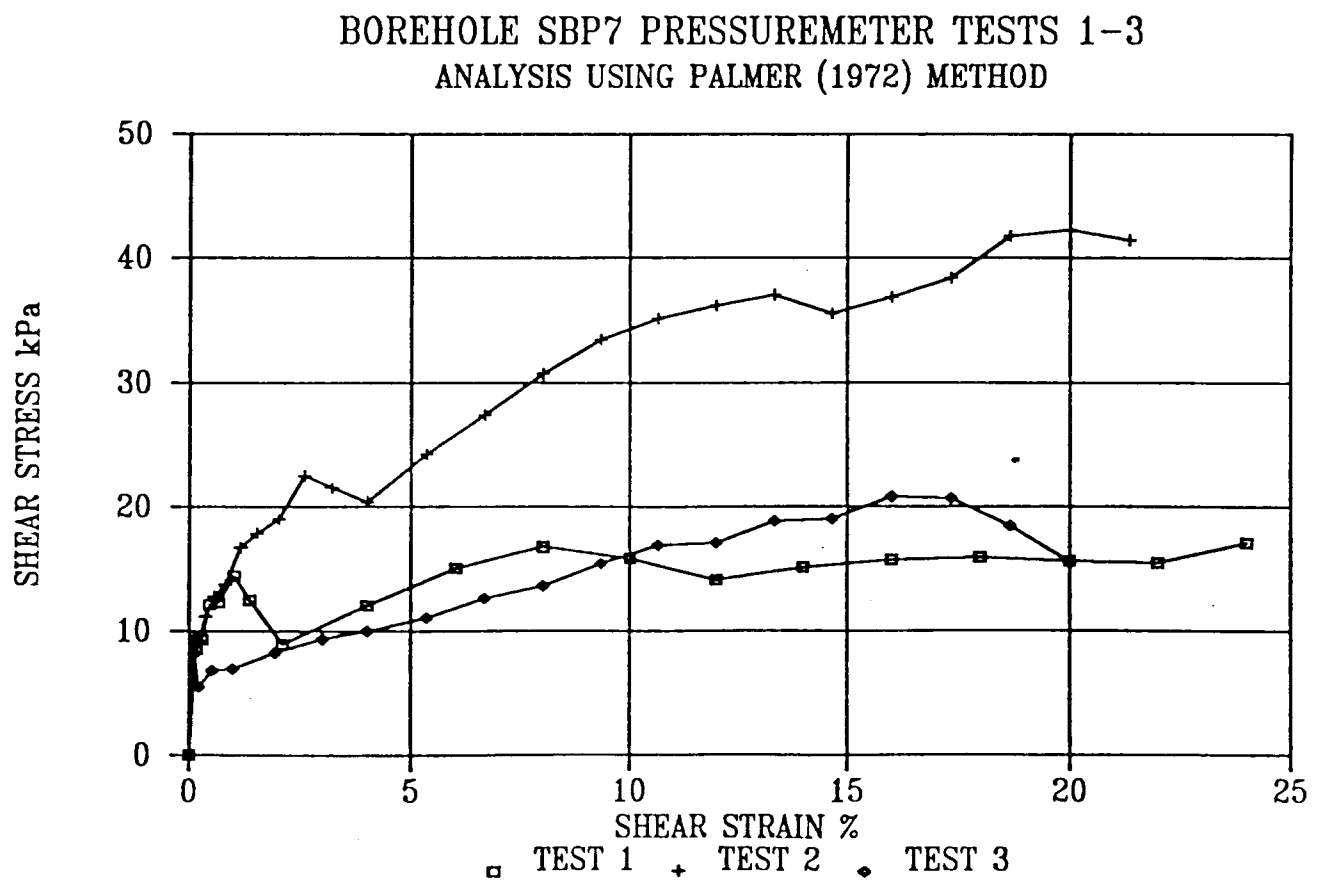

Figure 4.7 Palmer (1972) analysis of presuremeter tests SBP7/1-3 (North of the NOS)

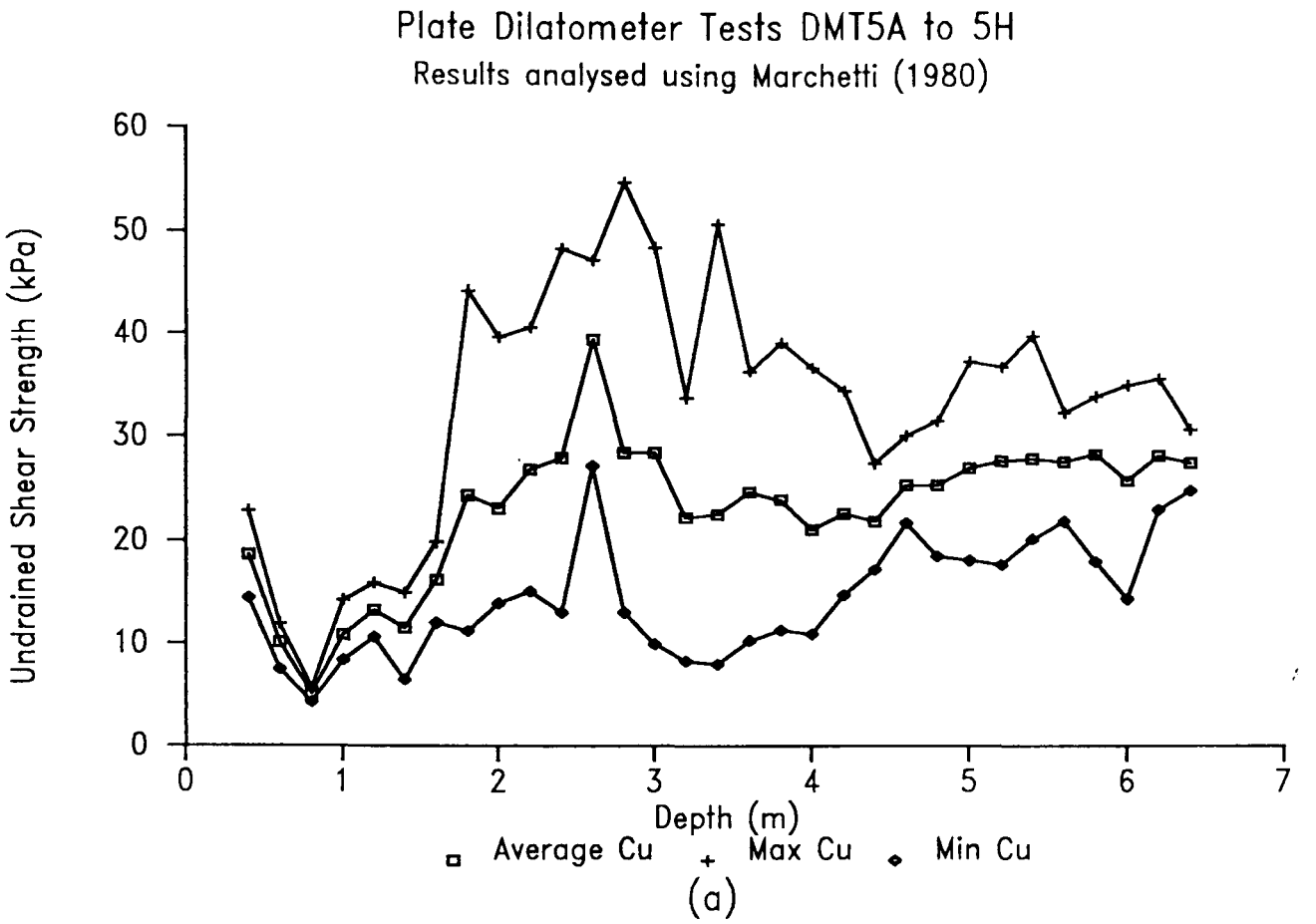

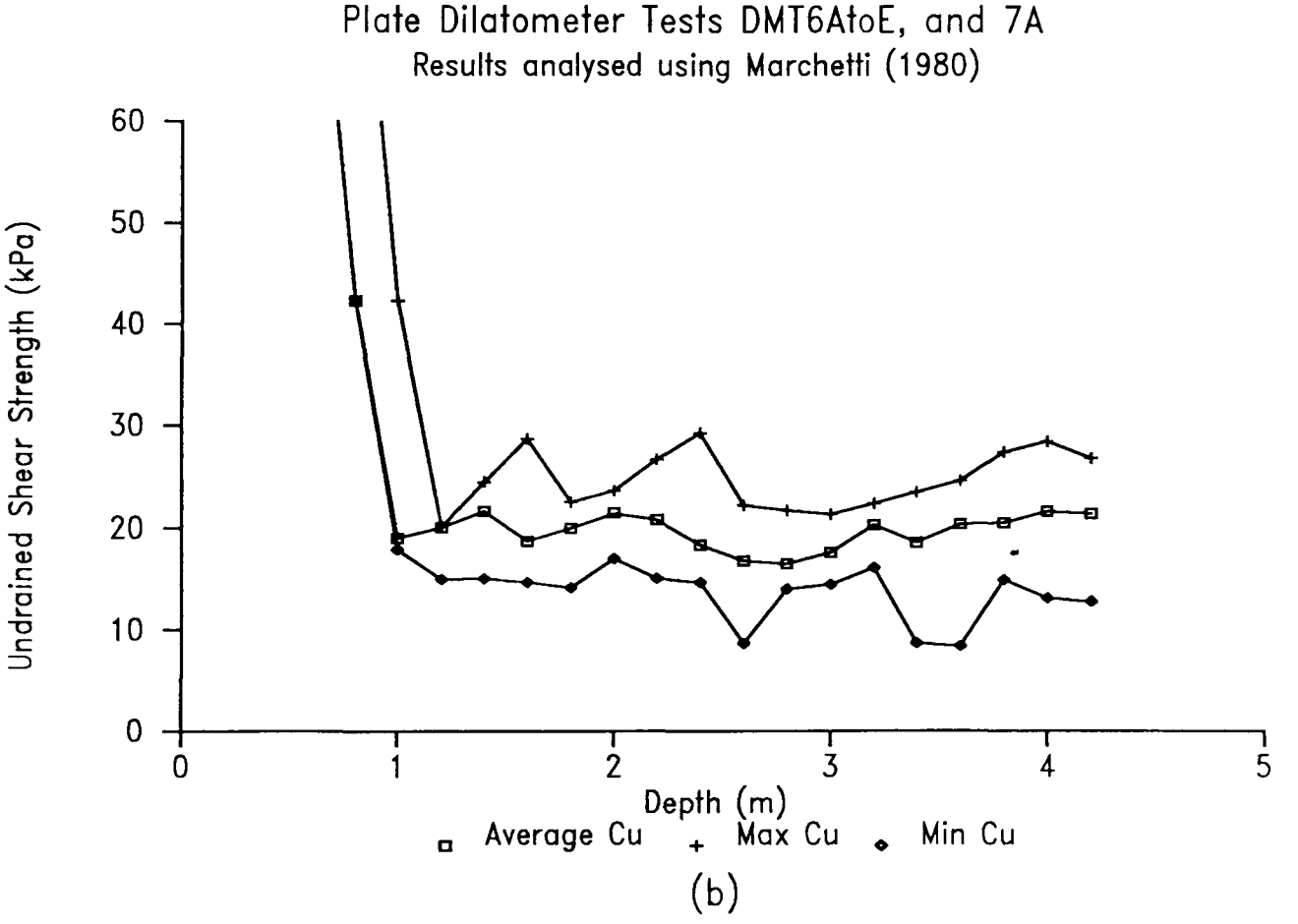

Figure 4.8 Plate Dilatometer – Undrained Shear Strength

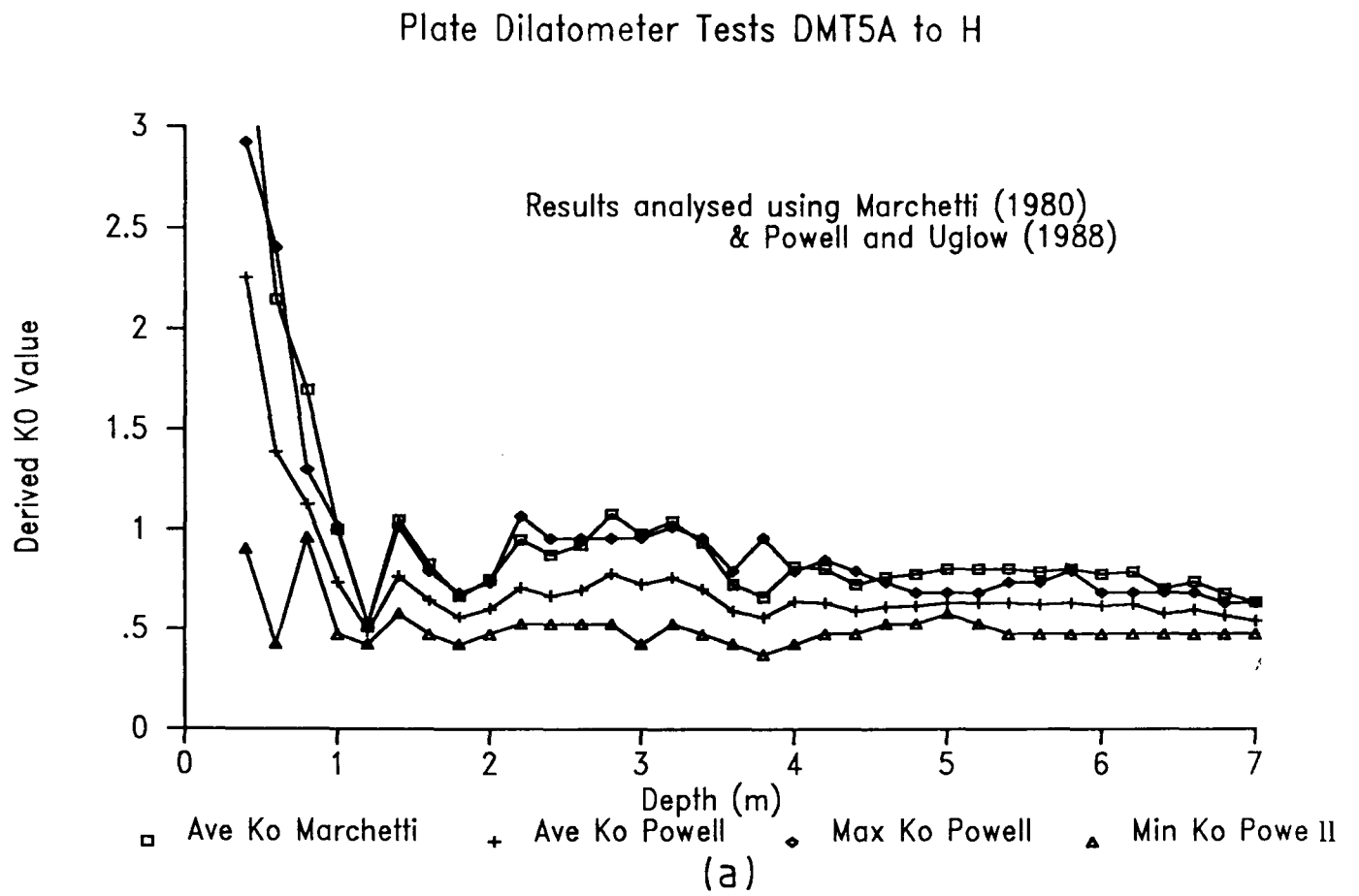

Figure 4.9 Plate Dilatometer – In Situ K_o

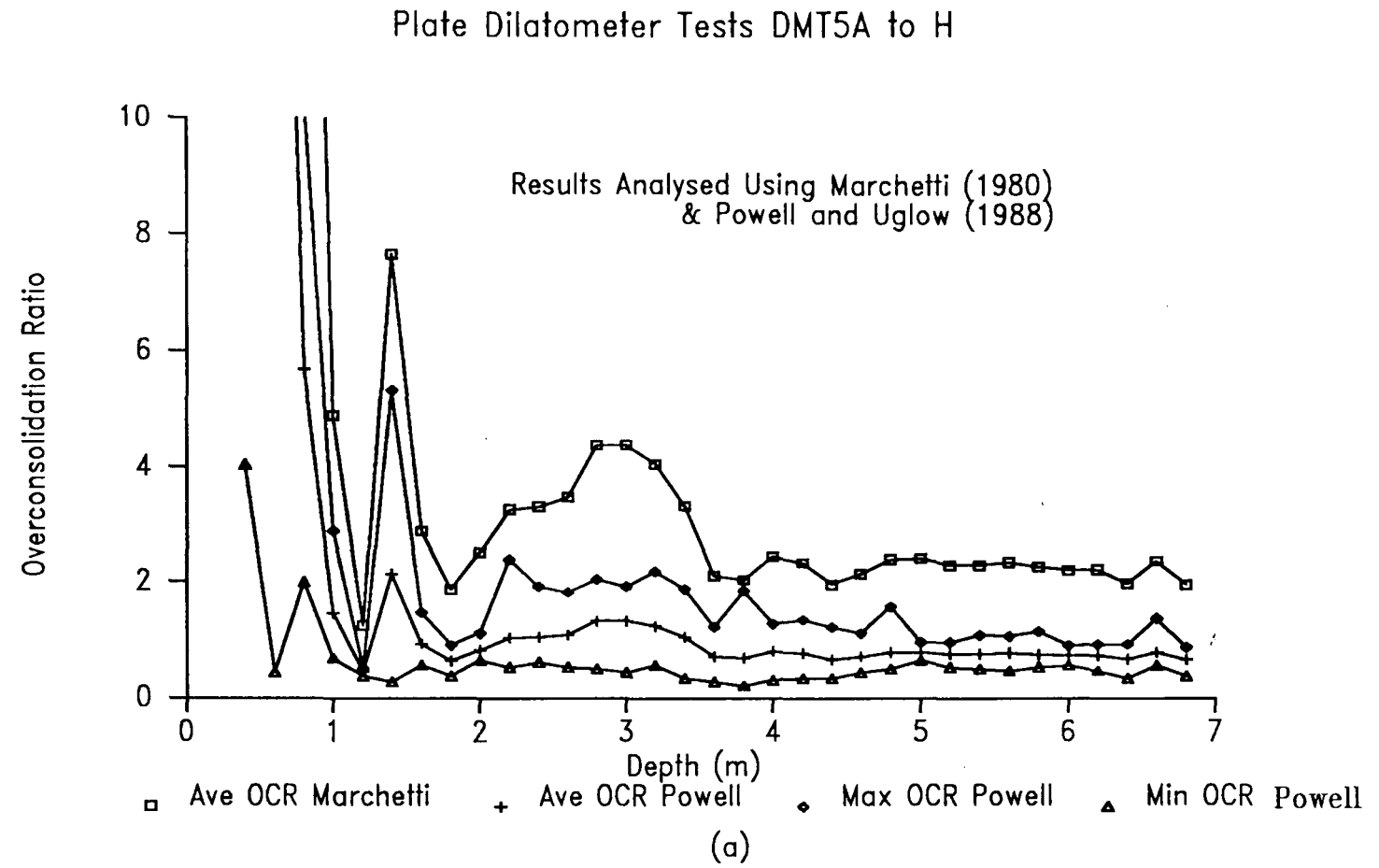

Figure 4.10 Plate Dilatometer – Overconsolidation Ratio

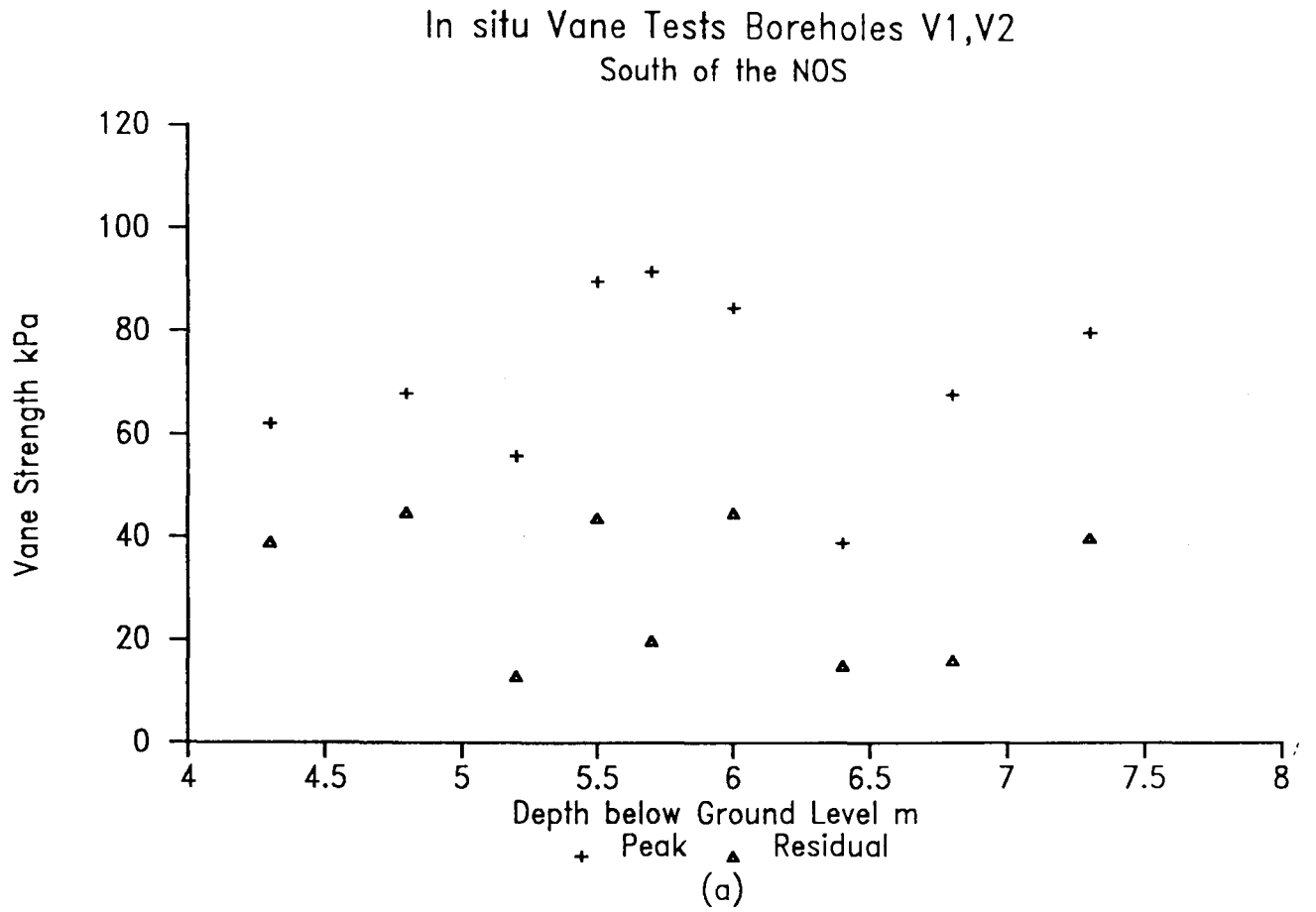

Figure 4.11 In Situ Shear Vane Test Results

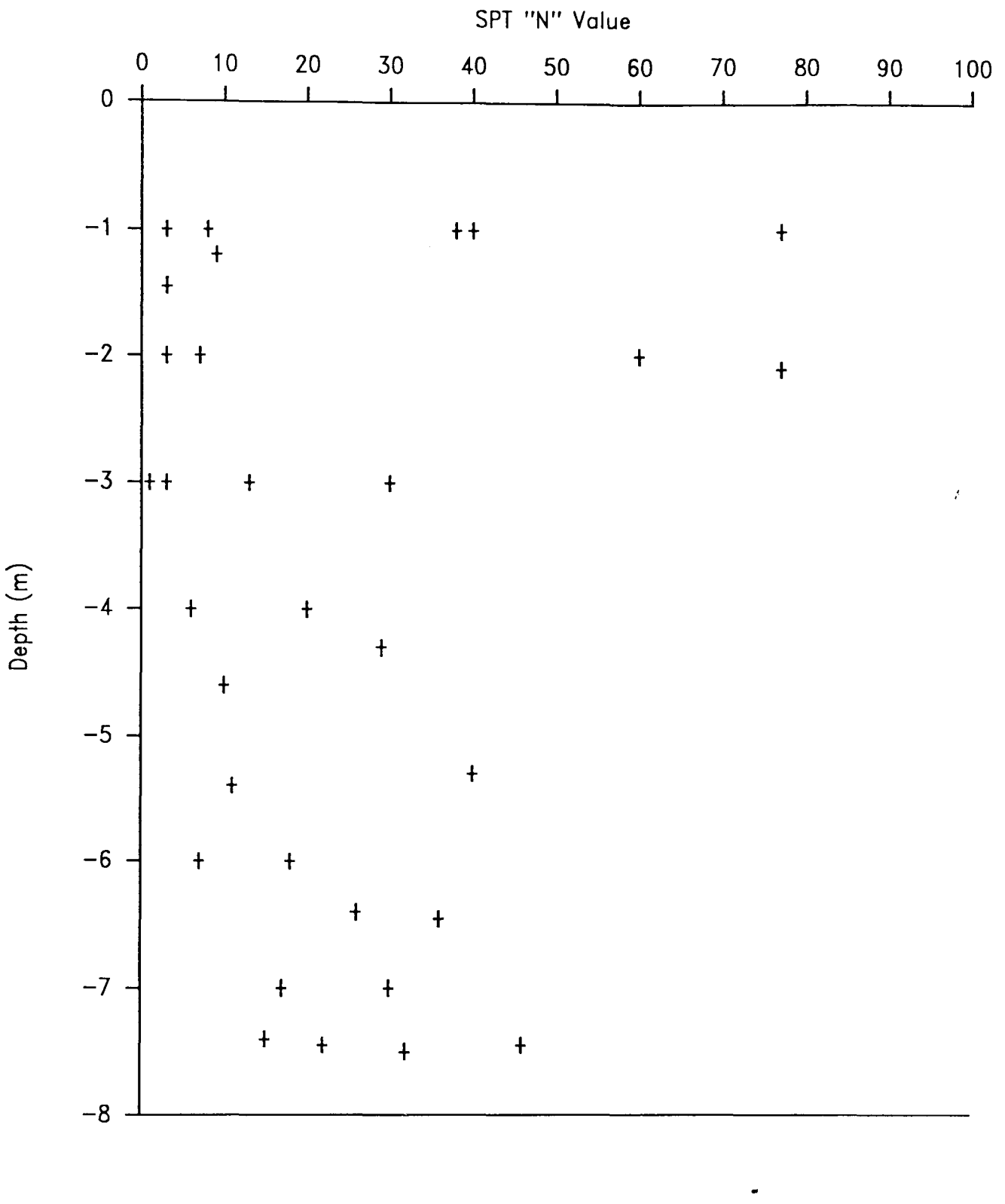

Figure 4.12 Standard Penetration Test results, south of the NOS

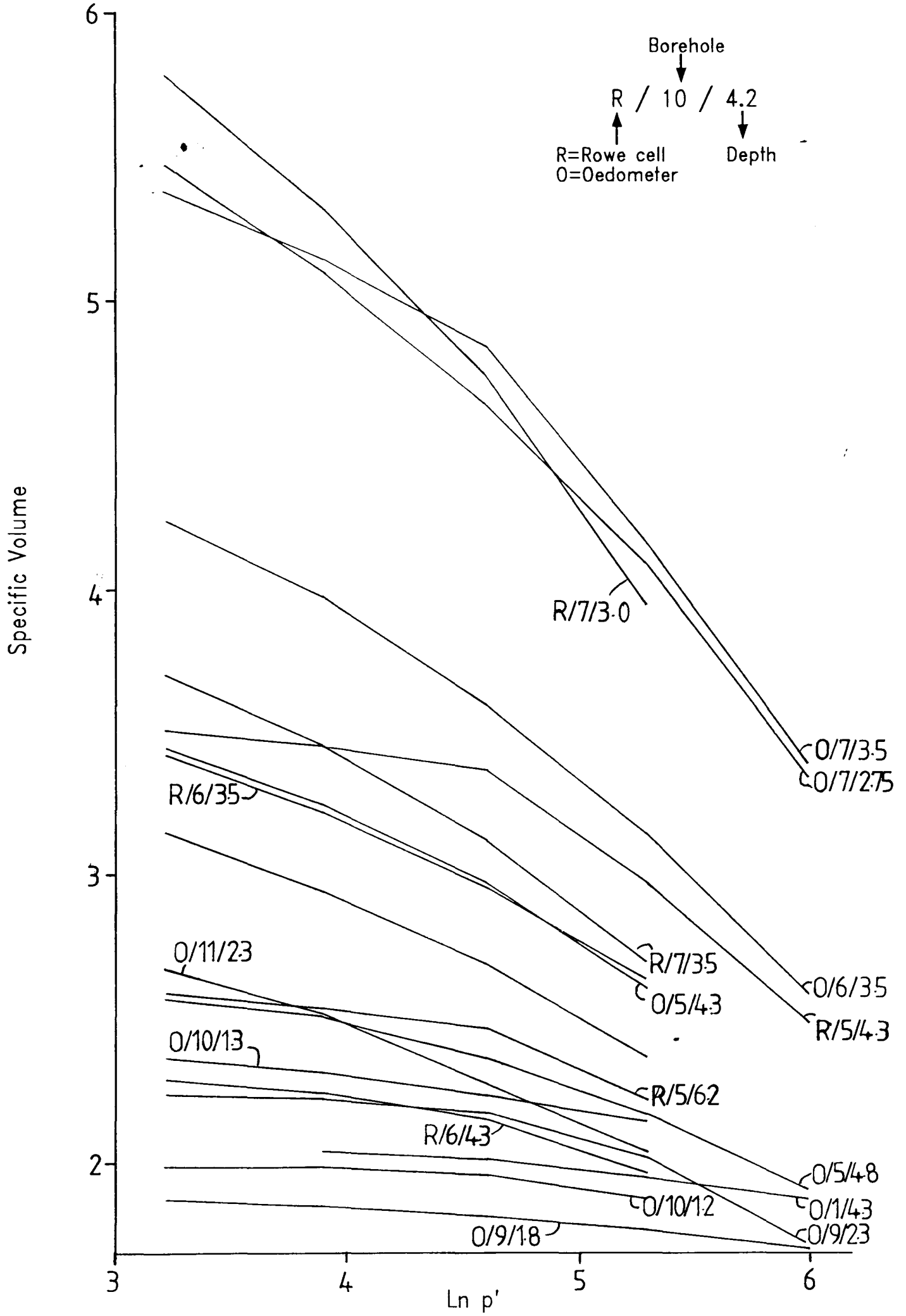

Figure 4.13 Summary of results of Rowe cell and oedometer tests

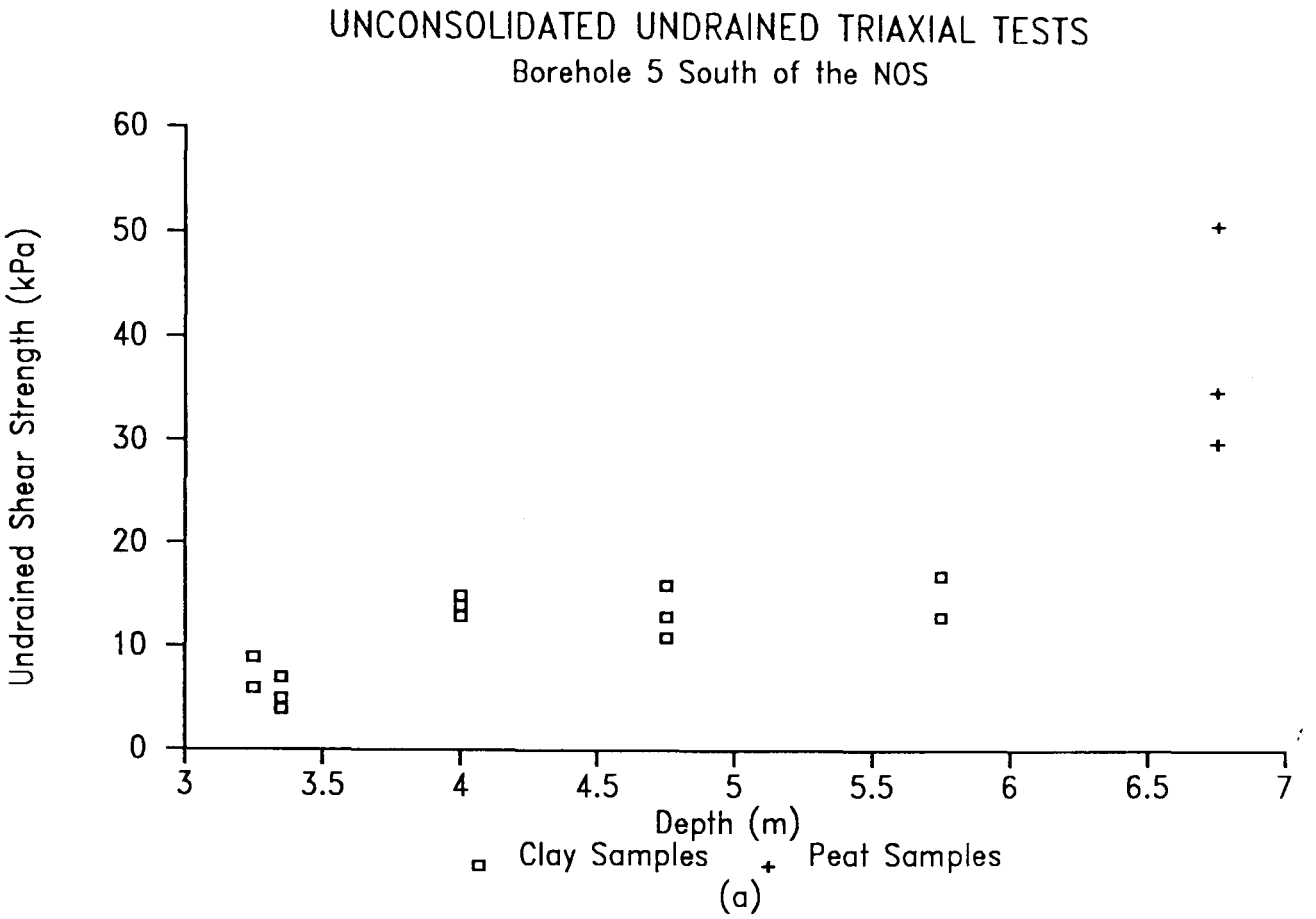

Figure 4.14 Unconsolidated Undrained Triaxial Test Results

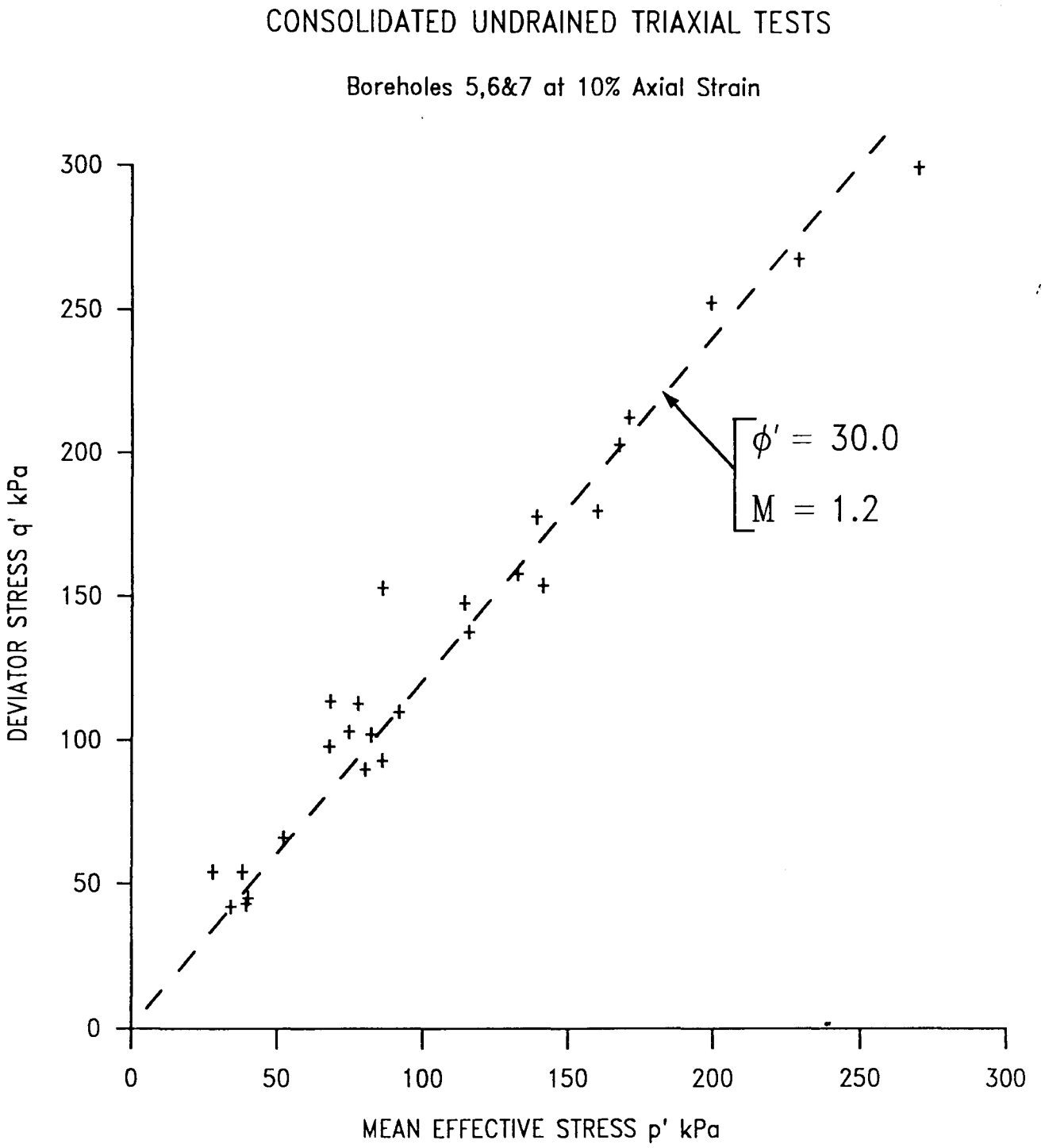

Figure 4.15 Consolidated Undrained Triaxial Test Results

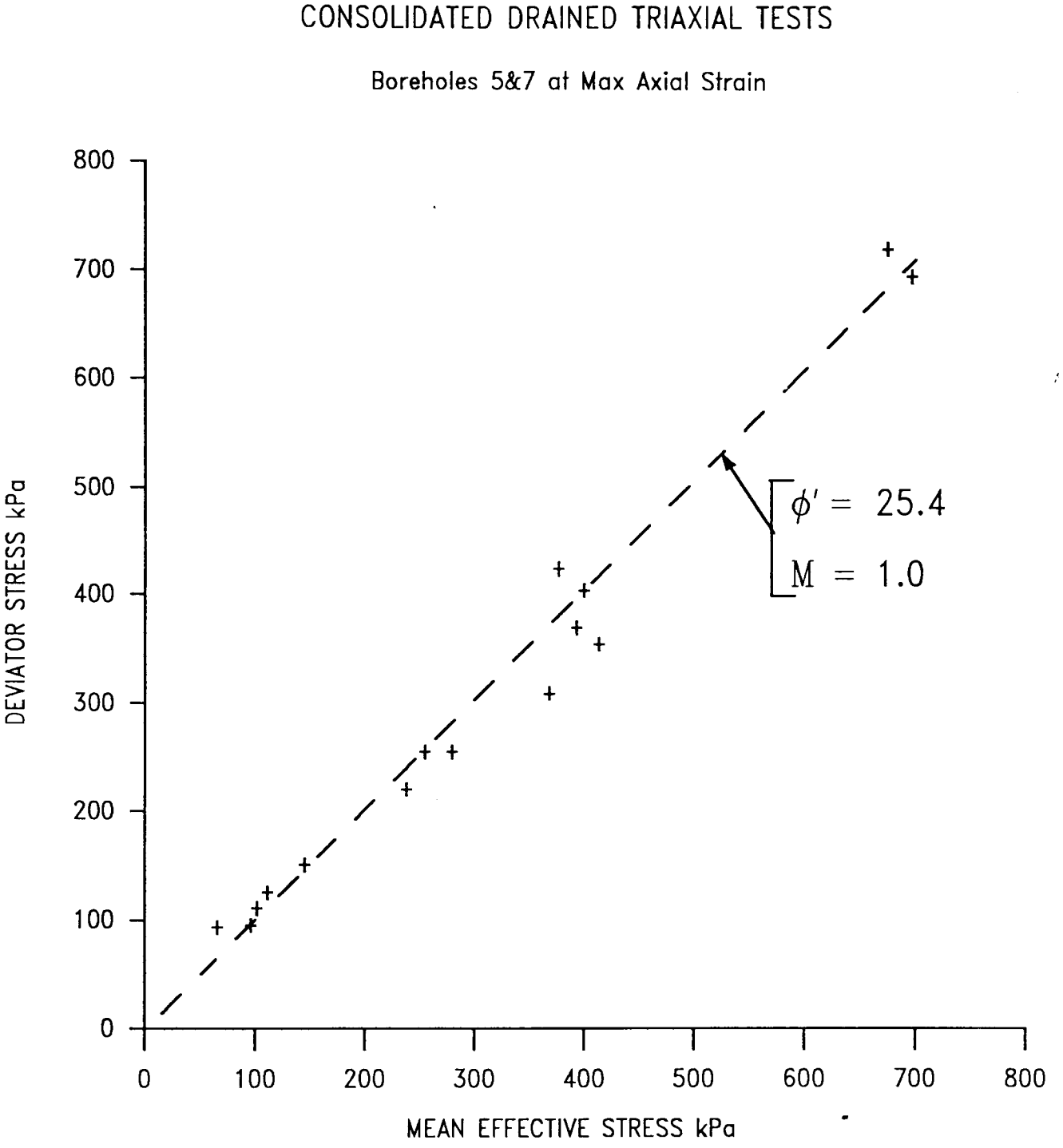

Figure 4.16 Consolidated Drained Triaxial Test Results

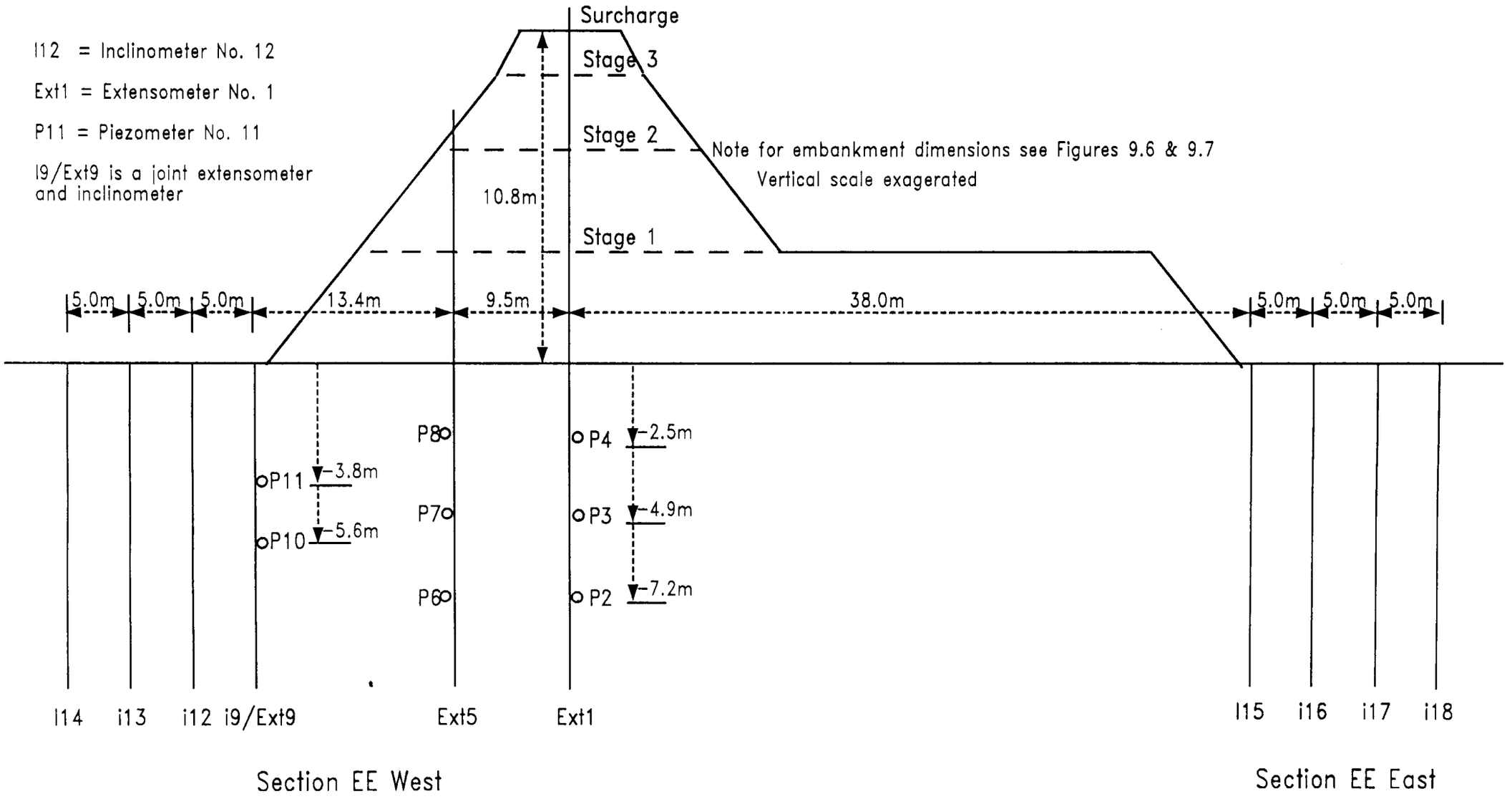

Figure 5.1 Position of instrumentation at section EE East and West

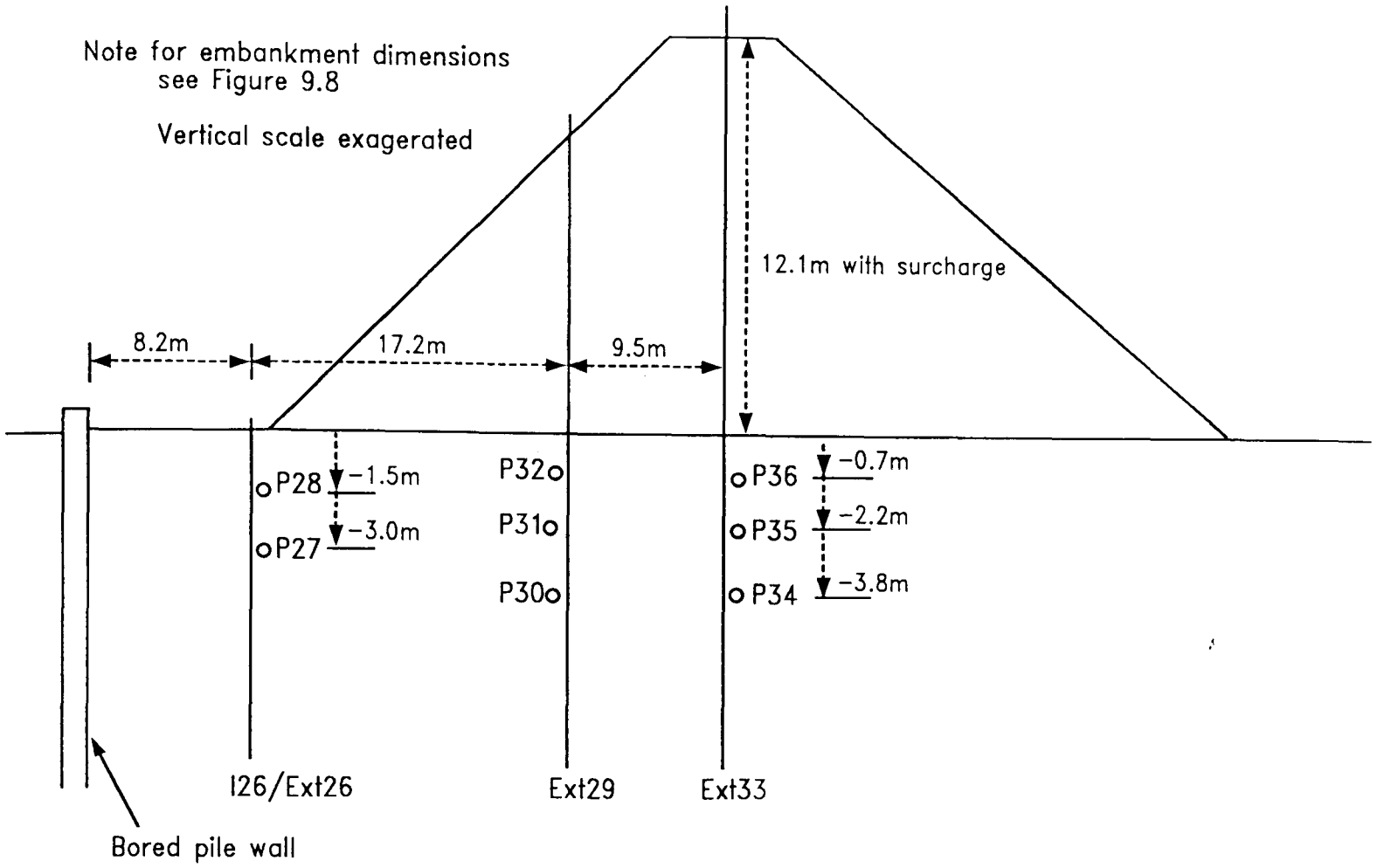

(a) Section DD

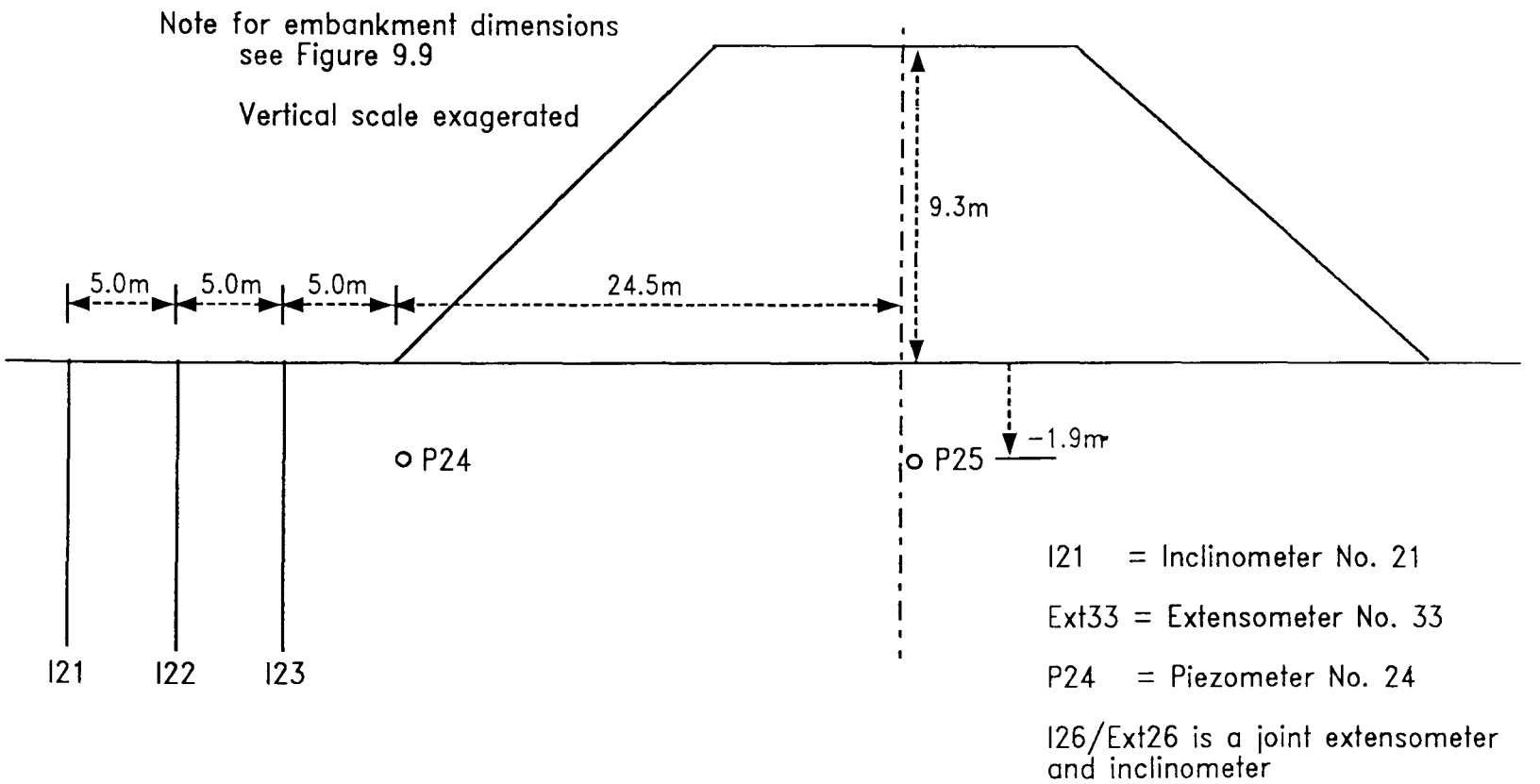

(b) Section CC

Figure 5.2 Position of instrumentation at sections DD and CC

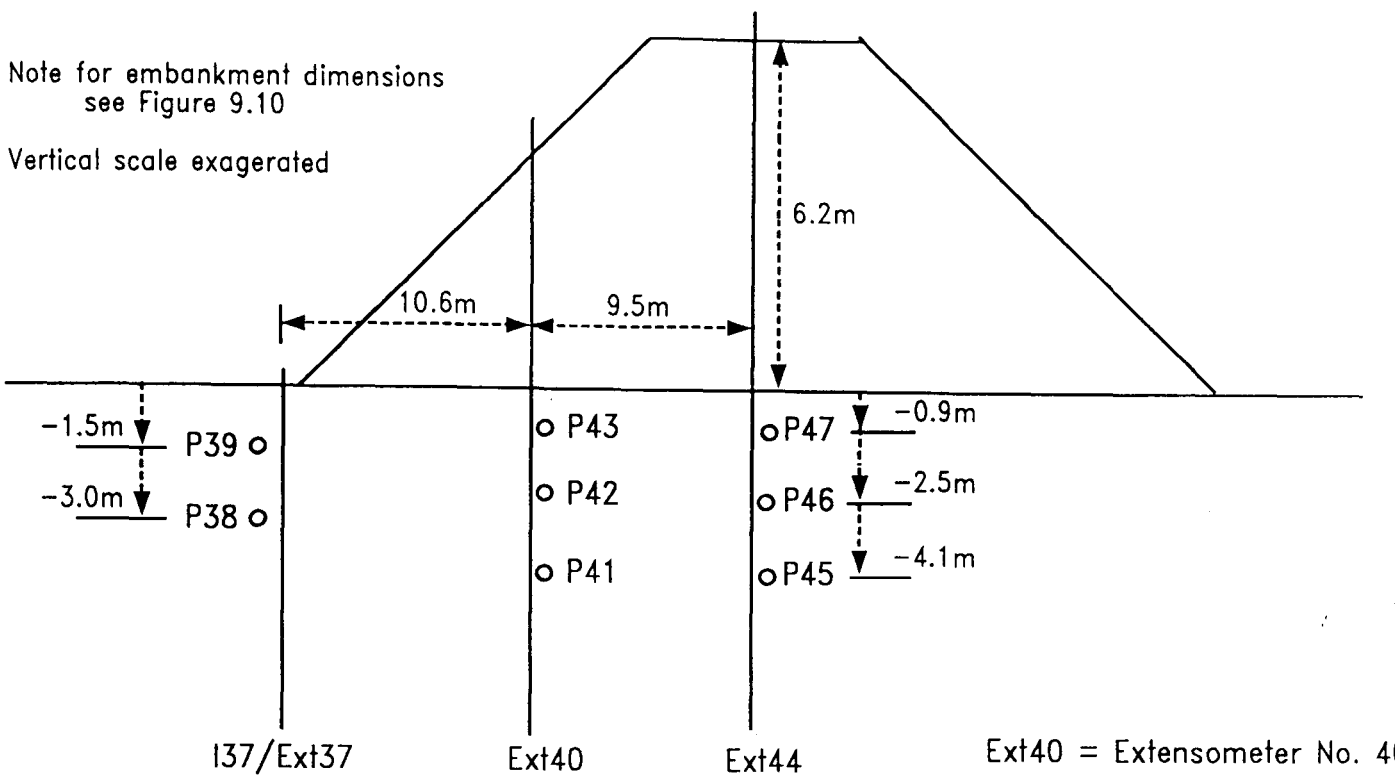

(a) Section AA

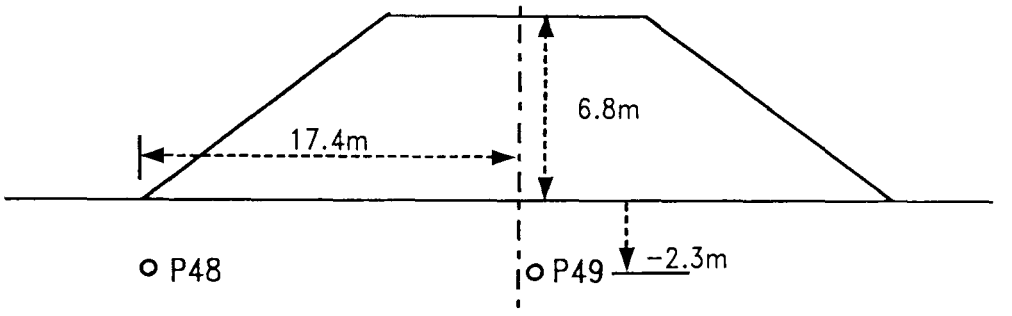

(b) Section BB

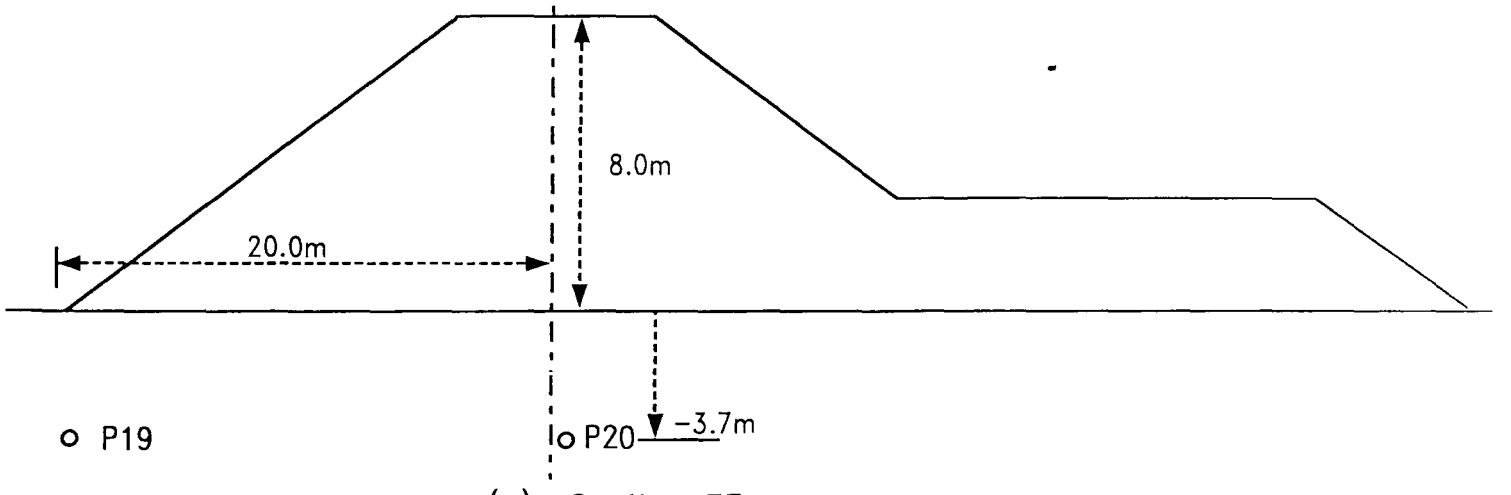

(c) Section FF

Figure 5.3 Position of instrumentation at sections AA, BB and FF

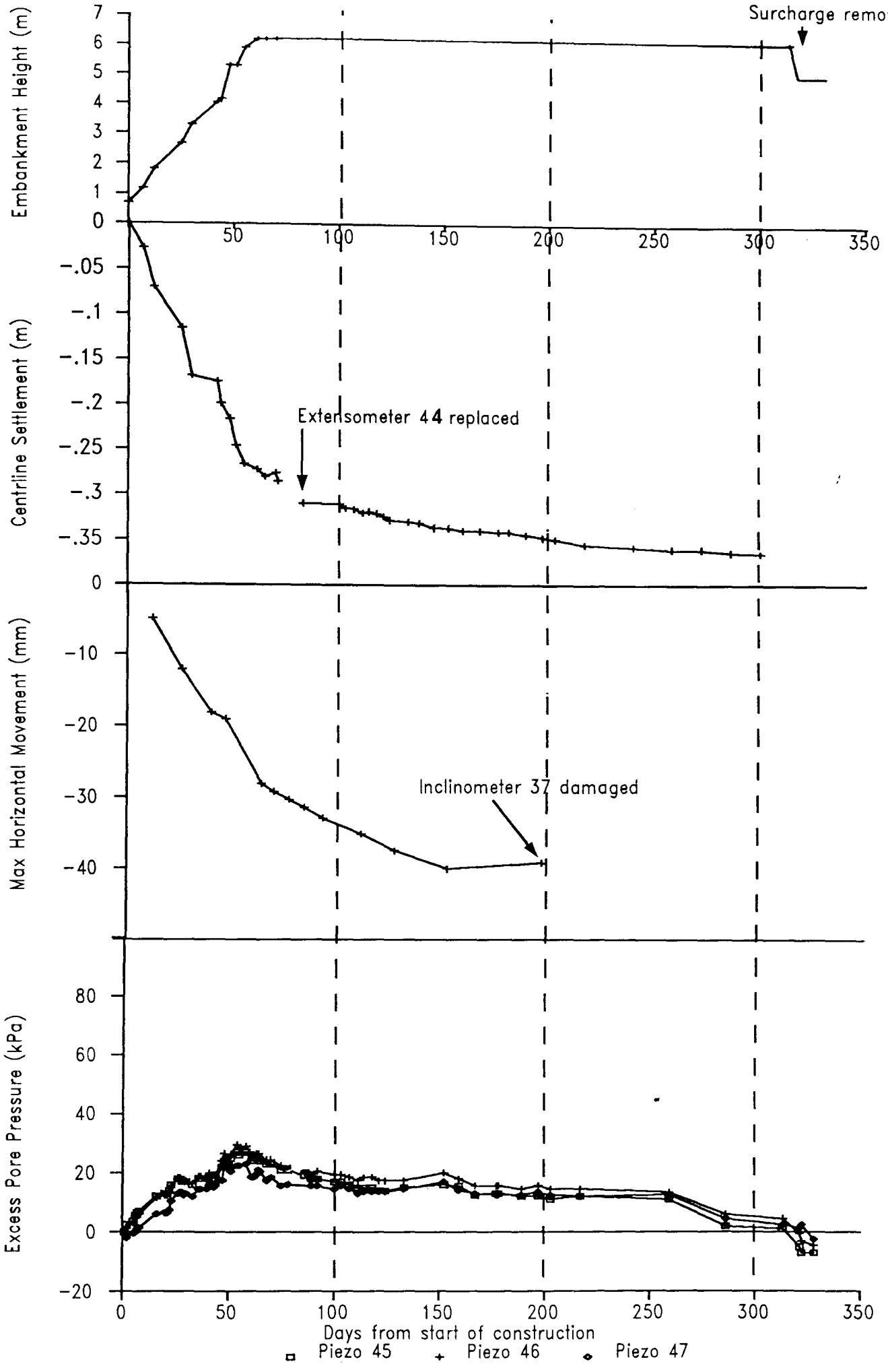

Figure 5.4 Summary of monitoring results at Section AA

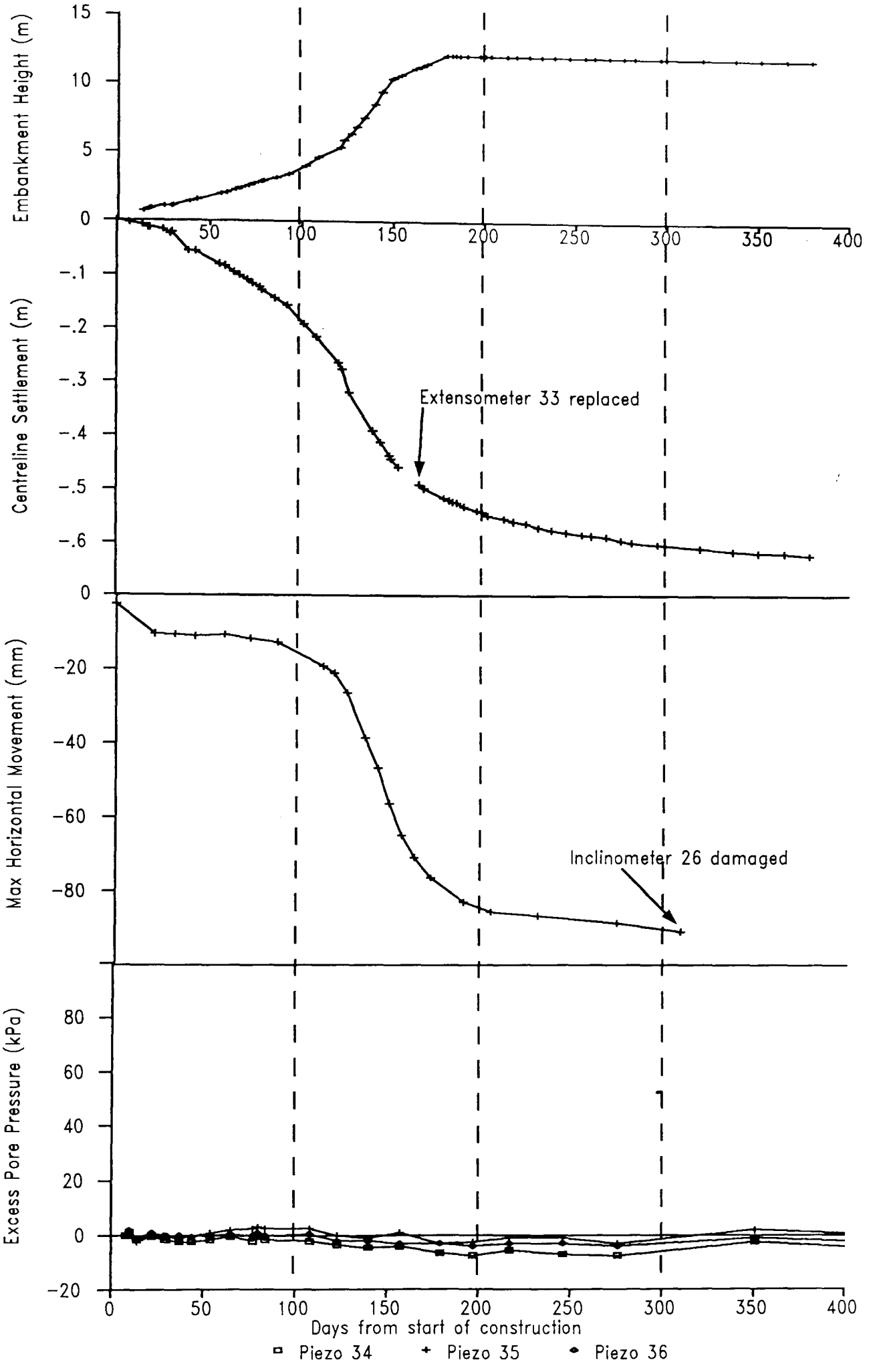

Figure 5.5 Summary of monitoring results at Section DD

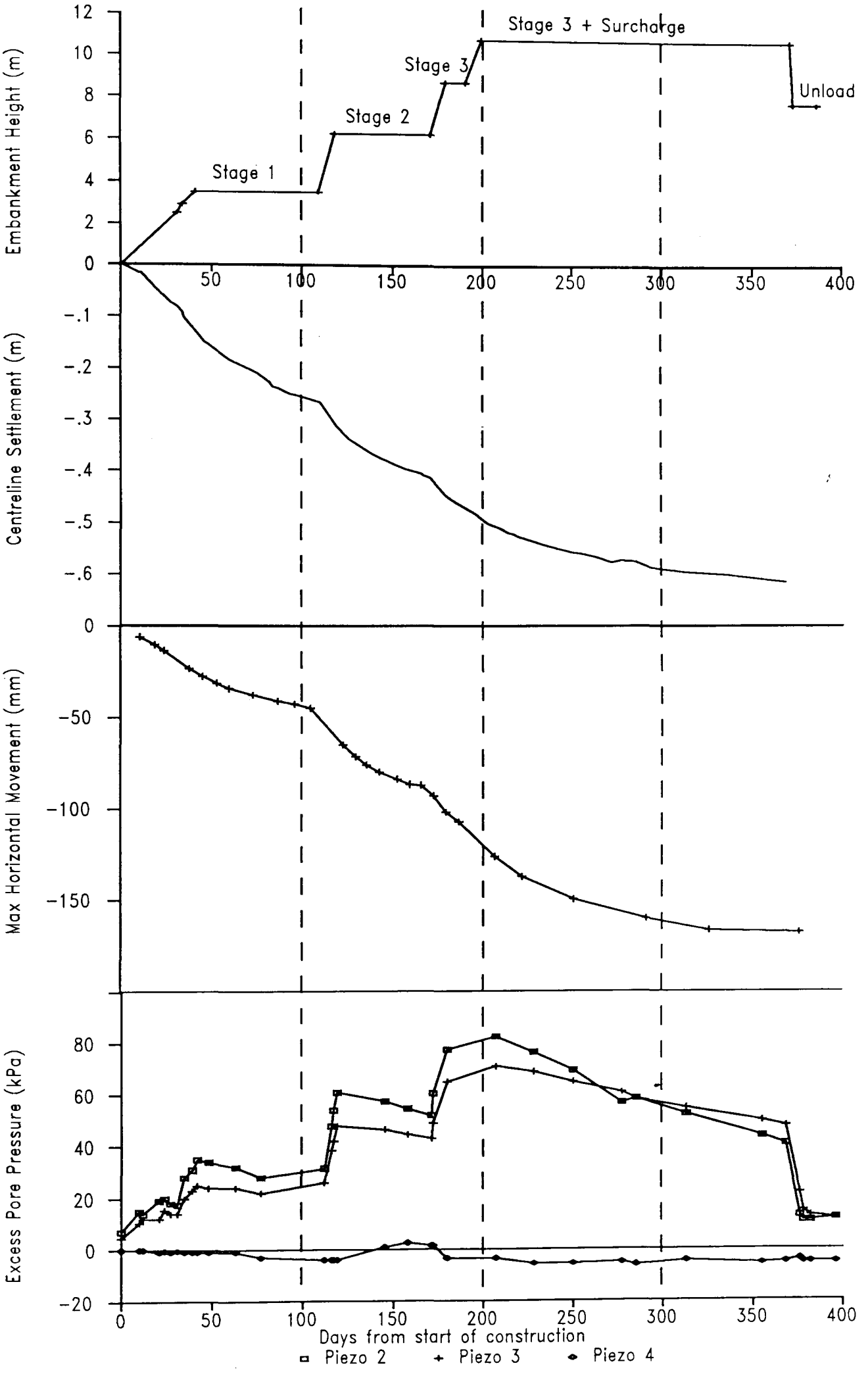

Figure 5.6 Summary of monitoring results at Section EE

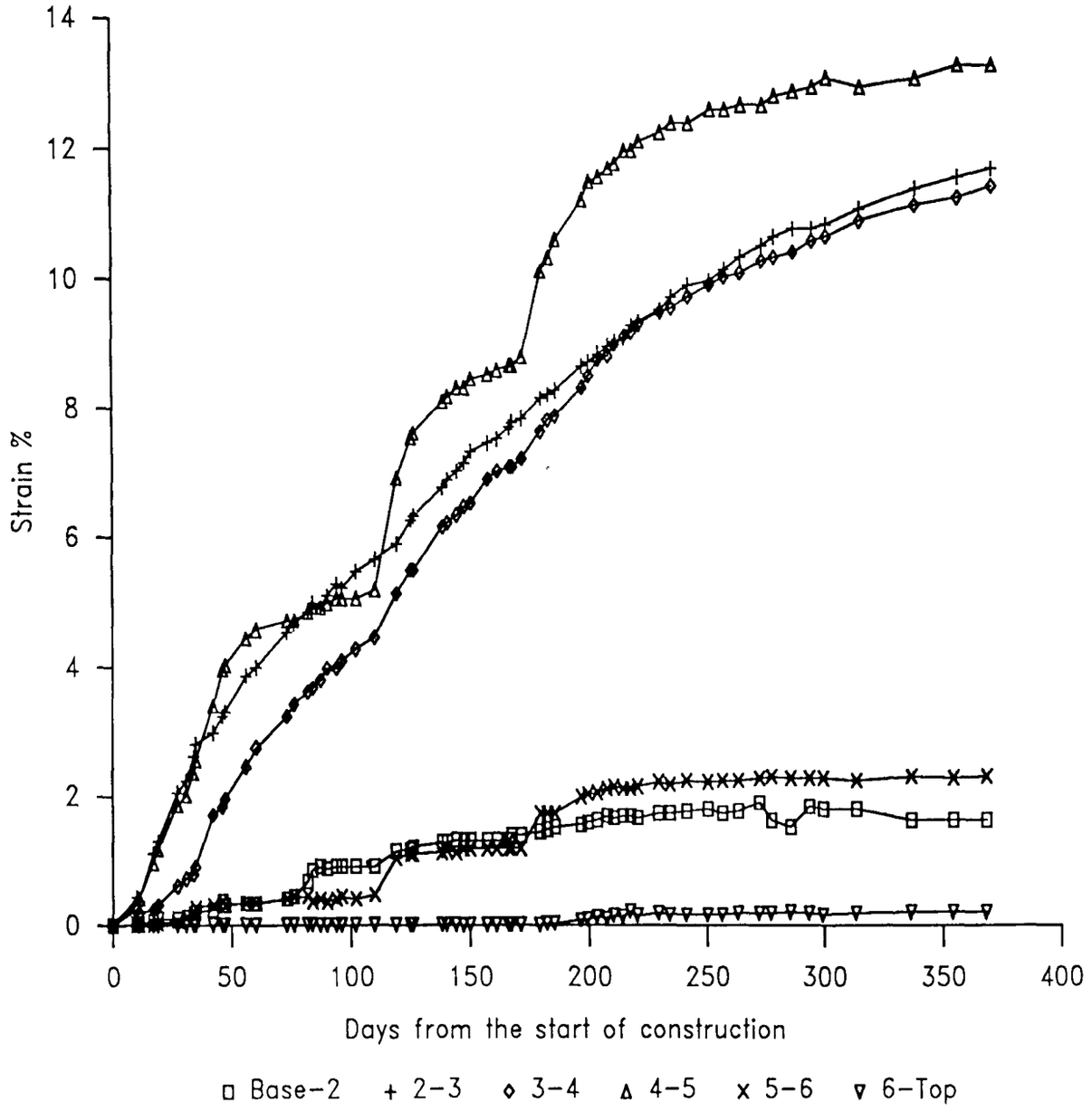

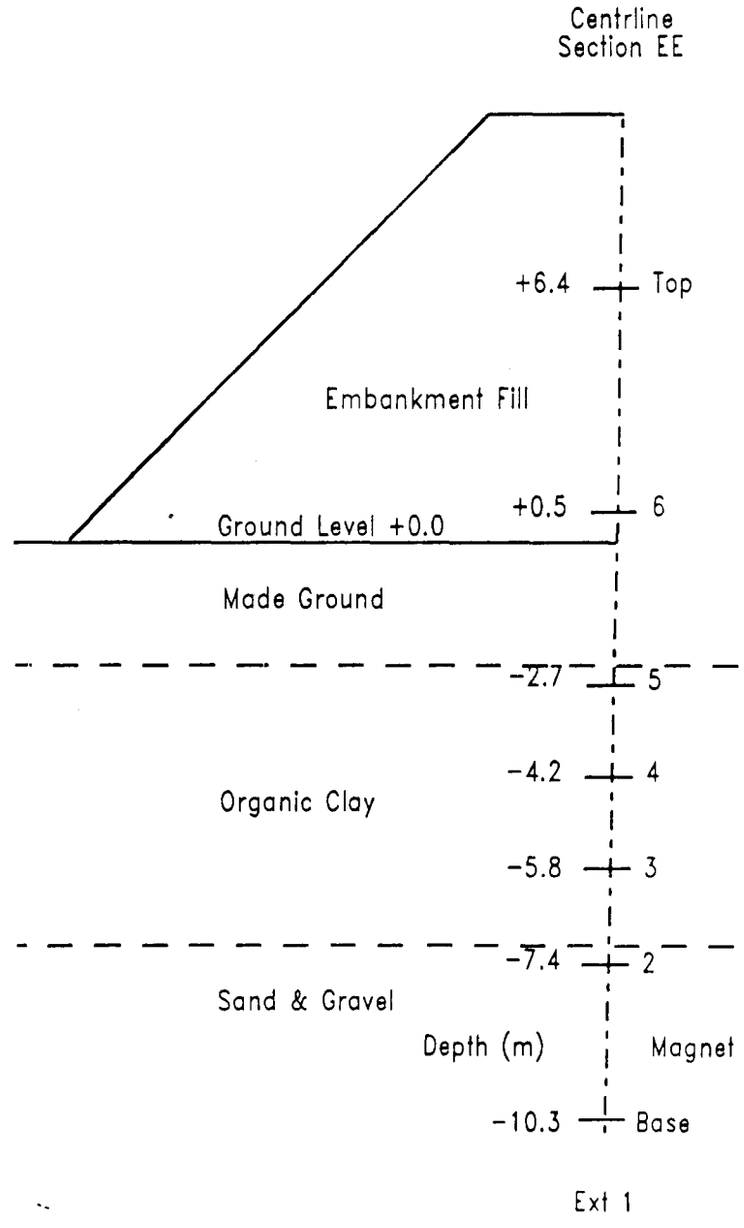

Figure 5.7 Vertical strains in soil layers at the centreline of Section EE

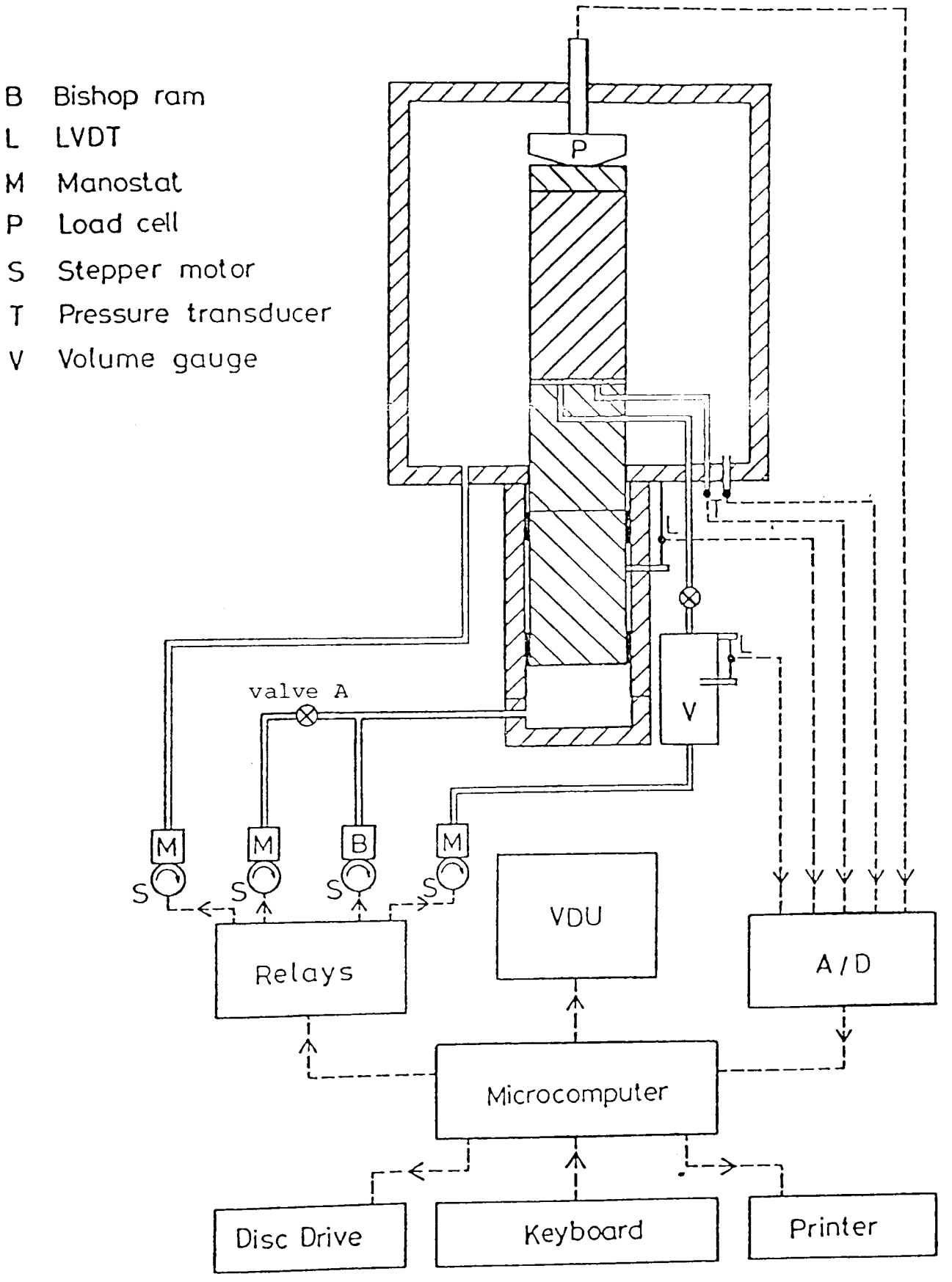

Figure 6.1 Diagramatic layout of the BBC stress path testing equipment (after Atkinson and Clinton, 1984)

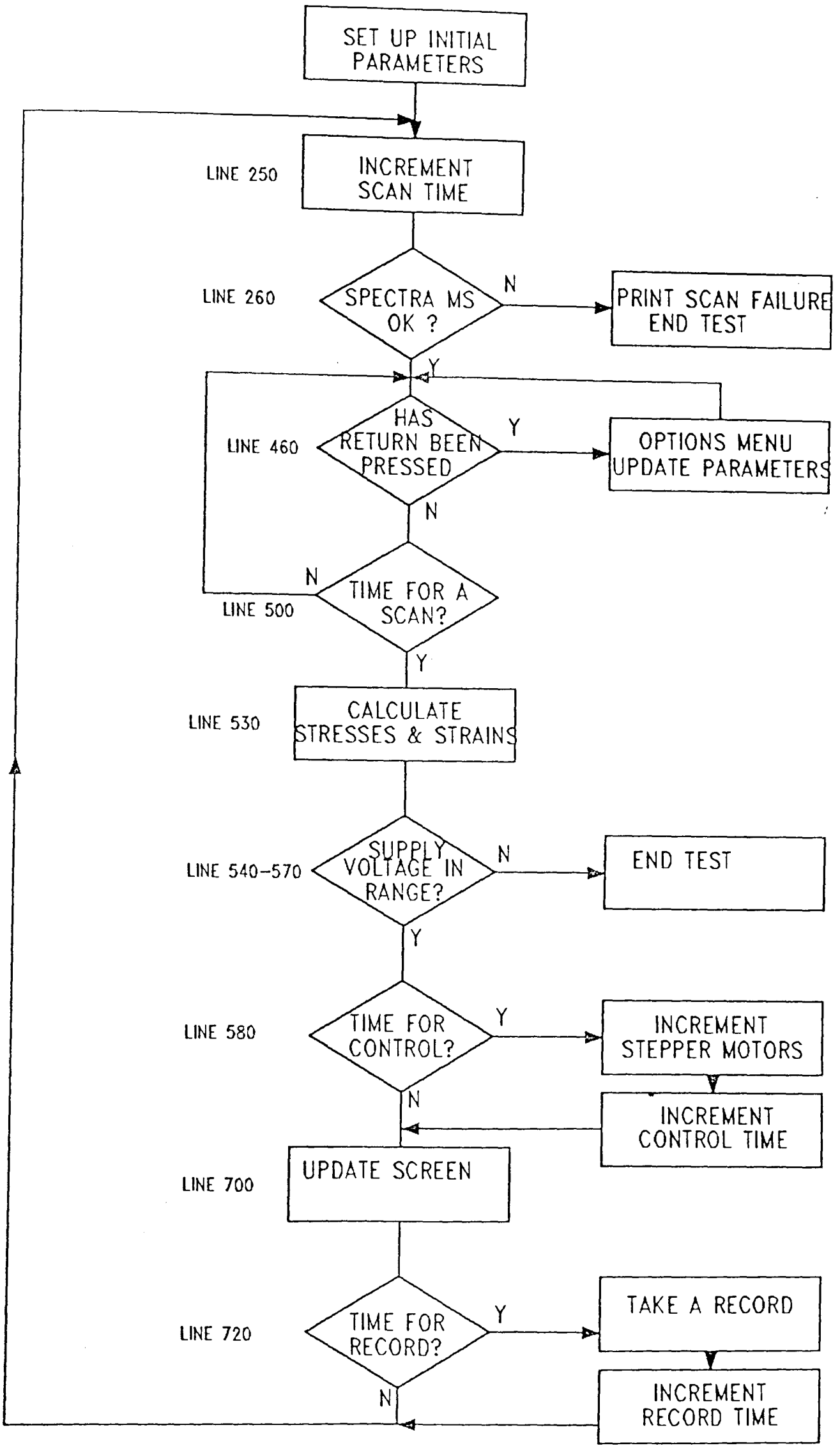

FIGURE 6.2 TRILOG3 MAIN CONTROL LOOP

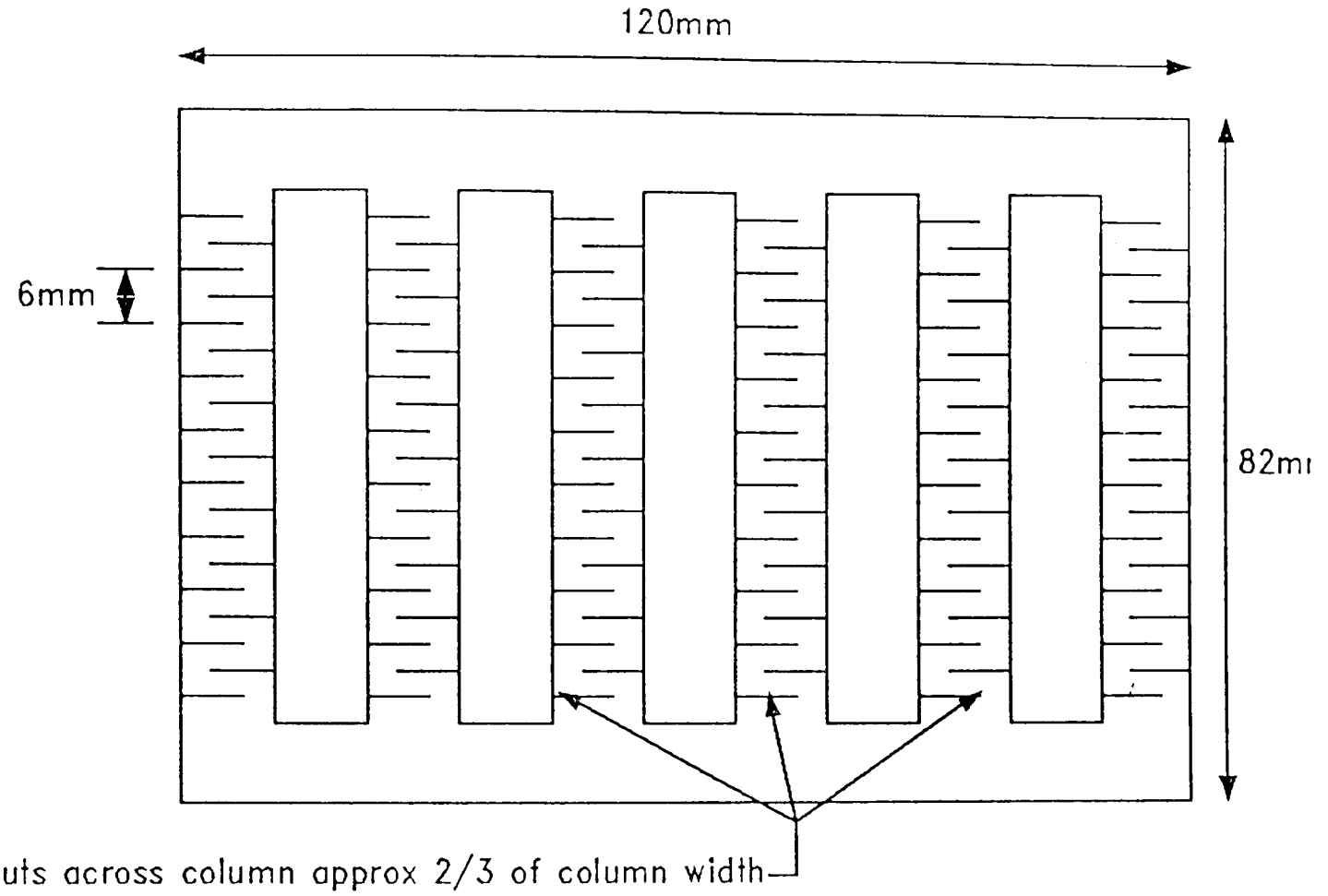

FIGURE 6.3 Wykeham Farrance Type WF10670 Sidedrain Modified for Extension Tes

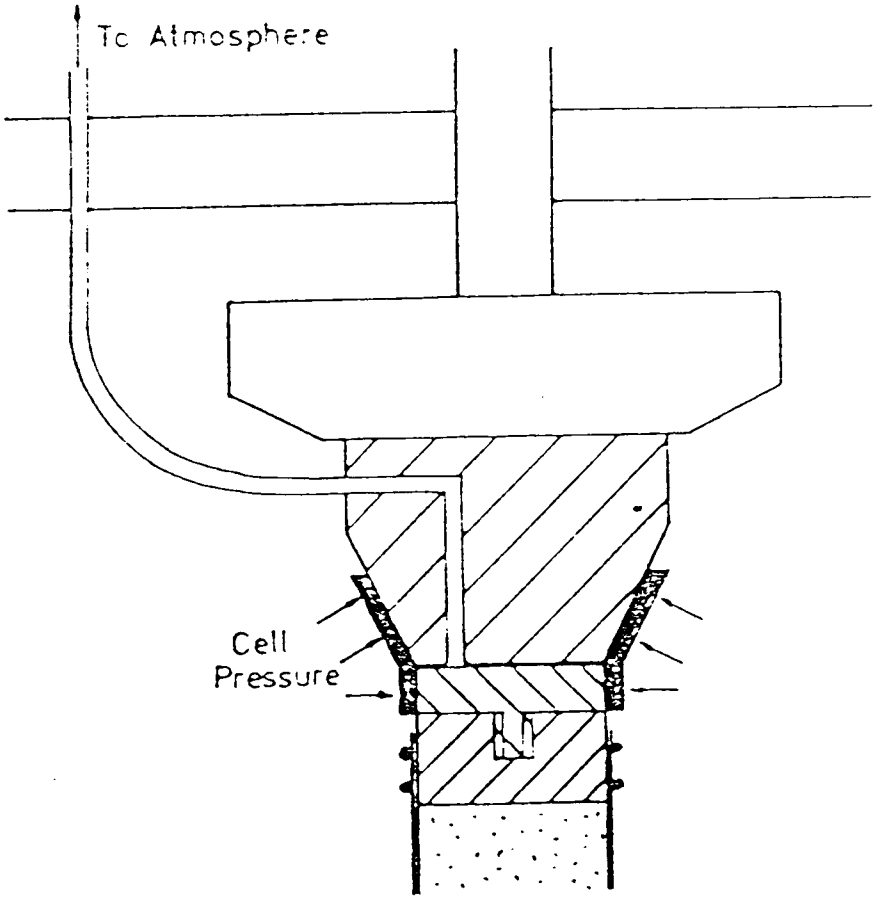

FIGURE 6.4 Top Platen and Suction Cap Fitting Arrangement (after Clinton 1987)

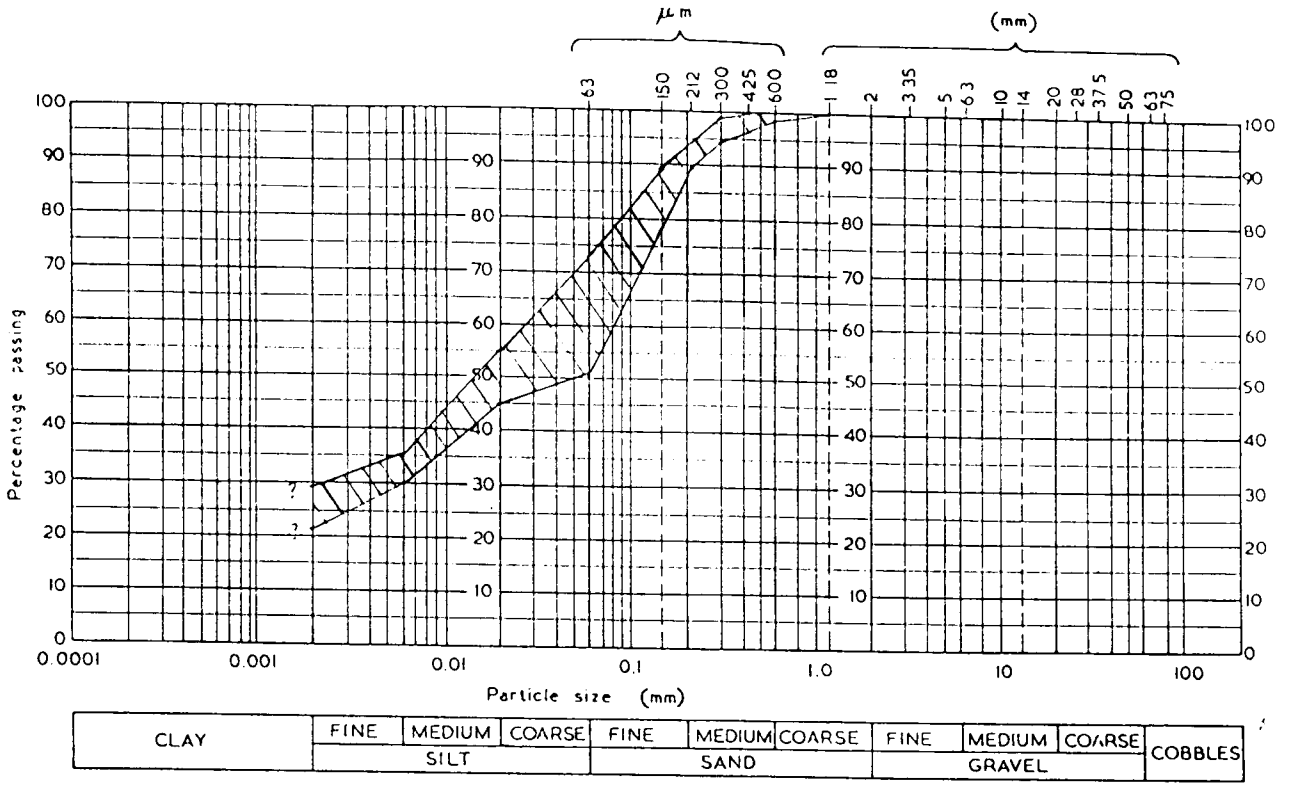

Operator: A. R. Pickles Job: Ph. D. Thesis Site: Eastern Gateway Access Road

Date: November 1987 Borehole No: Various

Description of soil: Grey mottled brown soft silty organic peaty clay with very occassional fine gravel fragments Sample No: Various

Depth of sample Various

Grading envelope from 8 tests British Standard test sieves

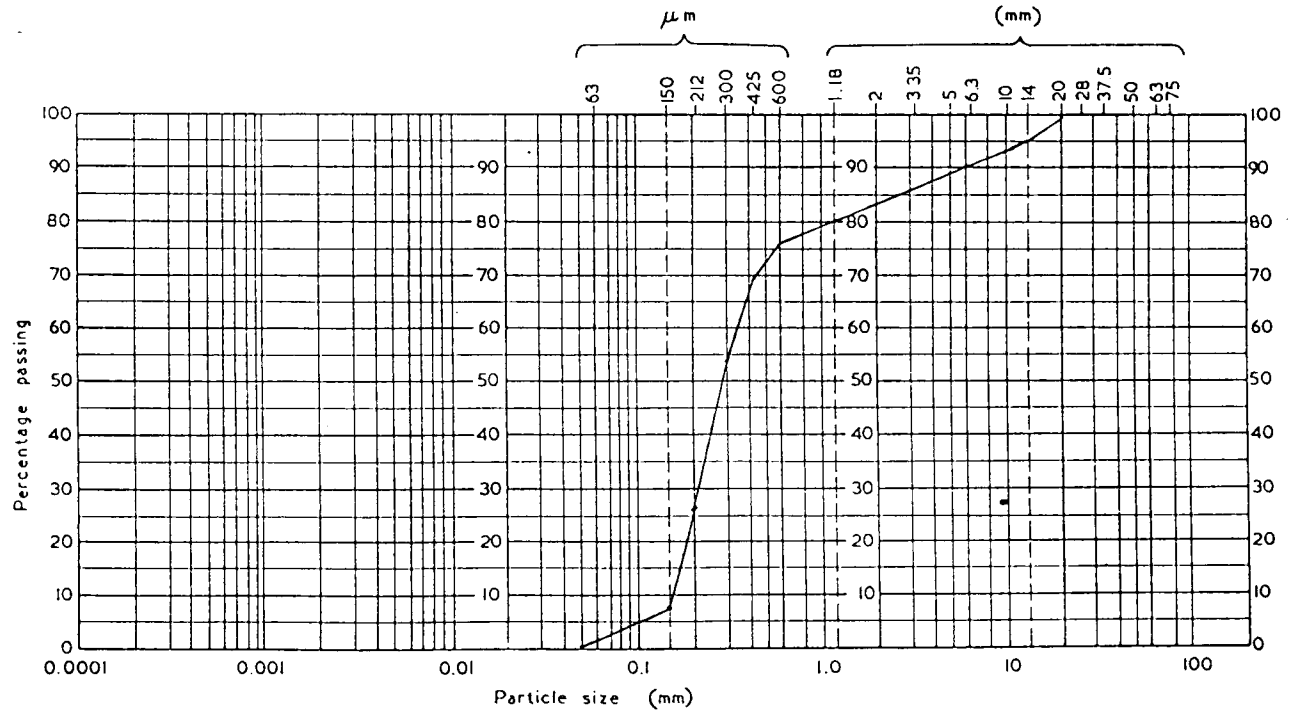

Operator: A. R. Pickles Job: Ph.D. Thesis Site: Eastern Gateway Access Road

Date: November 1987 Borehole No:

Description of soil: fine to medium sand with occassional fine to medium rounded gravel and shells Sample No: } Embankment fill mixed sample

Depth of sample }

British Standard test sieves

Figure 7.1 Results of grading analyses on organic clay and embankment sand fill samples.

Isotropic Compression Tests on Samples at Different Organic Contents

Incremental Loading – 24 Hours/Increment

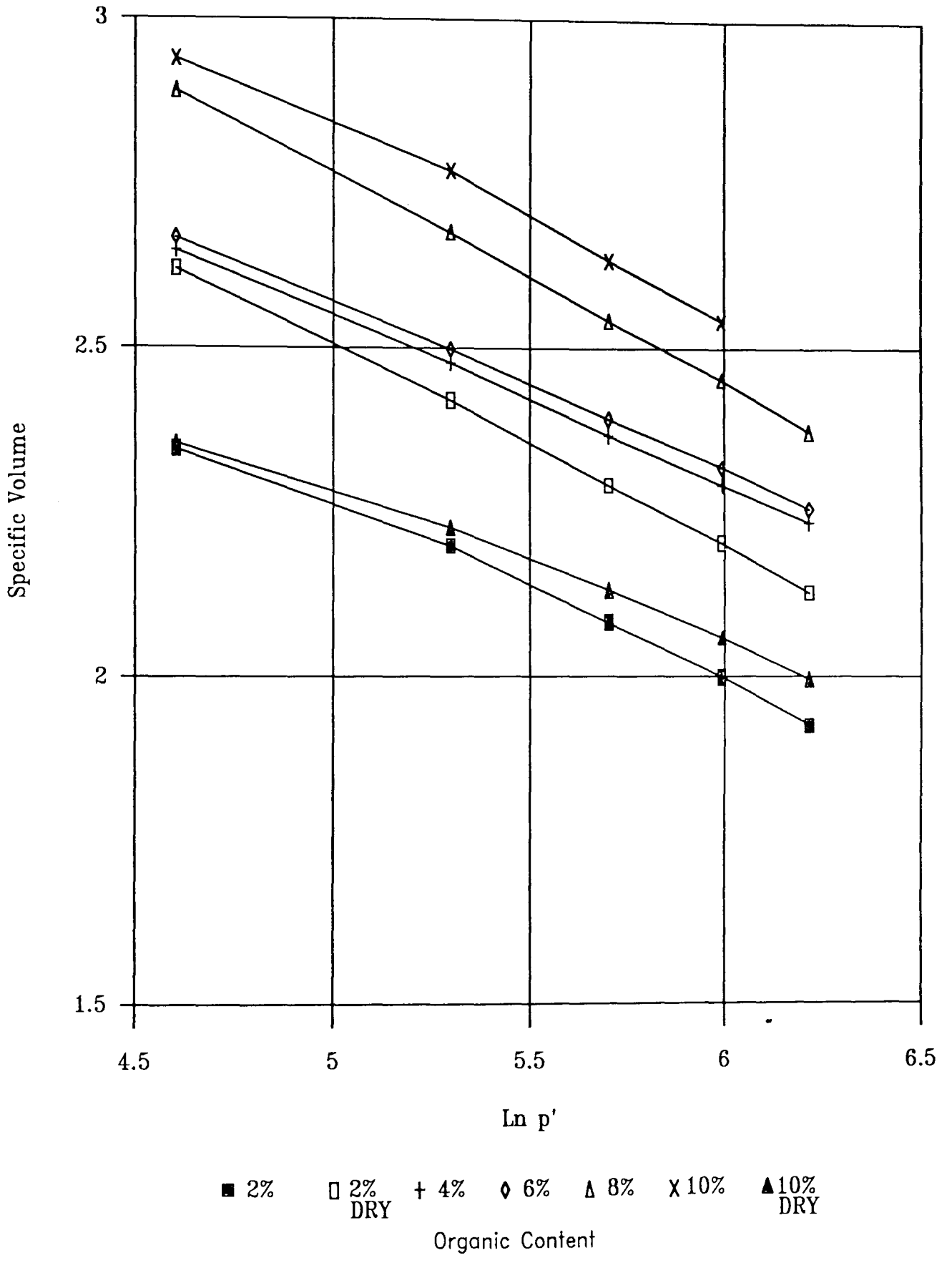

FIGURE 7.2 Compression Test Results at Different Organic Contents

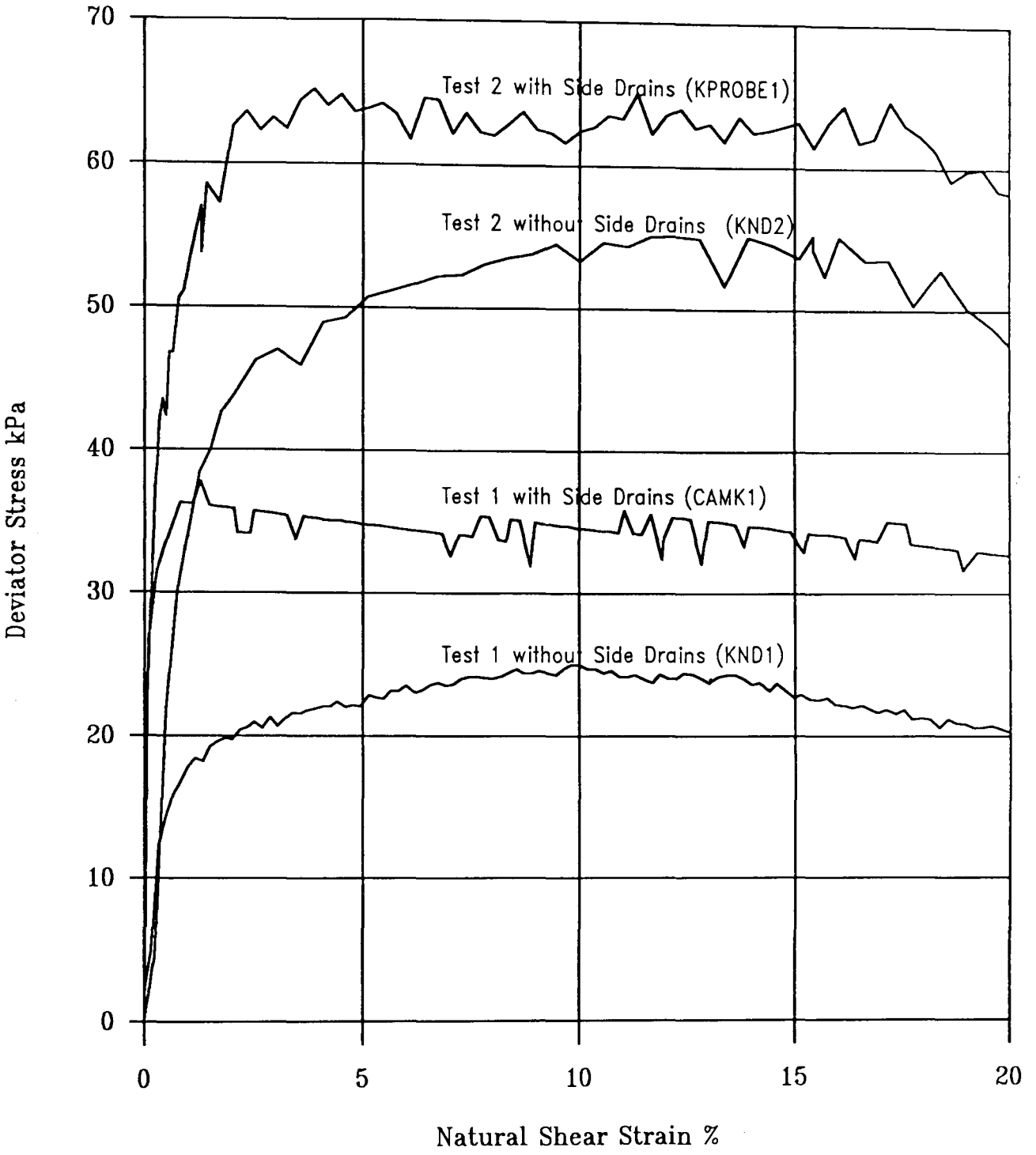

Test 1 P'_p = 75 kPa OCR = 1.5 ISOTROPIC CONSOLIDATION

Test 2 P'_p = 150 kPa OCR = 1.0 ISOTROPIC CONSOLIDATION

Figure 7·3 Results of Tests on Kaolin to determine Side Drain Stiffness

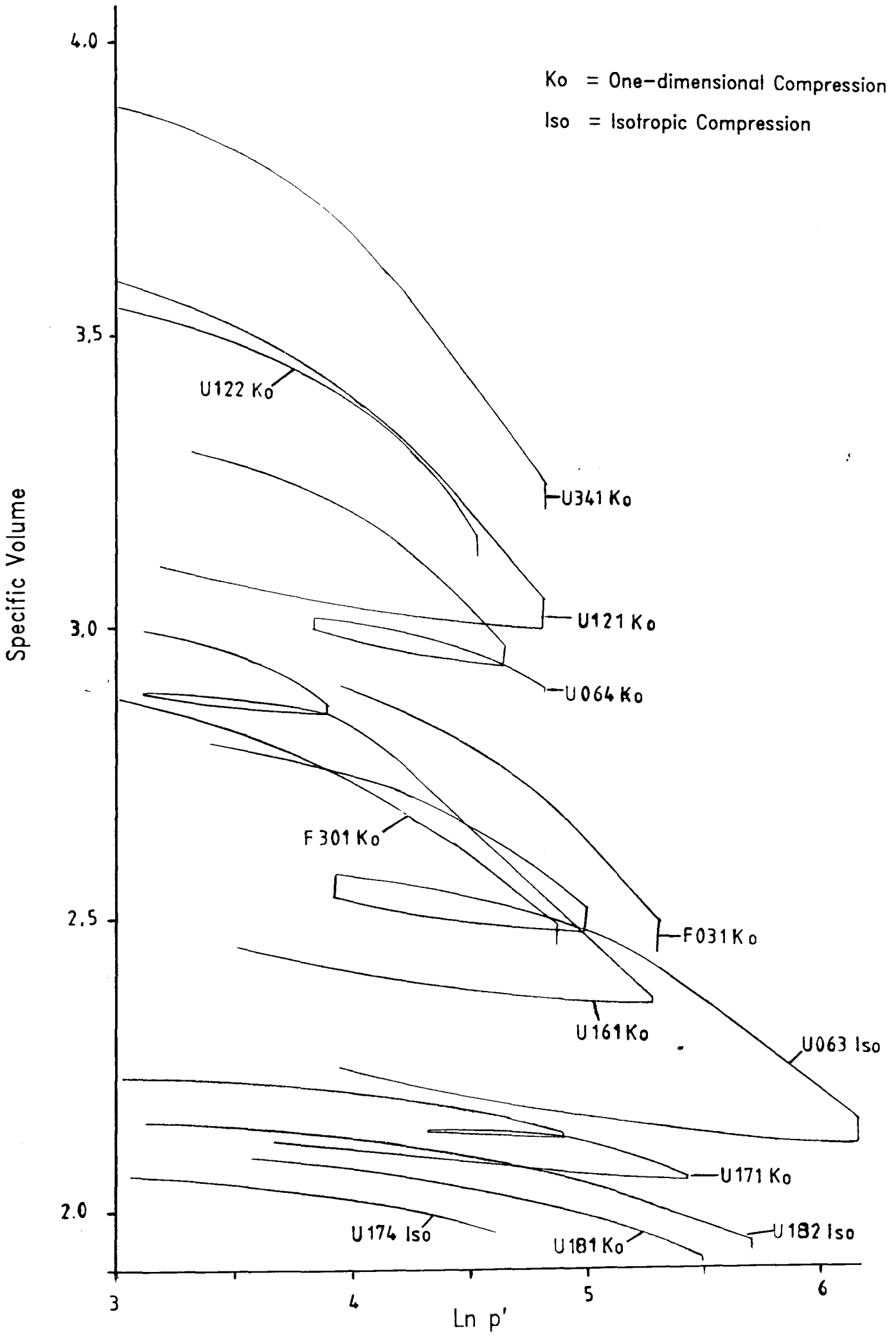

Figure 7.4 Summary of compression test data for organic clay piston samples

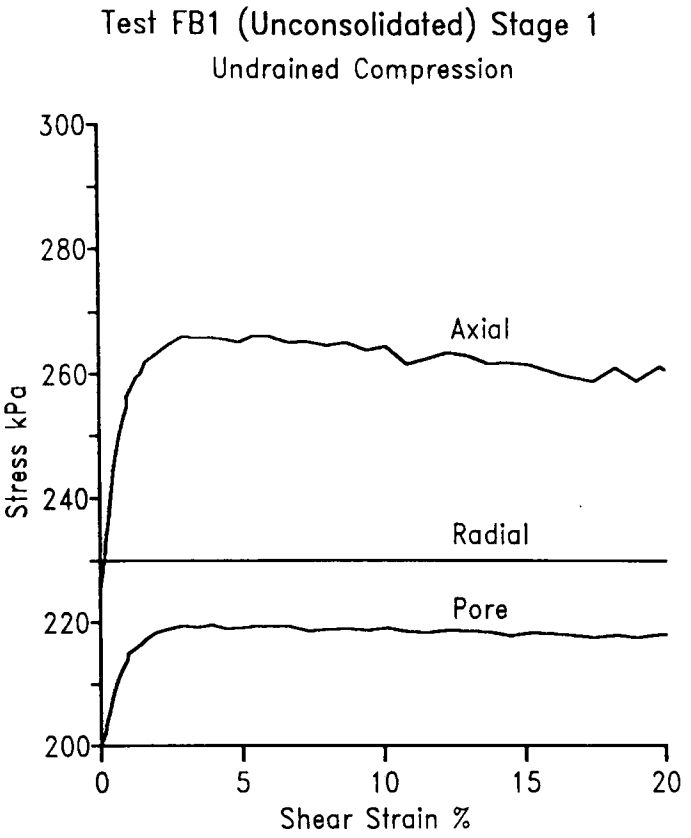

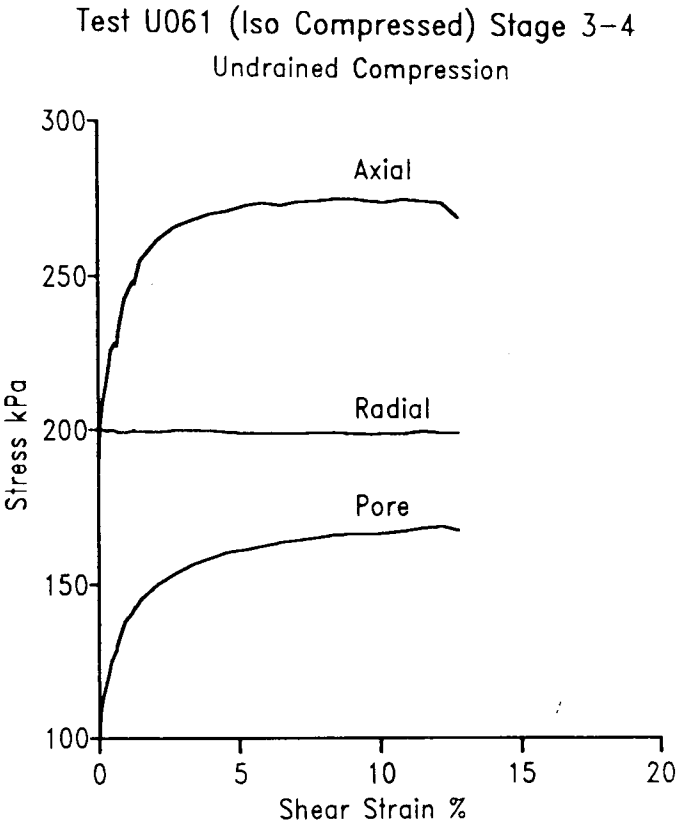

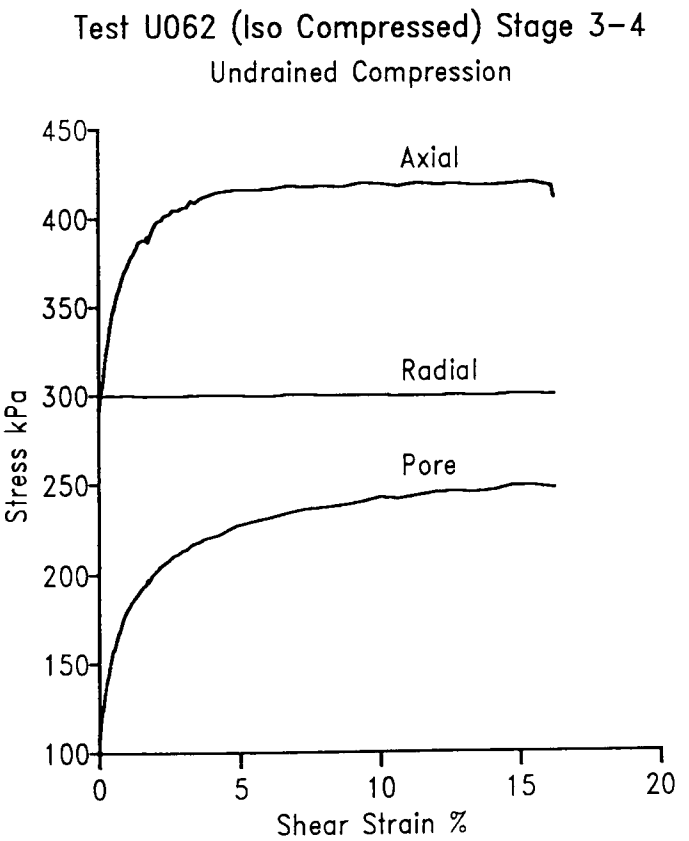

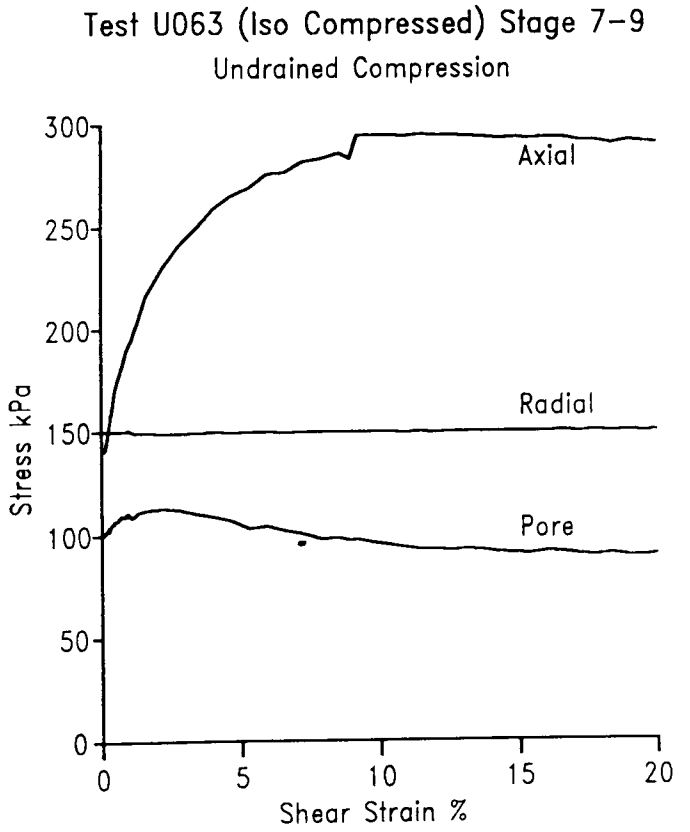

Figure 7.5 Shearing stages on organic clay piston samples – Basic test data (Sheet 1 of 3)

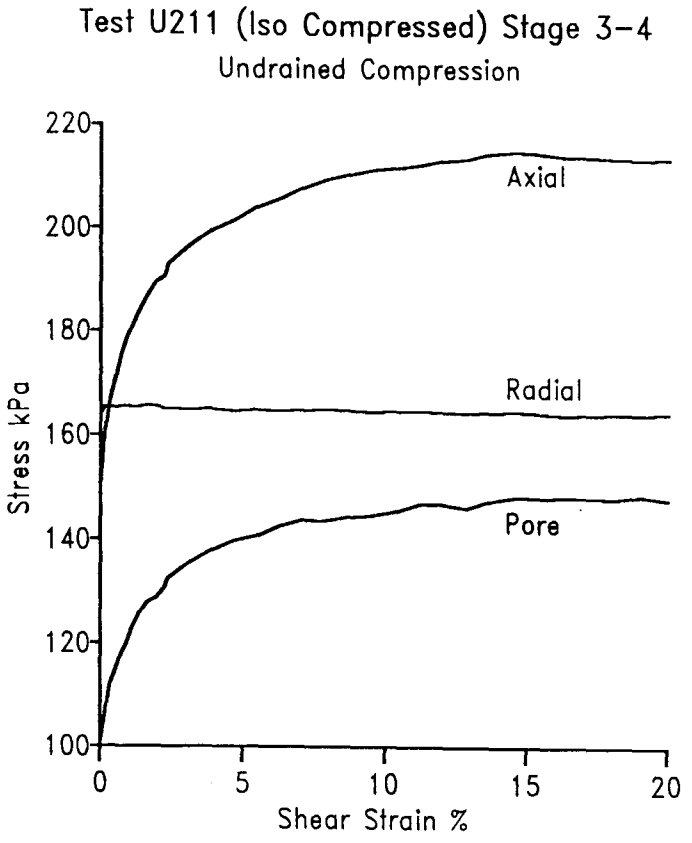

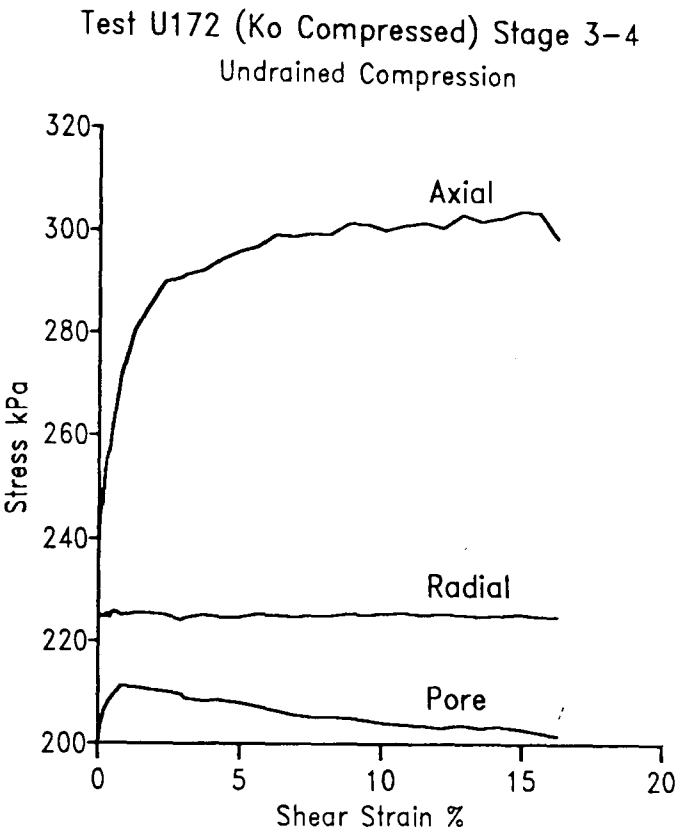

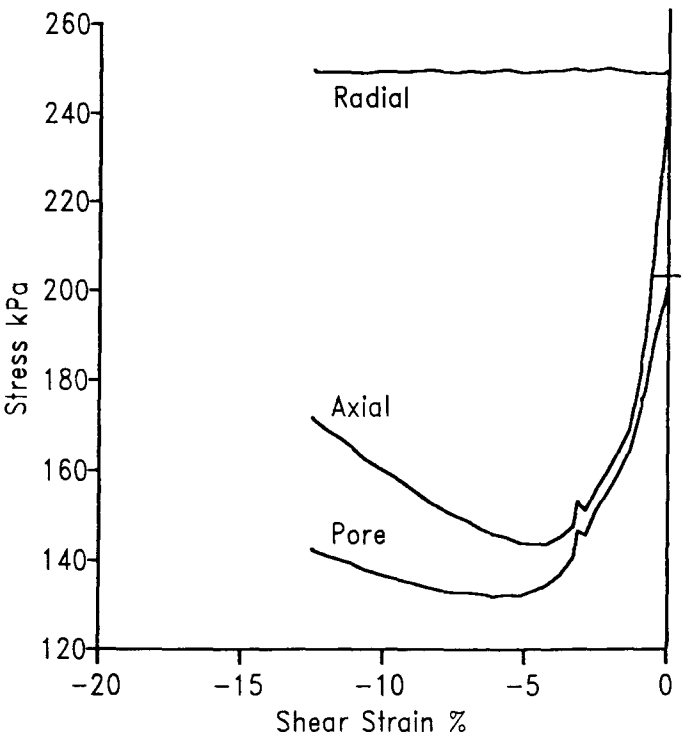

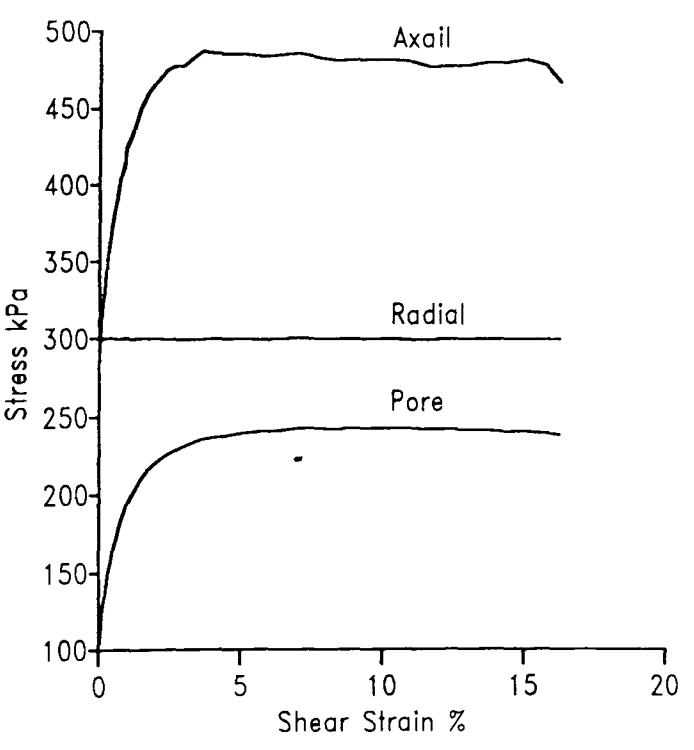

Figure 7.5 Shearing stages on organic clay piston samples – Basic test data (Sheet 2 of 3)

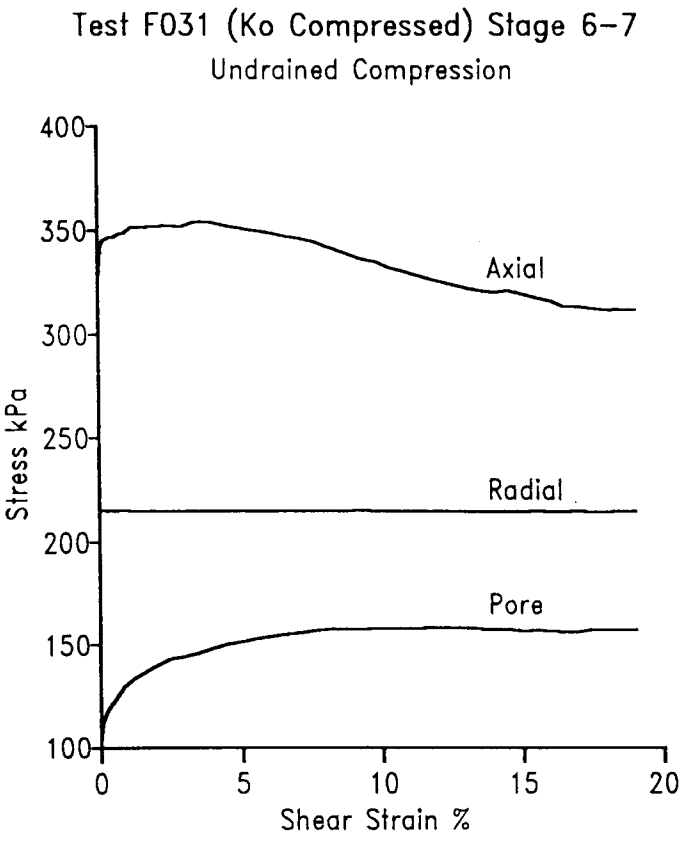

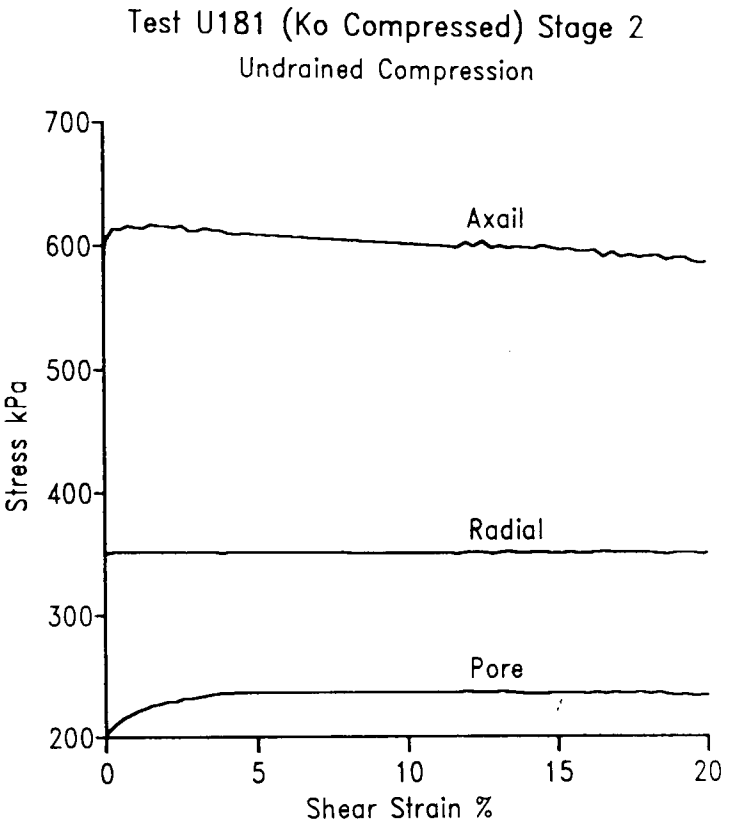

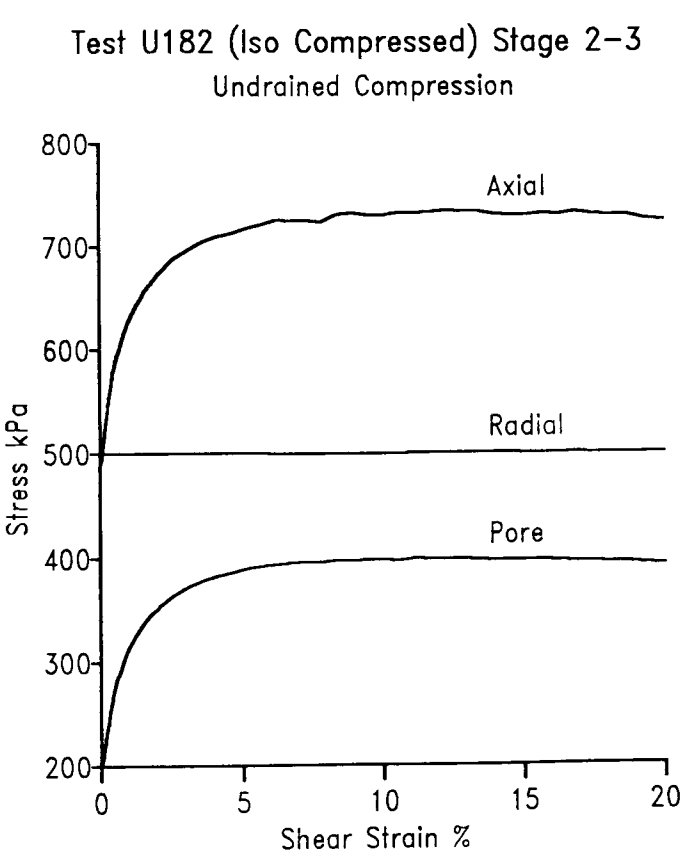

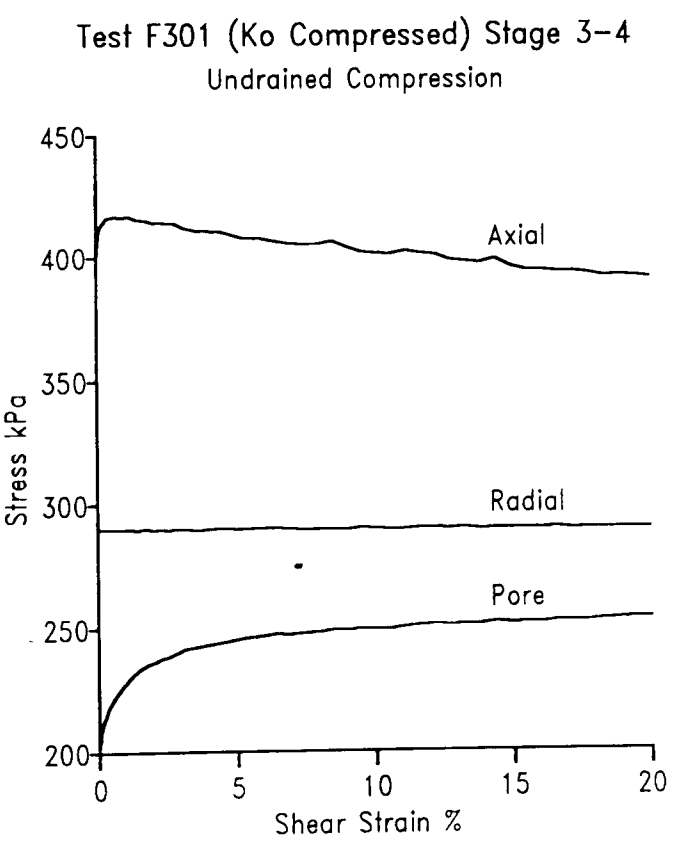

Figure 7.5 Shearing stages on organic clay piston samples – Basic test data (Sheet 3 of 3)

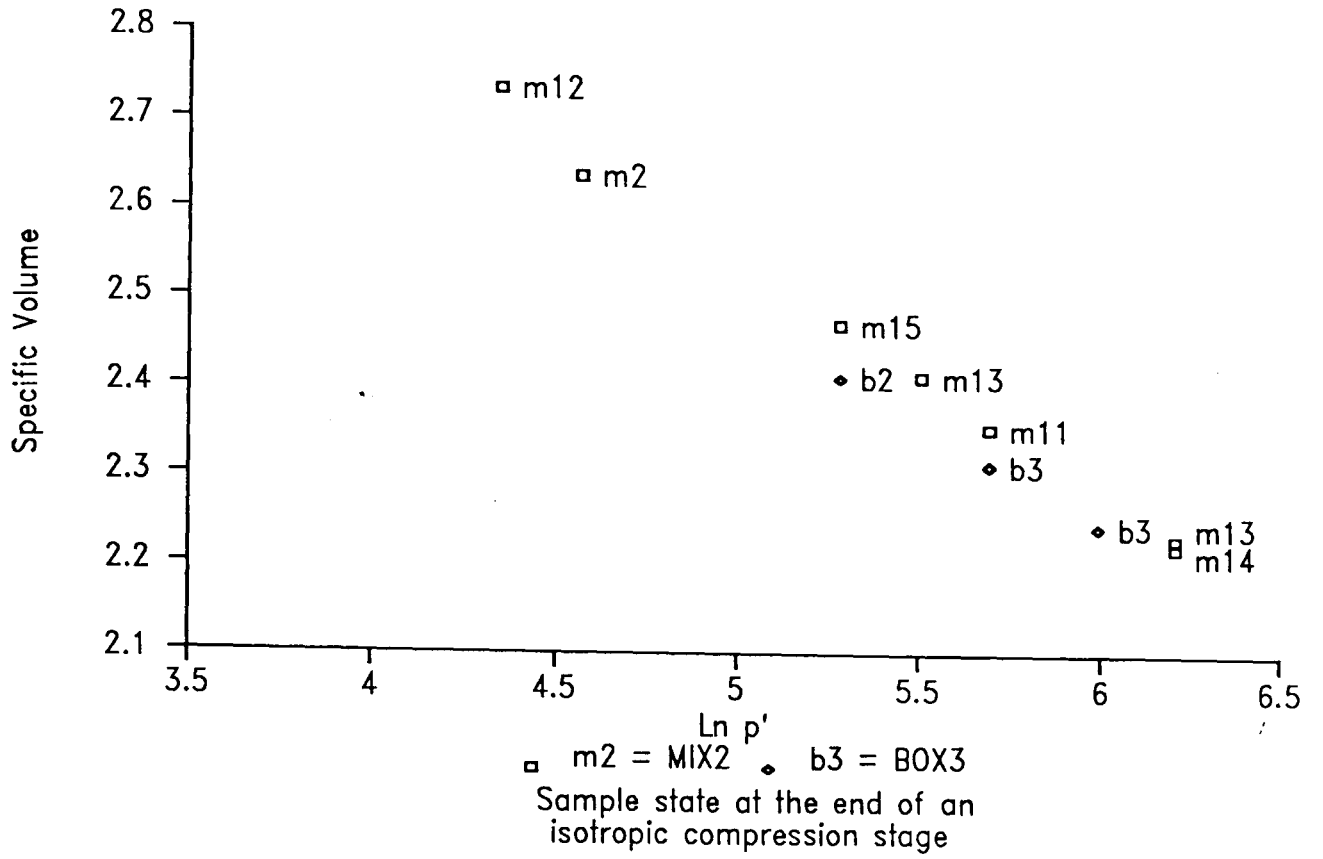

Figure 7.6 Compression test results for isotropically compressed reconstituted organic clay samples

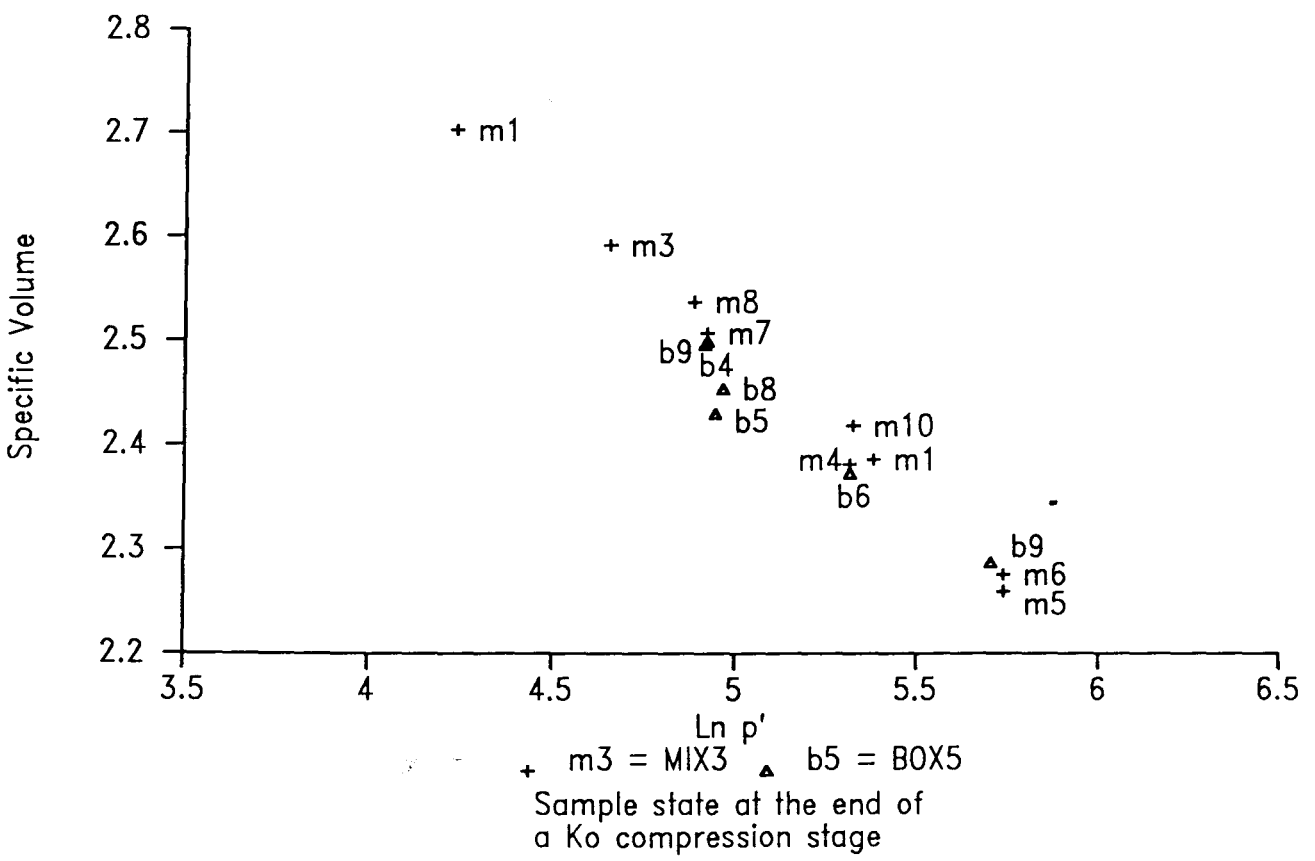

Figure 7.7 Compression test results for Ko compressed reconstituted organic clay samples

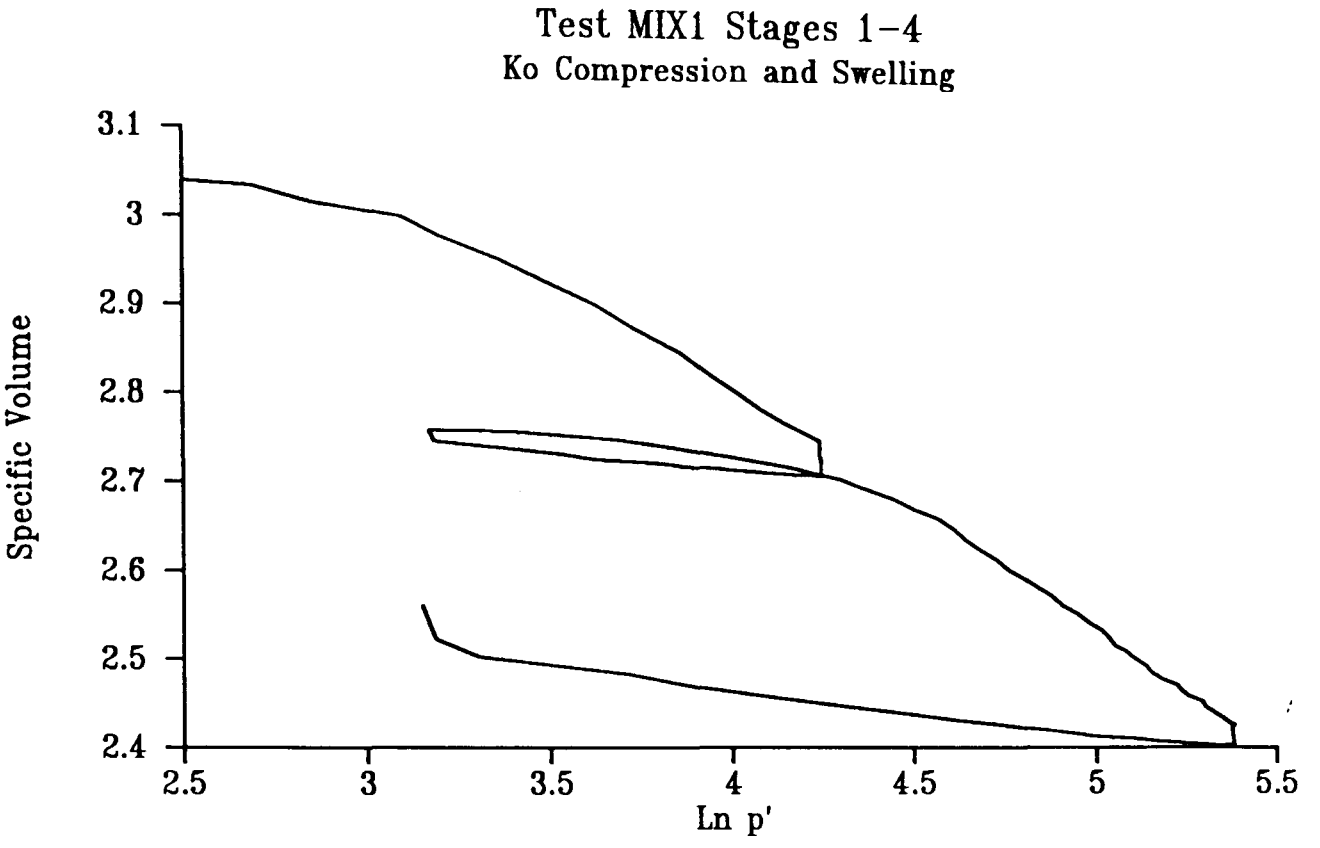

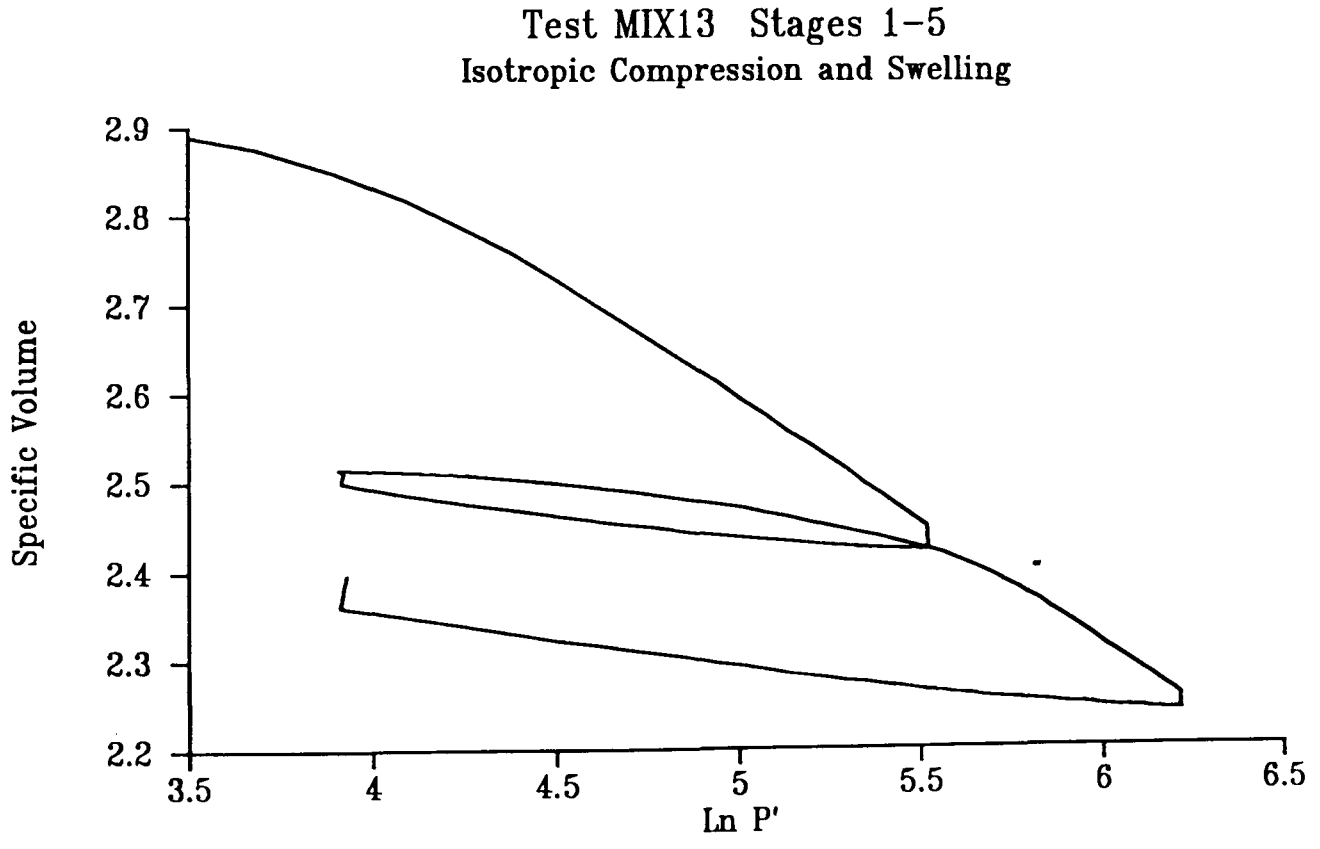

Figure 7.8 MIX1 and MIX13 Compression test results

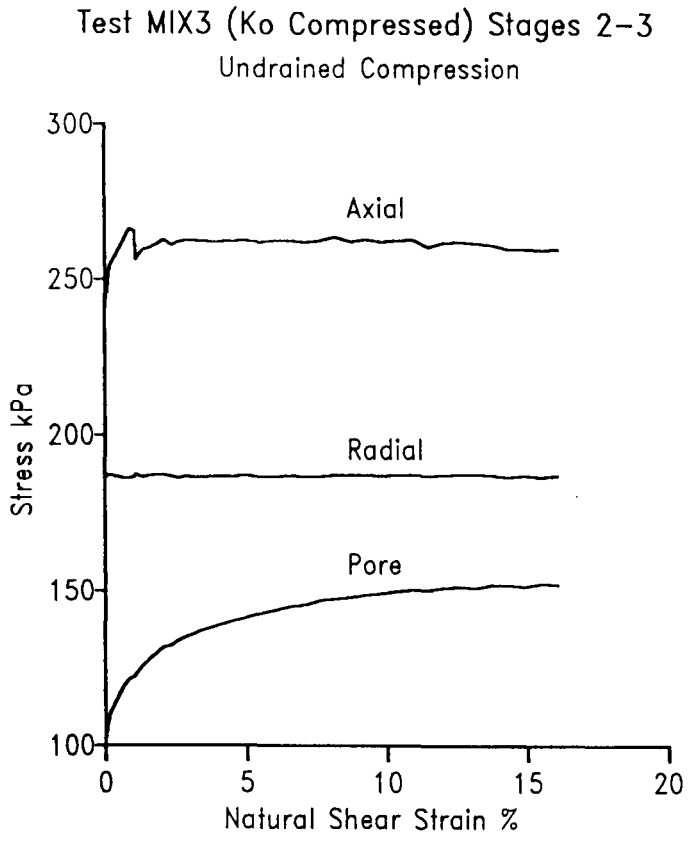

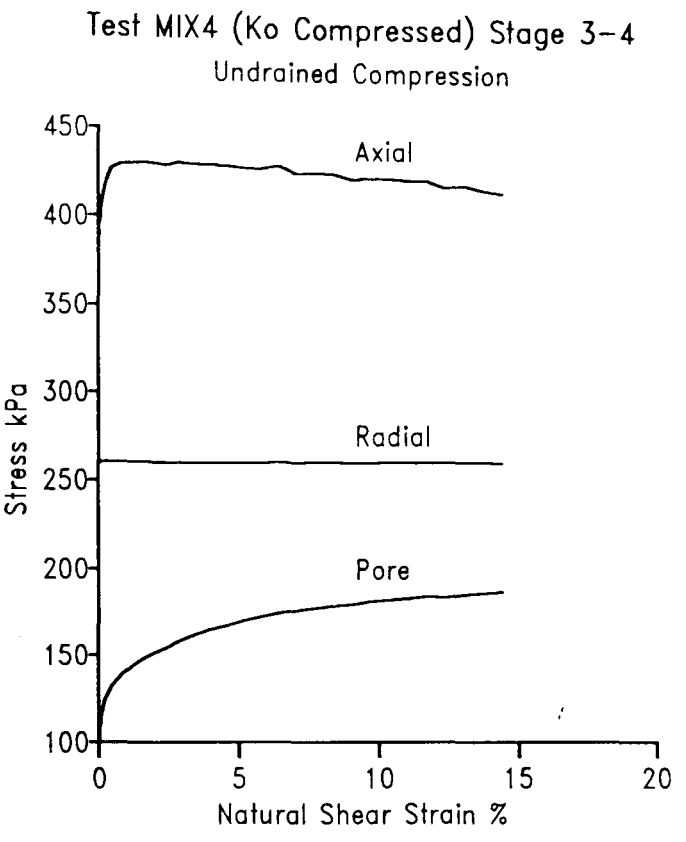

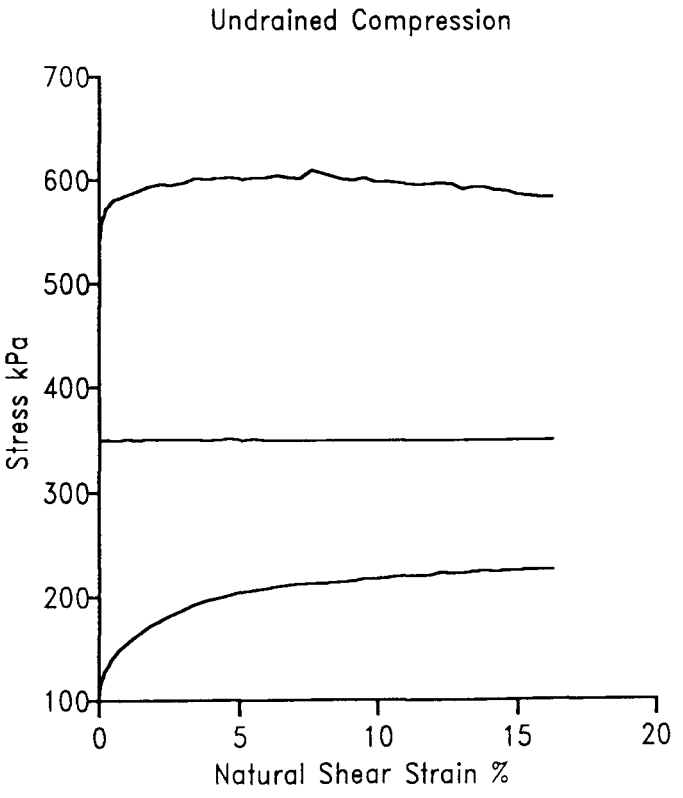

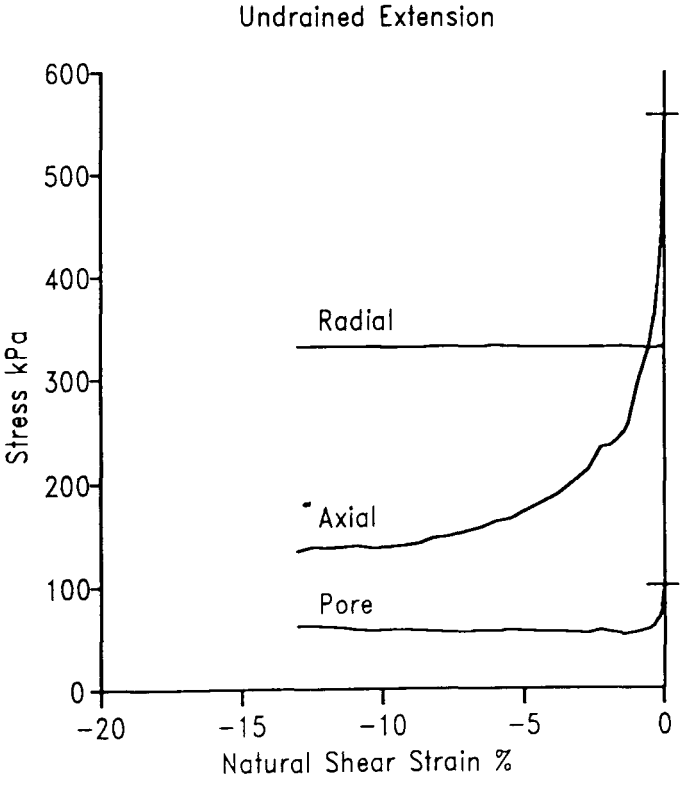

Figure 7.9 Shearing stages on reconstituted organic clay samples – Basic test data (Sheet 1 of 4)

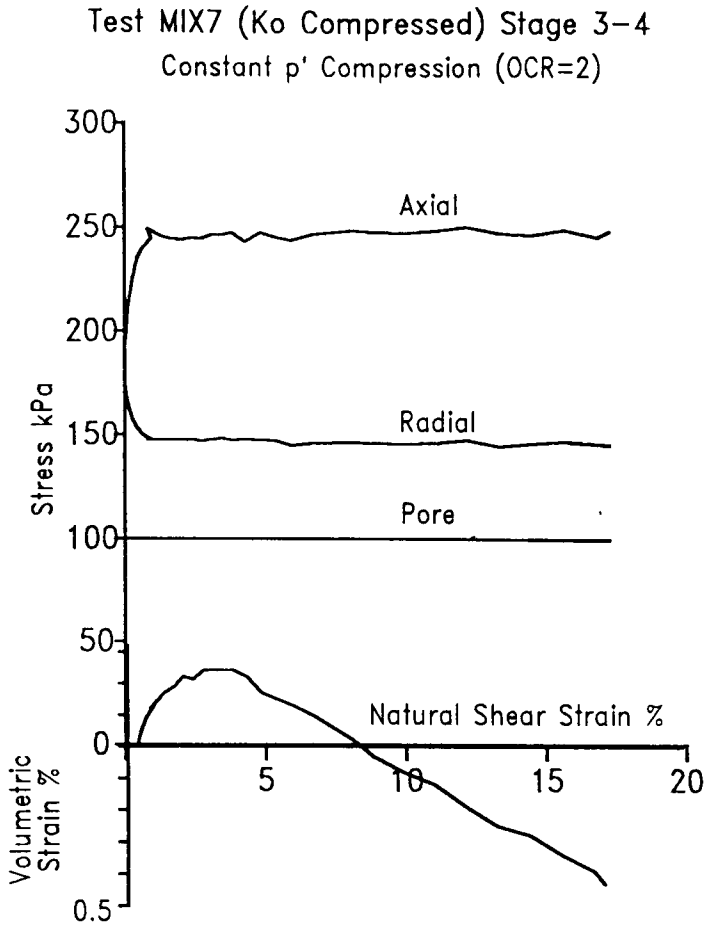

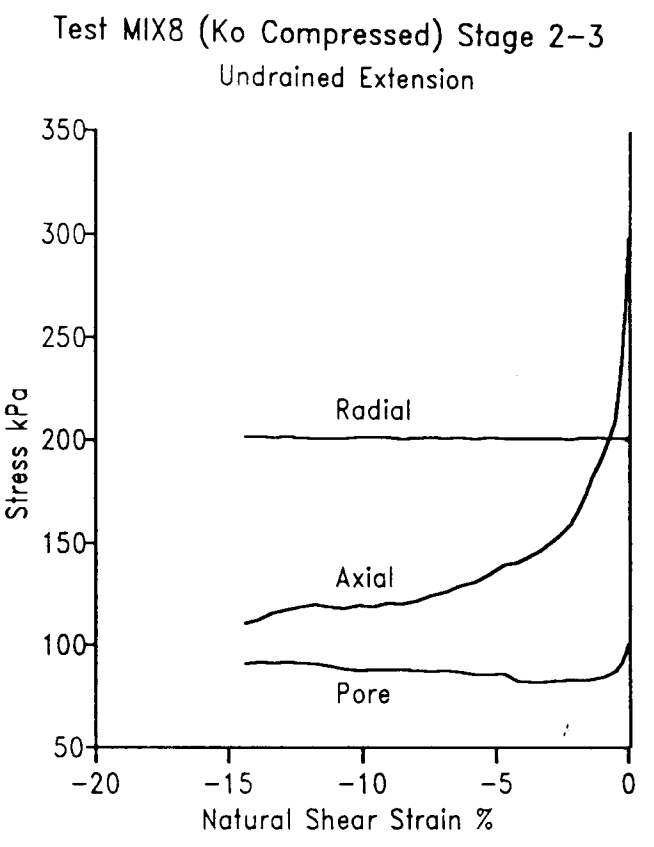

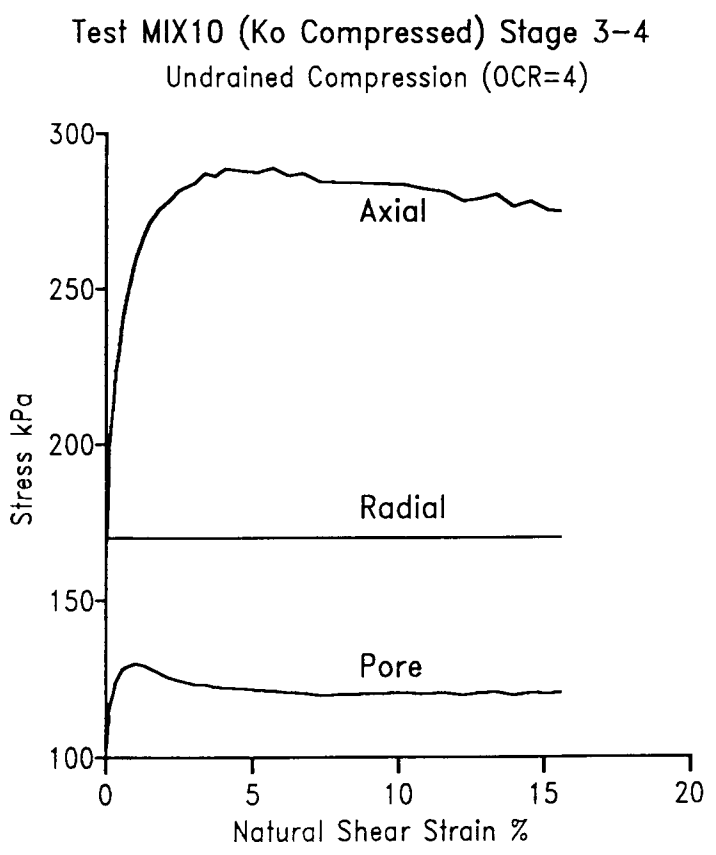

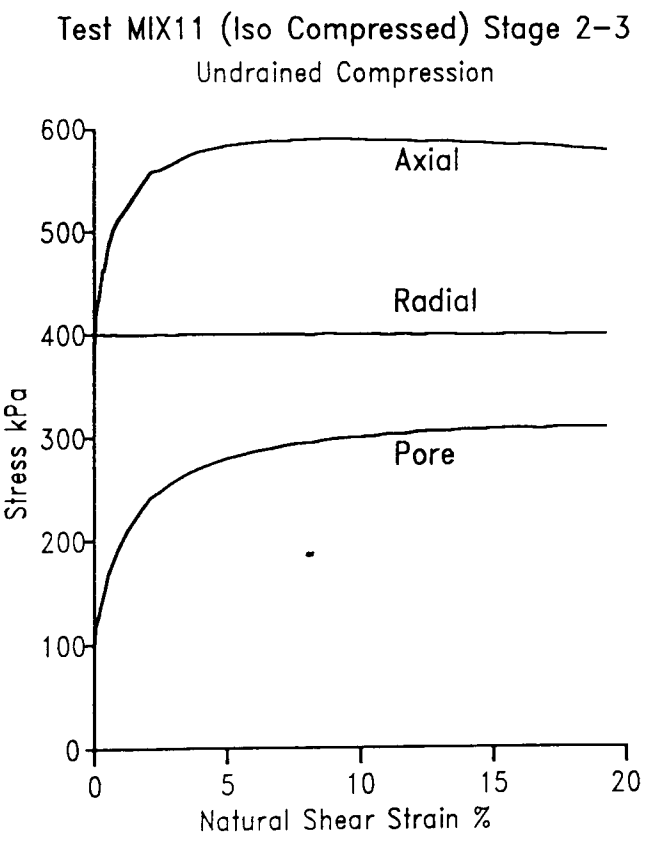

Figure 7.9 Shearing stages on reconstituted organic clay samples – Basic test data (Sheet 2 of 4)

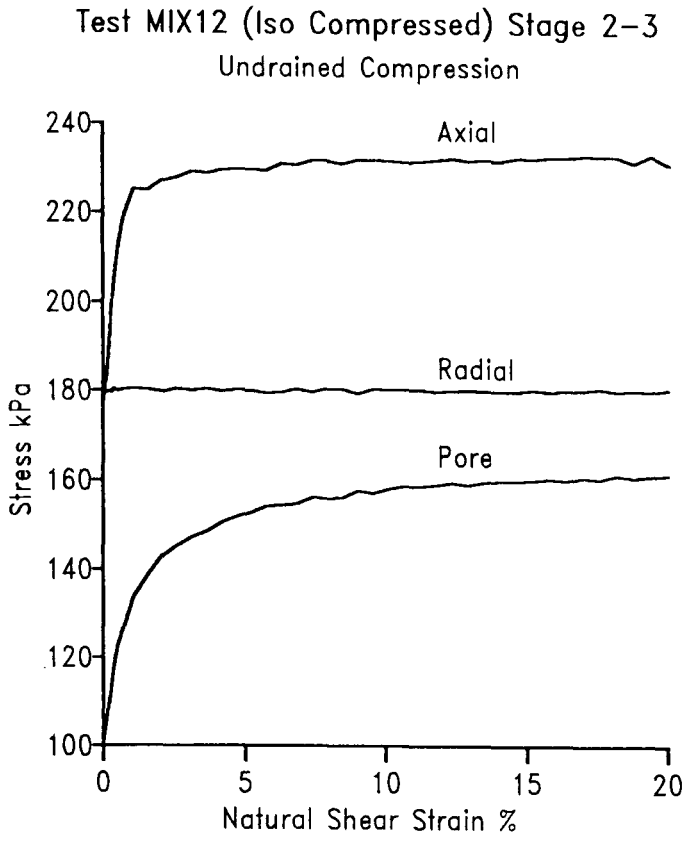

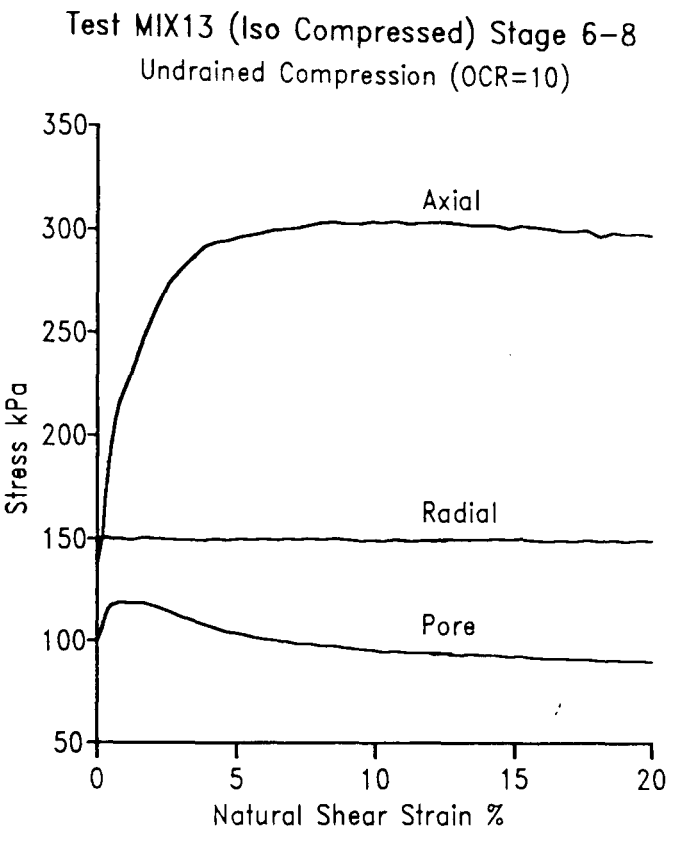

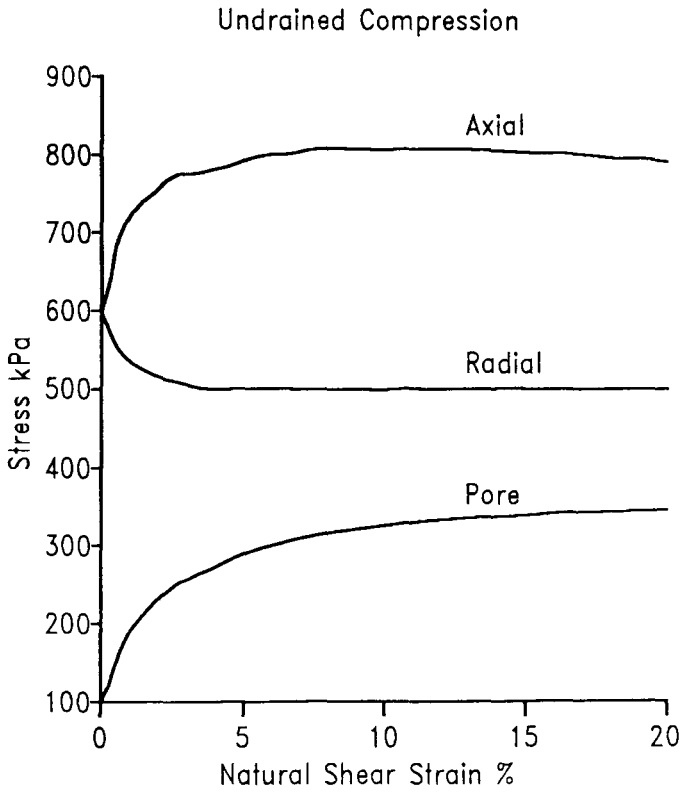

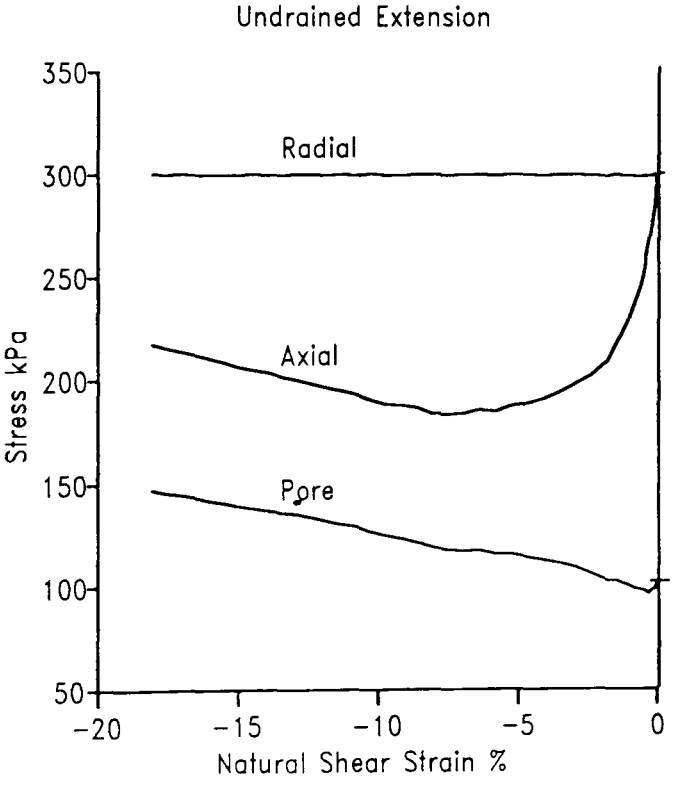

Figure 7.9 Shearing stages on reconstituted organic clay samples – Basic test data (Sheet 3 of 4)

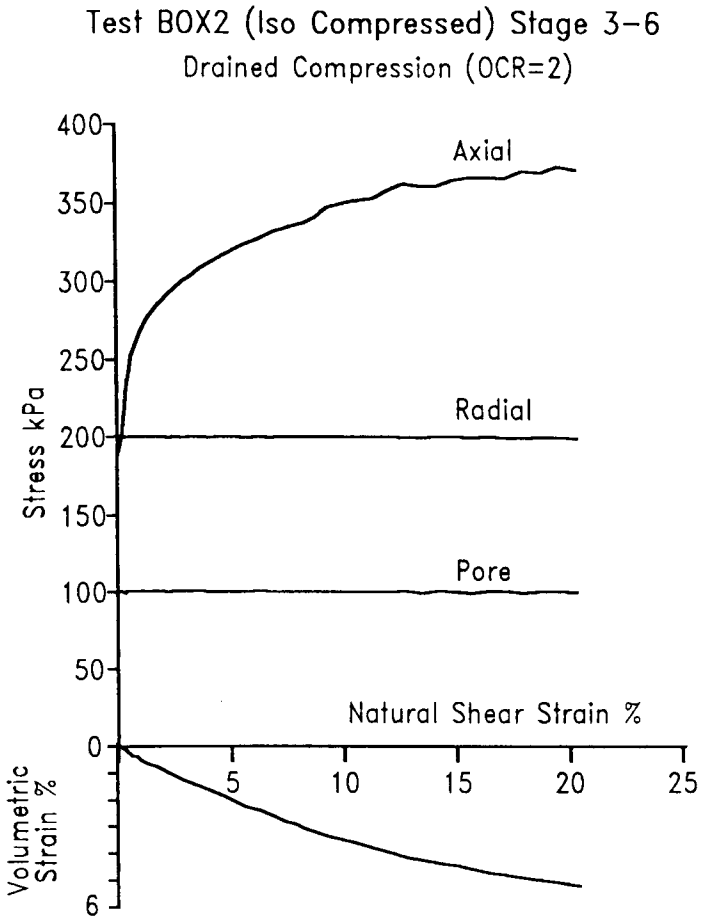

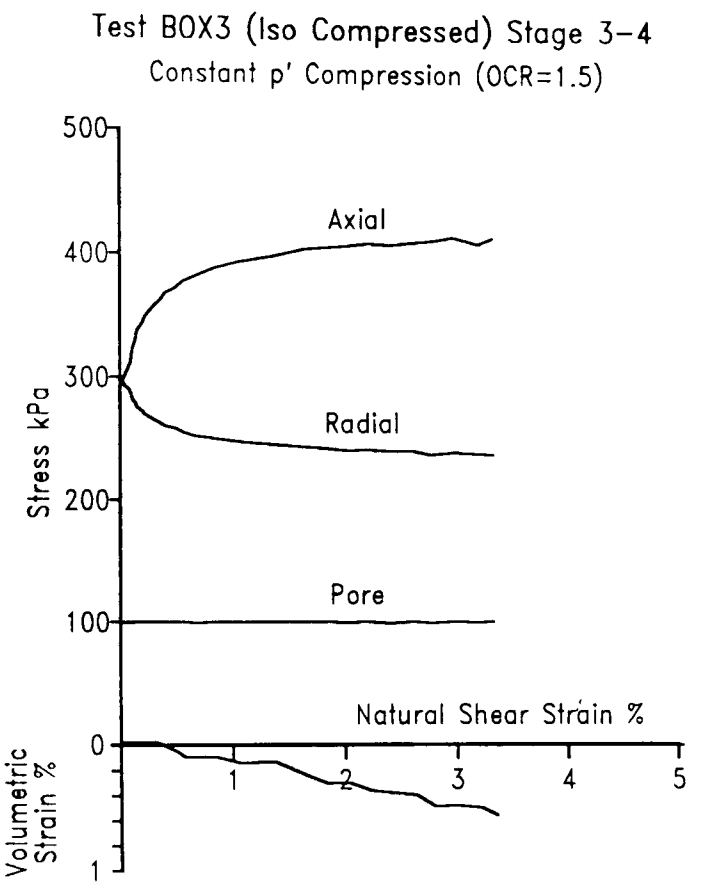

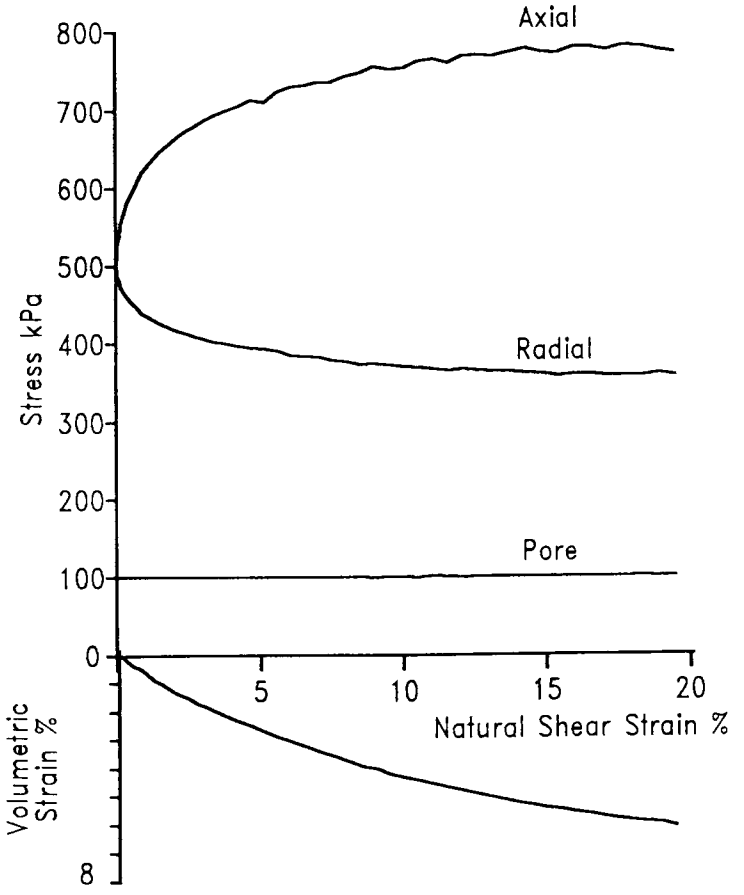

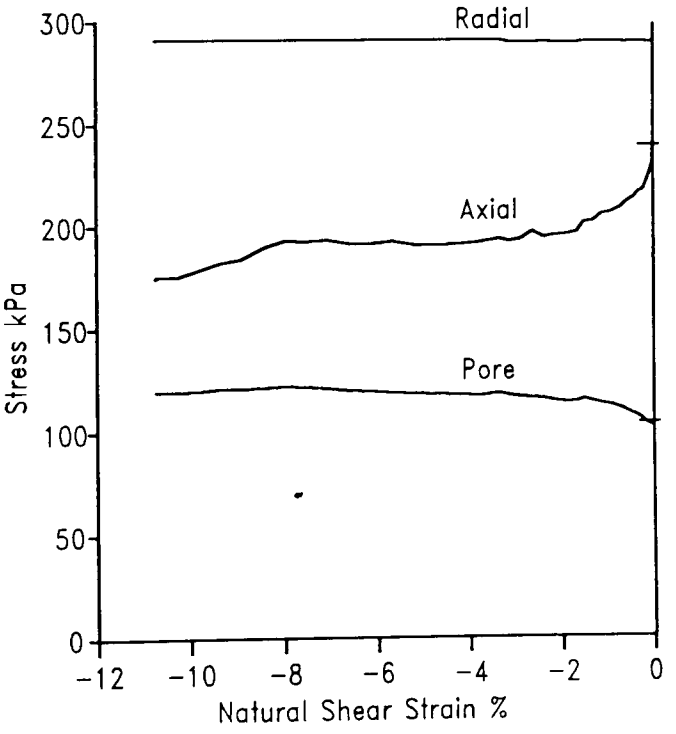

Figure 7.9 Shearing stages on reconstituted organic clay samples – Basic test data (Sheet 4 of 4)

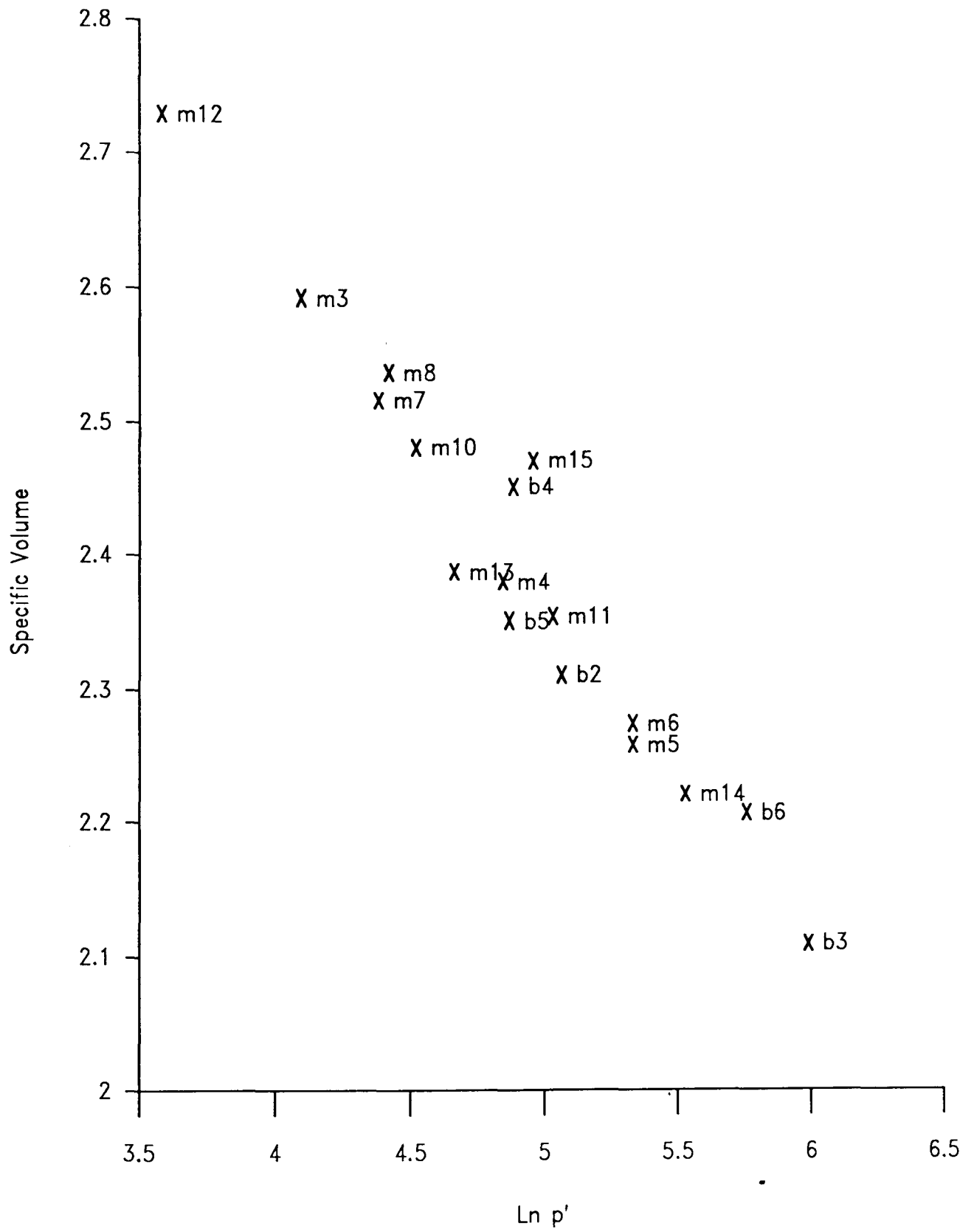

NOTE:- m6 = MIX6 , b3 = BOX3

Figure 7.10 Ultimate state of reconstituted organic clay samples at the end of the shearing stages

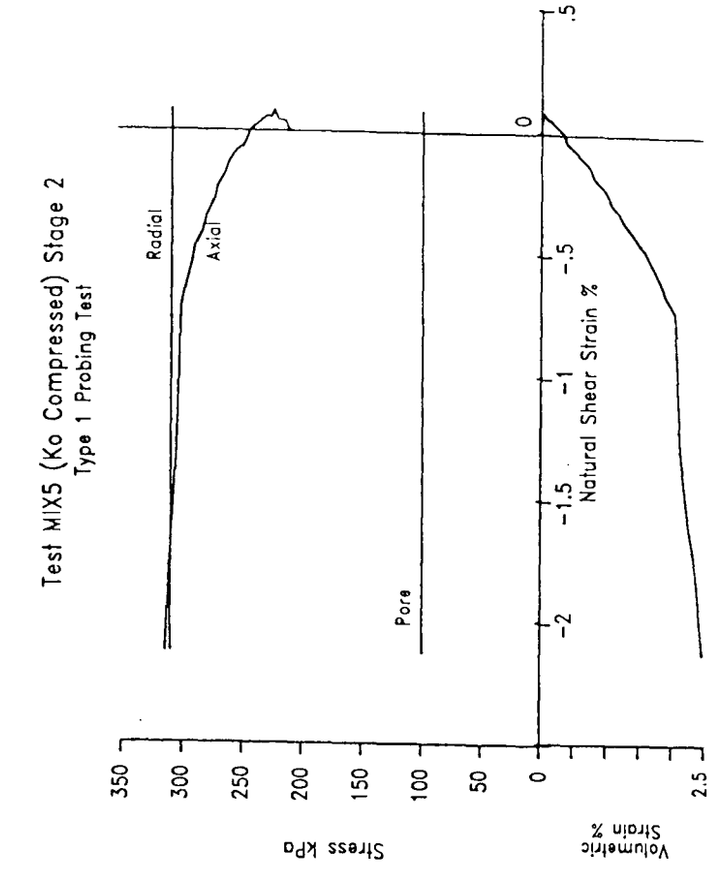

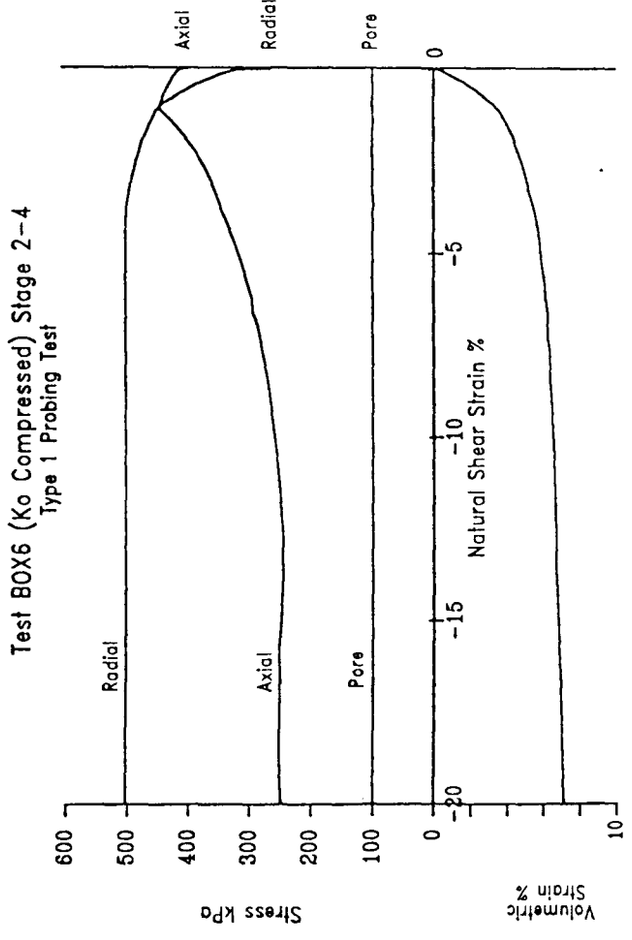

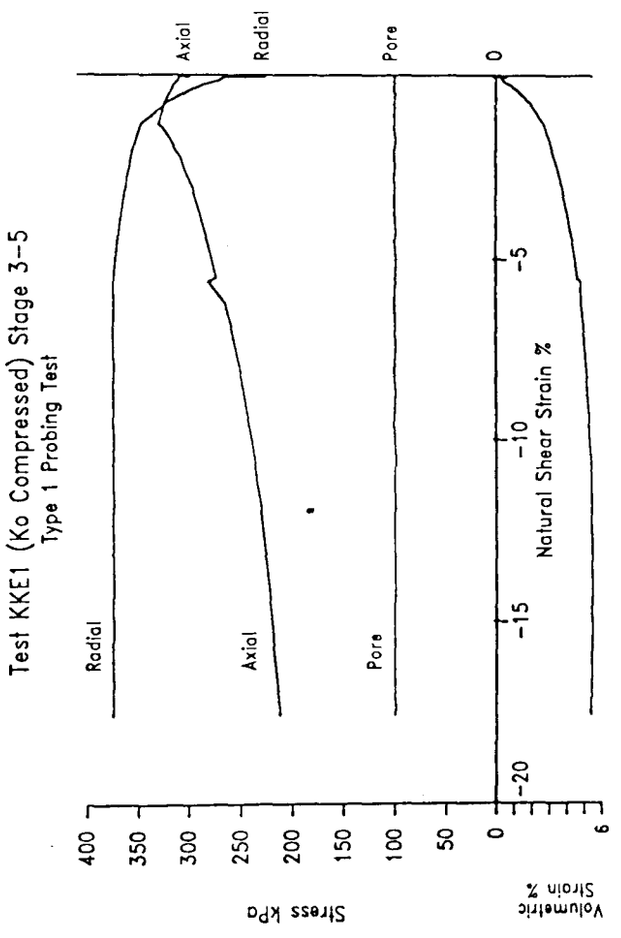

Figure 7.11 Type 1 Probing Tests – Basic Test Data

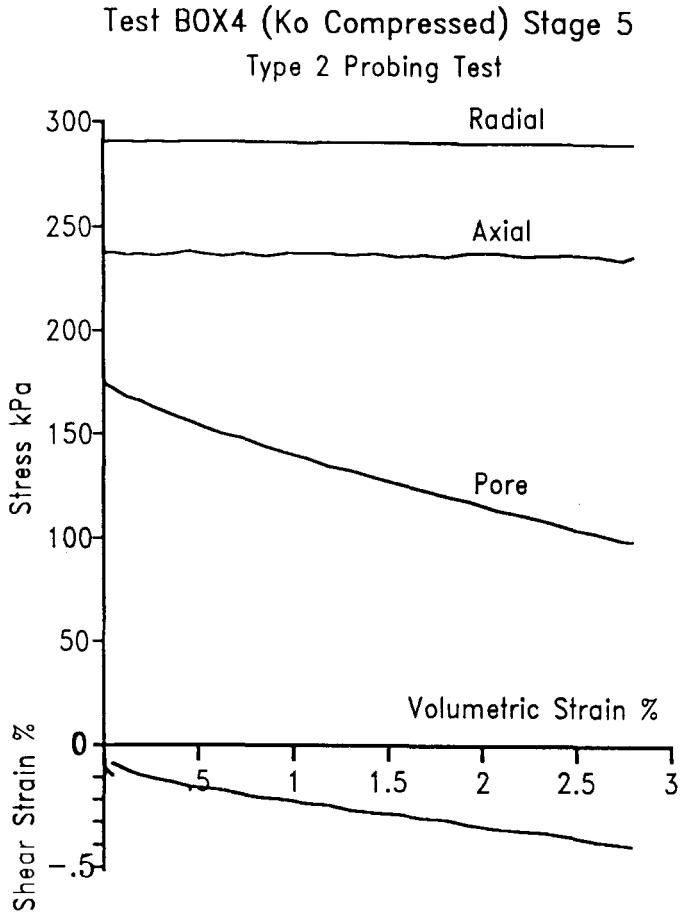

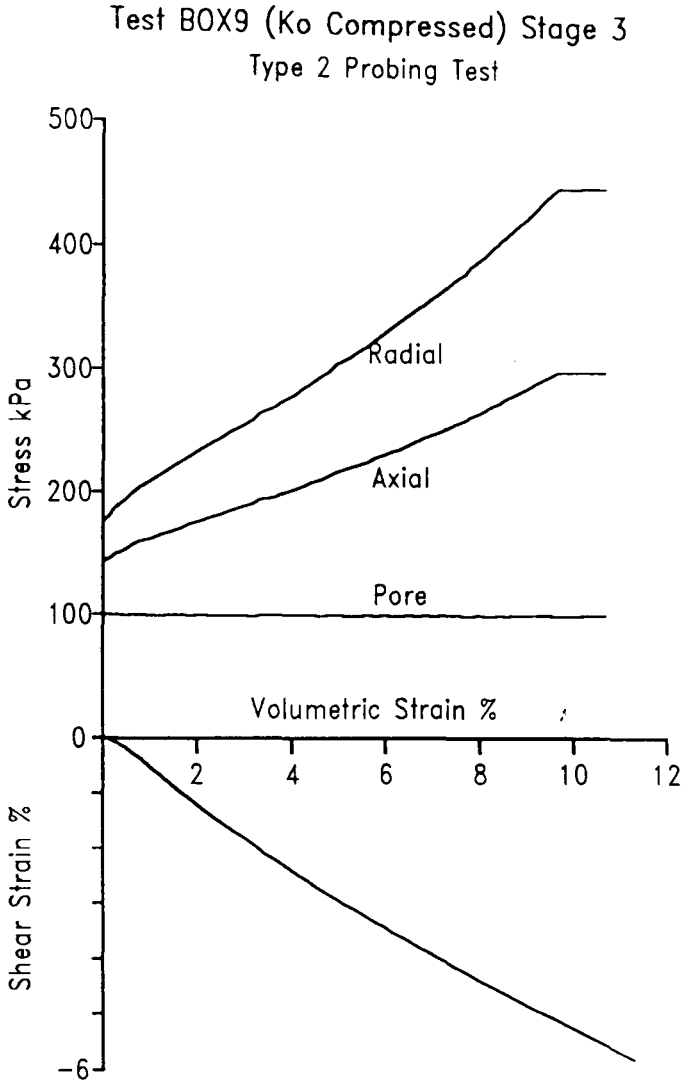

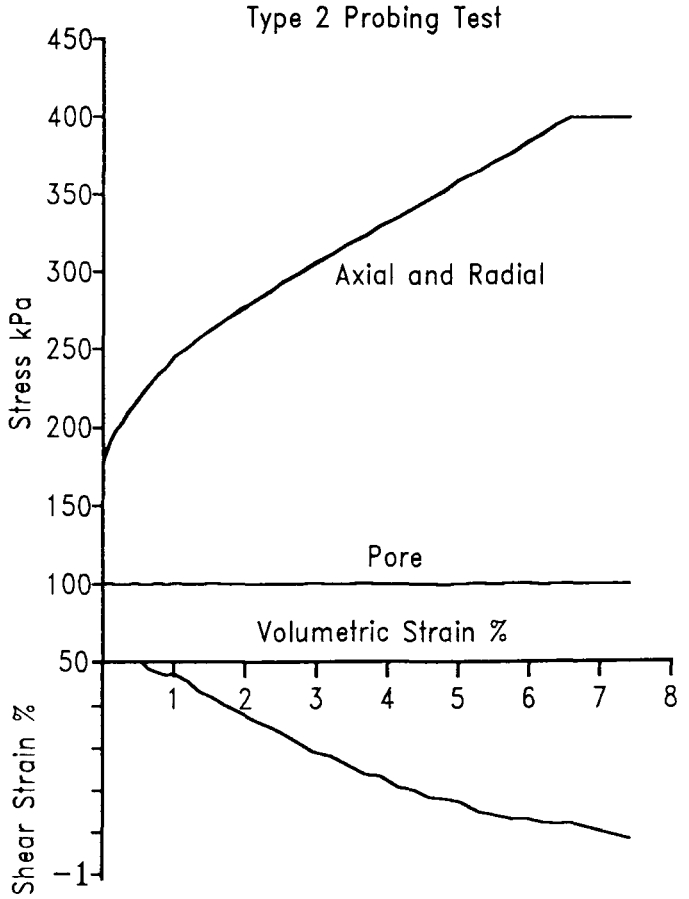

NOTES:-

Test BOX4 Constant q' Compression (q=-54)

Test BOX8 Isotropic Compression

Test BOX9 Compression along q'/p'=-0.5

Figure 7.12 Type 2 probing tests – Basic test data

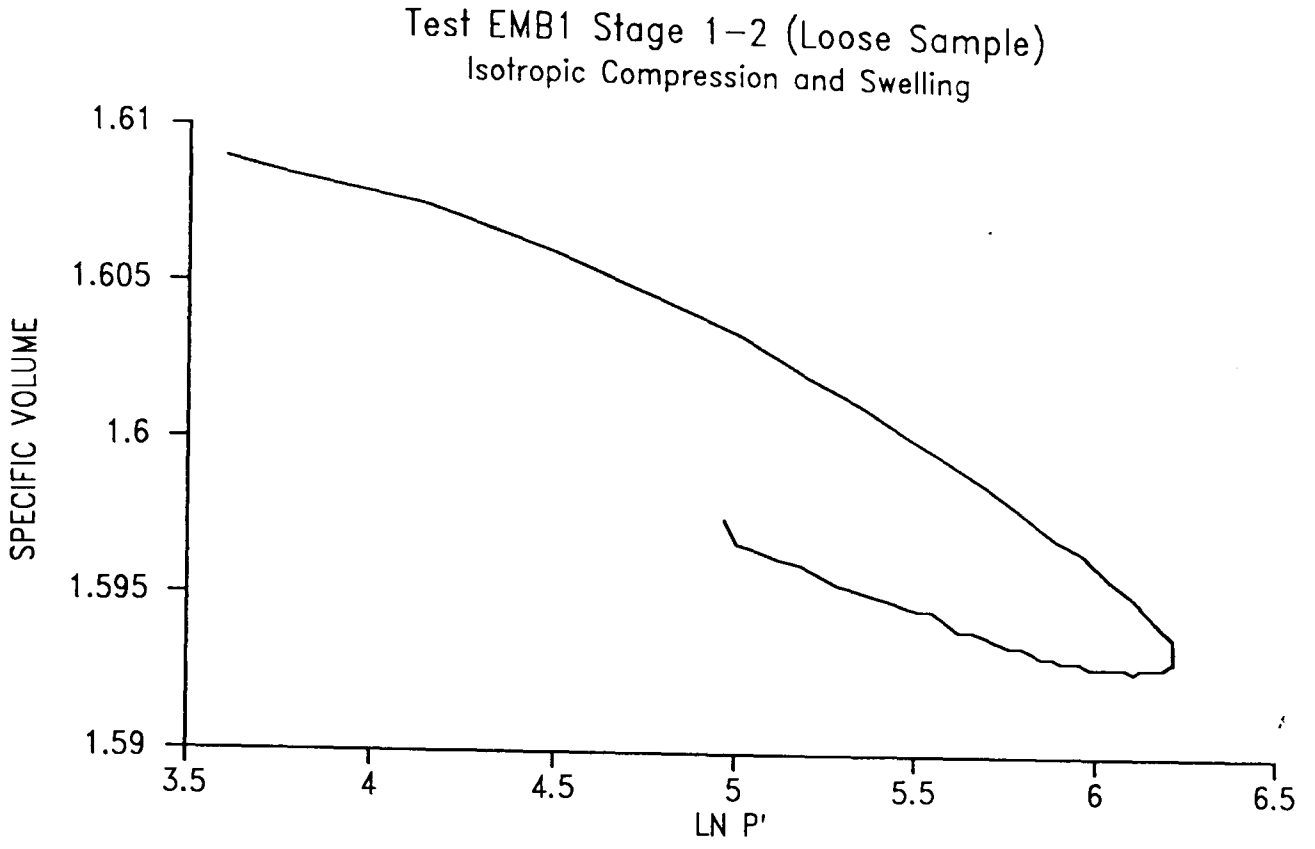

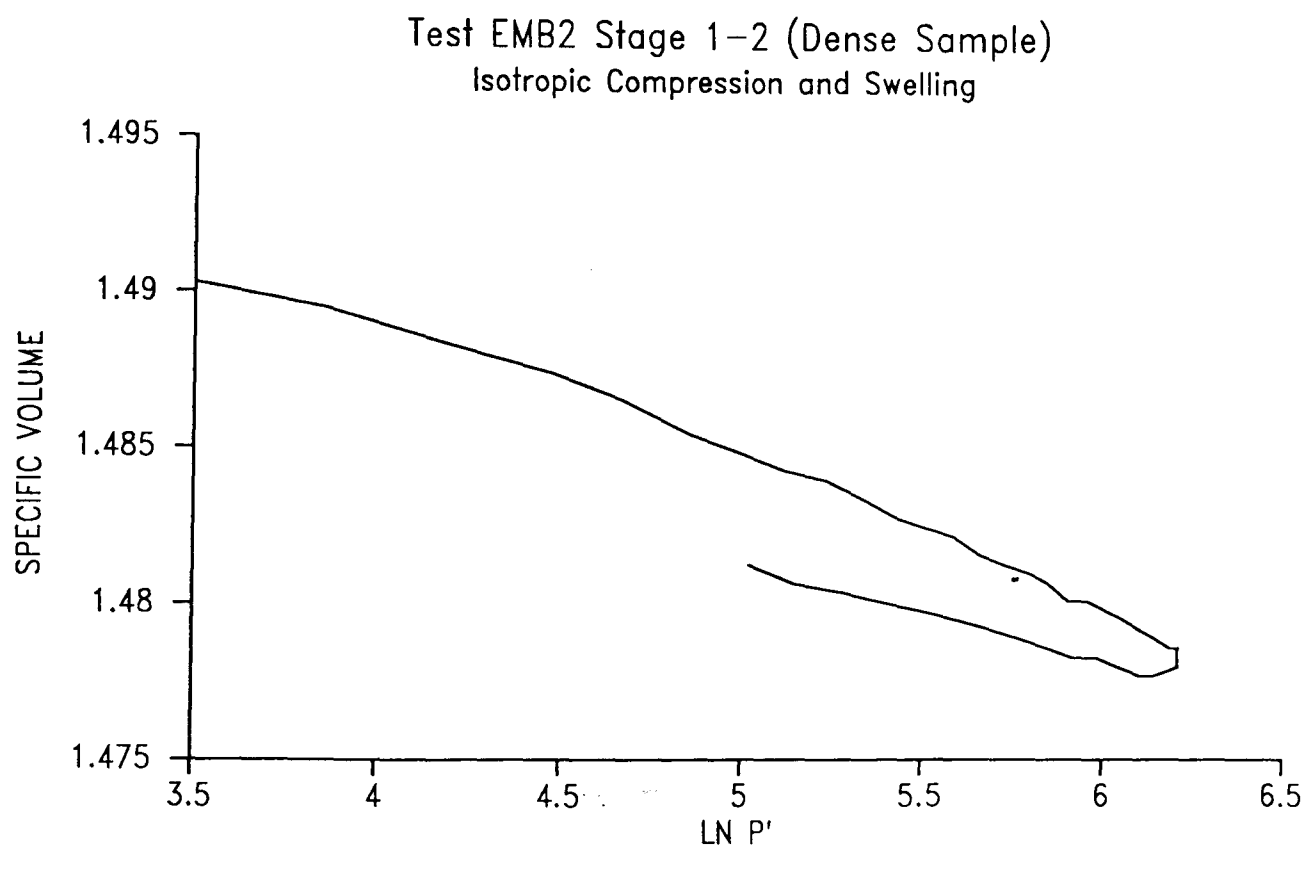

Figure 7.13 Embankment fill sand samples compression test results

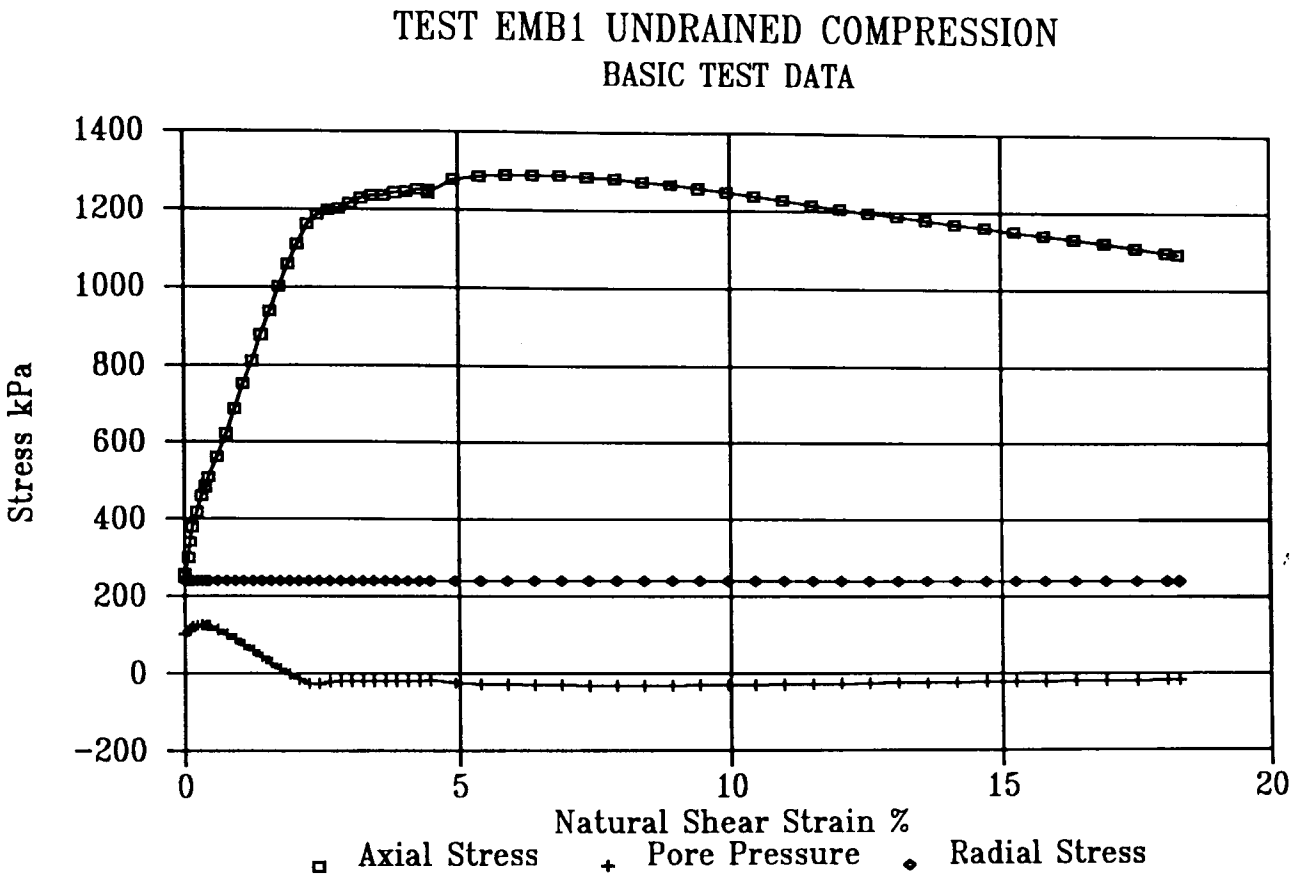

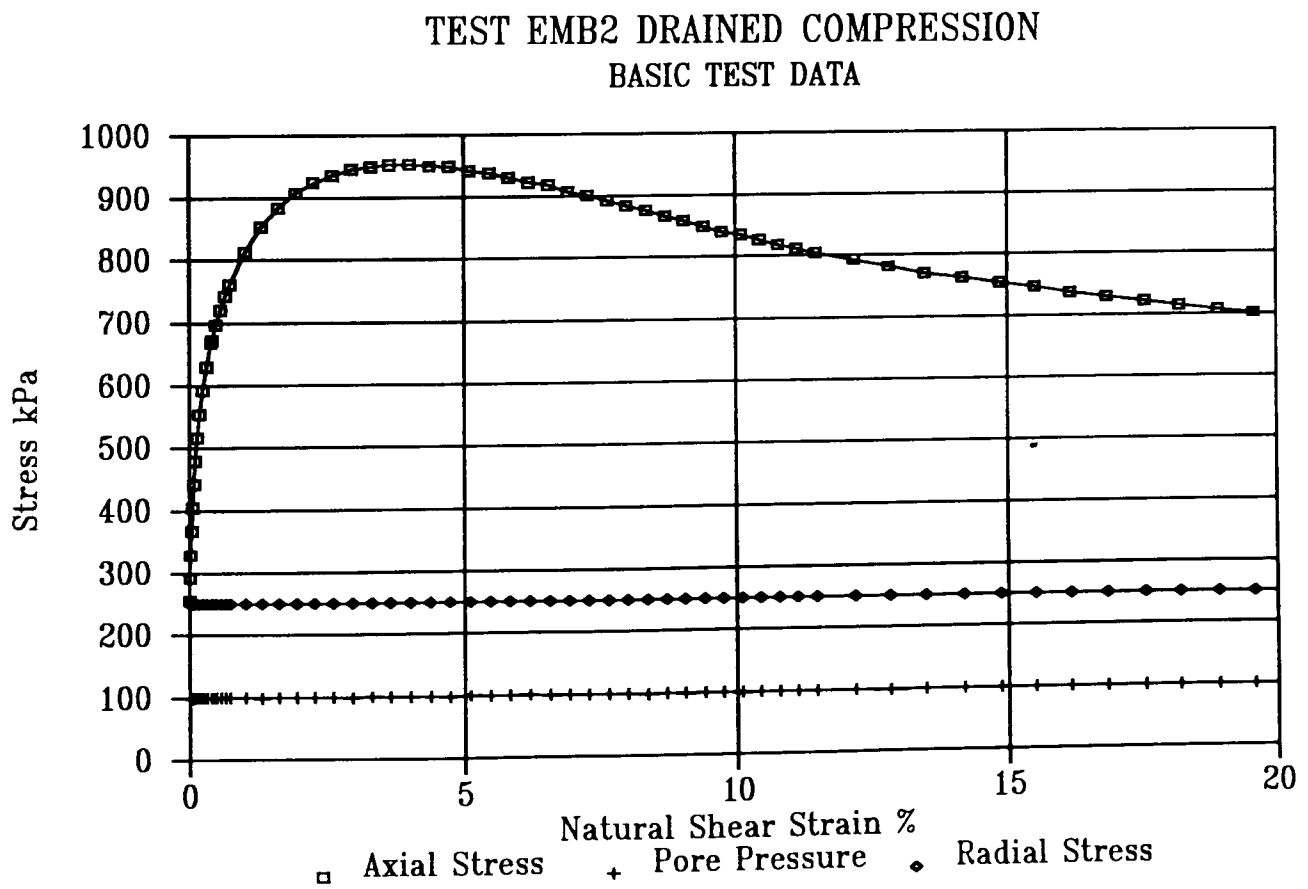

Figure 7.14 Shearing test results on embankment sand fill samples
Basic test data

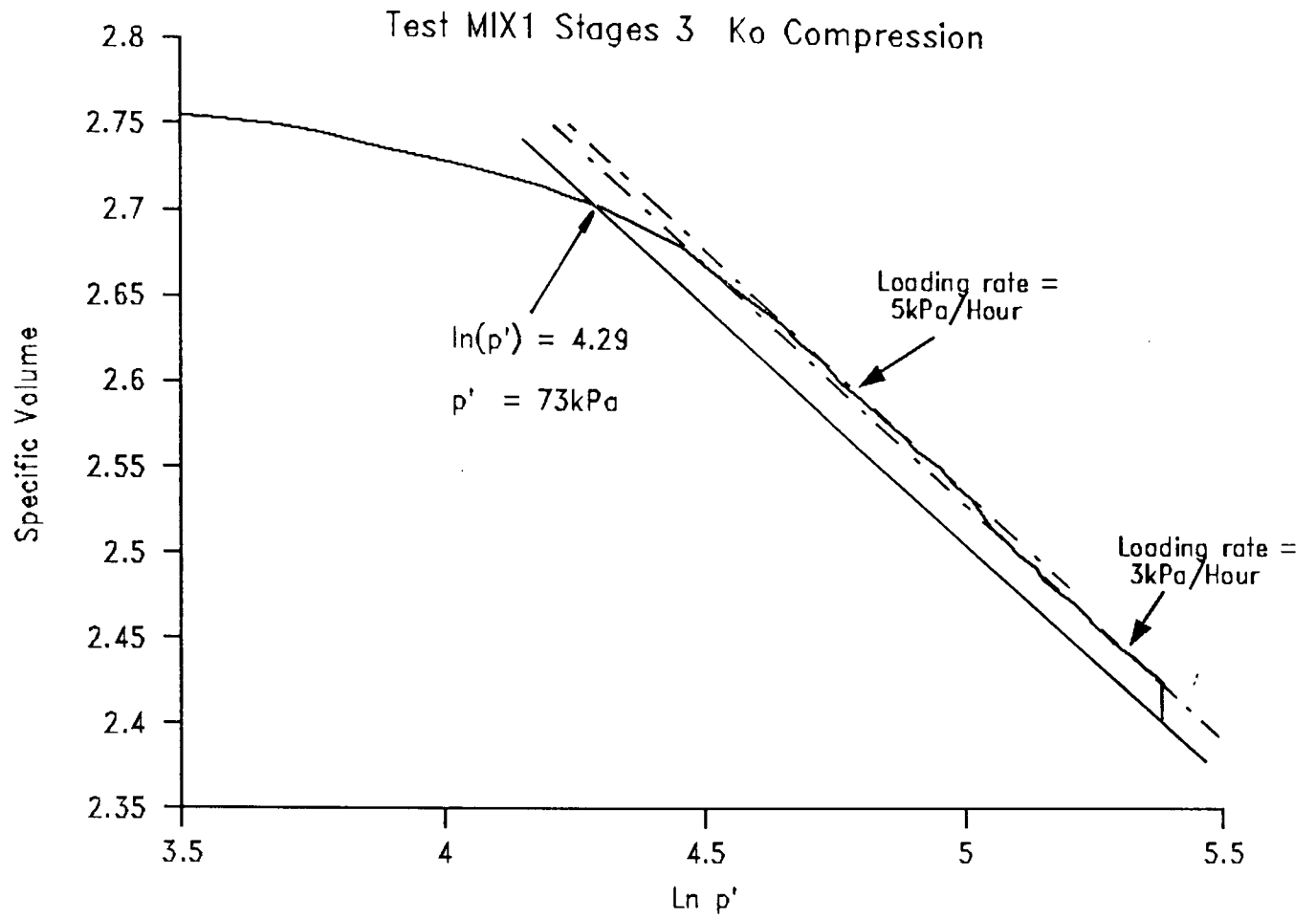

Figure 8.1 The Lambda construction for determining the SBS yield stress – Ko compressed sample

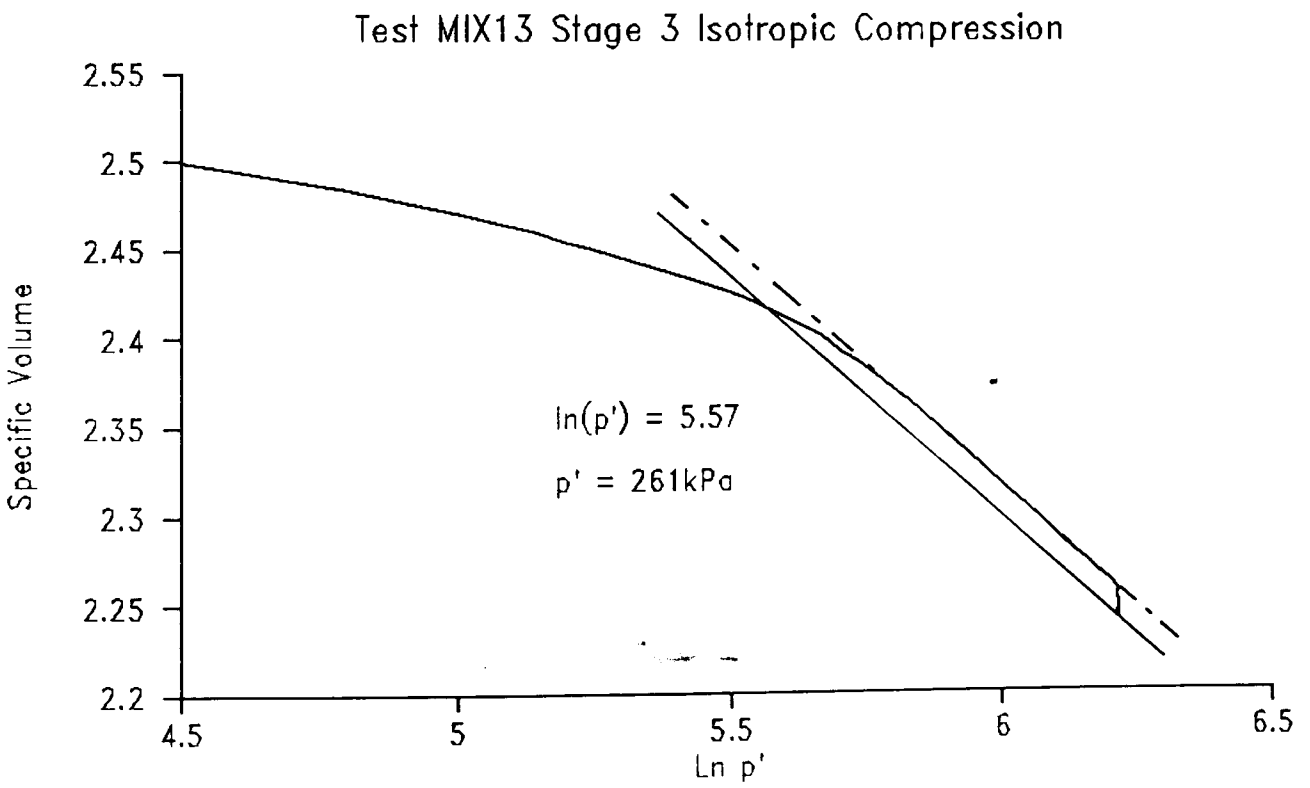

Figure 8.2 The Lambda construction for determining the SBS yield stress – isotropically compressed sample

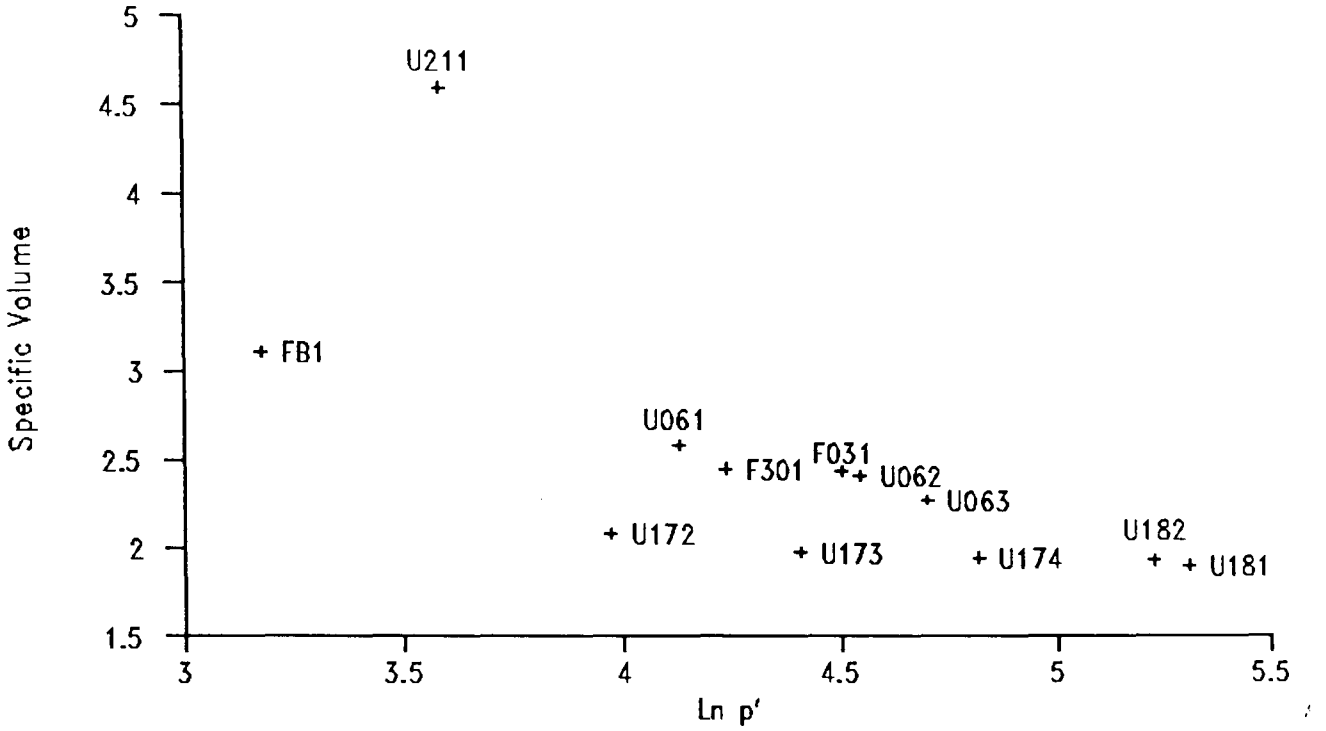

Figure 8.3 Ultimate state of piston samples at the end of shearing stages in V : Ln(p') space

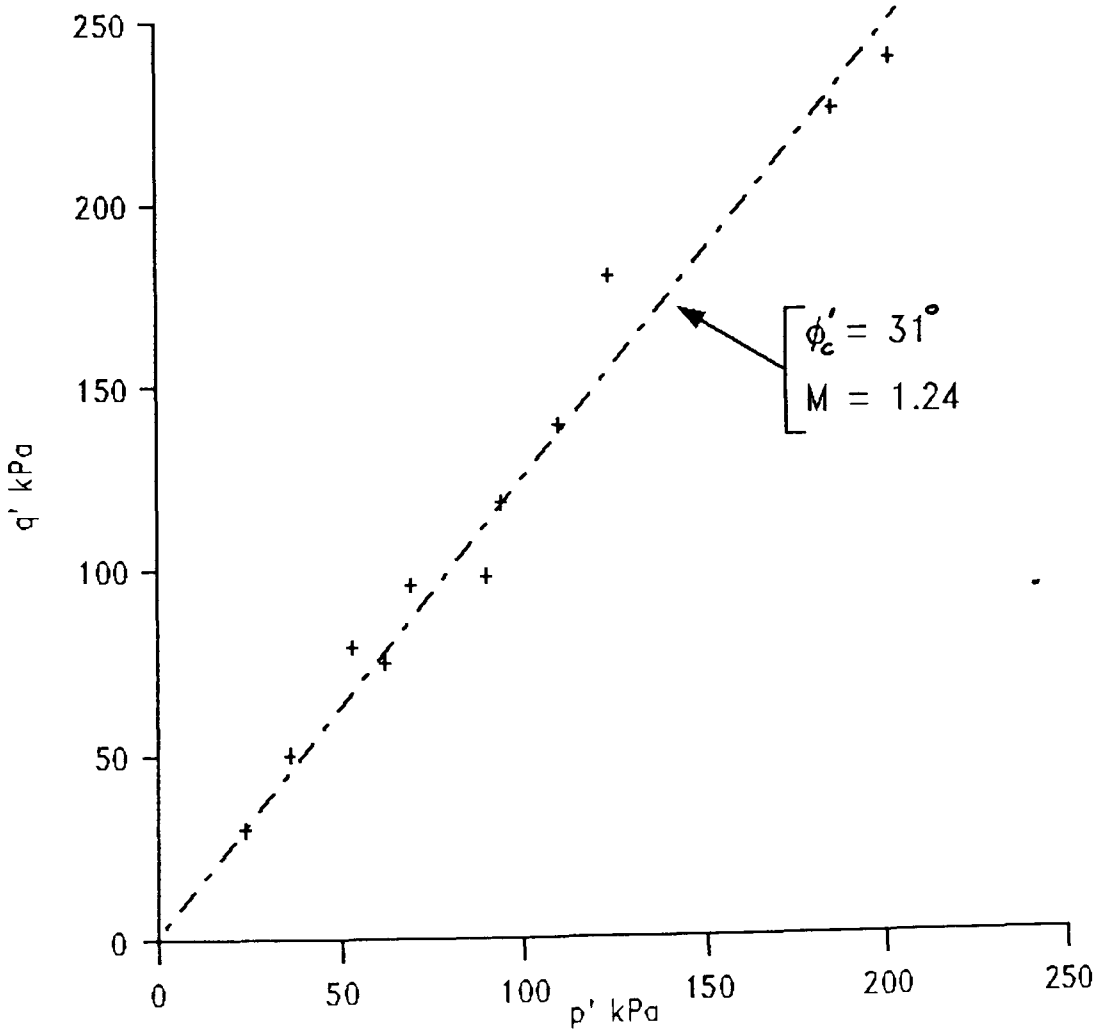

Figure 8.4 Ultimate state of piston samples at the end of undrained compression shearing stages in q' : p' space

Normalised Constant Volume Stress Paths
Organic Clay Piston Samples

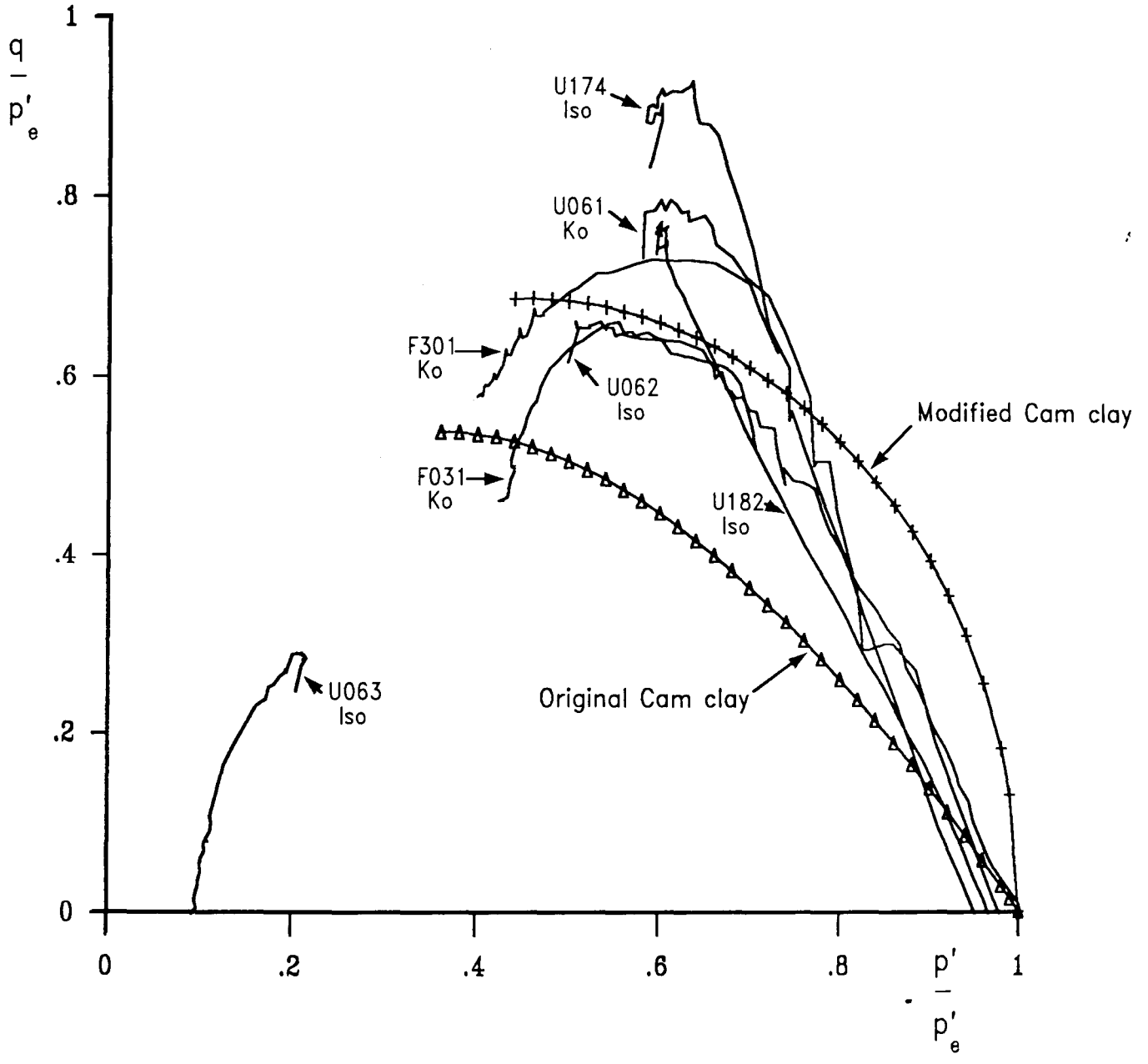

Iso = Isotropically compressed sample

Ko = One-dimensionally compressed sample

Figure 8.5 Constant volume stress paths for piston samples, normalised with respect to p'_e

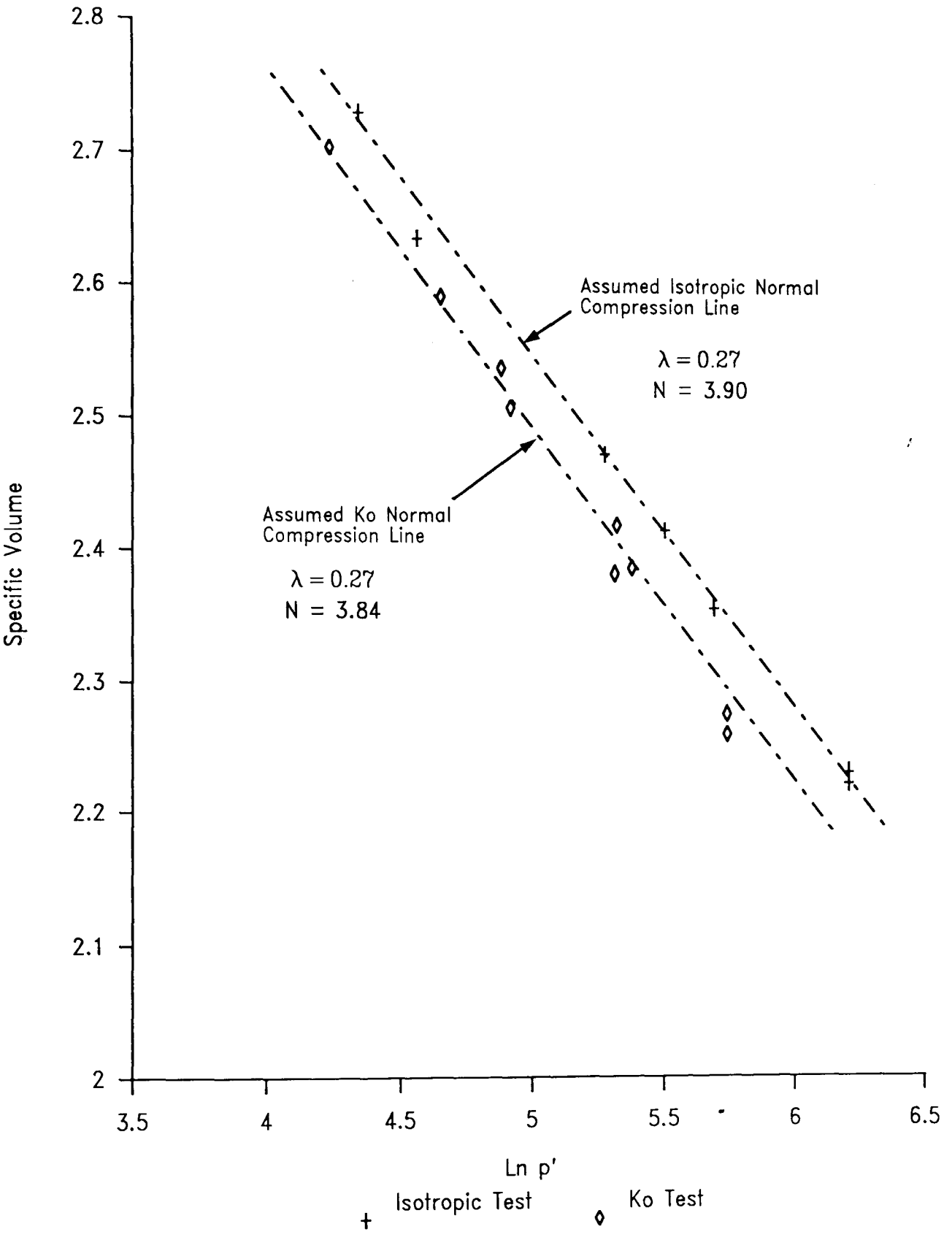

Figure 8.6 State of MIX reconstituted samples at end of Isotropic and Ko Compression stages

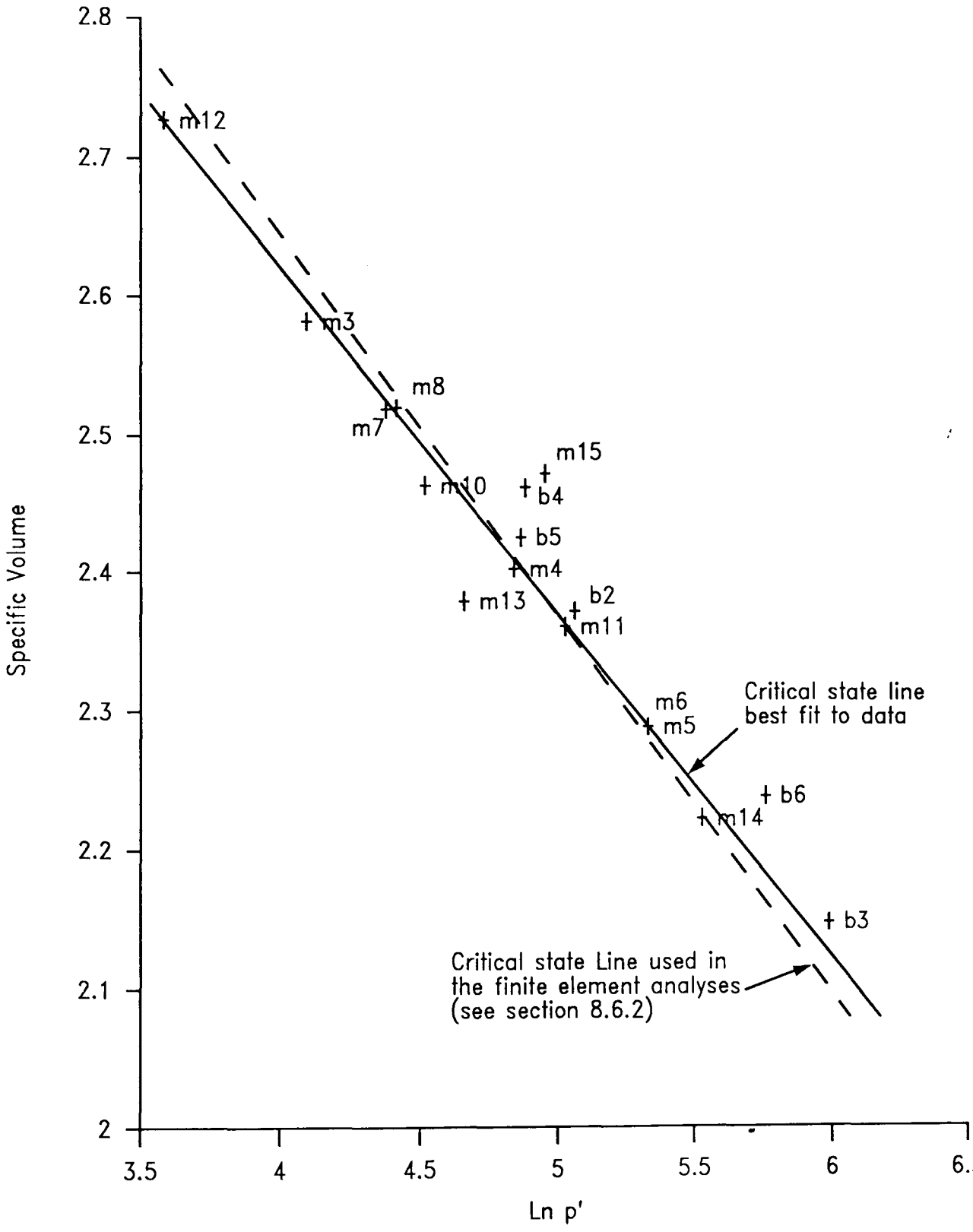

Figure 8.7 Corrected critical state points for reconstituted organic clay samples

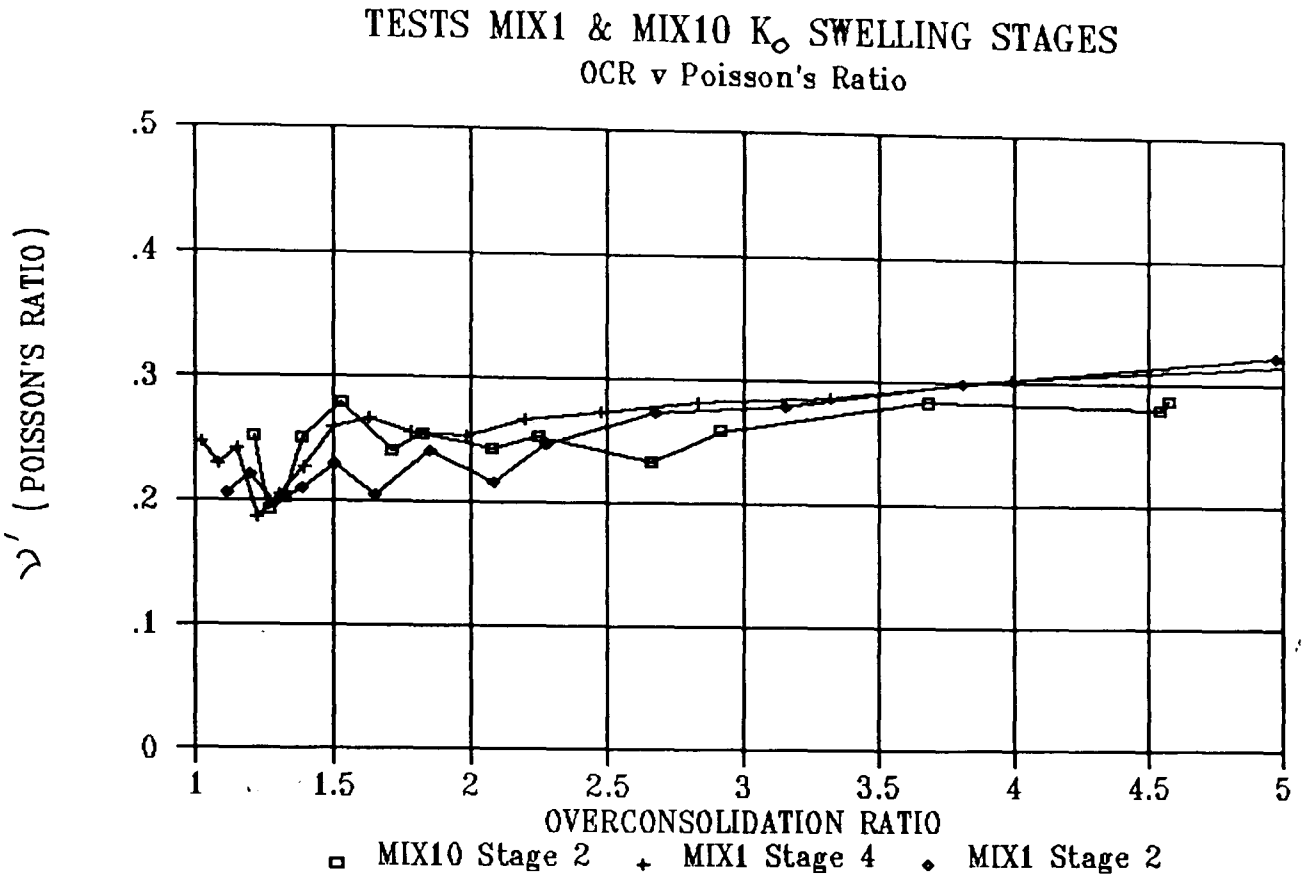

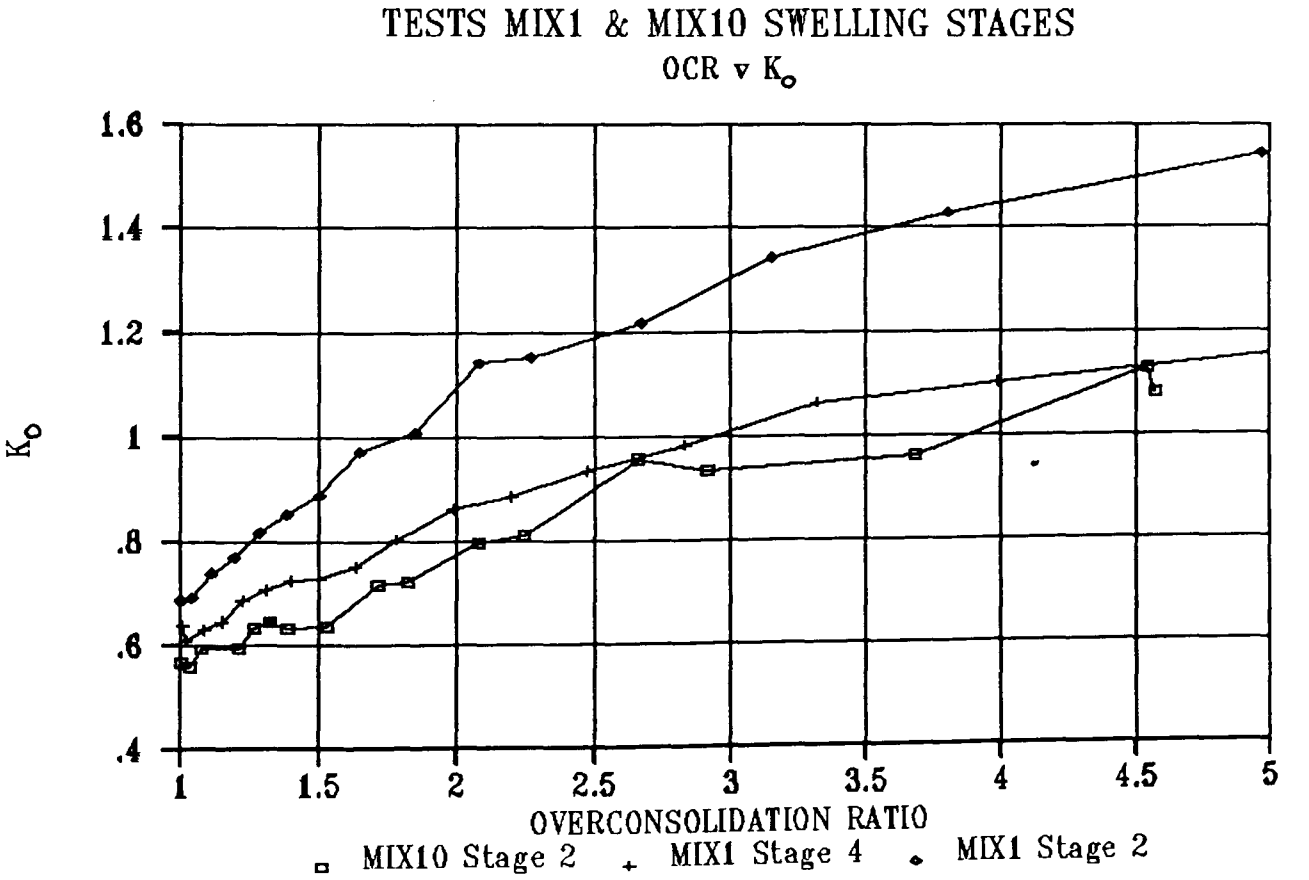

Figure 8.8 Determination of ν' from swelling test results

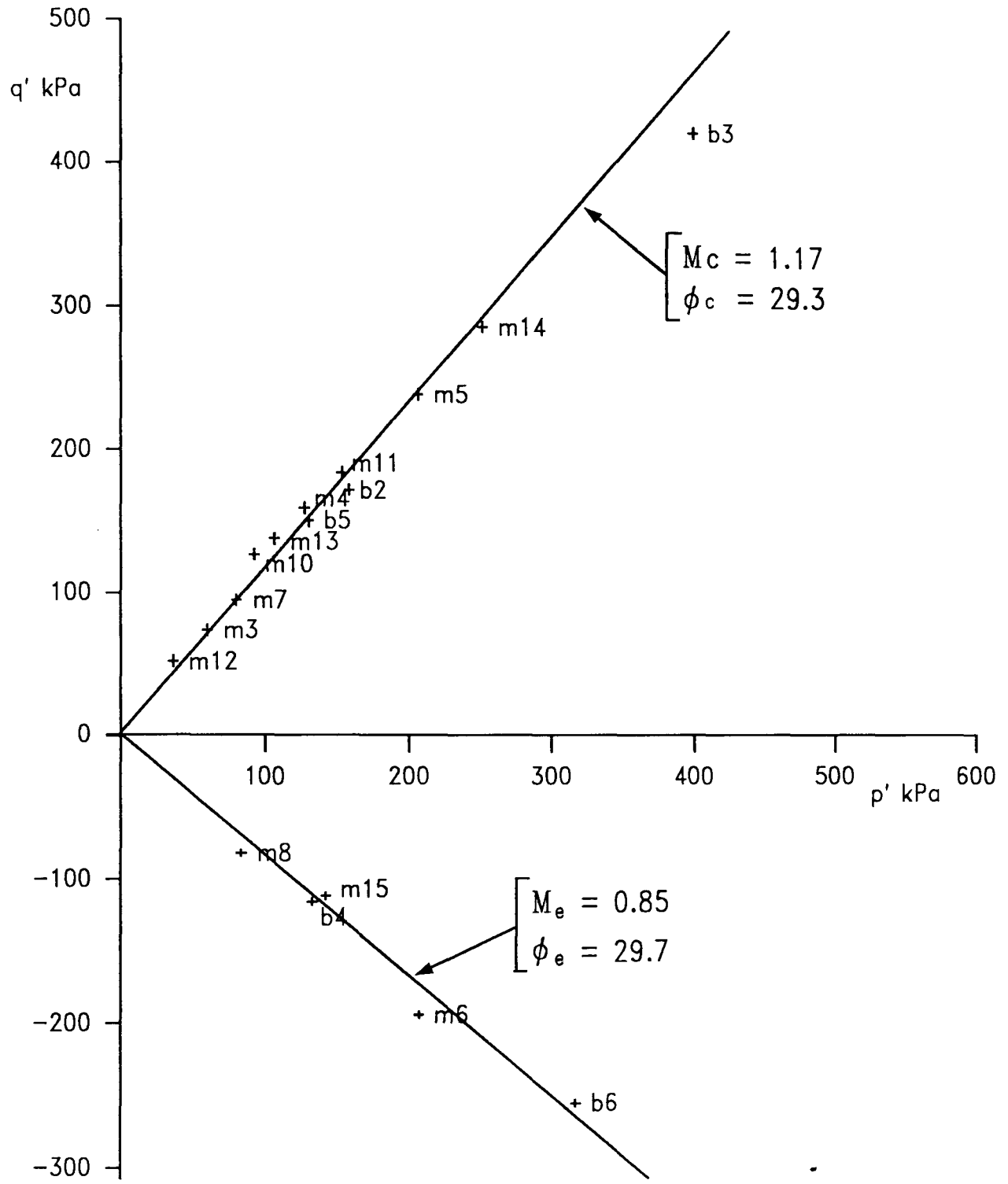

m15 = MIX15 , b3 = BOX3 etc.

Figure 8.9 Ultimate state of reconstituted organic clay samples at the end of shearing stages in q' : p' space

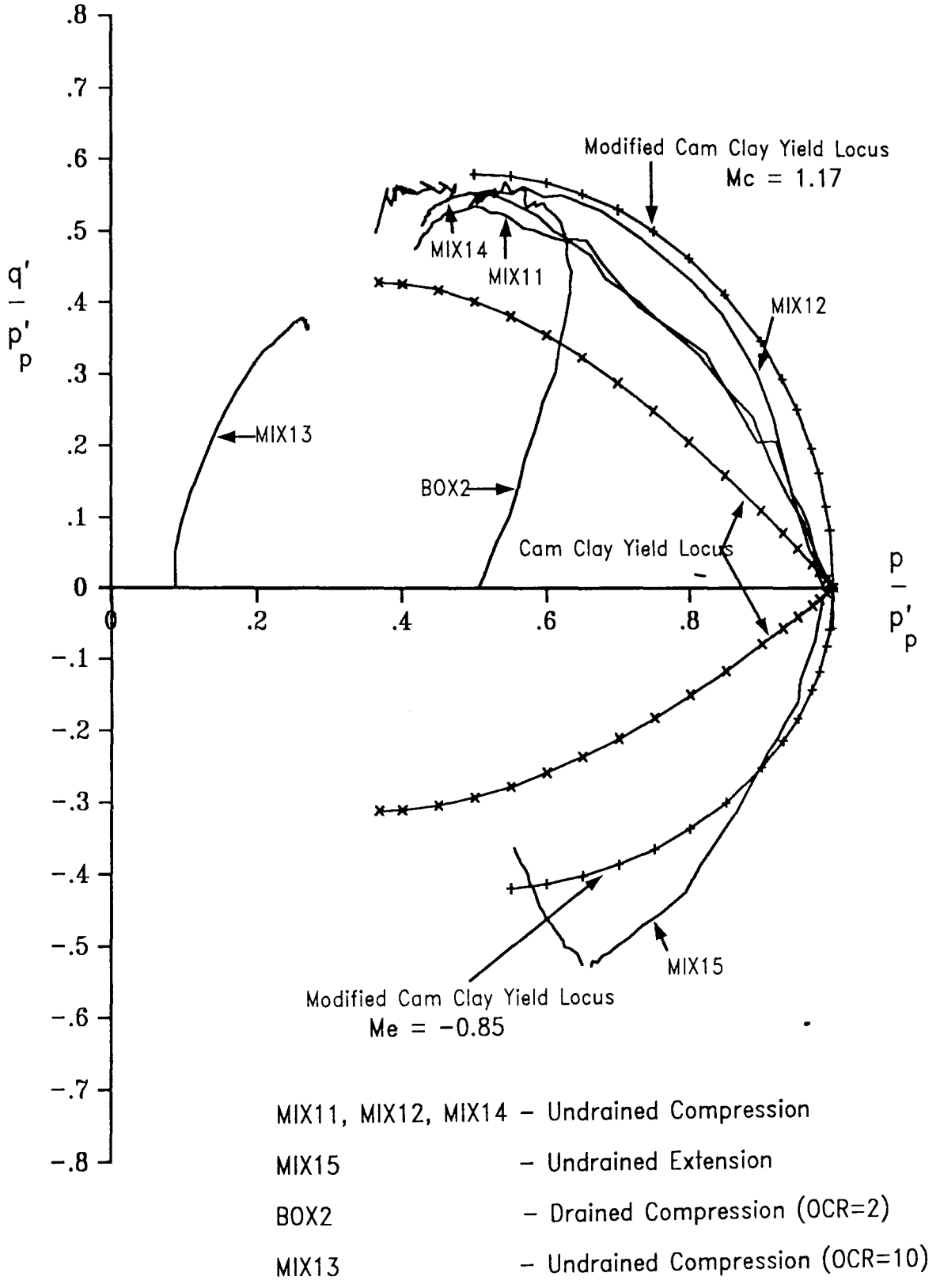

Figure 8.10 Stress paths for isotropically compressed samples normalised with respect to Pp'

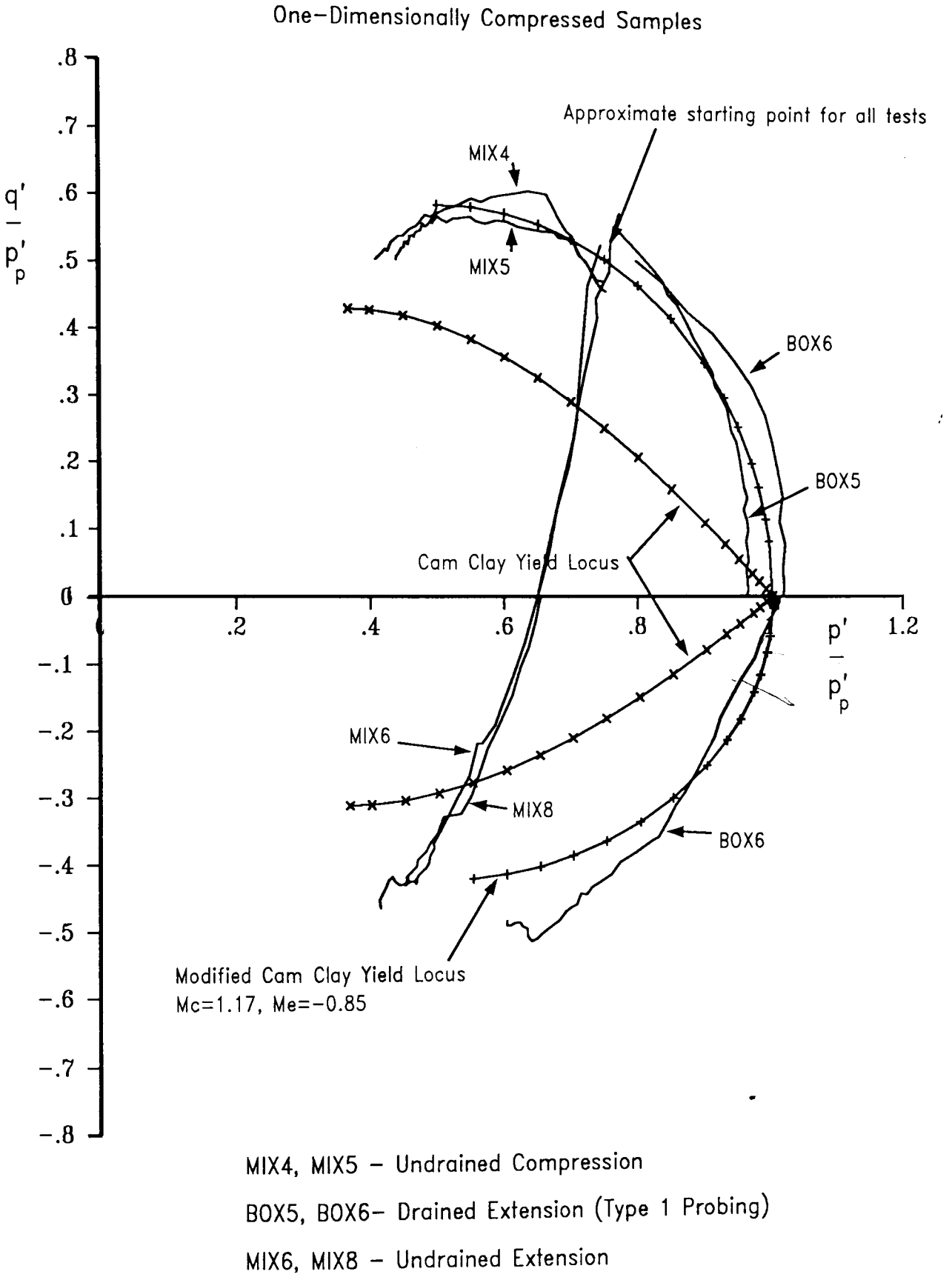

Figure 8.11 Stress paths for Ko normally compressed samples normalised with respect to Pp'

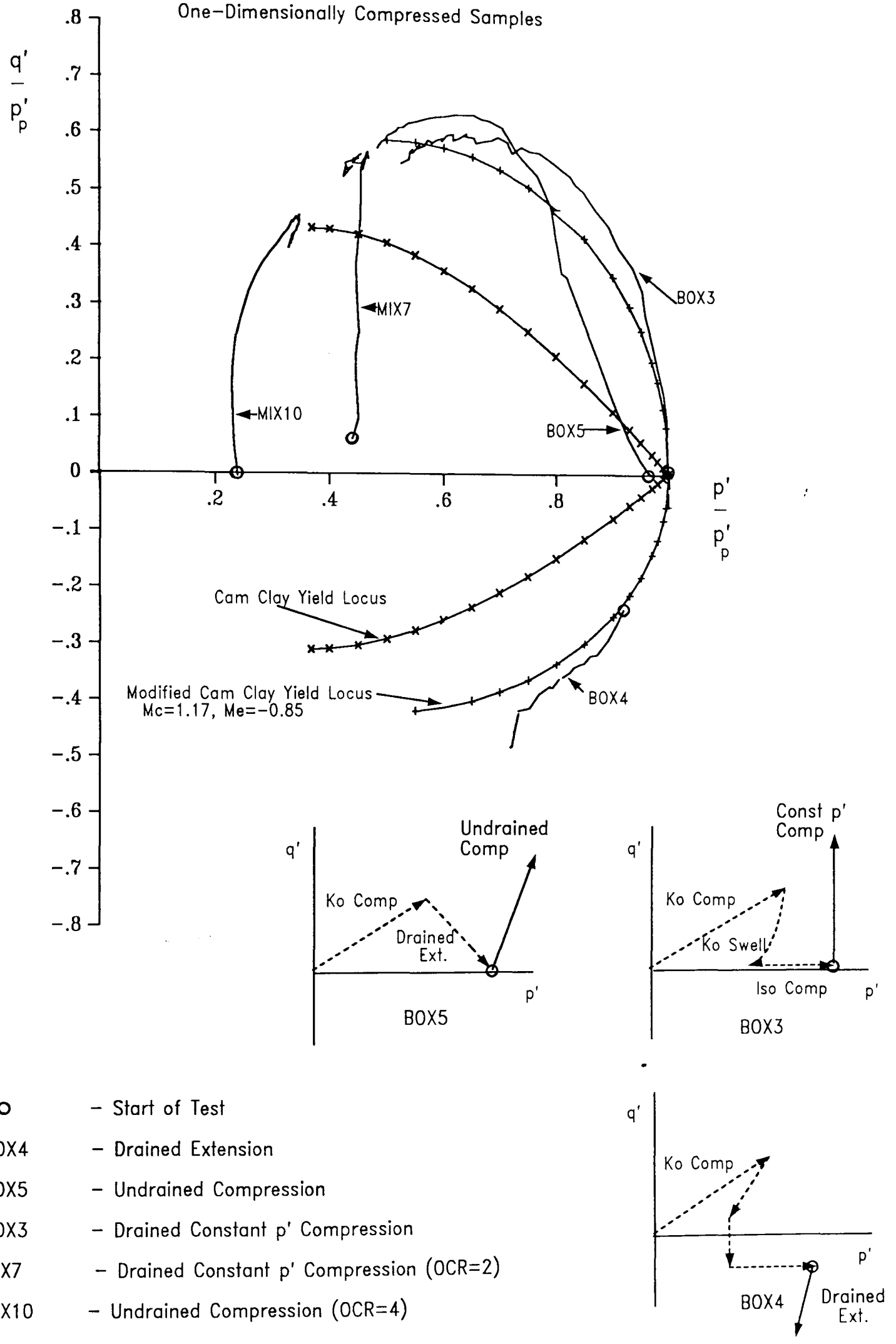

O	– Start of Test
BOX4	– Drained Extension
BOX5	– Undrained Compression
BOX3	– Drained Constant p' Compression
MIX7	– Drained Constant p' Compression (OCR=2)
MIX10	– Undrained Compression (OCR=4)

Figure 8.12 Stress paths for Ko compressed samples normalised with respect to Pp'

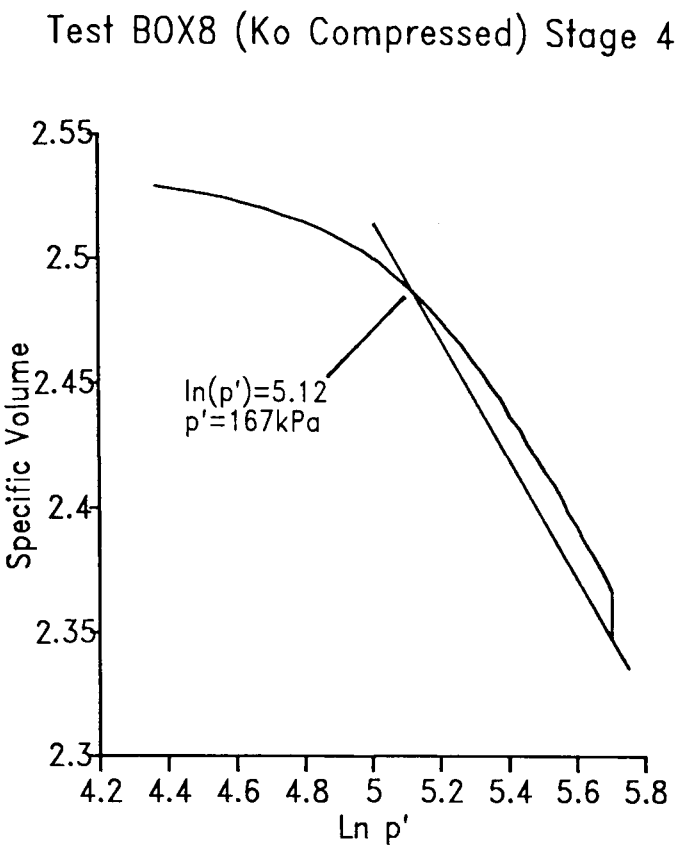

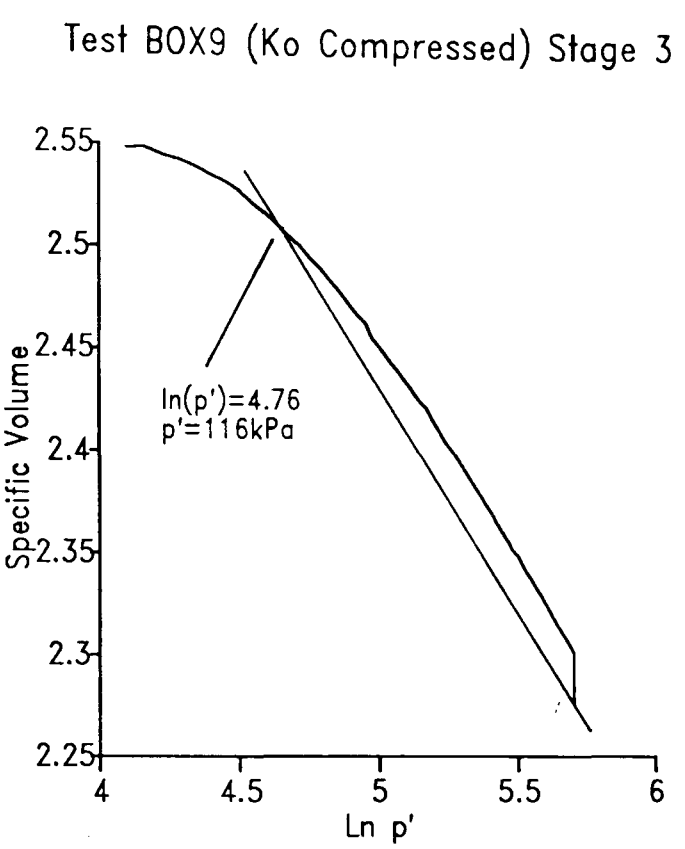

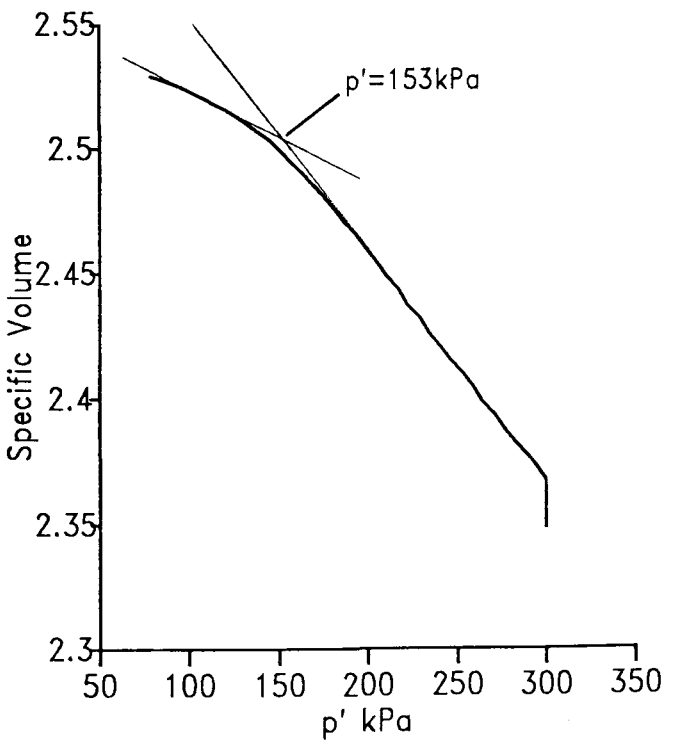

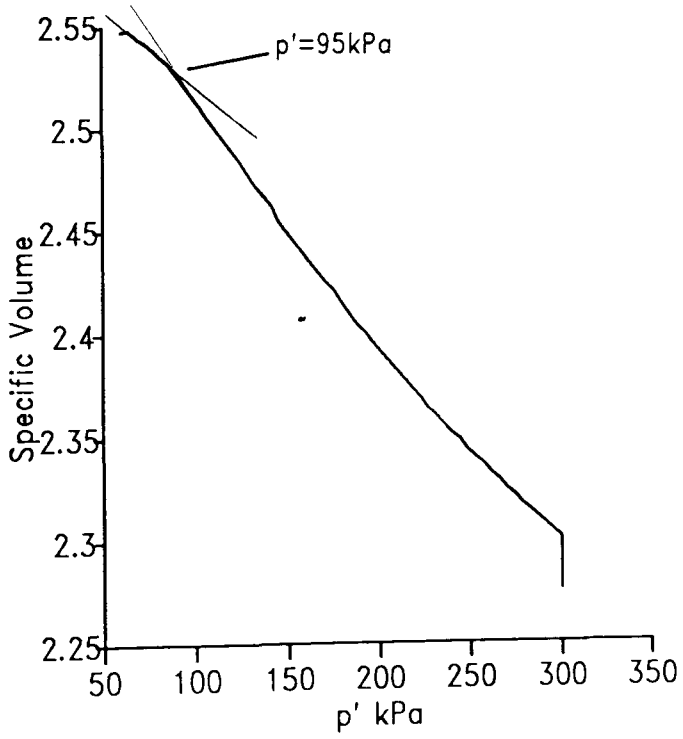

Figure 8.13 BOX8 & BOX9 Type 2 probing test results

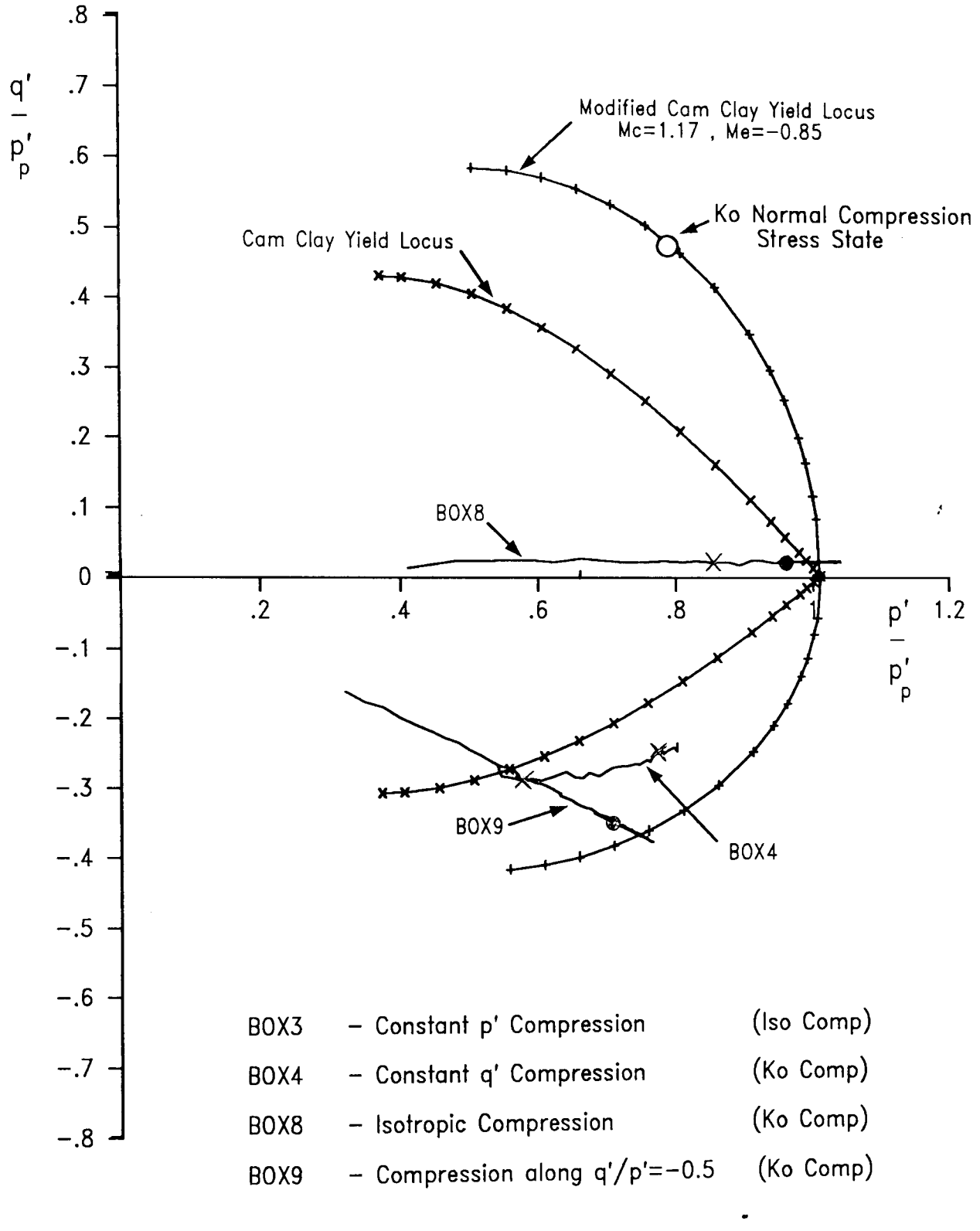

Position of the State Boundary Surface

● – Determined using the Lambda Construction

× – Determined using the Bi-linear Construction

Figure 8.14 Normalised stress paths for Type 2 probing tests

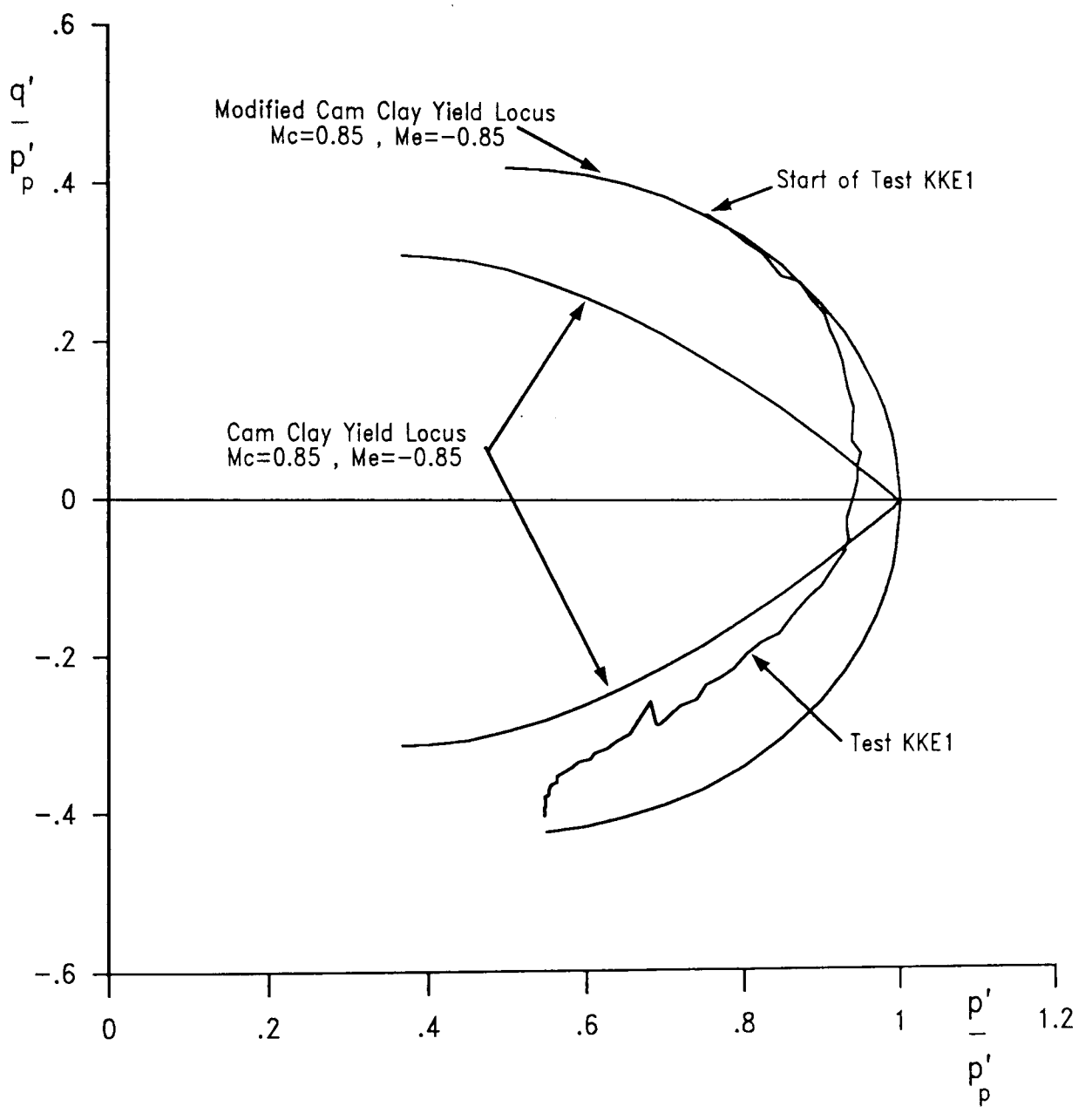

Figure 8.15 Normalised stress path for Type 1 probing test on reconstituted kaolin sample KKE1

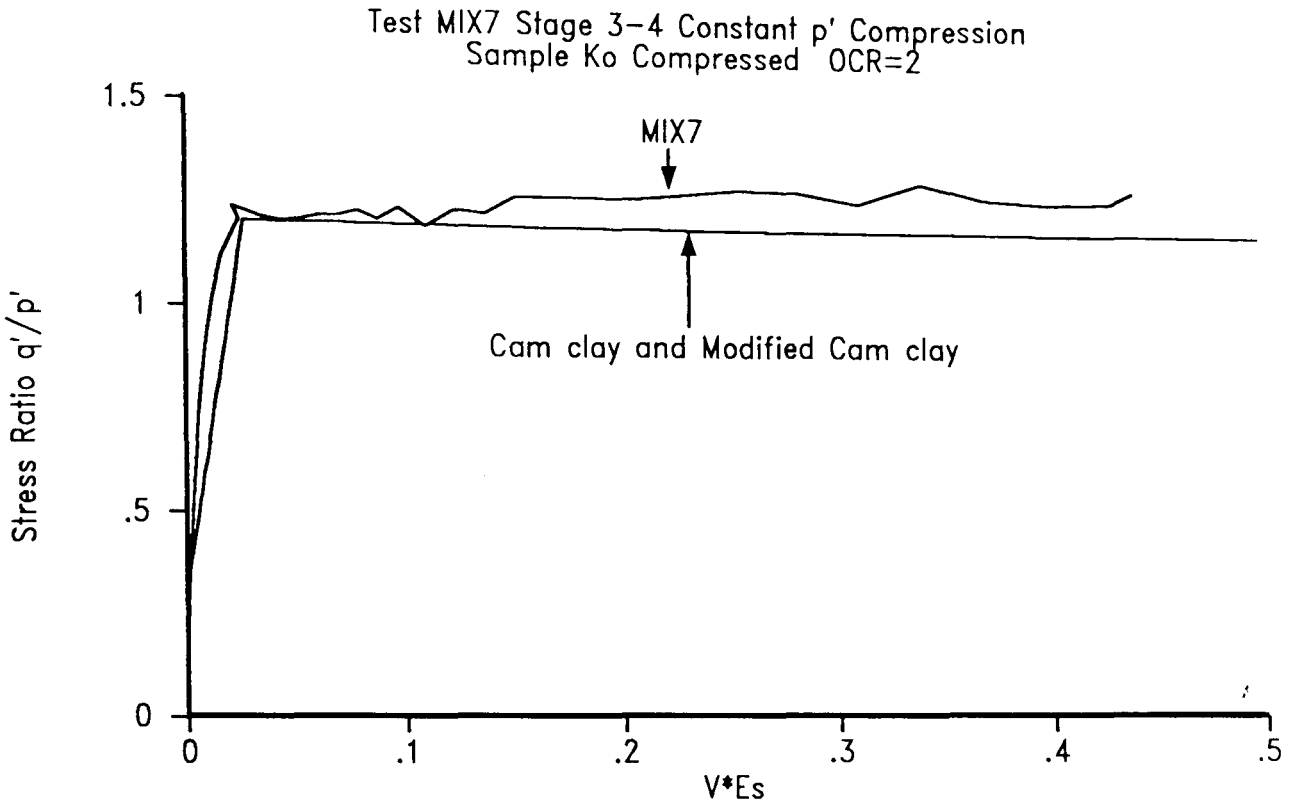

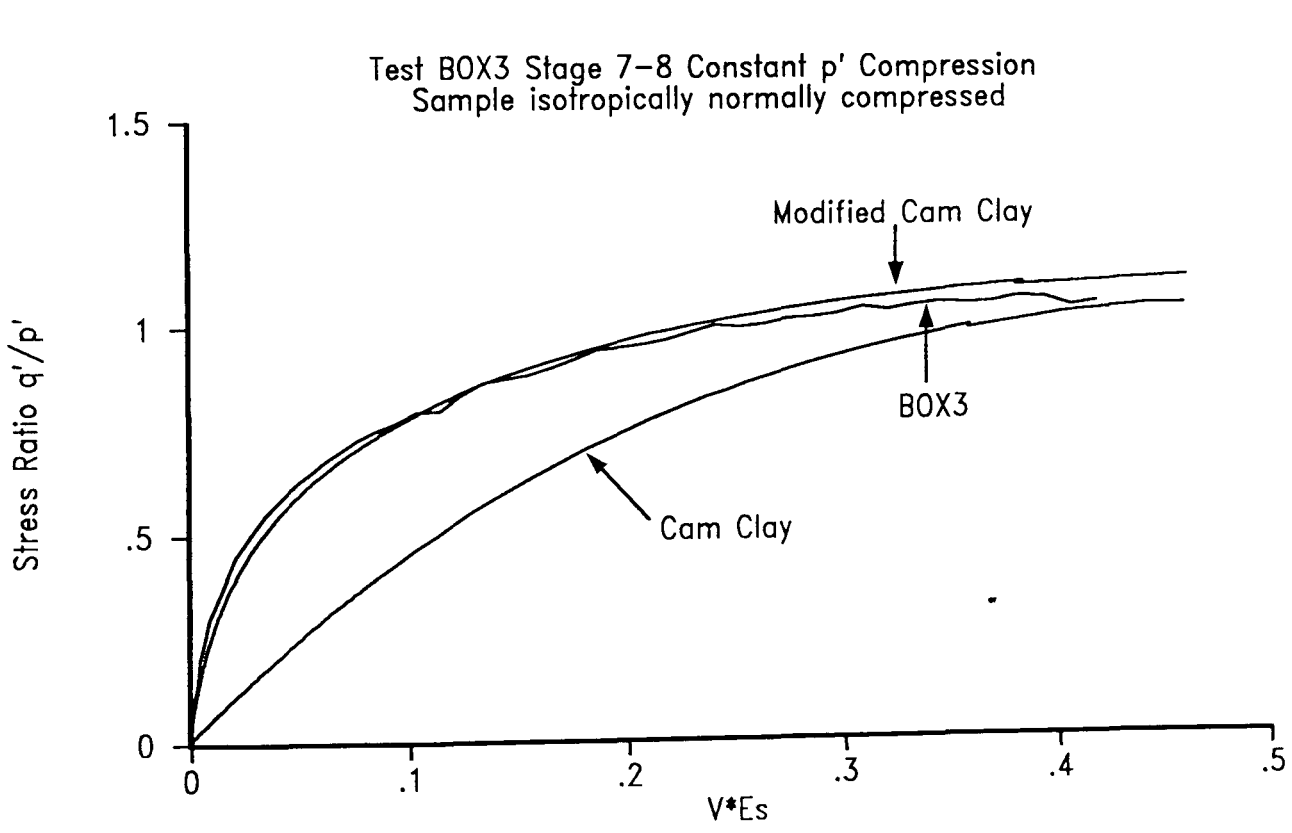

Figure 8.16 Normalised stress strain plots for drained tests on reconstituted clay (Sheet 1 of 2)

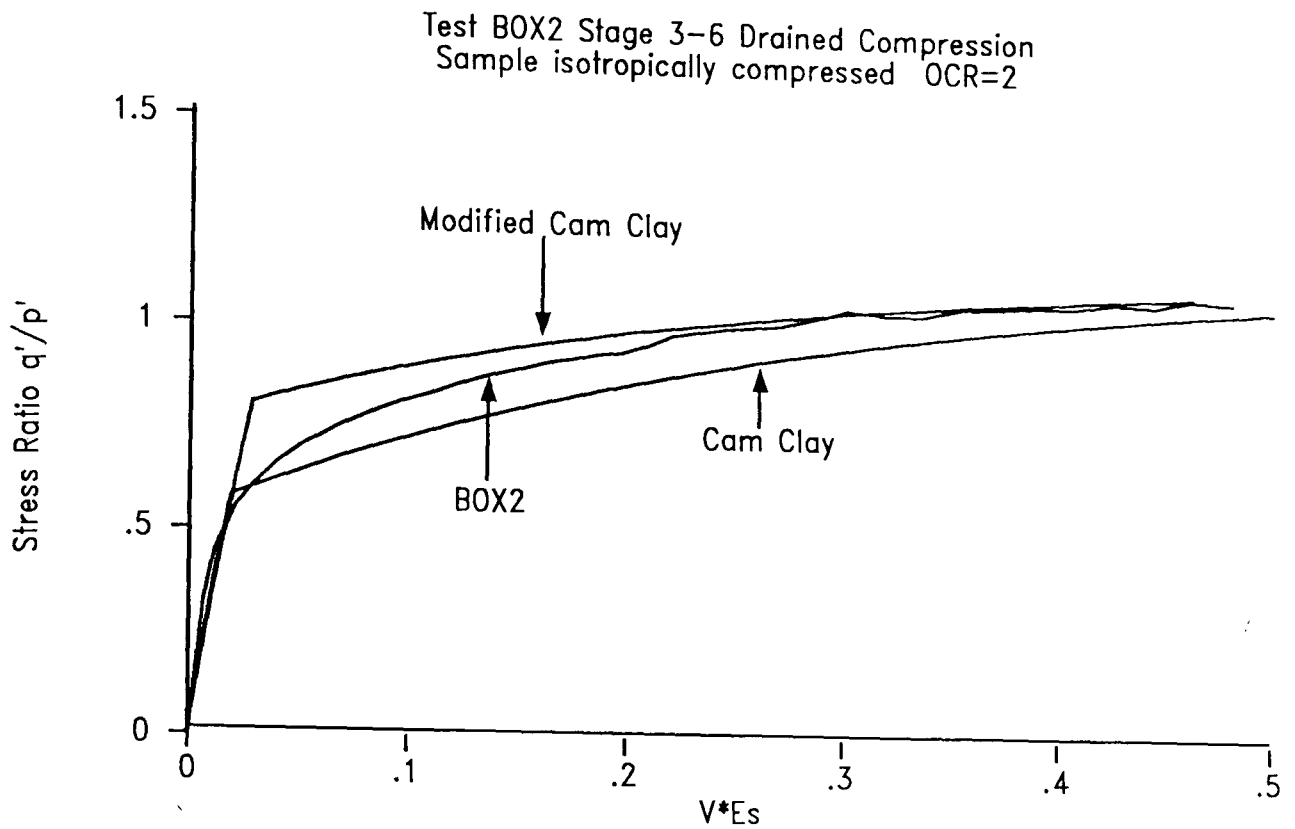

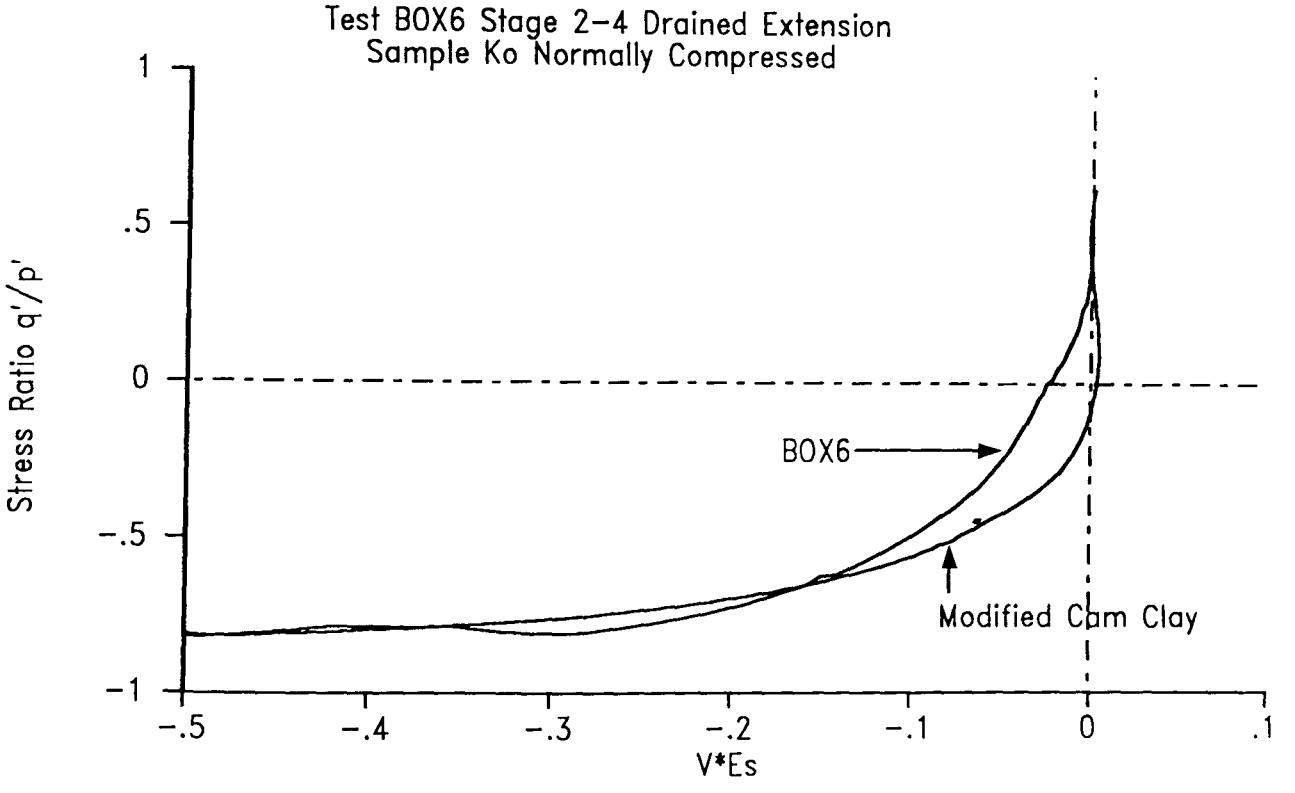

Figure 8.16 Normalised stress-strain plots for drained tests on reconstituted clay (Sheet 2 of 2)

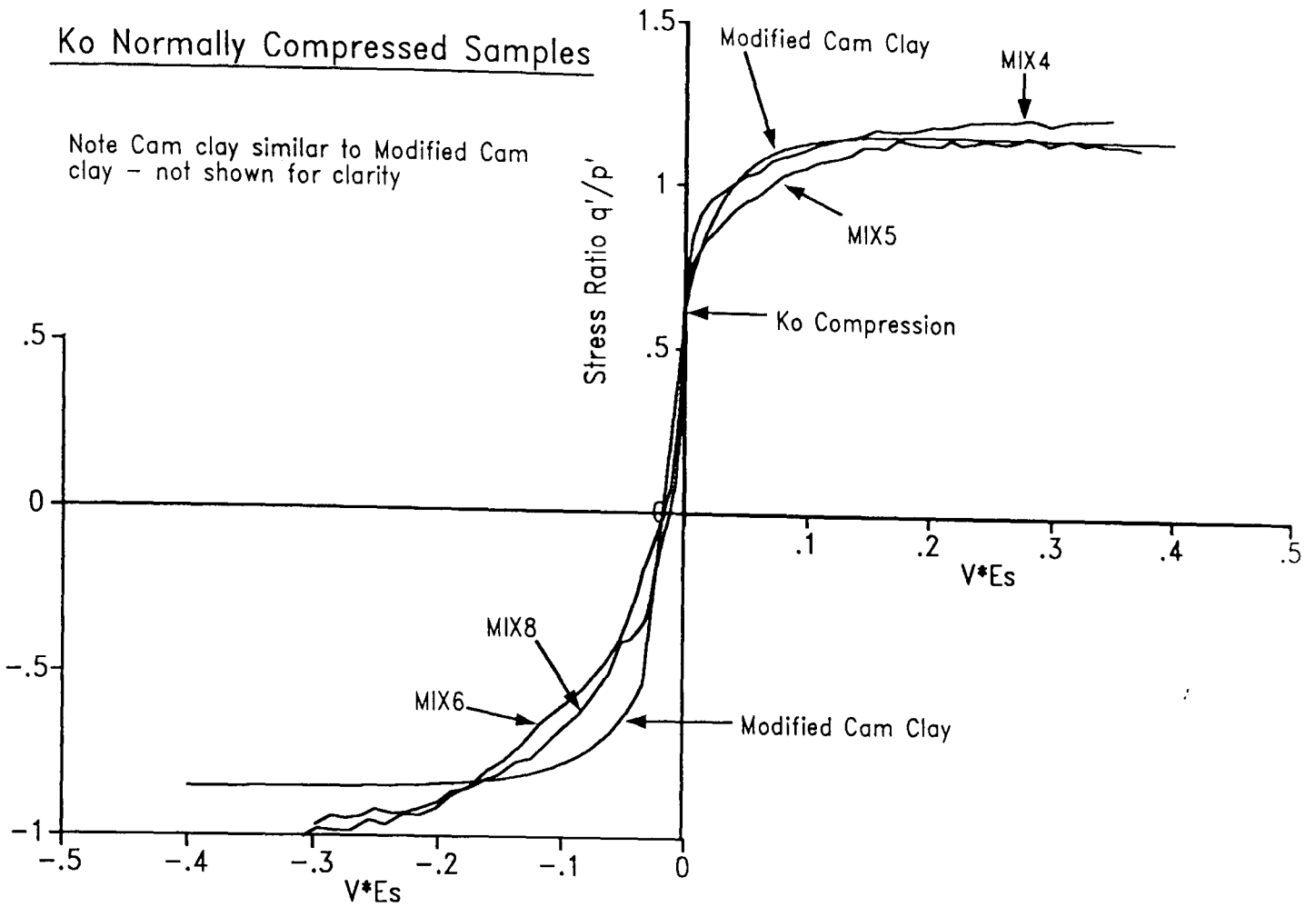

Figure 8.17 Normalised stress-strain plots for undrained tests on reconstituted clay

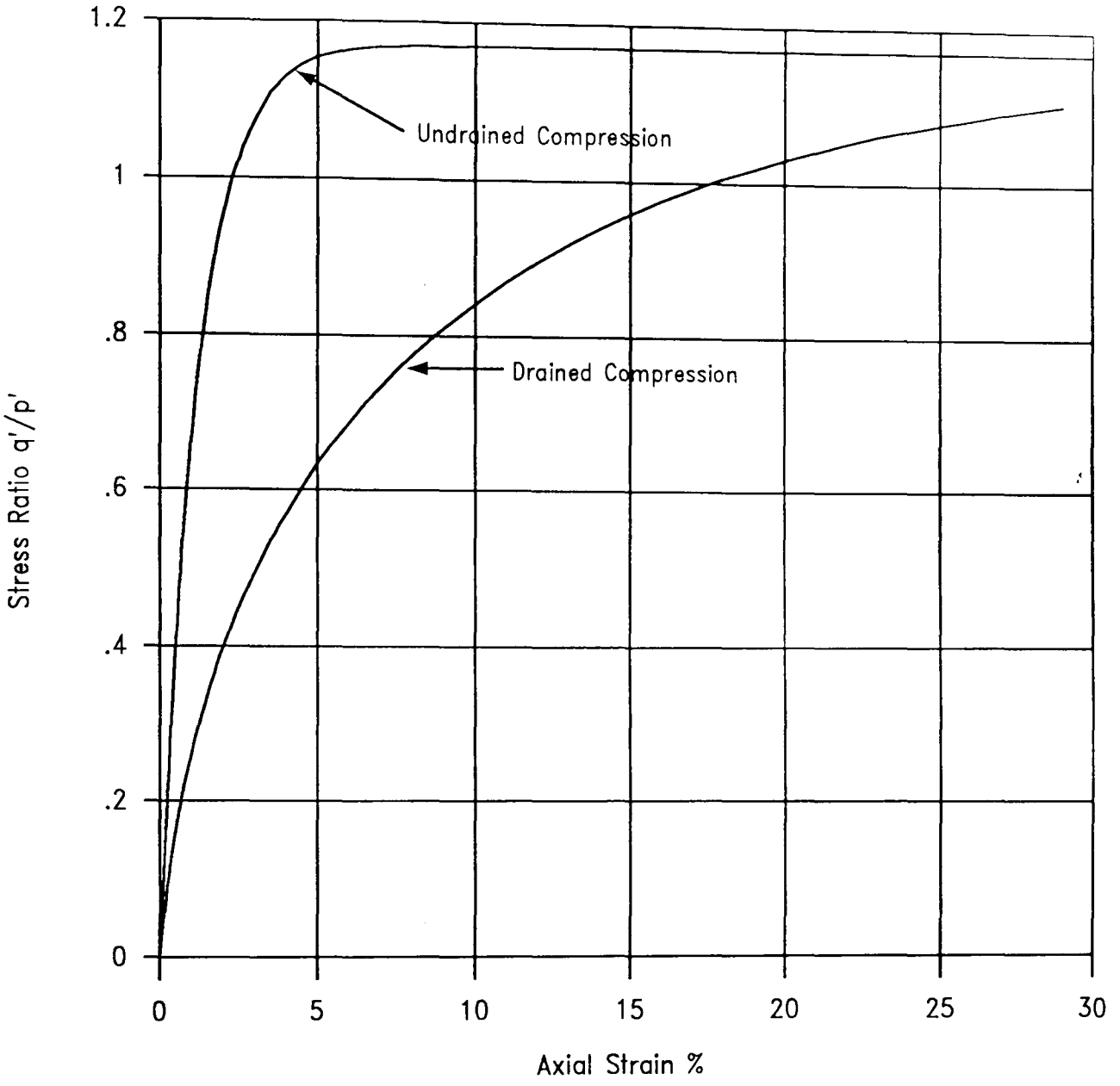

Figure 8.18 Comparison of drained and undrained shearing in compression using the Modified Cam clay soil model

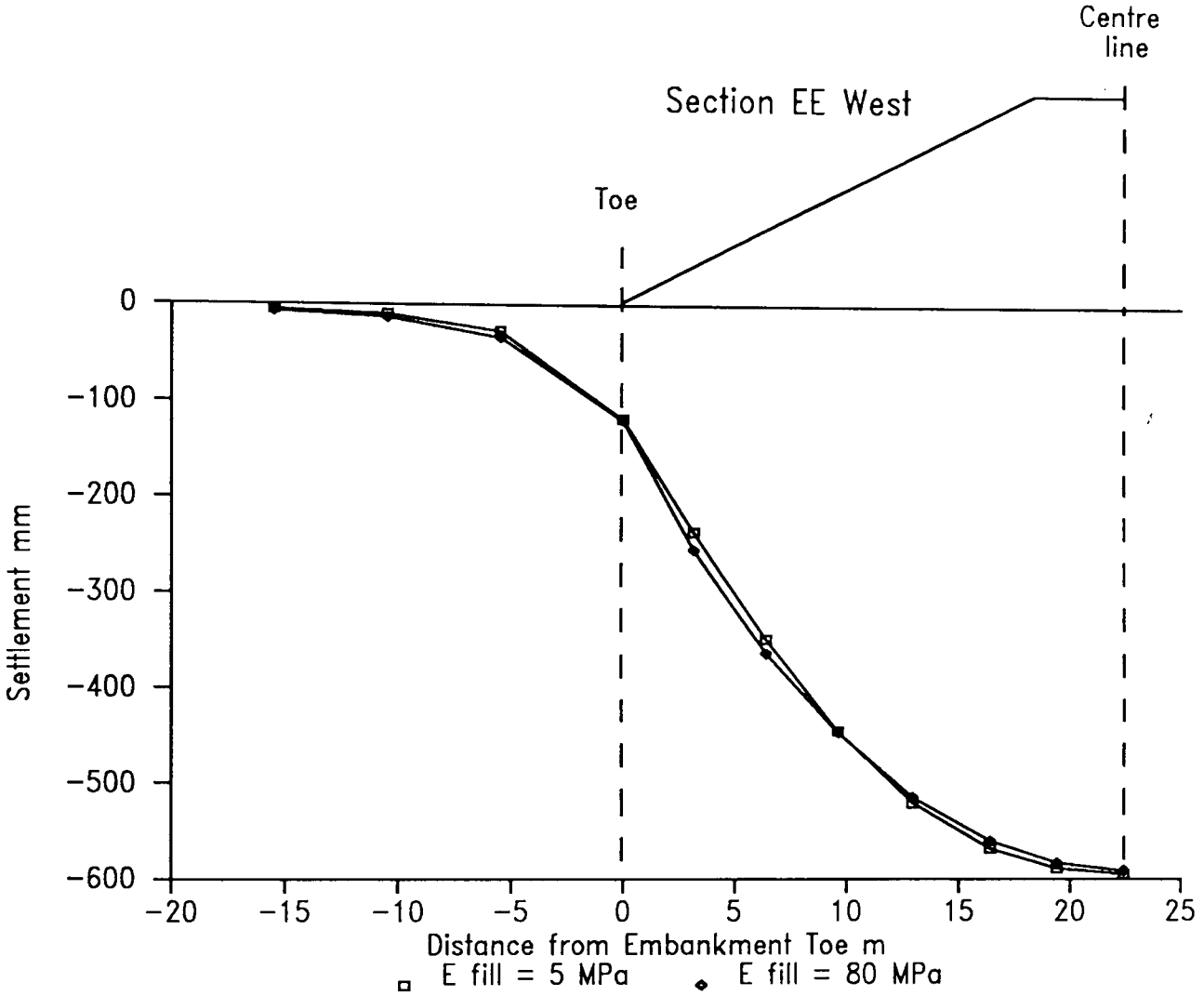

Figure 9.1 Influence of embankment stiffness on the settlement profile

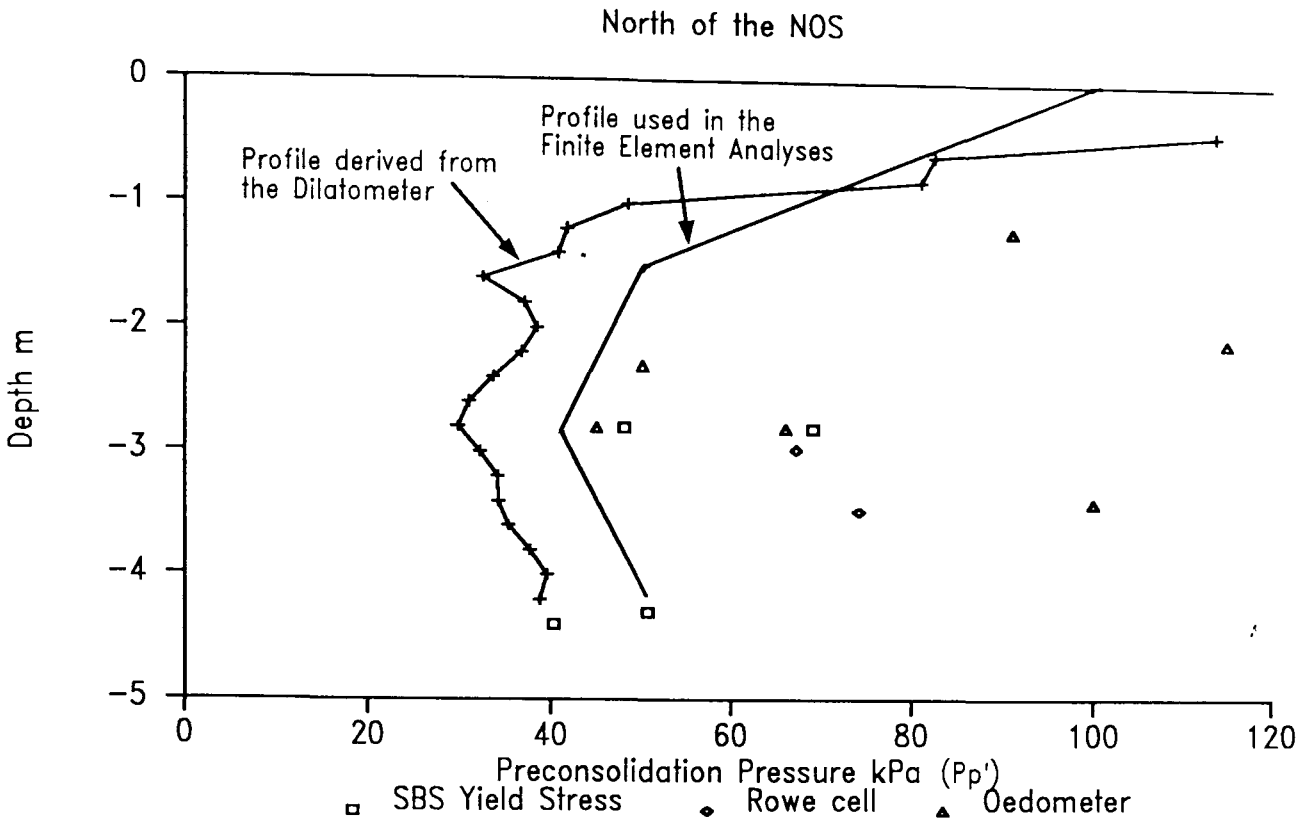

Figure 9.2 Profile of preconsolidation pressure used in the finite element analyses

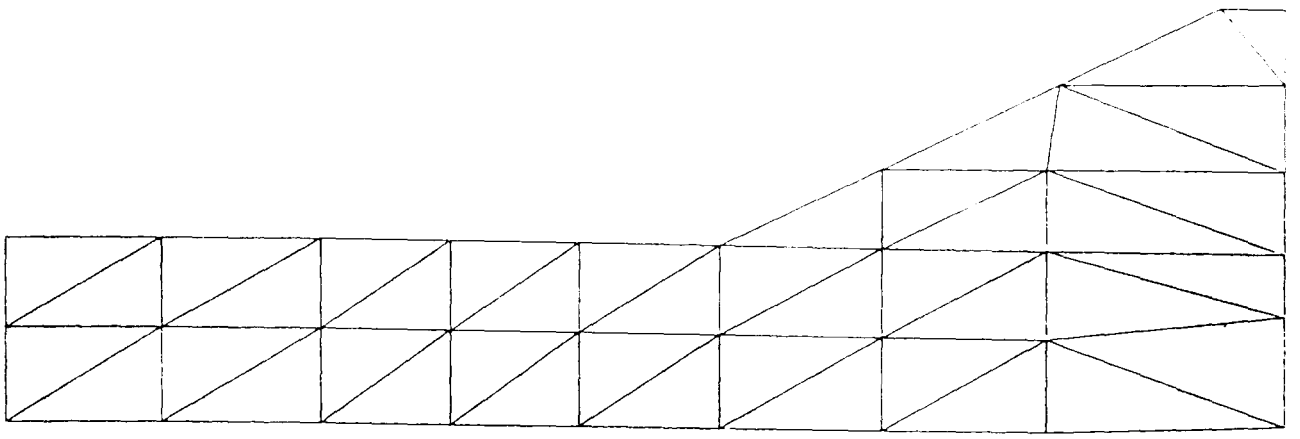

MESH ewl1 & ewc1

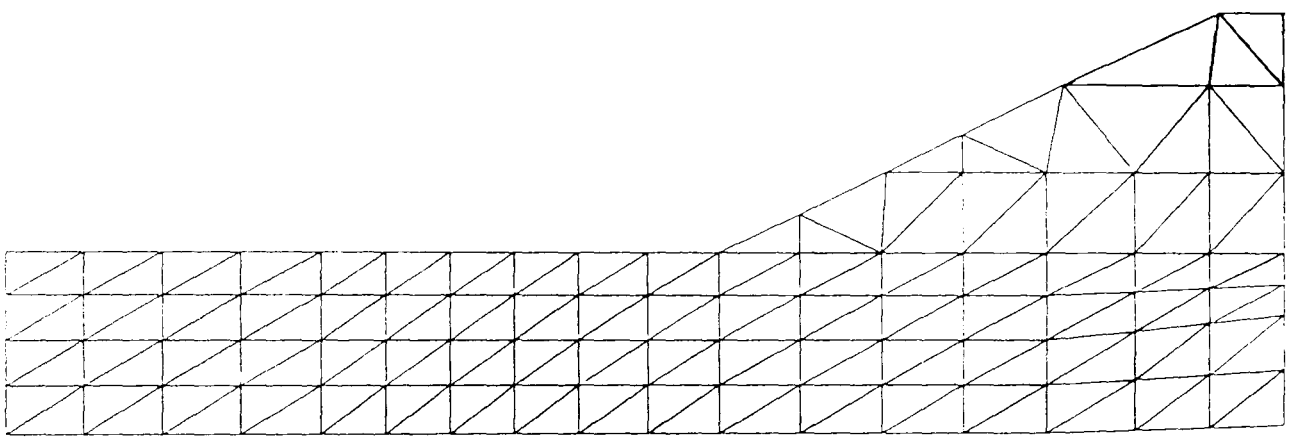

MESH ewl2

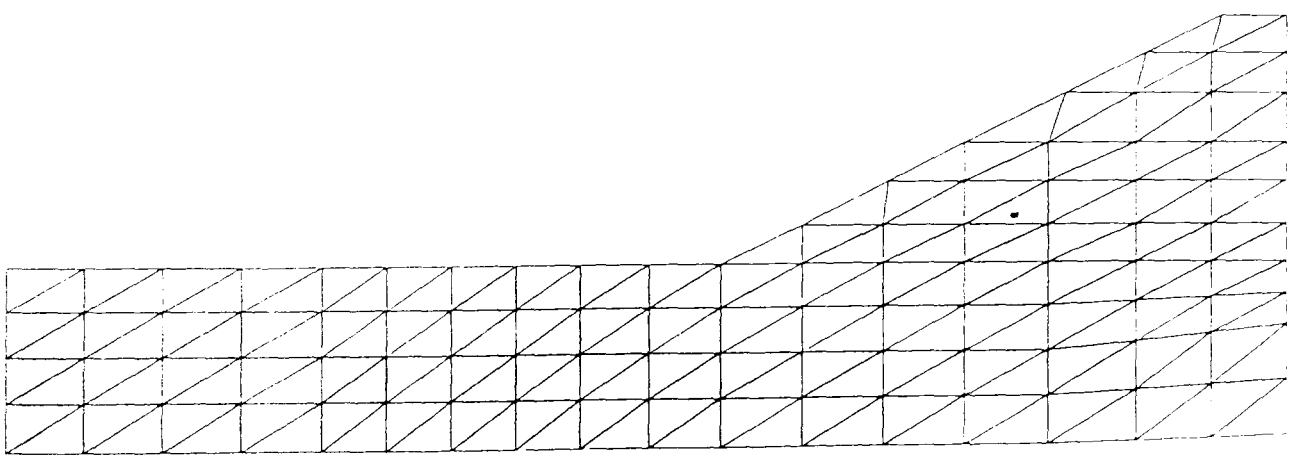

MESH ewl3

Figure 9.3 Finite element meshes for Section EE West

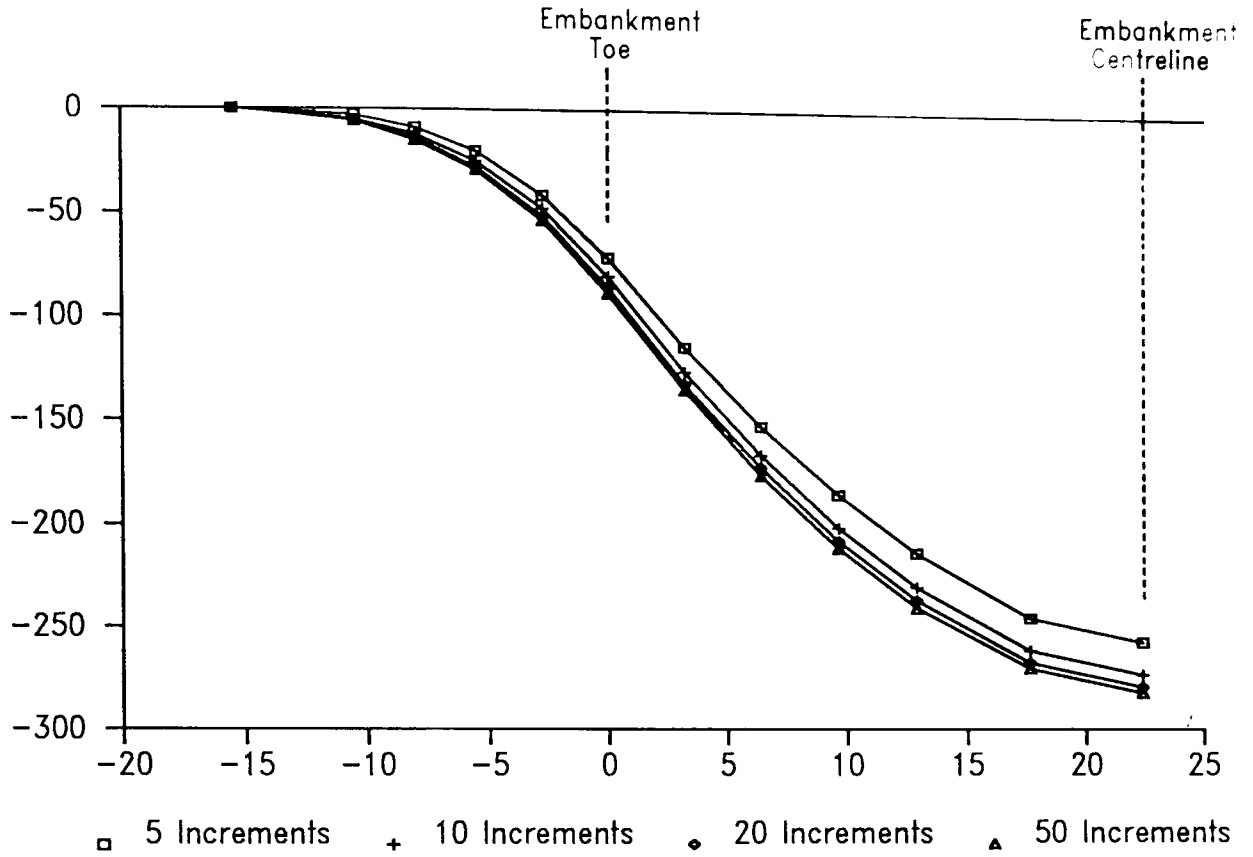

Figure 9.4 Influence of varying the number of loading increments on the finite element results

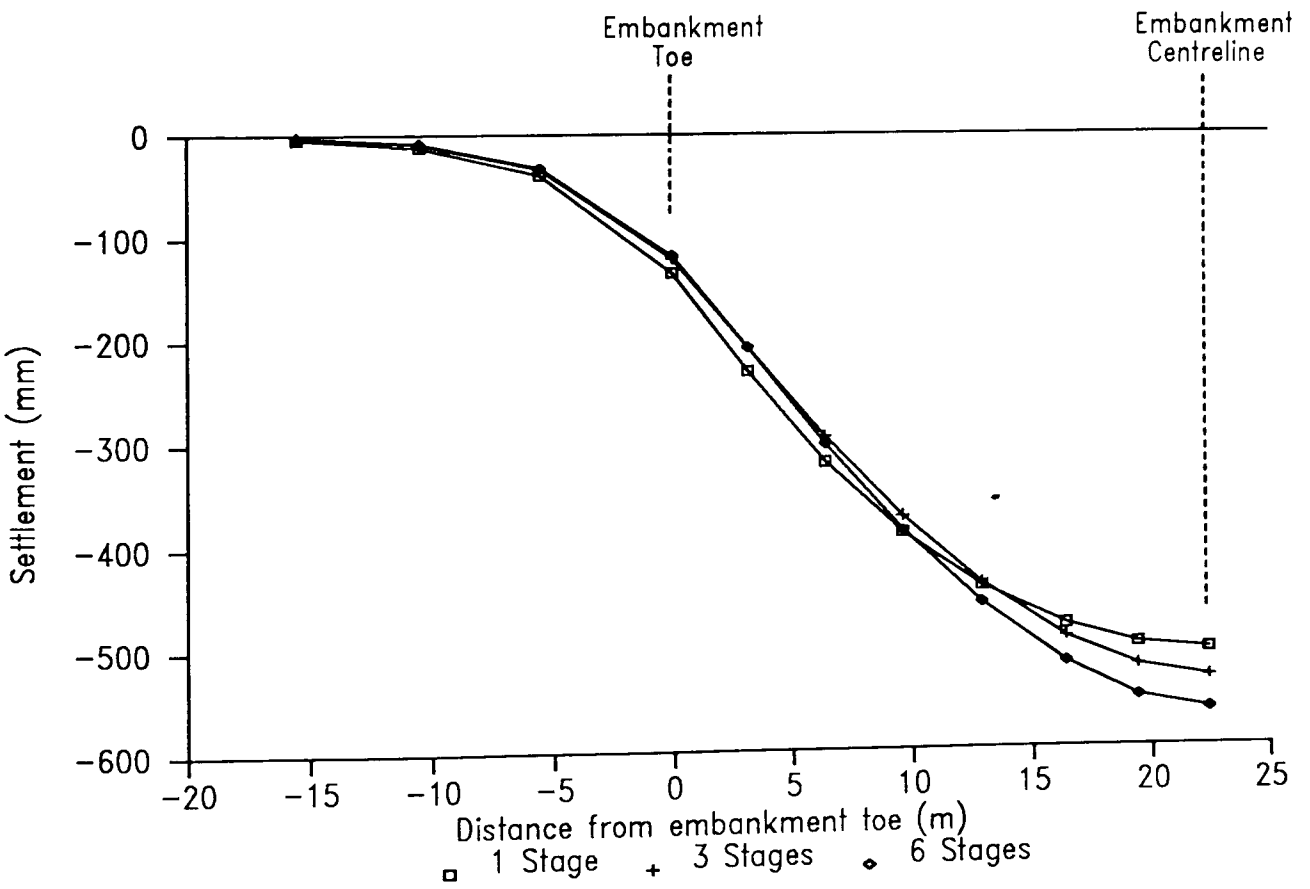

Figure 9.5 Influence of varying the number of construction stages on the finite element results

Node	X Coord m	Y Coord m
A	0.0	0.0
B	0.0	1.9
C	0.0	3.7
D	0.0	4.7
E	0.0	7.2
F	27.6	7.2
G	47.2	18.0
H	50.0	18.0
I	50.0	13.9
J	50.0	10.4
K	50.0	7.2
L	50.0	4.7
M	50.0	3.7
N	50.0	1.9
O	50.0	0.0
P	19.6	13.7
Q	41.2	20.4

IN SITU STRESSES				
Level	v' kPa	h' kPa	Pore kPa	P_p' kPa
E-K	0.0	0.0	0.0	0
D-L	37.5	29.0	0.0	50
C-M	52.5	29.0	0.0	50
A-O	74.0	41.1	37.0	70

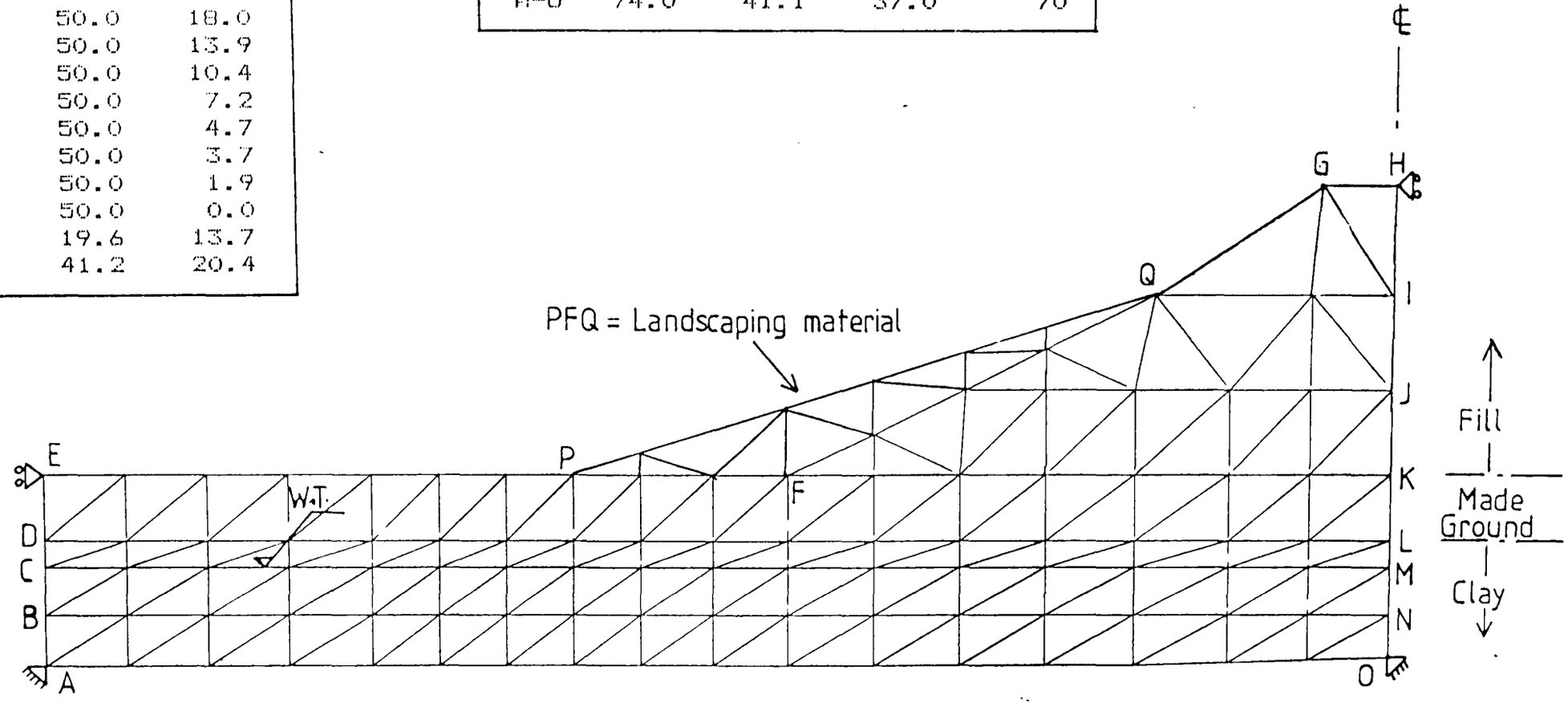

Section EE West Mesh ew14

Figure 9.6

Node	X Coord m	Y Coord m
A	0.0	0.0
B	0.0	1.9
C	0.0	3.8
D	0.0	5.0
E	0.0	6.2
F	27.6	6.2
G	34.0	9.6
H	50.0	9.6
I	50.0	7.9
J	50.0	6.2
K	50.0	5.0
L	50.0	3.8
M	50.0	1.9
N	50.0	0.0
X	0	2.8
Y	50	2.8

IN SITU STRESSES

Level	v' kPa	h' kPa	Pore kPa	P_p' kPa
E-J	0.0	0.0	0.0	0
C-L	36.0	29.0	0.0	50
X-Y	52.0	29.0	0.0	50
A-N	68.8	37.8	28.0	63

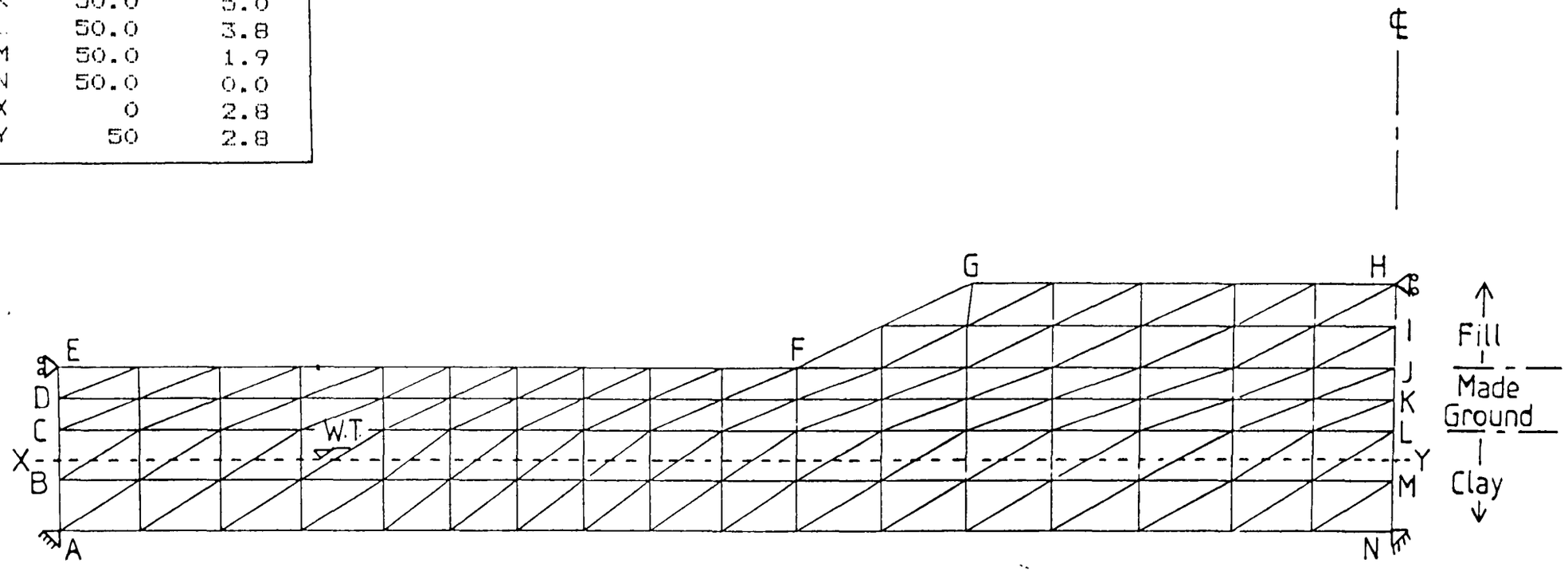

Section EE East Mesh ee13

Figure 9.7

Node	X Coord m	Y Coord m
A	0.0	0.0
B	0.0	1.4
C	0.0	2.8
D	0.0	4.3
E	8.2	4.3
F	32.0	16.4
G	35.0	16.4
H	35.0	13.2
I	35.0	10.4
J	35.0	7.4
K	35.0	5.1
L	35.0	4.3
M	35.0	2.8
N	35.0	1.4
O	35.0	0.0

IN SITU STRESSES

Level	σ_v' kPa	σ_h' kPa	Pore kPa	P_o' kPa
D-L	24.0	24.0	-24.0	100
C-M	24.0	24.0	0.0	50
B-N	32.4	21.0	14.0	40
A-O	40.8	26.0	28.0	50

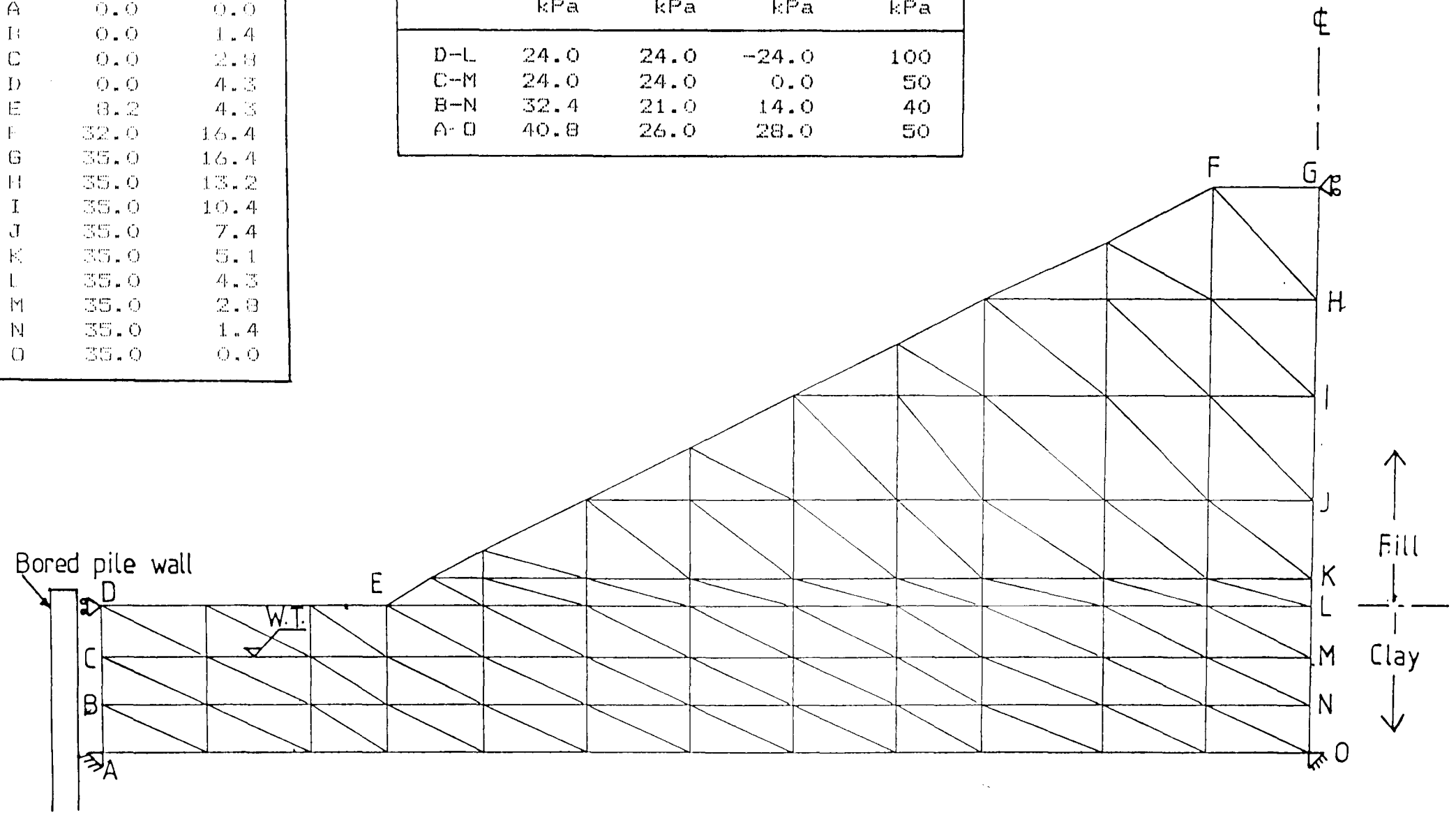

Section DD Mesh d11

Figure 9.8

Node	X Coord m	Y Coord m
A	0.0	0.0
B	0.0	1.3
C	0.0	2.6
D	0.0	4.0
E	27.0	4.0
F	45.5	13.3
G	51.5	13.3
H	51.5	10.0
I	51.5	7.0
J	51.5	4.7
K	51.5	4.0
L	51.5	2.6
M	51.5	1.3
N	51.5	0.0
O	19.5	4.0
P	36.0	8.5

IN SITU STRESSES				
Level	$\sigma v'$ kPa	$\sigma h'$ kPa	Pore kPa	P_p' kPa
D-K	22.4	22.4	-22.4	100
C-L	22.4	22.4	0.0	50
B-M	30.2	19.5	13.0	40
A-N	38.0	24.5	26.0	50

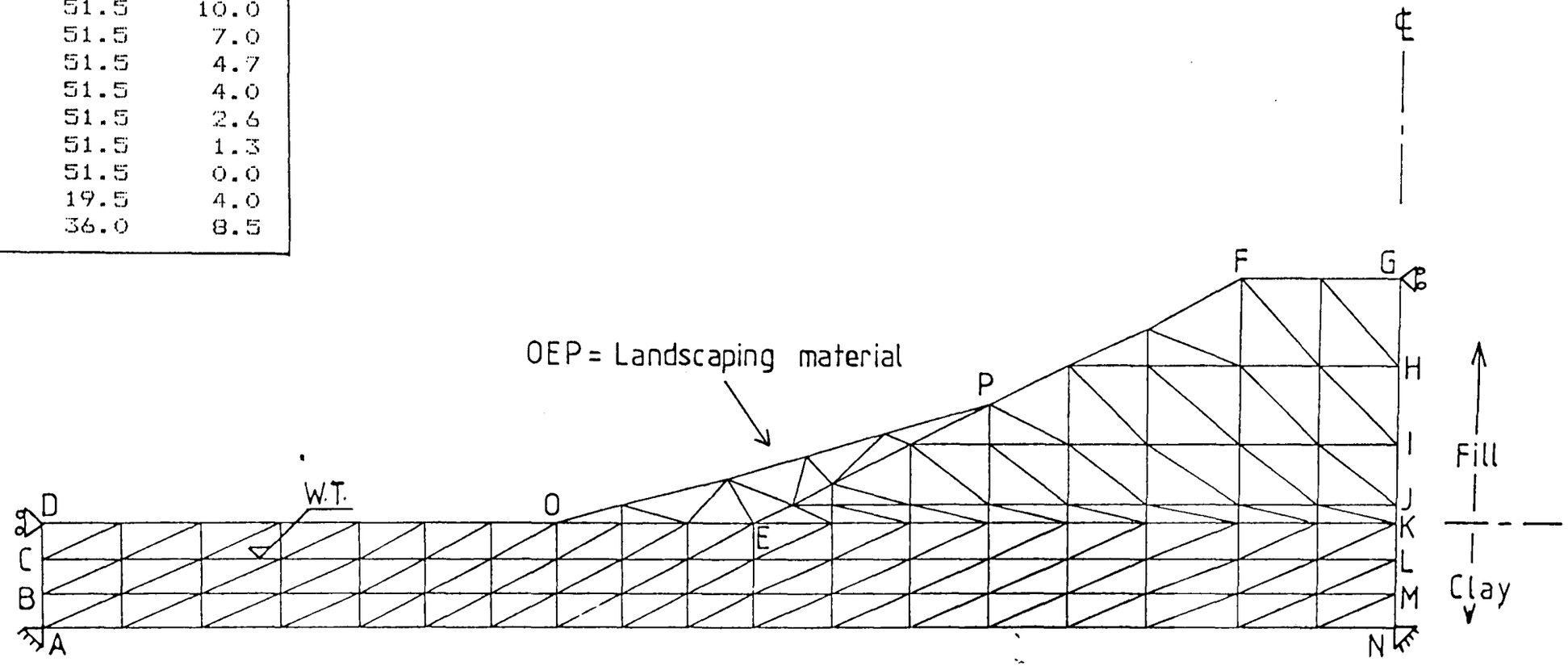

Section CC Mesh c12

Figure 9.9

Node	X Coord m	Y Coord m
A	0.0	0.0
B	0.0	1.4
C	0.0	2.8
D	0.0	4.2
E	18.0	4.2
F	30.4	10.4
G	37.0	10.4
H	37.0	7.4
I	37.0	4.9
J	37.0	4.2
K	37.0	2.8
L	37.0	1.4
M	37.0	0.0

IN SITU STRESSES				
Level	σ_v' kPa	σ_h' kPa	Pore kPa	P_β' kPa
D-J	22.4	22.4	-22.4	100
C-K	22.4	22.4	0.0	50
B-L	30.8	20.0	14.0	40
A-M	39.2	25.0	28.0	50

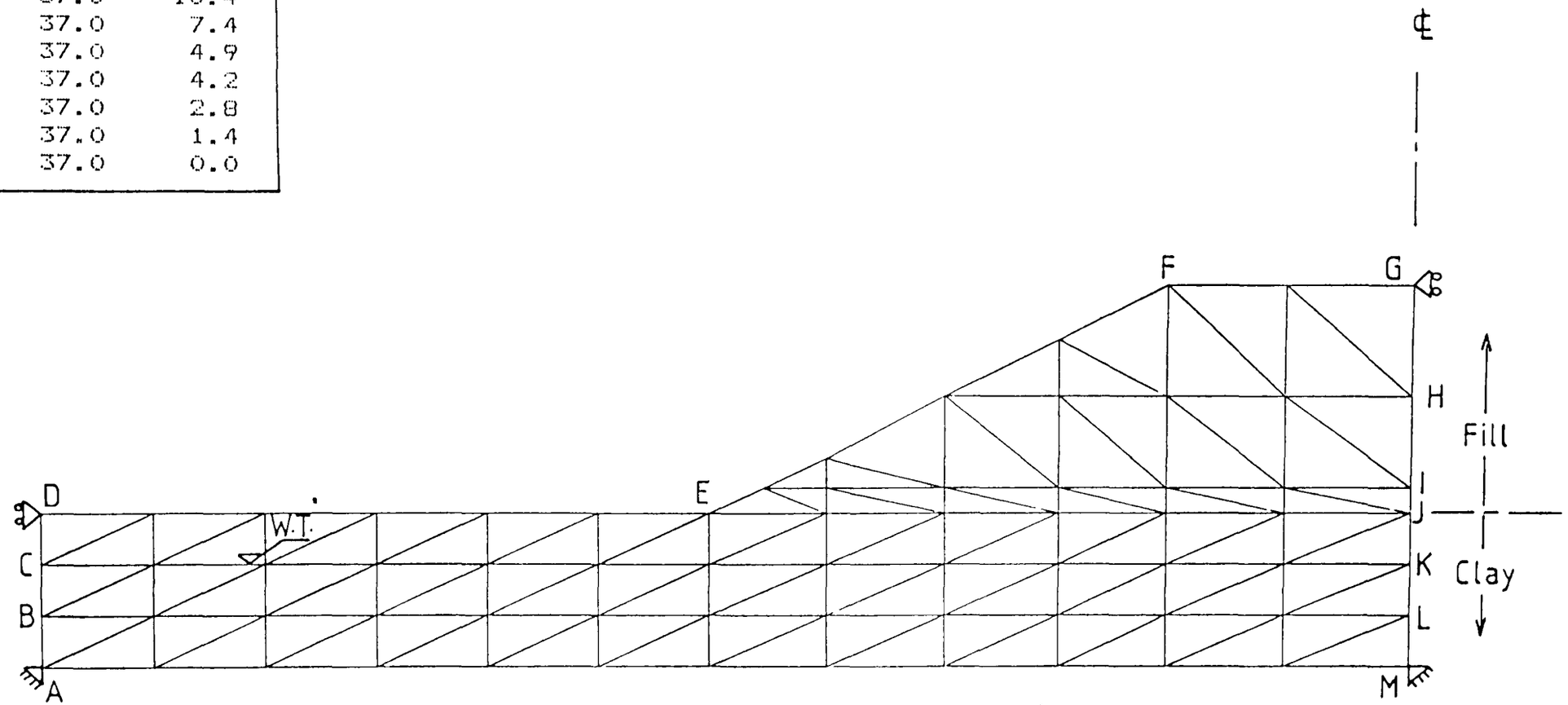

Section AA Mesh a11

Figure 9.10

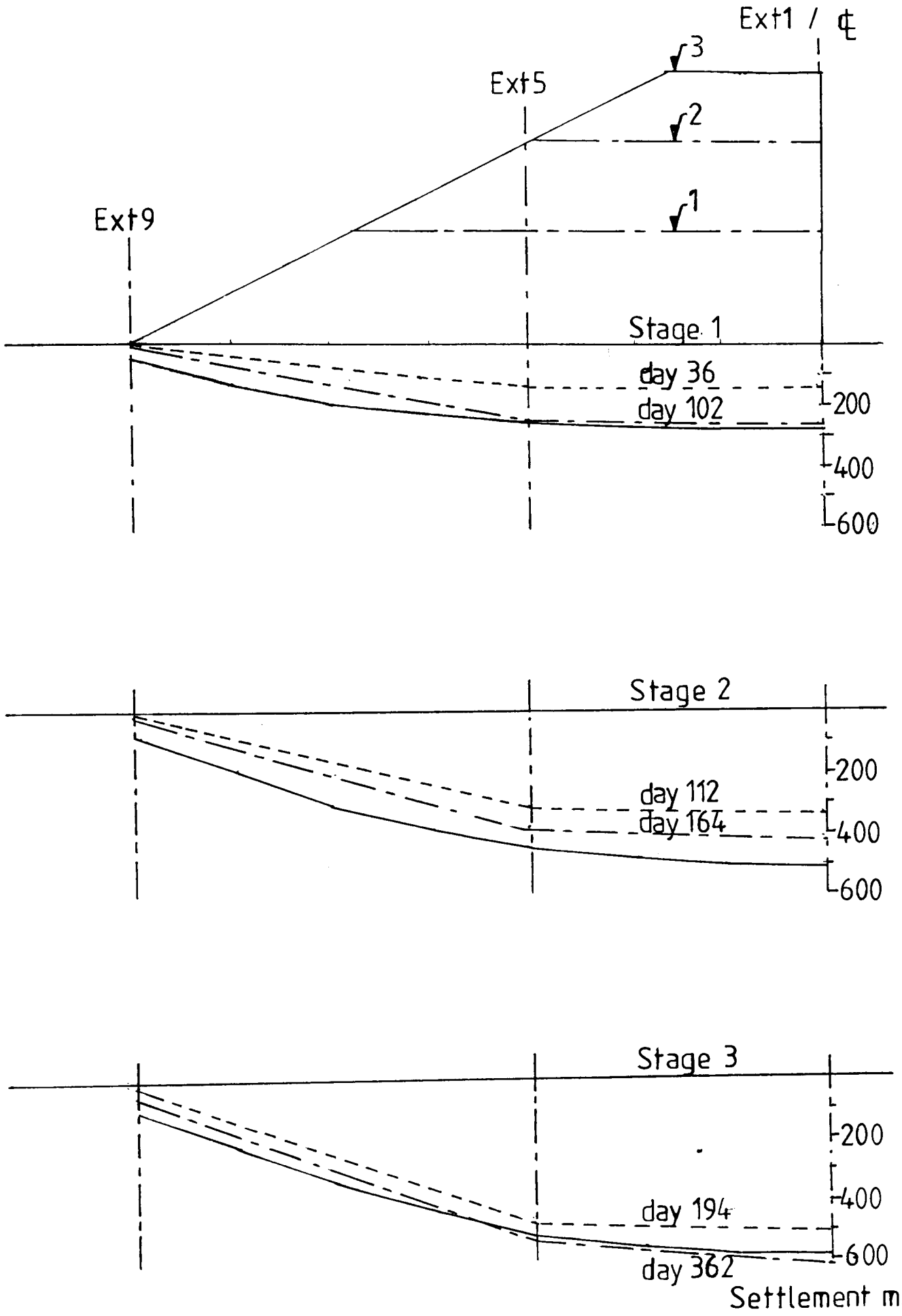

Figure 9.11 Predicted and actual settlements at Section EE West

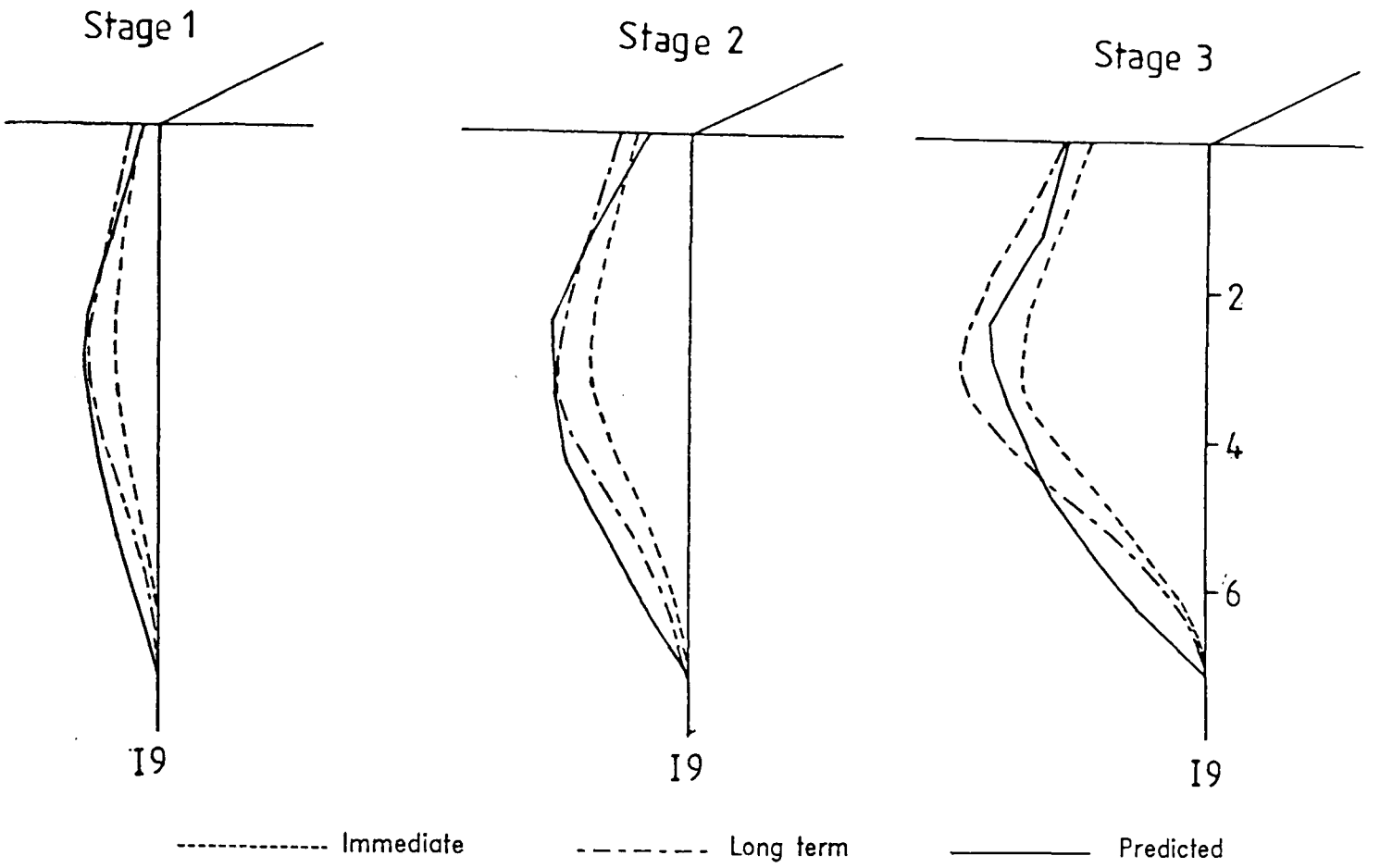

a) Deformation at the embankment toe during construction (see section 9.3.1)

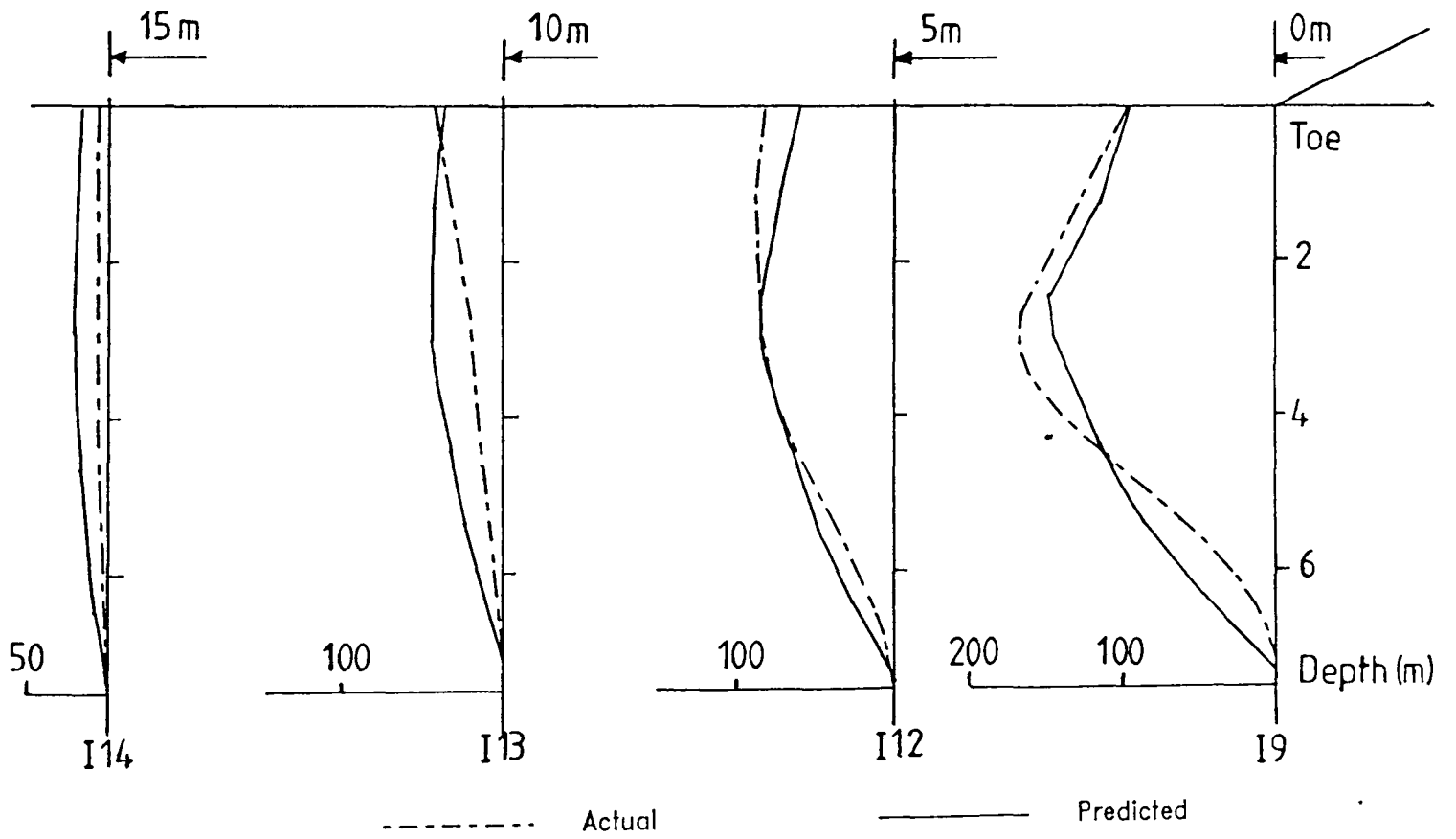

b) Final deformation profiles after landscaping (day 380)

Figure 9.12 Predicted and actual horizontal deformation profiles Section EE West

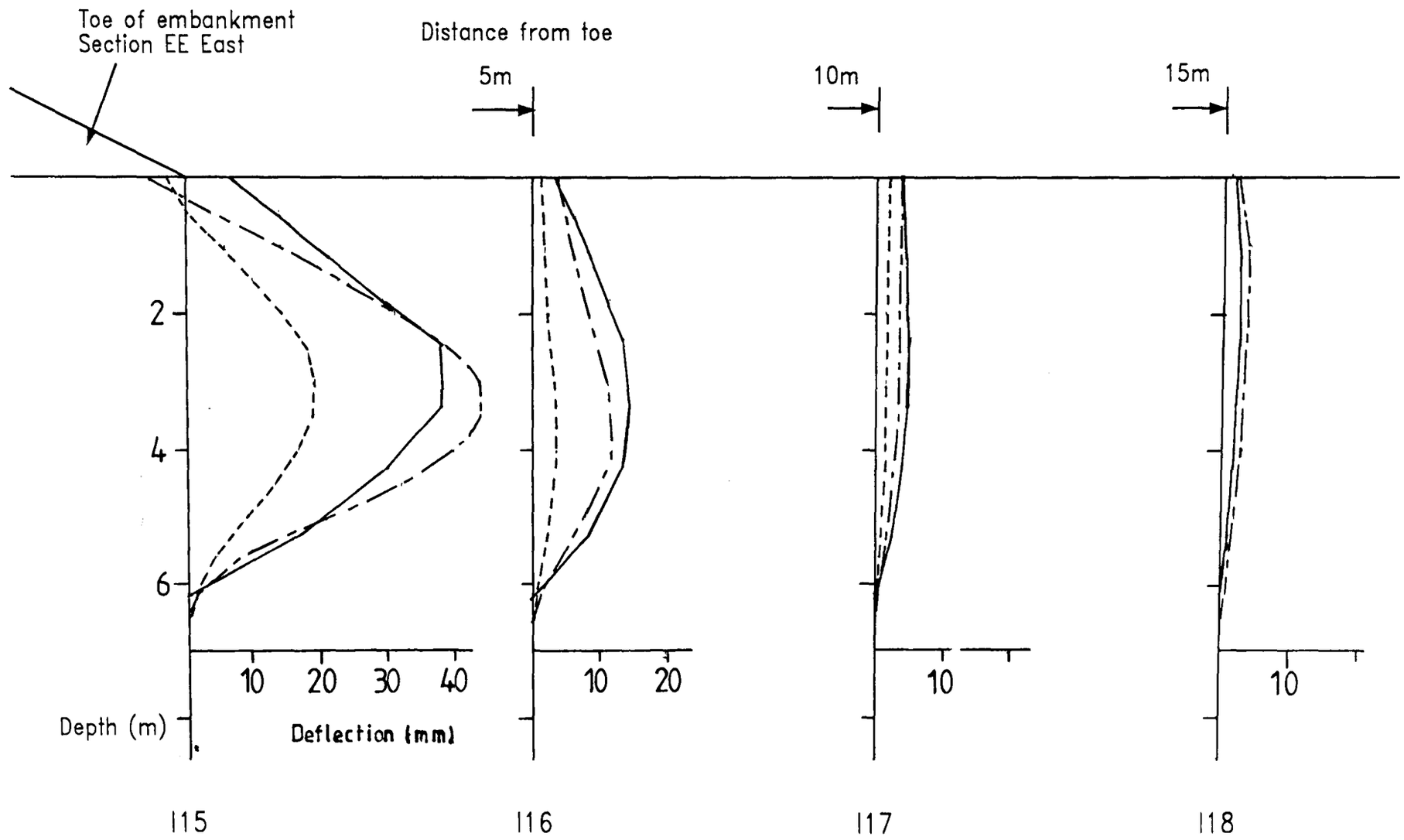

Figure 9.13 Predicted and actual ground deformations at section EE east

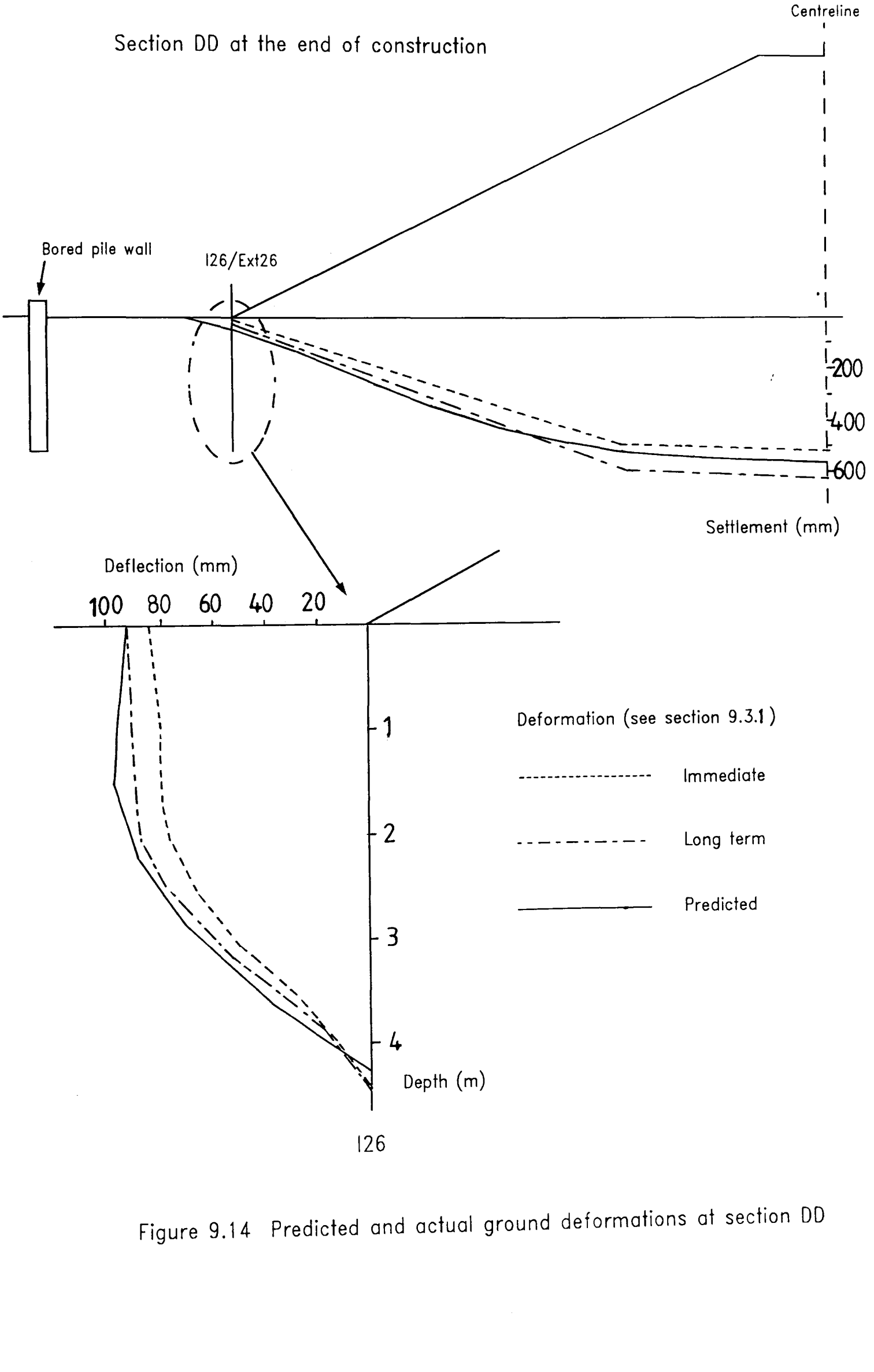

Figure 9.14 Predicted and actual ground deformations at section DD

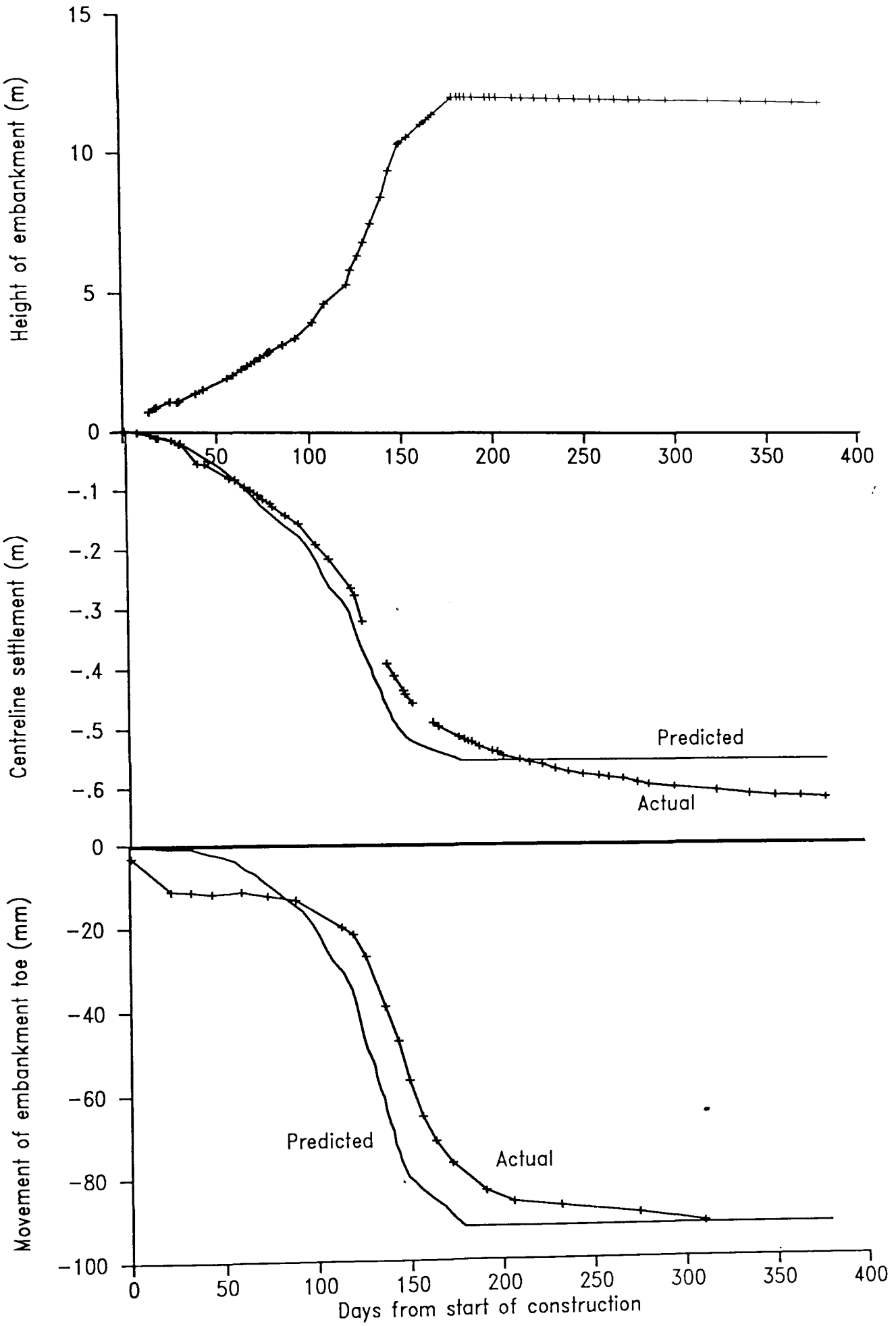

Figure 9.15 Maximum horizontal and vertical deformations versus embankment height at section DD

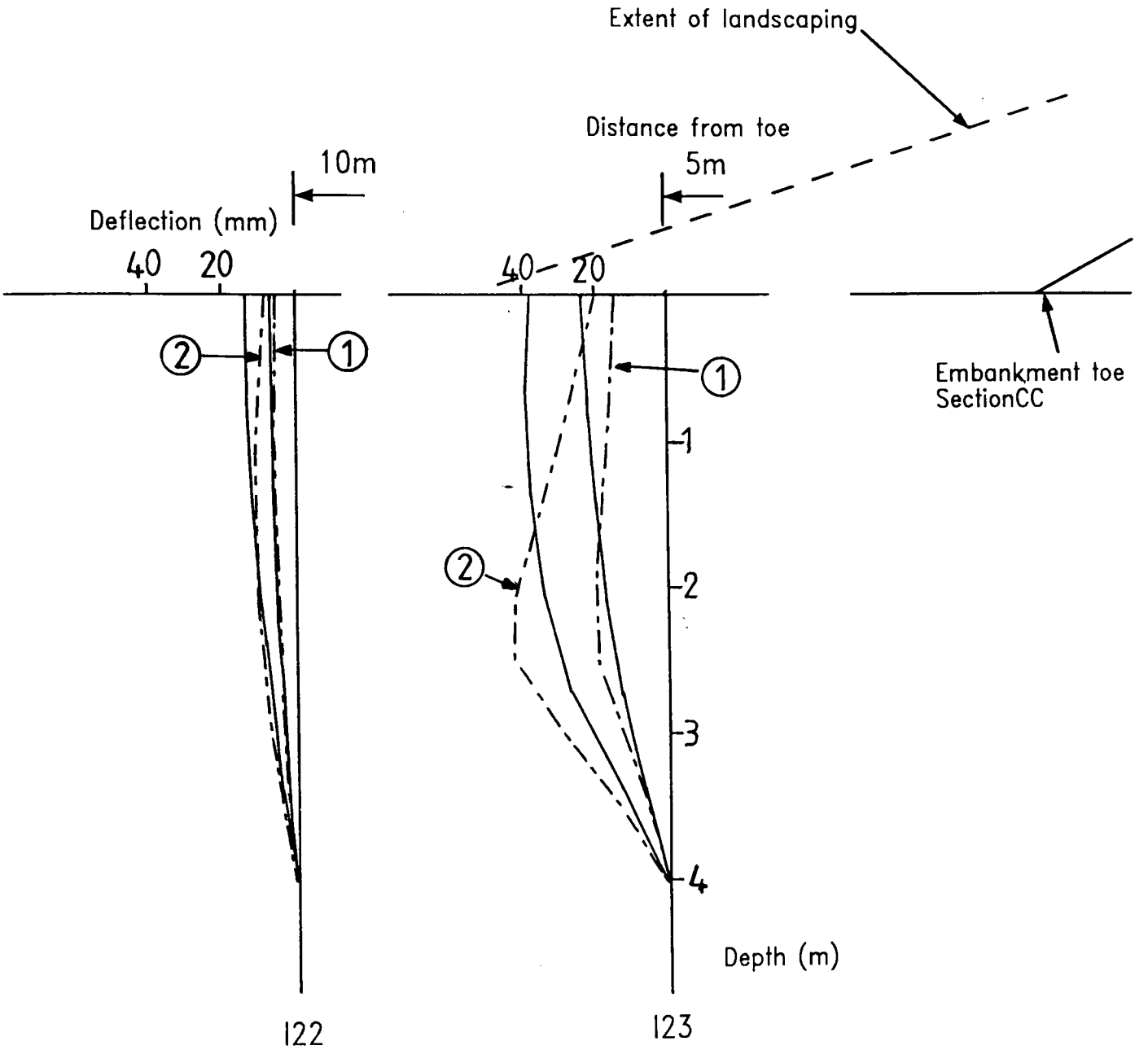

Deformation profiles (see section 9.3.5)

---------- Actual

———————— Predicted

① end of embankment construction

② after landscaping

Figure 9.16 Predicted and actual deformations at section CC

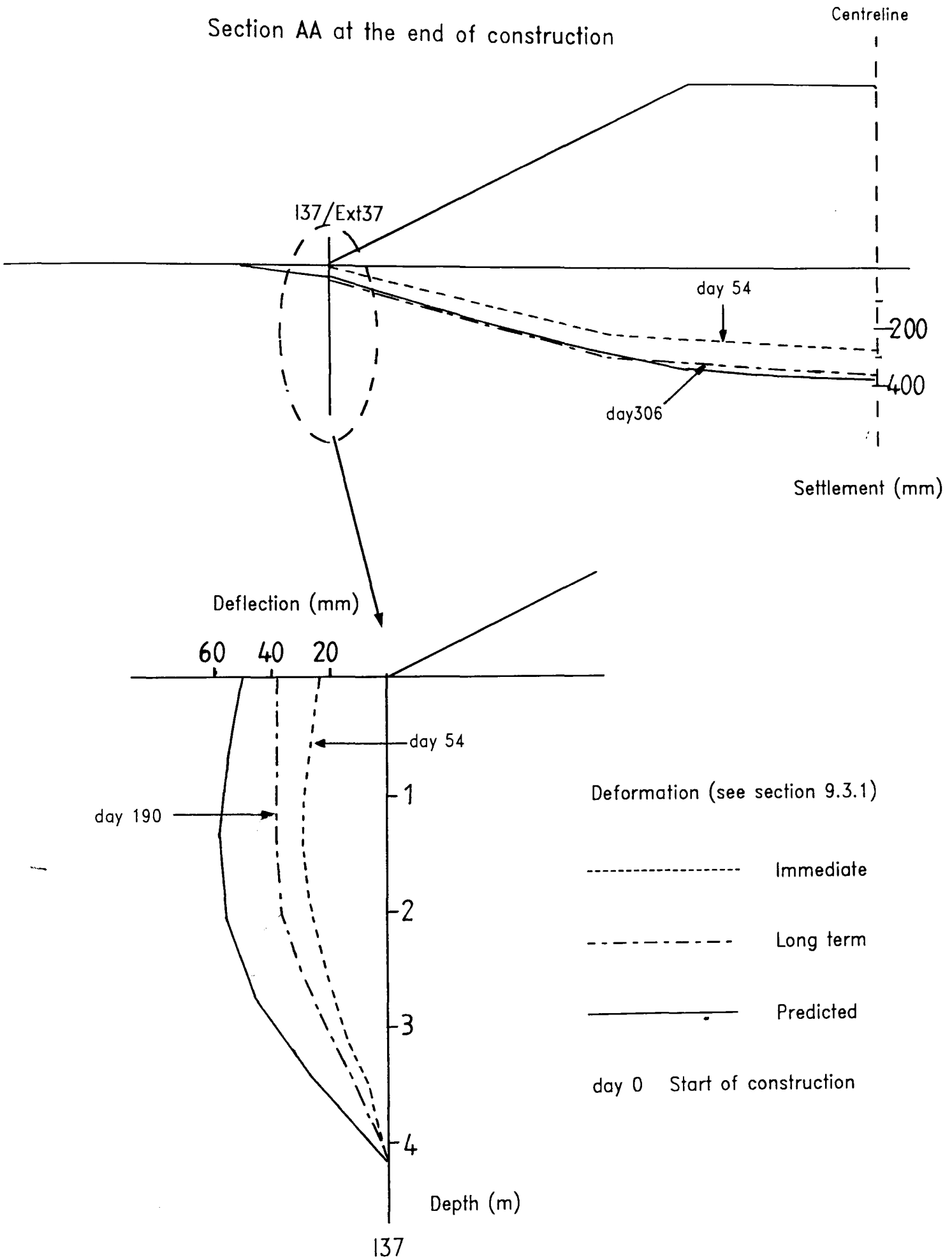

Figure 9.17 Predicted and actual ground deformations at section AA